TEXTE
60/2014

Modelling and mapping of atmospheric nitrogen and sulphur deposition and critical loads for ecosystem specific assessment of threats to biodiversity in Germany – PINETI (Pollutant INput and EcosysTem Impact)

Substudy Report 1

For our Environment

Umwelt Bundesamt

TEXTE 60/2014

Environmental Research of the
Federal Ministry for the
Environment, Nature Conservation,
Building and Nuclear Safety

Project No. (FKZ) 3710 63 246
Report No. (UBA-FB) 002007/1

Modelling and mapping of atmospheric nitrogen and sulphur deposition and critical loads for ecosystem specific assessment of threats to biodiversity in Germany – PINETI (Pollutant INput and EcosysTem Impact)

Substudy Report 1

by

Roy Wichink Kruit, Martijn Schaap, Arjo Segers, Dick Heslinga, Peter Builtjes
Netherlands Organisation for Applied Scientific Research TNO,
Utrecht, The Netherlands

Sabine Banzhaf
Freie Universität Berlin, FB Geowissenschaften, Institut für Meteorologie,
Berlin, Germany

Thomas Scheuschner
Gesellschaft für Ökosystemanalyse und Umweltdatenmanagement mbH
(ÖKO-DATA), Strausberg, Germany

On behalf of the Federal Environment Agency (Germany)

Imprint

Publisher:
Umweltbundesamt
Wörlitzer Platz 1
06844 Dessau-Roßlau
Tel: +49 340-2103-0
Fax: +49 340-2103-2285
info@umweltbundesamt.de
Internet: www.umweltbundesamt.de

/umweltbundesamt.de
/umweltbundesamt

Study performed by:
Netherlands Organisation for Applied Scientific Research TNO
P.O.Box 80015
3508 TA Utrecht
The Netherlands

Study completed in:
2014

Edited by:
Section II 4.3 Air Pollution and Terrestrial Ecosystems
Dr. Jakob Frommer, Markus Geupel

Publication as pdf:
http://www.umweltbundesamt.de/publikationen/modelling-mapping-of-atmospheric-nitrogen-sulphur

ISSN 1862-4804

Dessau-Roßlau, December 2014

The Project underlying this report was supported with funding from the Federal Ministry for the Environment, Nature Conservation, Building and Nuclear safety under project number FKZ 3710 63 246. The responsibility for the content of this publication lies with the author(s).

Kurzbeschreibung

Die Biodiversität in Europa ist durch den Eintrag von Schwefel- und Stickstoffverbindungen in die Ökosysteme gefährdet. Innerhalb des PINETI Projektes werden daher die atmosphärischen Einträge dieser Schad- und Nährstoffe für Deutschland für die Jahre 2008 und 2009 ermittelt. Die trockenen, nassen und feuchten Einträge von NH_x, NO_y, SO_x und die Einträge der basischen Kationen Ca^{2+}, Mg^{2+}, K^+ und Na^+ werden berechnet und zur Gesamtdeposition aufsummiert. Anhand der Ergebnisse und den Critical Load werden die Überschreitungen der Critical Load für empfindliche Ökosysteme berechnet.

Im Folgenden wird eine Zusammenfassung der verwendeten Methoden und der Projektergebnisse präsentiert. Nach einer kurzen Einleitung werden zunächst die Eingangsdaten zur Ermittlung der atmosphärischen Einträge erläutert. Anschließend werden die Methoden zur Bestimmung der trockenen, nassen und feuchten Deposition jeweils kurz beschrieben. Die erstellten Karten zur Gesamtdeposition werden präsentiert und die Ergebnisse mit den Resultaten des Vorgängerprojektes MAPESI und Ergebnissen des EMEP Modells verglichen. Im Anschluss werden die, innerhalb des Projektes durchgeführten Modellweiterentwicklungen und Modellevaluationen zusammenfassend beschrieben und weitere mögliche Modellentwicklungen benannt und empfohlen. Abschließend wird die Bewertung des Eintrages in Bezug auf Risiken für terrestrische Ökosysteme zusammenfassend dargestellt. Das Prinzip der Critical Load wird kurz erläutert und die zeitlichen Trends der Überschreitungen der Critical Load für Versauerung und für Eutrophierung werden präsentiert.

Abstract

Biodiversity in Europe is strongly affected by the deposition of nitrogen and sulfur on terrestrial ecosystems. Therefore, the deposition of these atmospheric substances is assessed for the years 2008 and 2009 within the PINETI project. Dry, wet and occult deposition of NH_x, NO_y, SO_x and the base cations Ca^{2+}, Mg^{2+}, K^+ und Na^+ are calculated and added up to the total deposition. By means of the latter and the Critical Load the Critical Load exceedances for sensitive ecosystems are assessed.

In the following, a summary of the applied methods and the results of the project is presented. A short introduction is followed by the description of the input data used to assess the atmospheric deposition. The methods applied for the calculation of dry, wet and occult deposition are summarized. Thereafter, the maps of the assessed total deposition are presented and the results are compared to those of the EMEP model and the MAPESI project. Moreover, the model developments and model evaluations that have been performed within the project are described and further recommended model developments are shortly introduced. Finally, the assessment of the atmospheric input with respect to risks for terrestrial ecosystems is presented. The approach of Critical Loads is shortly explained and the temporal trends of the exceedances of the Critical Load for acidification and eutrophication are presented.

Table of Contents

Table of Figures

List of Tables

Zusammenfassung

Die Biodiversität in Europa ist u.a. durch den Eintrag von Schwefel- und Stickstoffverbindungen in die Ökosysteme gefährdet. Ein wesentliches Ziel des PINETI Projektes (durchgeführt von TNO, FU-Berlin und ÖKO-DATA) war es daher die atmosphärischen Substanzen dieser Schad- und Nährstoffe für Deutschland für die Jahre 2008 und 2009 zu ermitteln (Teilbericht 1) und anhand der Ergebnisse die Überschreitungen der Critical Load für empfindliche Ökosysteme zu berechnen (Teilbericht 4).

Dafür wird sowohl der atmosphärische Eintrag von NH_x, NO_y, SO_x, als auch der Eintrag der basischen Kationen Ca^{2+}, Mg^{2+}, K^+ und Na^+ benötigt. Der atmosphärische Eintrag dieser Substanzen berechnet sich aus der Summe der folgenden drei Depositionswege: der trockenen Deposition, der nassen Deposition und der feuchten Deposition. Anders als die nasse Deposition kann die trockene Deposition nicht routinemäßig an einer Vielzahl von Standorten gemessen werden. Daher beruht die Abschätzung des Schadstoffeintrages durch trockene Deposition auf Modellrechnungen mit dem chemischen Transport Modell LOTOS-EUROS. Für die nasse Deposition stehen Messergebnisse aus verschiedenen Messnetzen an über 100 Stationen in Deutschland zur Verfügung. Je nach Messnetz werden die Daten zu den Konzentrationen von Stickstoff, Schwefel und den basischen Kationen in den gesammelten Niederschlagsproben wöchentlich, 2-wöchentlich oder 4-wöchentlich bereitgestellt. Durch die Kombination der Messungen mit den modellierten Feldern der nassen Deposition wurde eine hochaufgelöste Karte des Schadstoffeintrages durch die nasse Deposition in Deutschland erstellt. Die feuchte Deposition wurde anhand des modellierten Nebel-/Wolkenwassereintrages und der Stoffkonzentration im Nebel-/Wolkenwasser ermittelt. Dafür wurde die Stoffkonzentration im Nebel-/Wolkenwasser anhand einer empirisch ermittelten Funktion aus der Stoffkonzentration im Niederschlag berechnet. Durch die Addition von trockener, nasser und feuchter Deposition wurden Karten der Gesamtdeposition von SO_x, NO_y, NH_x und den basischen Kationen über Deutschland erstellt. Mit den so ermittelten Stoffeinträgen wurden anschließend geprüft, ob die ökologischen Belastungsgrenzen, die Critical Load, eingehalten oder überschritten wurden. Daraus kann dann abgeleitet werden, ob die Ökosysteme einem Schadstoffrisiko ausgesetzt oder aber vor Versauerung und Eutrophierung geschützt sind.

Um eine gute Abschätzung der Gesamtdeposition von SO_x, NO_y, NH_x und der basischen Kationen für Deutschland zu erhalten, ist die Schließung der Massenbilanz innerhalb des Systems zur Ermittlung der Gesamtdeposition von großer Bedeutung. Innerhalb des Vorgängerprojektes MAPESI (Builtjes et al., 2011) basierte die Ermittlung des Schadstoffeintrages durch die nasse Deposition ausschließlich auf Messungen und war somit unabhängig von den Modellberechnungen mit dem chemischen Transport Modell LOTOS-EUROS. Der Grund hierfür war, dass das Modell den nassen Depositionsfluss deutlich unterschätzt hat und somit die Verwendung der Messungen der nassen Deposition als Grundlage zur Erstellung der Karten der Verwendung des Modells vorgezogen wurde. Innerhalb des Modells sind die Prozesse der nassen Deposition und der trockenen Deposition jedoch über die Berechnung der Massenbilanz verbunden und somit nicht unabhängig voneinander. So wird zum Beispiel eine geringe nasse Deposition durch eine erhöhte trockene Deposition kompensiert. Werden die Karten der nassen Deposition auf Grundlage der Messungen erstellt und die Karten der trockenen Deposition basierend auf Modelldaten, kann dies daher zu einer Überschätzung der Gesamtdeposition führen. Eines der wichtigen Ziele dieses Projektes ist daher die Verbesserung der Modellierung der nassen Deposition (Teilbericht 2). Da das Modell trotz Unterschätzung der nassen Deposition zur Kenntnis ihrer räumlichen Verteilung beitragen kann, wurde innerhalb von PINETI eine neue Methodik zur Ermittlung

der Felder der nassen Deposition entwickelt. Innerhalb der neuen Methodik werden neben den Messungen auch modellierte Felder der Konzentrationen im Niederschlag in die Berechnung der Felder der nassen Deposition miteinbezogen. Allerdings ist auch mit der neuen Methodik die Schließung der Massenbilanz noch nicht gewährleistet.

Eine weiterer Eintrag, welcher nicht in die Berechnung der Massenbilanz einbezogen ist, d.h. außerhalb des Modellsystems LOTOS-EUROS berechnet wird, ist die feuchte Deposition. Wie bereits innerhalb des Vorgängerprojektes MAPESI, wird letztere derzeit in einem den Modellrechnungen nachgeschalteten Verfahren berechnet. Die innerhalb des PINETI Projektes berechnete feuchte Deposition für die Jahre 2008 und 2009 liegt jedoch deutlich unter den Werten, die innerhalb des MAPESI Projektes für das Jahr 2007 ermittelt wurden.

Die methodischen Unterschiede zwischen den Projekten MAPESI und PINETI führen zu Unterschieden in der berechneten Gesamtdeposition, welche in einer separaten Studie innerhalb des PINETI Projektes genauer untersucht wurden (Teilbericht 3).

In Teilbericht 1 werden die Methoden, die in PINETI zur Berechnung der Gesamtdeposition verwendet wurden im Detail beschrieben und die Ergebnisse für die Jahre 2008 und 2009 präsentiert. Innerhalb dieses Teilberichts werden auch die Unterschiede zwischen den TNO Ergebnissen zur Gesamtdeposition auf einem 1 x 1 km^2 Gitter (basierend auf LOTOS-EUROS Simulationen auf 7 x 7 km^2) und den ÖKO-DATA Karten auf einem 1 x 1 km^2 Gitter, die zur Berechnung der Überschreitungen der Critical Load verwendet werden, diskutiert. Des Weiteren ist ein Vergleich der PINETI Ergebnisse für 2008 mit den Ergebnissen von EMEP für 2008 und mit den Ergebnissen aus MAPESI für 2007 in Teilbericht 1 enthalten. In einem separaten Kapitel werden die Unsicherheiten bei der Erhebung der Gesamtdepositionsfelder diskutiert.

Die durchgeführten Arbeiten und die erzielten Ergebnisse sind (teilweise in englischer Sprache) in vier Teilberichten detailliert dargestellt und diskutiert. Nachfolgend werden die wichtigsten Eingangsdaten, Methoden und Ergebnisse zusammengefasst.

Eingangsdaten: Emissionen, Landnutzung und Meteorologie

Die in PINETI verwendeten Emissionen für Deutschland für die Jahre 2008 und 2009 basieren auf den deutschen Gesamtemissionen des Jahres 2005 und deren räumlicher Verteilung für Deutschland für das Jahr 2005, die innerhalb des PAREST Projektes vom Institut für Zukunftsstudien und Technologiebewertung (IZT) und dem Institut für Energiewirtschaft und Rationelle Energieanwendung (IER) an der Universität Stuttgart aufbereitet wurden (Jörß et al., 2010). Die Emissionen für die Jahre 2008 und 2009 wurden aus dieser Verteilung durch flächenkonstante Faktoren für jede Spezies berechnet. Die Skalierungsfaktoren geben dabei das Verhältnis der totalen Emissionen des Jahres 2008 bzw. 2009 (offizielle UNECE/EMEP-Berichterstattung 2012; UBA 2012) zu den entsprechenden PAREST-Emissionen des Jahres 2005 an (siehe Tabelle 1). Die räumliche Verteilung der Emissionen aus PAREST für das Jahr 2005 bleibt dabei erhalten. Die Skalierungsfaktoren berücksichtigen den berichteten Rückgang der Emissionen, sowie methodische Weiterentwicklungen in der Ermittlung der Emissionen. Abweichungen des Skalierungsfaktors von 1 für das Jahr 2005 (und spätere Jahre) können zum einen durch Unterschiede im Ansatz, siehe z.B. das Inlandsprinzip, und zum anderen durch neue Erkenntnisse in Bezug auf die Emissionsquellen, siehe z.B. NMVOC Emissionen aus der Landwirtschaft, hervorgerufen werden.

Tabelle 1. Emissionssummen und Skalierungsfaktoren, um die gemeldeten Länderemissionen des UNECE/EMEP Emissionskatasters für 2012 aus den PAREST 2005 Emissionen abzuleiten. Hierbei wird angenommen, dass für die Jahre 2005, 2008 und 2009 der relative Anteil der SNAP Sektoren unverändert bleibt. Der tiefe Wert bei NMVOC beruht auf der zwischenzeitlichen Herausnahme der landwirtschaftlichen NMVOC-Emissionen aus der offiziellen Berichterstattung

Gesamtsumme [Gg yr^{-1}]	NO_x	NMVOC	SO_x	NH_3	$PM_{2.5}$	PM_{10}	CO	CH_4
2005 PAREST	1544	1438	562	607	136	262	4043	2268
2005 UNECE/EMEP	1576	1143	517	573	121	207	3651	2725
2008 UNECE/EMEP	1415	1015	490	568	110	195	3387	2441
2009 UNECE/EMEP	1318	929	435	576	106	187	3002	2324
Skalierungsfaktor zwischen PAREST 2005 und UNECE/EMEP Emissionen								
2005	1.021	0.795	0.921	0.944	0.892	0.789	0.903	1.201
2008	0.916	0.706	0.873	0.936	0.809	0.742	0.838	1.076
2009	0.854	0.646	0.774	0.949	0.778	0.713	0.743	1.025

Im chemischen Transportmodell LOTOS-EUROS wird derzeit der CORINE Land Cover Landnutzungsdatensatz für das Jahr 2000 (CLC2000) zur Berechnung der Konzentrationen und Depositionen verwendet. Die Überschreitungen der Critical Load werden jedoch anhand einer aktualisierten Version des CLC2000 Datensatzes, dem höher aufgelösten CLC2006 Datensatz (250 x 250 m^2) berechnet.

Das bei TNO betriebene Modell LOTOS-EUROS wird mit meteorologischen Daten des ECMWF (www.ecmwf.int) angetrieben, welche vom Königlich-Niederländischen Meteorologischen Institut (KNMI) (www.knmi.nl), bereitgestellt werden. Der meteorologische Input wird auf einem 0.5° x 0.25° Längen/Breiten Gitter (ca. 28 x 28 km^2) und geländefolgend bereitgestellt. Bei der Berechnung der nassen Deposition wird zusätzlich in der Nachbearbeitung der vom DWD (http://www.dwd.de) bereitgestellte Jahresniederschlag auf einem 1 x 1 km^2 Gitter verwendet. Für die Berechnung der feuchten Deposition wird der Flüssigwassergehalt des vom DWD betriebenen COSMO-EU Modells verwendet. Die horizontale Auflösung des COSMO-EU-Modells beträgt ca. 7 x 7 km^2. In der Vertikalen wird auf 40 vertikalen Schichten/Flächen gerechnet, wobei die unterste Schicht etwa 10 Meter über Grund liegt. Für die Berechnung des Eintrages durch feuchte Deposition wird der Flüssigwassergehalt dieser untersten Schicht innerhalb eines der LOTOS-EUROS Simulation nachgeschalteten Programms verwendet.

Ermittlung der trockenen Deposition

Der Eintrag durch trockene Deposition in Deutschland wird anhand des LOTOS-EUROS Modells berechnet. Chemische Transportmodelle, wie LOTOS-EUROS werden verwendet, um den 3-dimensionalen Transport, die chemischen Umwandlungen und die Deposition verschiedener atmosphärischer Substanzen mit verschiedenen Gitterauflösungen in z.B. Europa oder Deutschland zu berechnen. Hierbei werden die Konzentrationsänderungen stündlich für jeden Gitterpunkt berechnet.

Die Eingangsdaten eines chemischen Transportmodells sind stündliche meteorologische Daten, zeit- und temperaturabhängige stündliche Emissionen und Landnutzungsdaten. Das Modell enthält Parametrisierungen für den Transport, die chemischen Umwandlungen sowie für die trockene und nasse Deposition von gasförmigen und partikulären atmosphärischen Substanzen. In jeder Gitterbox wird eine Bilanz zwischen den verschiedenen Prozessen berechnet, somit ist die Gesamtberechnung masseerhaltend. Das bedeutet, die Konzentration einer Substanz in einer Gitterzelle ist das Resultat vieler verschiedener vorrausgegangener Prozesse. Wird z.B. ein Mol NHx durch trockene Deposition aus einer Gitterzelle entfernt, wird die Masse in der Gitterzelle auch um ein Mol reduziert.

Der Fluss F der trockenen Deposition berechnet sich aus der Konzentration C der Substanz in einer Referenzhöhe und verschiedenen Widerständen (turbulenter Transferwiderstand R_a, quasi-laminarer Transferwiderstand R_b und Oberflächenwiderstand R_c):

$$F = \frac{C}{R_a+R_b+R_c} = v_d \cdot C \qquad \text{(Eq. 1)}$$

Der Kehrwert der Summe der Widerstände wird auch Depositionsgeschwindigkeit (v_d) genannt. Die trockene Deposition ist für die Masse in einer Gitterzelle im Chemischen Transportmodell ein Verlustterm. In PINETI ist die Berechnung der trockenen Deposition direkt in der Massenbilanzberechnung enthalten, um die Erhaltung der Masse im Modellsystem zu gewährleisten.

Die Methodik der Modellierung der trockenen Deposition wurde innerhalb des PINETI-Projekts verbessert. Darüber hinaus können vier weitere Gründe zu den Unterschieden in den Karten der trockenen Deposition zwischen PINETI und dem Vorgängerprojekt MAPESI für voneinander abweichende Jahre führen:

1. Unterschiede aufgrund von Änderungen in den Emissionen in Deutschland und Europa
2. Verschiebungen in den chemischen Gleichgewichten als Folge von Emissionsänderungen
3. Unterschiede aufgrund unterschiedlicher meteorologischer Bedingungen
4. Methodische Änderungen in den Stabilitätsfunktionen

Die modellierten trockenen Depositionsflüsse des PINETI Vorhabens sind im Mittel 5-15% niedriger als die des MAPESI Vorhabens, wobei die größten Differenzen für Wälder zu verzeichnen sind.

<u>Ermittlung der nassen Deposition</u>

Die nasse Deposition ist der vertikale Eintrag von luftgetragenen Stoffen auf die Erdoberfläche durch Niederschlag. Luftgetragenen Schadstoffe, welche in Wolkentropfen, Regentropfen oder Schnee enthalten oder gelöst sind, werden entweder durch den sogenannten ‚rain-out' (= die Auswaschung innerhalb der Wolke (in-cloud scavenging)) oder durch den sogenannten ‚wash-out' (= die Auswaschung unterhalb der Wolke (below-cloud scavenging)) zum Erdboden transportiert. Das LOTOS-EUROS Modell tendiert zur Unterschätzung der beobachteten nassen

Deposition von SOx, NOy und NHx. Im LOTOS-EUROS Modell wird bei der Modellierung der nassen Deposition ausschließlich ein Koeffizient zur Auswaschung unterhalb der Wolke (='below-cloud scavenging') berechnet, welcher in der Vertikalen auf die komplette Säule angewendet wird. Ein Koeffizient, der die Auswaschung innerhalb der Wolke (='in-cloud scavenging') beschreibt ist in der Parametrisierung des Prozesses nicht enthalten. Die Auswaschung innerhalb der Wolke ist jedoch effektiver als die Auswaschung unterhalb der Wolke und somit ist das fehlende ‚in-cloud scavenging' in LOTOS-EUROS einer der Gründe für die Unterschätzung der nassen Deposition. Innerhalb des Vorgängerprojektes MAPESI (Builtjes et al., 2011) basierte die Ermittlung des Schadstoffeintrages durch die nasse Deposition daher ausschließlich auf Messungen und war somit unabhängig von den Modellberechnungen mit LOTOS-EUROS. Da das Modell trotz Unterschätzung der nassen Deposition wichtige zusätzliche Informationen zu ihrer räumlichen Verteilung liefert, wurde die Methodik zur Ermittlung der nassen Deposition weiterentwickelt. Innerhalb der neuen Methodik wird die nasse Deposition durch eine Kombination von LOTOS-EUROS Modellberechnungen und Messungen erstellt. Für die nasse Deposition stehen Messergebnisse aus über 100 Stationen mehrerer Messnetze in Deutschland zur Verfügung. Die an den Messstellen vorliegenden Daten der Stoffkonzentration im Niederschlag wurden mit Hilfe von modellierten Feldern aus LOTOS-EUROS interpoliert (residual kriging). Zur flächendeckenden Ermittlung der nassen Deposition wurde die so erhaltene Verteilung der Stoffkonzentrationen anschließend mit den jährlichen Niederschlagshöhen (DWD, 1 km^2 Raster) kombiniert.

Der Vergleich der Ergebnisse der nassen Deposition aus den Vorhaben MAPESI und PINETI für das Jahr 2007 (Teilbericht 3) zeigt, dass die mittleren Frachten für oxidierte Schwefel- und Stickstoffverbindungen gut übereinstimmen, wohingegen für reduzierte Stickstoffverbindungen eine Abweichung von knapp 20% auftritt. Für die nasse Deposition von reaktivem Stickstoff ergibt sich deshalb im Mittel eine systematische Differenz zwischen der PINETI- und der MAPESI-Methodik von ca. 1 kg N ha^{-1} a^{-1}. Kreuzvalidierungen und detailliertere Analysen im Bereich des bayerischen Waldes (Teilbericht 3) zeigen, dass die in PINETI weiterentwickelte Methode zu einer besseren Abbildung der räumlichen Verteilung der nassen Deposition führt.

Ermittlung der feuchten Deposition

Nährstoff- oder Schadstoffeinträge, die mit der Ablagerung von Nebel- oder Wolkentropfen einhergehen, werden als feuchte Deposition bezeichnet. Die Berechnung der feuchten Deposition beruht auf einer weiterentwickelten Version des Ansatzes nach Bleeker et al. (2000) und wird innerhalb eines, der LOTOS-EUROS Simulation nachgeschalteten Programms ermittelt. Das heißt, die feuchte Deposition wird nicht mit LOTOS-EUROS berechnet. Die feuchte Deposition, die in PINETI berechnet wird, bezieht sich auf den Wassereintrag durch sogenannte „hill clouds". Bei „hill clouds" handelt es sich entweder um Nebel bzw. Wolken, die durch Aufgleiten an der Orographie entstanden sind oder um advektierte Wolken, die aufgrund der erhöhten Orographie auf Grund treffen (Bleeker et al., 2000). Der Flüssigwassergehalt, welcher zur Berechnung der feuchten Deposition nach Bleeker et al. (2000) benötigt wird, stammt, wie bereits in MAPESI, zeitlich hoch aufgelöst auf einem horizontalen Gitter von 7 x 7 km^2 für ganz Deutschland aus dem COSMO-EU Modell. Letzteres führt zu einer besseren Beschreibung lokaler Begebenheiten als der ursprünglich in Bleeker et al. (2000) verwendete klimatologische Wert von 1400 Stunden Nebel-/Wolkenvorkommen in Bodennähe, welcher auf Messungen im Schwarzwald beruht. Werte in dieser Größenordnung sind lediglich in Gebirgsregionen zu erwarten. Im Mittel ist die Anzahl der Stunden mit Nebel-/Wolkenvorkommen in Bodennähe übers Jahr geringer und liegt im Bereich von 200 Stunden, was deutlich unterhalb dem in Bleeker et al. (2000) verwendeten Wert liegt. Es sei darauf

hingewiesen, dass in der aktuellen Methode zur Berechnung der Deposition von Nebel-/Wolkentropfen die Depositionsgeschwindigkeit grober Partikel verwendet wird, was suggeriert, der Eintrag durch feuchte Deposition sei ein vertikaler Prozess. In der Realität hat der Eintrag von Nebel-und Wolkenwasser jedoch auch eine horizontale Komponente. Dies wurde in einer separaten Studie untersucht, welche in Teilbericht 3 beschrieben ist.

Ein Vergleich der Felder der feuchten Deposition zwischen den Vorhaben PINETI und MAPESI zeigt, dass die räumliche Verteilung gut übereinstimmt, wohingegen die in PINETI ermittelte mittlere Fracht der feuchten Deposition verglichen mit der entsprechenden mittleren Fracht aus MAPESI deutlich kleiner ist. Die Unterschiede werden in Teilbericht 3 erläutert und diskutiert.

Ermittlung der Gesamtdeposition

Die Gesamtdeposition wird aus der Summe der trockenen, der nassen und der feuchten Deposition gebildet. Die Gesamtdeposition resultiert somit aus der Summe von sowohl landnutzungsabhängigen als auch landnutzungsunabhängigen Feldern und ist daher abhängig von der Landnutzung. Abbildung 1 zeigt die modellierte Gesamtdeposition des Jahres 2009 für ein 1 x 1 km^2-Raster. Die Ergebnisse des LOTOS-EUROS Modellgitters (trockene Deposition) wurden dafür vom 7 x 7 km^2-Gitter auf ein 1 x 1 km^2-Raster interpoliert. Innerhalb einer Gitterzelle von 7 x 7 km^2 (aber auch innerhalb einer 1 x 1 km^2 Gitterzelle) können unterschiedliche Vegetationstypen mit deutlich voneinander abweichenden resultierenden Depositionsflüssen enthalten sein. Die Werte in jeder 7 x 7 km^2 Gitterzelle werden aus den landnutzungsabhängigen Depositionsflüssen und dem jeweiligen Anteil der entsprechenden Landnutzungsklasse berechnet. Steht ein höher aufgelöster Landnutzungsdatensatz zur Verfügung, können anhand dessen und der landnutzungsabhängigen Depositionskarten auf dem 1 x 1 km^2 Gitter höher aufgelöste Informationen aus den Daten gewonnen werden. Letzteres wird für die Berechnung der Überschreitungen der Critical Load unter Verwendung der CLC2006 Landnutzungsdaten durchgeführt. Die über Deutschland gemittelten Gesamtdepositionen der verschiedenen Komponenten für 2008 und 2009 sind in Tabelle 2 zusammengefaßt. Die Unsicherheit der über das Jahr gemittelten N-Gesamtdeposition in Deutschland liegt bei etwa 30% und ist hauptsächlich durch die Unsicherheit in der trockenen Deposition bedingt.

Abbildung 1. Gesamtdeposition von NH_x, NO_y, SO_x, Na^+, Ca^{2+}, Ca^{2+}-nss, Mg^{2+}, Mg^{2+}-nss, K^+, K^+-nss und Gesamt-N in Deutschland für das Jahr 2009.

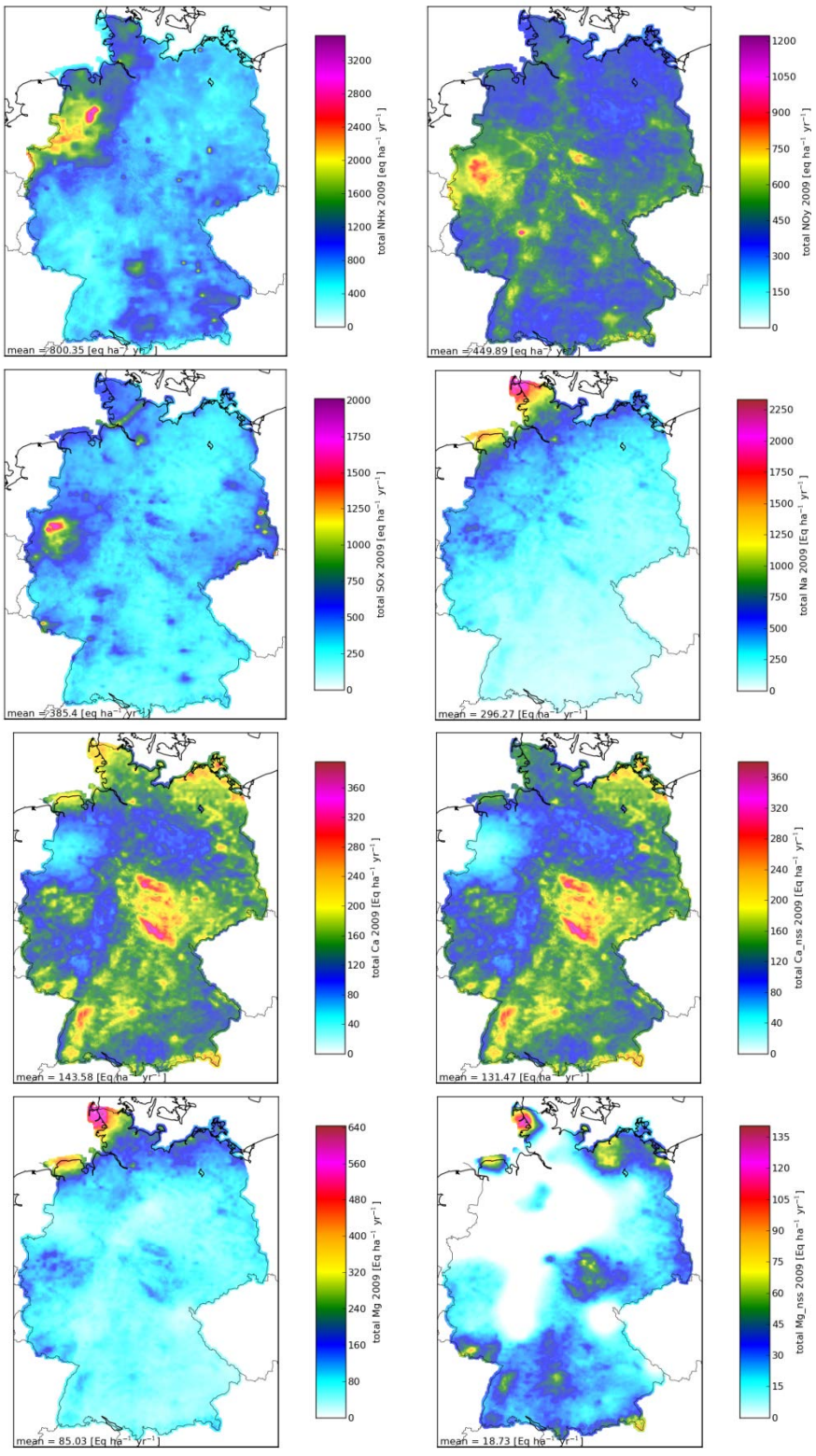

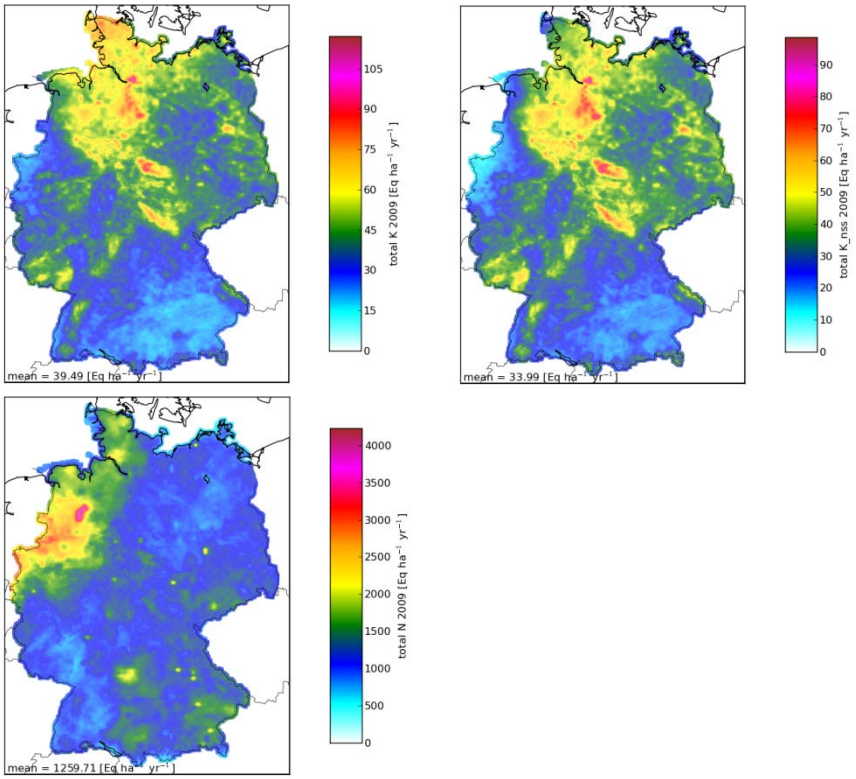

Tabelle 2. Überblick der PINETI Ergebnisse zum Gesamtdepositionsfluss.

TOTAL DEPOSITION		2008 PINETI	2009 PINETI
SO_x-S-nss	eq ha^{-1} yr^{-1}	364.9	349.9
SO_x-S	eq ha^{-1} yr^{-1}	412.8	385.4
NH_x-N	eq ha^{-1} yr^{-1}	803.5	800.4
	kg ha^{-1} yr^{-1}	11.25	11.21
NO_y-N	eq ha^{-1} yr^{-1}	450.8	449.9
	kg ha^{-1} yr^{-1}	6.31	6.30
N	eq ha^{-1} yr^{-1}	1254.9	1250.7
	kg ha^{-1} yr^{-1}	17.57	17.51
Na^+	eq ha^{-1} yr^{-1}	399.6	296.3
Ca^{2+}	eq ha^{-1} yr^{-1}	162.3	143.6
Mg^{2+}	eq ha^{-1} yr^{-1}	110.3	85.0
K^+	eq ha^{-1} yr^{-1}	38.7	39.5
Ca^{2+}-nss	eq ha^{-1} yr^{-1}	145.8	131.5
Mg^{2+}-nss	eq ha^{-1} yr^{-1}	18.7	18.7
K^+-nss	eq ha^{-1} yr^{-1}	31.2	34.0
BC-nss	eq ha^{-1} yr^{-1}	195.7	184.2

Vergleich mit EMEP und MAPESI

Die Gesamtdepositionsflüsse aus PINETI stimmen in Betrag und räumlicher Verteilung gut mit den Ergebnissen des EMEP Modells überein (Unterschiede innerhalb ± 15%). Die PINETI Ergebnisse zeigen allerdings ein deutlich detaillierteres Bild der Depositionen in Deutschland. So sind z.B. ‚hot spots' in den PINETI Karten deutlich sichtbar, die in den EMEP Daten nicht erkennbar sind. Nahe der polnischen Grenze sind zum Beispiel Kraftwerke in den SOx Depositionsfeldern deutlich zu sehen.

Im Vergleich zu den Ergebnissen aus dem Vorgängervorhaben MAPESI liegt die in PINETI ermittelte mittlere Gesamtdeposition von Stickstoff um ca. 20% (oder 4 kg ha^{-1} a^{-1}) tiefer. Die Unterschiede sind zum Teil auf interannuelle Variationen in der Meteorologie (so war der Niederschlag im Jahr 2008 um 183 mm geringer als im Jahr 2007, was mit einer Abnahme der nassen Deposition einhergeht) sowie die Abnahme der Emissionen zurückzuführen, zum Teil aber auch auf die methodischen Weiterentwicklungen (feuchte und nasse Deposition). Dies erschwert den direkten Vergleich zwischen den beiden Vorhaben deutlich. Die räumliche Verteilung der Deposition ist in den Ergebnissen beider Vorhaben sehr ähnlich; allerdings enthalten die Karten aus dem PINETI-Vorhaben erhöhte Depositionen um einzelne Punktquellen. Dies ist auf die Berücksichtigung der LOTOS-EUROS-Modellergebnisse bei der Ermittlung der nassen Deposition und ein modifiziertes Verfahren für die Interpolation der trockenen Deposition vom 7 x 7 km^2-Gitter auf das 1 x 1 km^2-Raster zurückzuführen. Im MAPESI-Vorhaben wurde dafür ebenfalls eine Kriging-Interpolation genutzt, die es erlaubt die räumliche Abhängigkeit der Werte zu berücksichtigen, allerdings, v.a. bei singulären Extremwerten, auch zu einer Glättung der Daten führt. Zur Vermeidung dieser unerwünschten Glättung werden die Rastermittelpunkte des 7 x 7 km^2-Gitters in PINETI bilinear auf das 1 x 1 km^2-Raster interpoliert. Die so ermittelte, erhöhte trockene und nasse Deposition im Umfeld großer Punktquellen ist plausibel und aus lokalen Messungen bekannt; Ausmaß und räumlicher Umfang des modellierten Effektes konnten im Vorhaben allerdings noch nicht systematisch verifiziert werden.

Weiterentwicklung der Modellierung der nassen und feuchten Deposition

Die mit LOTOS-EUROS ermittelte Fracht der nassen Deposition findet in der derzeitigen Modellkombination keine direkte Berücksichtigung (die Höhe der nassen Depositionsfracht wird durch die Messergebnisse bestimmt; die Modellergebnisse werden derzeit nur für die Interpolation verwendet). Die Tatsache, dass LOTOS-EUROS die nasse Deposition systematisch unterschätzt führt jedoch, durch die Kopplung der Prozesse der nassen und trockenen Deposition im Modell, tendenziell zu einer (leichten) Überschätzung der trockenen Deposition. Ein weiteres wichtiges Ziel im PINETI-Vorhaben war es deshalb, die Modellierung der nassen Deposition zu verbessern, um diesen Effekt zukünftig so klein wie möglich zu machen und die Erstellung zuverlässiger Depositionsszenarien zu ermöglichen (vgl. Teilbericht 2). Ein besonderes Augenmerk galt dabei der Parametrisierung der Auswaschung von Stoffen innerhalb der Wolke. Derzeit wird im LOTOS-EUROS Modell bei der Modellierung der nassen Deposition ausschließlich ein Koeffizient zur Auswaschung unterhalb der Wolke (='below-cloud scavenging') berechnet, welcher in der Vertikalen auf die komplette Säule angewendet wird. Ein Koeffizient, der die Auswaschung innerhalb der Wolke (='in-cloud scavenging') beschreibt ist in der Parametrisierung des Prozesses derzeit nicht enthalten. Die Auswaschung innerhalb der Wolke ist jedoch effektiver als die Auswaschung unterhalb der Wolke und somit ist das

fehlende ‚in-cloud scavenging' in LOTOS-EUROS einer der Gründe für die Unterschätzung der nassen Deposition.

Für die Untersuchungen zur Verbesserung der Modellierung der nassen Deposition wurde eine Forschungsversion des chemischen Transportmodells REM-Calgrid (RCG) weiterentwickelt und verbessert. Die operationelle Version des RCG berücksichtigt bei der Berechnung der nassen Deposition, wie LOTOS-EUROS, nur die Auswaschung von Schadstoffen unterhalb der Wolke. Bereits innerhalb des Vorgängerprojektes MAPESI wurde die Modellierung durch die Einführung der Auswaschung innerhalb der Wolke verbessert. Die Auswaschung von Gasen und die Sulfatbildung in Wolkenwasser sind vom pH-Wert des Regen- bzw. Wolkentropfens abhängig. Während in der bisherigen Modellversion ein konstanter Tropfen-pH-Wert in der Modellatmosphäre angenommen wurde, wird dieser in der neu entwickelten Modellversion modelliert und ist somit variabel. Nach Einführung des modellierten Tropfen-pH-Wertes wurde die Sensitivität der neuen Modellversion auf Änderungen des pH-Wertes untersucht. Des Weiteren wurde das Modell anhand von Messungen für ausgewählte Zeiträume in den Jahren 2005 und 2009 evaluiert. Die Evaluation zeigt, dass die Modellgüte durch die Einführung des modellierten Tropfen-pH-Wertes erneut verbessert werden konnte. Die Weiterentwicklungen der Modellierung der nassen Deposition, die innerhalb des MAPESI- und des PINETI-Projekts, für das RCG durchgeführt wurden, können und sollten nun zukünftig in das LOTOS-EUROS-Modell integriert werden.

Um Möglichkeiten für eine Weiterentwicklung der Methode zur Ermittlung der feuchten Deposition zu evaluieren, wurden eine Literaturstudie durchgeführt und vorausgegangene Messkampagnen, u.a. aus dem Bayerischen Wald (Forellenbachgebiet; FKZ 35101088), analysiert. Die Ergebnisse bestätigen frühere Studien, welche die hohe räumliche und zeitliche Variabilität sowohl des Nebel-/Wolkenwassereintrages als auch der Konzentrationen von Spurenstoffen im Nebel-/Wolkenwasser hervorheben. Die Ergebnisse legen nahe, dass die Rekonstruktion der feuchten Deposition mit regionalen bzw. nationalen Modellen durch die sehr kleinräumige Variabilität zu erheblichen Schwierigkeiten führt. Für einen Großteil der betroffenen Flächen dürften die im PINETI-Vorhaben ermittelten Werte der feuchten Deposition im Allgemeinen eine brauchbare Schätzung liefern; der Eintrag in stark exponierte, räumlich sehr begrenzte Gebiete (Gipfel, Kammlagen) wird hingegen unterschätzt. Mögliche Verbesserungen des Berechnungsverfahrens werden im Teilbericht 3 diskutiert.

Außerdem wird mit einem detaillierten Vergleich für das Jahr 2007 analysiert, wie sich der Weiterentwicklung der Methode zur Verarbeitung der Messwerte zur nassen Deposition auf den Unterschied zwischen MAPESI und PINETI auswirkt (Tabelle 3). Die methodischen Fortschritte führen zu einem Rückgang von 0.9 kg/ha/yr. Zusammenfassend zeigt sich daran anschließend, dass die methodischen Weiterentwicklungen etwa 50 % des Unterschieds zwischen der nassen Deposition für das Jahr 2007 (MAPESI) und der nassen Deposition für das Jahr 2008 (PINETI) ausmachen – der Rest ist auf meteorologische Unterschiede und veränderte Emissionen zurückzuführen.

Tabelle 3. Vergleich der nassen Deposition in Deutschland im Jahr 2007 mit MAPESI und PINETI Methode

	MAPESI 2007 [eq ha^{-1} yr^{-1}]	PINETI 2007 [eq ha^{-1} yr^{-1}]	Relative Änderung [-]	Differenz [eq ha^{-1} yr^{-1}]
SO_x-nss	237.63	226.00	0.95	-11.63
NH_x	416.46	346.28	0.83	-70.18
NO_y	268.55	275.53	1.03	6.98
Na^+	252.86	266.66	1.05	13.79
Ca^{2+}	115.25	92.59	0.80	-22.66
Mg^{2+}	69.87	70.06	1.00	0.18
K^+	37.18	27.92	0.75	-9.26
Ca^{2+}-nss	104.12	81.27	0.78	-22.85
Mg^{2+}-nss	8.91	12.65	1.42	3.74
K^+-nss	31.87	22.27	0.70	-9.60

Weitere Modellentwicklung

Bezüglich der weiteren Modellentwicklung sollte der Fokus auf der Schließung der Massenbilanz liegen. Eine der aktuellen Schwächen in der Modellierung ist die Unterschätzung der nassen Deposition, was im Modell zu einer leichten Überschätzung der trockenen Deposition führen kann. Während die modellierte nasse Deposition anhand von Messungen korrigiert wird, ist dies aufgrund fehlender Messungen für die trockene Deposition nicht möglich. Das bedeutet, die Reduzierung der Unterschätzung der nassen Deposition im Modell ist von großer Wichtigkeit, um Überschätzungen der trockenen Deposition und damit der Gesamtdeposition zu verhindern. Des Weiteren zeigen neue Erkenntnisse u.a. aus den Niederlanden über den Austausch von Ammoniak zwischen Erdoberfläche und Atmosphäre, dass die trockene Deposition von Ammoniak besonders in landwirtschaftlich geprägten Regionen überschätzt wird. Eine neue bidirektionale Parametrisierung des Austausches zwischen Erboberfläche und Atmosphäre wurde bereits entwickelt. Die neue Parametrisierung wird zu einer Verschiebung der Ammoniakdeposition von landwirtschaftlich genutzten Gebieten zu naturnahen Gebieten führen. Es wird empfohlen diese neue bidirektionale Parametrisierung des Austausches zwischen Erboberfläche und Atmosphäre für zukünftige Berechnungen ins Modell zu implementieren.

Bewertung des Eintrags in Bezug auf Risiken für terrestrische Ökosysteme

Zur Bewertung der Risiken, denen naturnahe Ökosysteme durch den Eintrag von Luftschadstoffen ausgesetzt sind, wurden die in Teil 1 des PINETI-Projekts ermittelten Depositionen mit wirkungsbezogenen Belastungsgrenzen verglichen (siehe Teilbericht 4). Solche Belastungsgrenzen, als Critical Load bezeichnet, werden für die naturnahen Ökosysteme,

die auf etwa 30 Prozent der Fläche Deutschlands vorzufinden sind, bestimmt und kartiert. Seit nunmehr 25 Jahren erfolgt auf Grundlage eines Methodenhandbuchs des Internationalen Kooperativen Programms zur Modellierung und Kartierung von Critical Load (ICP Modelling & Mapping, www.icpmapping.org) die Ausweisung von Belastungsgrenzen zum Schutz vor Versauerung und Eutrophierung.

Im Vergleich mit den jährlichen Depositionsfrachten zeigt sich, ob die Critical Loads eingehalten oder überschritten werden. Der Anteil von Ökosystemen, bei denen die Critical Loads nicht mehr überschritten werden, ist als ein Indikator für die Wirksamkeit von Maßnahmen zur Luftreinhaltung zu sehen und wurde in das Kernindikatorensystem des Umweltbundesamtes aufgenommen. Daher erfolgt mit den Ergebnissen dieses Projekts eine Fortschreibung und Aktualisierung dieser Indikatoren.

Ebenso ist die Einhaltung der Critical Loads eine Notwendigkeit zum Erhalt der biologischen Vielfalt. Die „Nationale Strategie zur biologischen Vielfalt“, mit der eine entsprechende europäische Konvention (Convention on Biological Diversity, CBD) für Deutschland umgesetzt wird, hat die anspruchsvolle Zielstellung formuliert, bis zum Jahr 2020 alle Ökosysteme vor Versauerung und Eutrophierung zu schützen. Das ist gleichbedeutend mit der Einhaltung der Critical Load auf allen Flächen, die im nationalen Datensatz erfasst sind. Der Anteil von Ökosystemen, bei denen die Critical Loads nicht mehr überschritten werden, wurde in das Indikatorenset zur Nationale Strategie zur Biologischen Vielfalt aufgenommen

Beim Schutz vor Versauerung zeigen die Maßnahmen zur Luftreinhaltung bereits große Wirkung. So verminderte sich der Anteil von Ökosystemen, die von Critical Load Überschreitungen betroffenen sind, von ehemals 85 Prozent im Jahr 1990 auf nunmehr nur noch 15 Prozent im Jahr 2009. Waren zwischen 1990 und 1995 etwa 60 % der Ökosysteme mit mehr als 1000 Äquivalente pro Hektar und Jahr überlastet, das entspricht 16 Kilogramm Schwefel, so trifft dies 2009 nur noch auf 1 % der Fläche zu (vgl. Abbildung 2).

Demgegenüber gibt es weiterhin einen hohen Anteil an Flächen, die dem Risiko einer Eutrophierung unterliegen. Zwar ist der Anteil von Ökosystemen, die mit mehr als 10 kg Stickstoff pro Hektar und Jahr über den Critical Load hinaus belastet werden von fast 90 % im Jahr 1990 auf unter 6 % im Jahr 2009 gesunken, doch bleiben auf der Hälfte aller Flächen die Belastungsgrenzen überschritten. Fortschritte gab es jedoch bei dem Anteil von Rezeptorflächen, bei denen die Critical Load eingehalten werden. So waren 1990 erst auf weniger als 1 % der Flächen die Critical Load nicht überschritten, dieser Anteil stieg auf 22,5 % im Jahr 2007 und weiter auf 50 % im Jahr 2009 (vgl. Abbildung 3).

Als Beitrag zur methodischen Weiterentwicklung wurde in diesem Vorhaben der Critical Load Ansatz auf Natura 2000 Gebiete ausgedehnt. Mit verschiedenen Ansätzen erfolgte eine Berechnung oder Zuweisung von Belastungsgrenzen auf FFH-Gebiete und die darin ausgewiesenen Lebensraumtypen. Grundsätzlich kann davon ausgegangen werden, dass die im deutschen Datensatz ausgewiesenen ökologischen Belastungsgrenzen auch die unter NATURA 2000 erfassten FFH-Gebiete repräsentieren. Demzufolge bleibt ein vorrangiges Ziel, die Critical Load im nationalen Maßstab einzuhalten.

Abbildung 2. Überschreitung der Critical Load für Versauerung im zeitlichen Trend

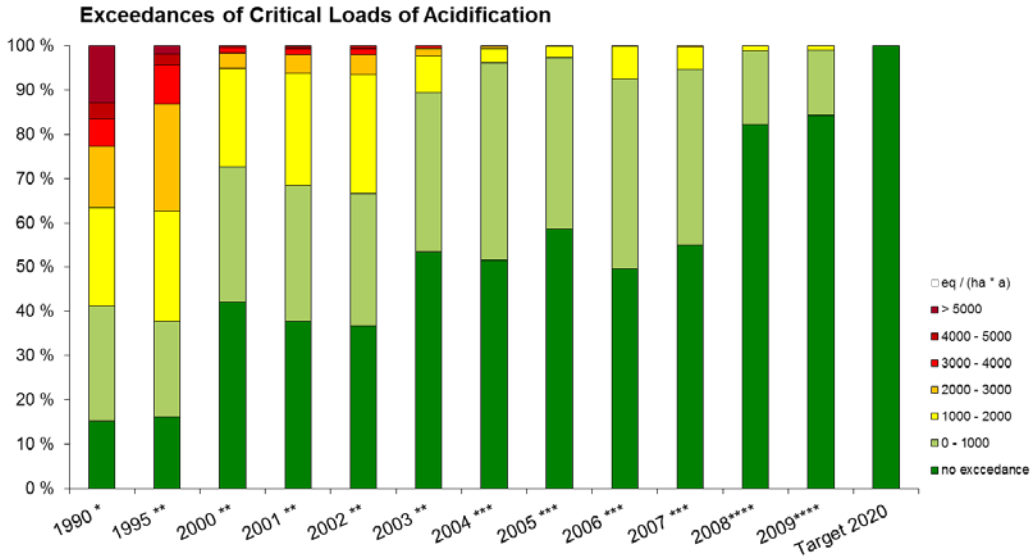

Source: Research projects of the Federal Environmental Agency (UBA): * FKZ 200 85 212 (2004), ** FKZ 204 63 252 (2008), *** FKZ 3707 64 200 (2011, MAPESI),****FKZ 3710 63 246 (2013, PINETI), Target 2020: to protect all ecosystems is a national CBD target for 2020 (BMU 2007)

Abbildung 3. Überschreitung der Critical Load für Eutrophierung im zeitlichen Trend

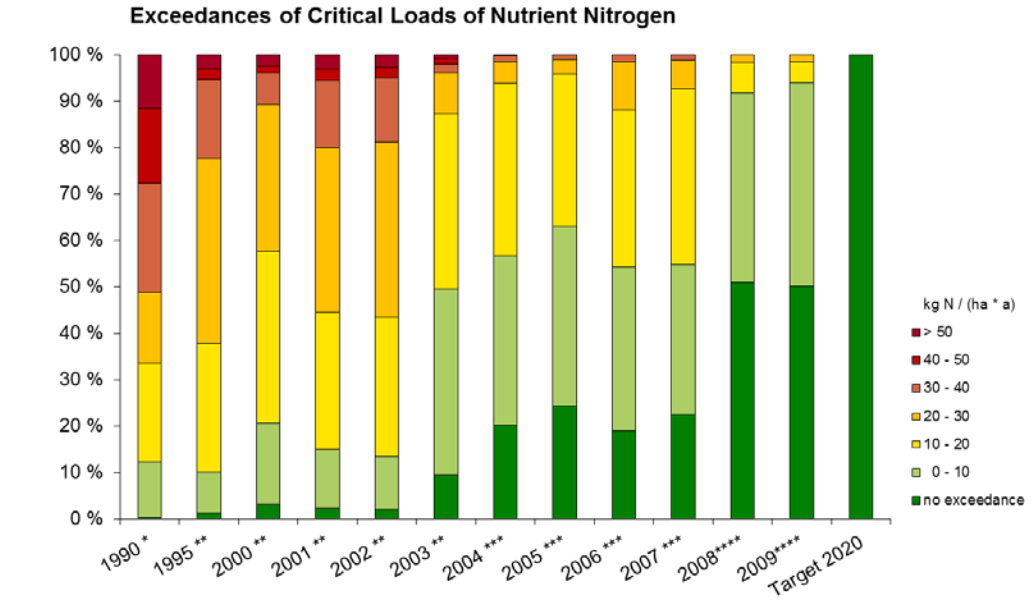

Source: Research projects of the Federal Environmental Agency (UBA) * FKZ 200 85 212 (2004), ** FKZ 204 63 252 (2008), *** FKZ 3707 64 200 (2011, MAPESI), **** FKZ 3710 63 246 (2013, PINETI), Target 2020: to protect all ecosystems is a national CBD target for 2020 (BMU 2007)

Summary

Biodiversity in Europe is strongly affected by the deposition of nitrogen and sulfur on terrestrial ecosystems. Therefore, TNO, FUB and ÖKO-DATA have assessed the deposition of these atmospheric substances over Germany for the years 2008 and 2009 (Teilbericht 1) and calculated the exceedance of critical loads for sensitive ecosystems (Teilbericht 4).

For the calculation of critical load exceedances, the atmospheric input of NH_x, NO_y, SO_x, as well as the base cations, Ca^{2+}, Mg^{2+}, K^+, Na^+, is needed. The atmospheric input of these substances occurs by means of three different forms of deposition: dry deposition, wet deposition and occult deposition. Measurements of dry deposition are very expensive and generally not available on a regular basis. Therefore, we relied on model calculations to estimate the dry deposition. For the wet deposition, however, there exist several networks with more than 100 measuring stations in total in Germany. These measuring stations provide weekly, 2-weekly or 4-weekly measurements of concentrations of nitrogen, sulfur and base cation concentrations in rainwater. By combining these measurements with the modeled wet deposition fields, a high resolution map of the wet deposition over Germany was obtained. The occult deposition was estimated from the modeled fog/cloud deposition and the concentrations of the different substances in the cloud or fog droplets (derived from the concentrations in rainwater from the wet deposition network). By adding the dry, wet and occult deposition, an overview of the total deposition over Germany was obtained, which was finally used to calculate the critical load exceedances for different vegetation types.

To make a good assessment of the total deposition of NH_x, NO_y, SO_x and the base cations over Germany, it is important to create a system that is mass conservative and consistent. In the previous MAPESI project (Builtjes et al., 2011), the wet deposition was based on the observed concentrations in rain water only and completely disconnected from the model calculations. The motivation for this approach was that modeled wet deposition and observed wet deposition differed substantially, i.e., the model underestimates the observed wet deposition. The obtained wet deposition field from the observations was considered to be more realistic than the rather low wet deposition field from the model. However, in the mass balance calculations in the model, the wet and dry deposition are connected, which means that a low wet deposition is compensated by a higher dry deposition. Taking the wet deposition from the observations and the dry deposition from the model can therefore lead to an overestimation of the total deposition. An important aim of this project is therefore to improve the modeling of the wet deposition (Teilbericht 2). As the model can still add spatial information to the wet deposition field, a new method to assess the wet deposition was developed within PINETI. In this new method both the modeled and the observed concentrations in precipitation are used. However, the new method has no feedback in the mass balance calculation yet.

Another inconsistency in the mass balance calculation is the calculation of the occult deposition, which is currently not considered in the model calculations. In this PINETI-project the occult deposition was calculated in a post-processing procedure similar as in the MAPESI project. However, considerably lower amounts of occult deposition were modeled in PINETI compared to MAPESI.

These methodological changes led to differences between the MAPESI and the PINETI project, which were investigated in more detail in a separate study within the PINETI project (see Teilbericht 3).

In Teilbericht 1, the methods that were applied to obtain the total deposition in PINETI are explained in detail and the results for 2008 and 2009 are presented. This Teilbericht also discusses the differences between the final TNO 1 x 1 km^2 deposition results and the sub-grid information that is used by ÖKO-DATA to calculate critical load exceedances. Furthermore, a comparison of the PINETI results for 2008 with the MAPESI results for the year 2007 and the EMEP results for 2008 are presented. The uncertainties in the total deposition are discussed in a separate chapter.

Input data: Emissions, Land use und Meteorology

The emissions for Germany for 2008 and 2009 rely on the emissions for Germany for 2005. These 2005 emissions have been produced by the Institut für Zukunftsstudien und Technologiebewertung (IZT) and the Institut für Energiewirtschaft und Rationelle Energieanwendung (IER) from the University of Stuttgart within the PAREST project (Jörß et al., 2010). In this project, the PAREST emissions are scaled by a constant factor (for each substance) to the officially reported emission totals in 2012 by UNECE/EMEP (UBA, 2012) (see Table 1), while the spatial distribution of PAREST is maintained. Deviations from a scaling factor of 1 for the year 2005 (and more recent years) can be caused by differences in approaches, i.e., the Inland-Prinzip, but also due to new insights in the emission sources, e.g., the agricultural emissions of NMVOC.

Table 1. Emission totals and scaling factors to obtain the reported country totals of the UNECE/EMEP emission inventory 2012 from original PAREST 2005 emissions assuming no changes in relative contribution of SNAP categories for the years 2005, 2008 and 2009. The low scaling factor for NMVOC is caused by the current exclusion of NMVOC-emissions from agriculture in the emission inventory.

totals [Gg yr^{-1}]	NO_x	NMVOC	SO_x	NH_3	$PM_{2.5}$	PM_{10}	CO	CH_4
2005 PAREST	1544	1438	562	607	136	262	4043	2268
2005 UNECE/EMEP	1576	1143	517	573	121	207	3651	2725
2008 UNECE/EMEP	1415	1015	490	568	110	195	3387	2441
2009 UNECE/EMEP	1318	929	435	576	106	187	3002	2324
scaling factor between PAREST 2005 and UNECE/EMEP emissions								
2005	1.021	0.795	0.921	0.944	0.892	0.789	0.903	1.201
2008	0.916	0.706	0.873	0.936	0.809	0.742	0.838	1.076
2009	0.854	0.646	0.774	0.949	0.778	0.713	0.743	1.025

The chemical transport model (CTM) LOTOS-EUROS currently uses the land use dataset Corine Land Cover for the year 2000, CLC2000, for concentration and deposition calculations. The critical load exceedance calculation is however based on an updated version of the CLC2000 database, i.e., CLC2006, which has a higher resolution of 250 x 250 m^2.

The LOTOS-EUROS model at TNO uses ECMWF meteorology (www.ecmwf.int), which is provided by the Royal Dutch Meteorological Institute, i.e., KNMI (www.knmi.nl). The meteorological input is provided on a 0.5° x 0.25° longitude/latitude resolution (~28 x 28 km^2) and is terrain

following. For the wet deposition calculation, the annual precipitation fields from DWD (http://www.dwd.de) are used on a 1 x 1 km^2 resolution in the post-processing. For the calculation of the occult deposition the liquid water content of DWD COSMO-EU is used. COSMO-EU runs at a 7 x 7 km^2 resolution and uses 40 vertical levels with the lowest level 10 meter above ground. For the occult deposition, only the data from this lowest level is used in the post-processing.

Assessment of dry deposition

The dry deposition over Germany is calculated with LOTOS-EUROS. CTMs calculate the 3-dimensional transport, chemical conversion and deposition of different atmospheric substances over an area typically the size of Europe or Germany. Concentration changes are calculated for each grid cell and for every hour.

The input data in a CTM consist of hourly meteorology, time and temperature dependent hourly emissions and land use data. The model contains parameterizations for transport, chemical conversion and dry and wet deposition for gaseous and particulate atmospheric substances. In each grid cell, the mass balance of the considered substance is calculated consistently based on the processes described above, where the total mass of the substance is maintained. So, the concentration of a substance in a grid cell is the result of many different processes, e.g., if one mole of NH_x is removed from a grid cell by dry deposition, the total mass in the grid cell is also reduced by one mole.

The dry deposition flux is calculated from the ambient concentration at a reference height and several resistances:

$$F = \frac{C}{R_a + R_b + R_c} = v_d \cdot C \qquad \text{(Eq. 1)}$$

The reciprocal of the sum of the resistances is also called the deposition velocity, i.e., v_d. The dry deposition flux is a loss term for mass in a CTM grid cell. This means that besides emissions, chemical conversions and transport in and out of a grid cell, wet and dry deposition fluxes also affect the mass and consequently the concentration in a grid cell. In PINETI, the calculated dry deposition flux is directly applied in the mass balance calculation to keep the modeling system mass conservative.

The method for the calculation of the dry deposition has been improved within the PINETI Project. In addition to this, there are four further reasons for differences in dry deposition between PINETI and MAPESI in different years:

1. Differences due to changes in the emissions in Germany and Europe
2. Changed chemical equilibriums due to the emissions changes
3. Differences caused by different meteorological circumstances
4. Methodological changes in stability functions

The modelled dry deposition fluxes in PINETI are on average 5-15% lower than those in MAPESI with forest classes at the high end of this range.

Assessment of wet deposition

Wet deposition is the vertical chemical input of airborne compounds to a ground surface via precipitation. Airborne pollutants, which are attached to and dissolved in cloud droplets, rain drops, and snow, respectively, are either transported downwards to the ground surface by 'rain-out' ('in-cloud scavenging'), or they are taken up from the atmosphere by hydrometeors during the precipitation event ('wash-out', 'below-cloud scavenging').

The LOTOS-EUROS model tends to slightly underestimate the observed wet deposition of SO_x, NO_y and NH_x. The wet deposition in LOTOS-EUROS is calculated using below-cloud scavenging coefficients only, leaving the in-cloud scavenging out of consideration, which likely explains part of the underestimation by the LOTOS-EUROS model. We have to mention here that the in-cloud scavenging was not included in the PINETI-project due to lacking meteorological input data. However, this shortcoming is likely partly compensated by the applied (higher) below-cloud scavenging coefficients. As many wet deposition measurements are available, the wet deposition maps in PINETI are obtained by applying a Kriging technique, which combines LOTOS-EUROS model calculations with wet deposition measurements. The concentrations of the different components in precipitation in Germany are measured by an extensive countrywide measurement network made up of various national and regional monitoring programs.

Assessment of occult deposition

Nutrient or pollutant input in ecosystems by deposition of fog or cloud droplets is called occult deposition. The computation of the occult deposition flux is performed following the approach by Bleeker et al. (2000) and is performed in a post-processing procedure, i.e., the occult deposition is not included in the LOTOS-EUROS model.

The occult deposition computed within PINETI refers to input by "hill clouds", which is the result of condensation processes in moist air lifted by mountains (= orographic cloud) or by intrusion of mountaintops into a low level cloud deck (Bleeker et al., 2000).

The climatological duration of cloud occurrences used in Bleeker et al. (2000) was derived for the mountainous area Schwarzwald and does not have to be valid in other mountainous areas. In fact, in this study, LWC is available on a high time resolution gridded over the whole of Germany from COSMO-EU at a 7 x 7 km^2 grid size resolution similar as in MAPESI. It appears that the climatological average duration of cloud occurrences of 1400 hours used in Bleeker et al. (2000) can only be found in a few mountainous areas. On average, the duration of cloud occurrences is much lower and is in the order of 200 hours. This is significantly lower than the climatological value of 1400 hours used by Bleeker et al. (2000). Although the method in PINETI was similar to the method in MAPESI, significantly lower occult deposition was modeled. These differences were investigated in Teilbericht 3.

Assessment of total deposition

The total deposition is calculated as the sum of dry, wet and occult deposition. The total deposition is the sum of land use dependent and land use independent data, which makes the total deposition dependent on land use in the end. Figure 1 shows the best estimate for the grid cell resolution of the model (7 x 7 km^2) interpolated to a 1 x 1 km^2 grid cell resolution over Germany in 2009. Within one grid cell of 7 x 7 km^2 (but also within the interpolated 1 x 1 km^2), different vegetation types might be present with significantly different deposition amounts. The values in Figure 1 are calculated from the fractions of each land use present in a

7 x 7 grid cell and their corresponding land use dependent depositions. If an accurate land use map is available, sub-grid information can be obtained by taking the actual land use and its corresponding interpolated 1 x 1 km^2 land use dependent deposition. Latter procedure is followed to calculate the Critical Load Exceedances using the CLC2006 land use map. The uncertainty of the total yearly averaged N-deposition over Germany will be close to 30 %, and is mainly determined by the uncertainty in the dry deposition.

The country average total depositions of the different components in Germany in 2008 and 2009 are given in Table 2.

Figure 1. Total deposition of NH_x, NO_y, SO_x-nss, Na^+, Ca^{2+}, Ca^{2+}-nss, Mg^{2+}, Mg^{2+}-nss, K^+, K^+-nss and total N in Germany in 2009.

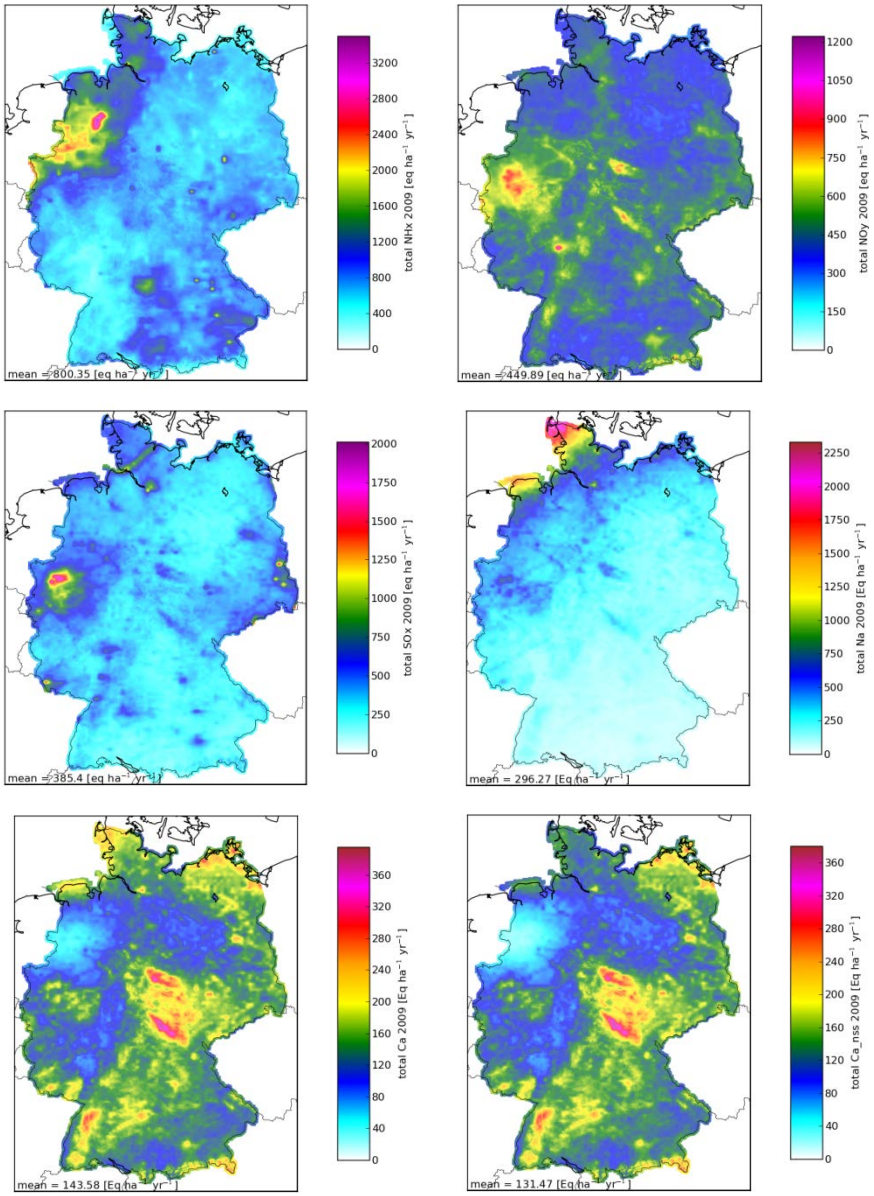

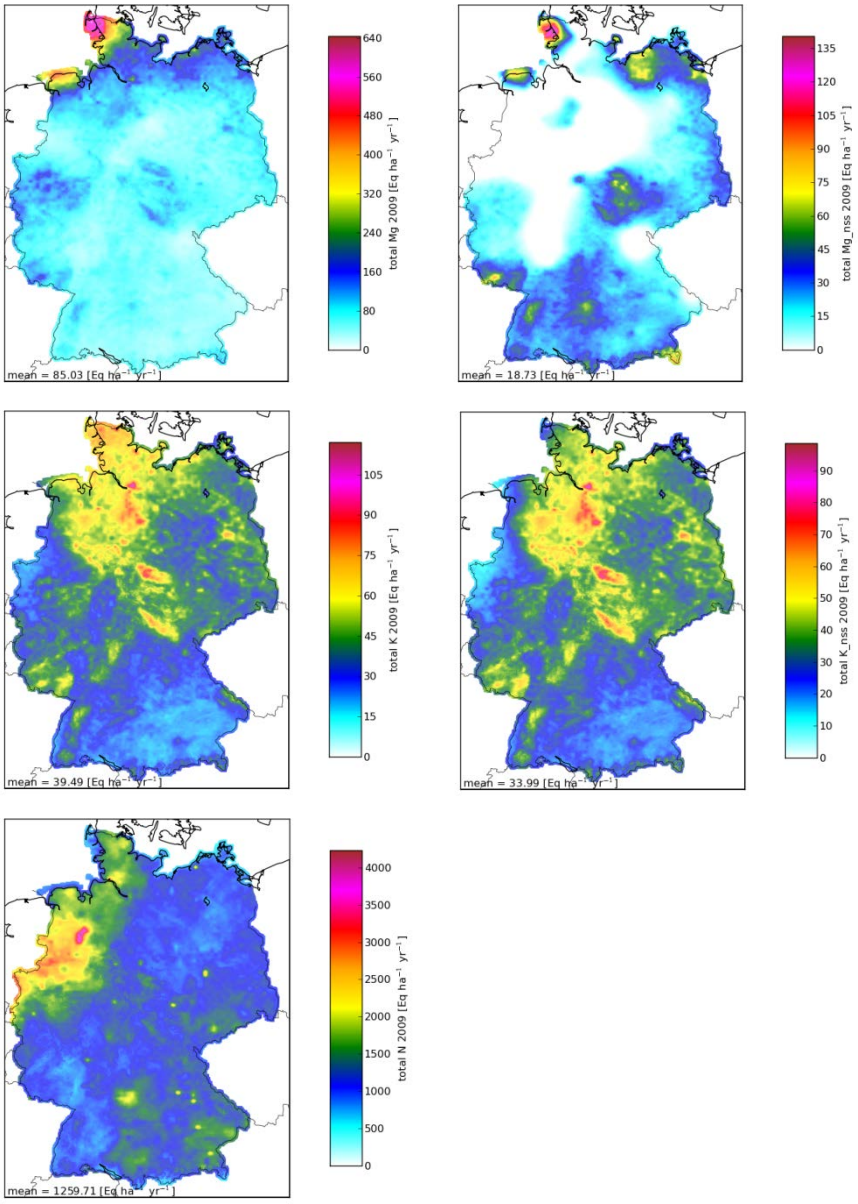

Table 2. Overview of the PINETI results of total deposition flux.

TOTAL DEPOSITION		2008 PINETI	2009 PINETI
SO_x-S-nss	eq ha^{-1} yr^{-1}	364.9	349.9
SO_x-S	eq ha^{-1} yr^{-1}	412.8	385.4
NH_x-N	eq ha^{-1} yr^{-1}	803.5	800.4
	kg ha^{-1} yr^{-1}	11.25	11.21
NO_y-N	eq ha^{-1} yr^{-1}	450.8	449.9
	kg ha^{-1} yr^{-1}	6.31	6.30
N	eq ha^{-1} yr^{-1}	1254.9	1250.7
	kg ha^{-1} yr^{-1}	17.57	17.51

Na^+	eq ha^{-1} yr^{-1}	399.6	296.3
Ca^{2+}	eq ha^{-1} yr^{-1}	162.3	143.6
Mg^{2+}	eq ha^{-1} yr^{-1}	110.3	85.0
K^+	eq ha^{-1} yr^{-1}	38.7	39.5
Ca^{2+}-nss	eq ha^{-1} yr^{-1}	145.8	131.5
Mg^{2+}-nss	eq ha^{-1} yr^{-1}	18.7	18.7
K^+-nss	eq ha^{-1} yr^{-1}	31.2	34.0
BC-nss	eq ha^{-1} yr^{-1}	195.7	184.2

Comparison with EMEP and MAPESI

In this project, it is shown that the magnitude of the total deposition fluxes and the distributions in PINETI compare well (within 15% difference) with the results of the EMEP model. The PINETI results give a much more detailed picture of the deposition fields over Germany than the EMEP results. This leads to 'hot spots' being clearly visible in the distributions and being much more pronounced than in the EMEP data. For example, power plants are clearly visible in the SO_x deposition fields close to the Polish border.

Also in comparison to MAPESI, 'hot spots' are much more pronounced in PINETI, because the modeled wet deposition is used in the final wet deposition field. In MAPESI, the wet deposition was based on measurements only, and these very local deposition patterns were not obtained by the former observational kriging method. Whether these high local depositions are realistic or not should be verified by measurements, but they don't seem to be unrealistic. Furthermore, we have seen some regional differences between PINETI 2008 and MAPESI 2007 results, which might be the result of the methodological change to calculate the wet deposition, e.g. a different Kriging method was applied in PINETI and the stations used for the Kriging were not the same. Besides the methodological reason, another reason for the differences is that the meteorology in the years is different, e.g., in 2008 on average there was 183 mm less precipitation over Germany than in 2007, which will reduce the amount of wet deposition.

For the dry deposition fields we also see some local 'hot spots' popping up. These differences are related to a conversion of the LOTOS-EUROS results from the TNO grid to the INS sub-grid in MAPESI. It is, however, not clear what exactly happened in this grid conversion, but it seems that these 'hot spots' disappeared in the conversion from the TNO grid to the INS sub-grid especially in urban areas (for dry deposition of SO_x) and airports (for dry deposition of NO_y). As there is not such a grid conversion involved anymore in PINETI, some local 'hot spots' pop up again. On the other hand, rather large reductions in the dry deposition over forests are observed, which are related to changes in the stability functions. In the MAPESI project, the stability function for heat was used to calculate the wind speed at 50 meters height from the 10 meter wind speed. In the PINETI project, the stability function for momentum was used for this calculation. This wind speed at 50 meters is used in the derivation of land use specific u^*, which are used in the calculation of deposition velocities. It appeared that especially over forest, this change leads to a reduction in u^* and consequently in the deposition velocities. Furthermore, some inconsistencies in the definition of the displacement height were corrected.

For the occult deposition, the differences between the MAPESI 2007 and PINETI 2008 results are also quite large, although the contribution of the occult deposition to the total deposition is

still relatively limited. These differences mainly seem to be due to differences in the applied method. It was, however, not exactly clear how the results in MAPESI were obtained. In this report, we have implemented the method as it was described by Bleeker et al. (2000) using the more accurate hourly liquid water content (LWC) data from COSMO-EU. In this way, we avoided the use of climatological values for the LWC and cloud duration, which made the method more general to apply. Note that the use of the deposition velocity for coarse particles makes the occult deposition a rather vertical process, while in reality the input from cloud water might be a more horizontal process. Therefore, a literature study was set up to actualize the state-of-science which is reported separately (see Teilbericht 3).

Besides the differences in methods that were described above, all the individual and consequently also the total deposition fields are affected by differences in meteorology and emissions between 2007 and 2008/2009, which makes a direct comparison between MAPESI results and PINETI results extremely complicated.

Concerning model development, future research should focus on closing the mass balance. One of the current weaknesses in the modeling is the underestimation of the wet deposition process, which likely leads to a slight overestimation of the dry deposition. Although the modeled wet deposition is corrected with wet deposition observations, the modeled dry deposition is not due to a lack of dry deposition observations. This means that reducing the underestimation of the modeled wet deposition is a key priority to avoid an overestimation of the dry deposition and consequently an overestimation of the total deposition. Besides, new insights in the surface-atmosphere exchange of ammonia in the Netherlands indicate that dry deposition of ammonia is overestimated in especially the agricultural areas. A new bi-directional surface-atmosphere exchange parameterization was developed. This new parameterization will lead to a shift of ammonia deposition from agricultural areas to (semi-) natural areas. It is recommended to include this new bi-directional surface-atmosphere exchange parameterization in future model calculations.

Improvement of the LOTOS-EUROS wet and occult deposition

In Teilbericht 2, the description of wet deposition modeling in the chemistry transport model RCG has been improved. In the operational version of RCG (and LOTOS-EUROS) only below-cloud scavenging is considered while in-cloud scavenging, which was found to contribute the major part of the scavenged material is neglected. A discrimination of below-cloud and in-cloud scavenging was already implemented within the MAPESI project.

However, the scavenging of gases and aqueous phase sulfate formation is dependent on droplet pH, which is not currently accounted for in RCG and LOTOS-EUROS. So far, a constant droplet pH was used. Within this subproject a modeled, variable droplet pH is implemented. The sensitivity of modeled concentrations and deposition fluxes to changes in droplet pH were investigated. Furthermore, the improved model version was evaluated against observations.

The wet deposition fluxes of SO_x, NO_y and NH_x of the improved model version of RCG and the fluxes calculated using the LOTOS-EUROS model were compared to observations at 191 measurement sites spread over Germany for the year 2009. The comparison showed that the model performance has been improved by implementing the variable droplet pH. A comparison of the calculated wet deposition by RCG and LOTOS-EUROS has shown that the improved model version of RCG better represents the observed wet deposition than the LOTOS-EUROS version that only considers below-cloud scavenging. Note that the developments in the wet deposition description from MAPESI and PINETI are currently only implemented in the

RCG model. As all necessary information is available to LOTOS-EUROS, it is possible to include the new wet deposition description in LOTOS-EUROS as well.

A comparison between the RCG model results at 7 x 7 km^2 and the SO_x, NO_y and NH_x wet deposition results at 1 x 1 km^2 from PINETI for the year 2009 have shown that despite the lower resolution, the RCG model represents the spatial distribution of the wet deposition rather well.

In Teilbericht 3, several questions that arose during the project, are answered. The first task was to evaluate the applied method to calculate occult deposition in PINETI. A literature study was carried out and previous measurement campaigns were analyzed. The results from this evaluation confirm earlier studies that emphasize the high spatial and temporal variability of cloud water deposition and concentrations of substances in fog/clouds and precipitation. A comparison with available observations at stations with elevated orography has shown that the cloud water deposition as calculated in PINETI is underestimated. Based on an approach by Katata et al. (2008, 2011), the modeling of cloud water deposition can be improved. An extensive evaluation of the new method would be desirable, but is currently not possible due to a lack of observations. The evaluation has also shown that the height-dependent functions derived by Bleeker et al. (2000) between the concentration in precipitation and the concentration in cloud water cannot describe the measurements from more recent studies satisfactorily. Above the cloud basis, the cloud liquid water content increases with height and as a result the concentrations of trace gases decrease. A series of test runs has shown, however, that the year-to-year variability in the cloud water deposition is much larger than the variability in the choice of the height-dependent functions between concentration in precipitation and the concentration in cloud water. In the method of Bleeker et al. (2000) and in PINETI, the cloud water deposition is based on annual average parameters, e.g., cloud liquid water content, deposition velocities, etc. For consistency reasons, these annual averages were also used in the method of Katata et al. (2008, 2011). For a more accurate estimate of the cloud water deposition an hourly calculation would be desirable.

The second task concerns the analysis of the spatial variation of dry, wet and occult deposition in the Bayerischer Wald area for the year 2008. For this task, additional observations of wet and occult deposition were available (FKZ 35101088). The spatial variation of the deposition does not differ much between the PINETI and the MAPESI results. A comparison of the wet deposition of NH_x from MAPESI with observations at the Forellenbach station and Bayerischer Wald (open space) for 2007 shows that the wet deposition is clearly overestimated for that area in MAPESI. Within the PINETI project, wet deposition was already found to be much lower in this area and in much better correspondence with the observations. As the modeling of occult and wet deposition are strongly connected, i.e., the concentration in cloud water is derived from the concentration in precipitation, also the occult deposition in PINETI in this area is much lower than in MAPESI. Unfortunately, there were no observations in 2007 available to verify this.

The third task concerns the comparison of wet deposition results from PINETI for the year 2007 with those from MAPESI for the year 2007. Significant differences are found between the MAPESI 2007 and PINETI 2007 results for the different components (Table 3). For SOx-nss, NHx and NOy, these differences are caused by differences in the observations that are used for the Kriging and by including model results in the Kriging (see also Figure 23 in Teilbericht 1 of the project), while for the other components the differences are only due to differences in the observations that are used for the Kriging. In general, the PINETI method gives similar or better

results than the MAPESI method, especially for the components in which the model results are included.

For nitrogen the analysis indicates a systematic difference between the average wet deposition calculated within MAPESI for 2007 (9.6 kg N/ha/yr) and PINETI 2007 (8.7 kg N/ha/yr) of about 0.9 kg N/ha/yr. In the PINETI results for 2008 the wet N-deposition was 7.8 kg N/ha/yr and the observed difference compared to the MAPESI results 1.8 kg N/ha/yr. This means that about 50% of the difference between the 2007 wet N-deposition (MAPESI) and the 2008 N-deposition (PINETI) are caused by methodological changes, while the remaining 50% result from changed meteorology and/or emissions.

Table 3. Overview table of the mean wet deposition over Germany in 2007 using the MAPESI and PINETI method.

	MAPESI 2007 [eq ha^{-1} yr^{-1}]	PINETI 2007 [eq ha^{-1} yr^{-1}]	relative difference [-]	difference [eq ha^{-1} yr^{-1}]
SO_x-nss	237.63	226.00	0.95	-11.63
NH_x	416.46	346.28	0.83	-70.18
NO_y	268.55	275.53	1.03	6.98
Na^+	252.86	266.66	1.05	13.79
Ca^{2+}	115.25	92.59	0.80	-22.66
Mg^{2+}	69.87	70.06	1.00	0.18
K^+	37.18	27.92	0.75	-9.26
Ca^{2+}-nss	104.12	81.27	0.78	-22.85
Mg^{2+}-nss	8.91	12.65	1.42	3.74
K^+-nss	31.87	22.27	0.70	-9.60

Assessment of ecosystem impact

In order to estimate risks of natural or semi-natural ecosystems concerning acidification and eutrophication due to air borne pollution the Critical Load for terrestrial ecosystems was calculated in Teilbericht 4. Comparing such thresholds for pollution and comparing it with estimations for current deposition loads was done for approximately 30% of the area of whole Germany. This method of modelling Critical Load according to the Mapping Manual of the International Cooperative Program for Modelling and Mapping Critical Load (ICP Modelling & Mapping, www.icpmapping.org) has a rather long history in Germany. For 25 years this procedure of developing this tool for ecosystem protection was applied.

The direct link of ecological threshold (Critical Load) with the yearly sum of air borne deposition highlights areas at risk to suffer from acidification and/or eutrophication. The share of ecosystems with no exceedance of the Critical Load is an indicator for the success of air pollution abatement measures. It is part of the system of the kernel indicators ("Kernindikatoren") of the German Federal Environmental Agency ("Umweltbundesamt"). This project is in line with the continuation and the update of these essential indicators.

The deposition load needs also to be in compliance with the Critical Load in order to preserve the biological diversity. Therefore the realization of the European convention on biological diversity (CBD) in Germany defined targets for Critical Load exceedance. This realization is called national strategy of biological diversity ("Nationale Strategie zur biologischen Vielfalt") and this document drafts the objective of protecting all ecosystems in Germany against acidification and eutrophication by 2020. This is equal with a 100% of no exceedance in the German Critical Load dataset. The share of ecosystems with no exceedance of the Critical Load has been added to the set of indicators for national biodiversity strategy.

The measures taken to reduce acidifying effects of air pollution seem to be rather successful. The share of ecosystems with Critical Load exceedance is clearly reduced comparing the years 1990 with 85% and 2009 with 15% (see Figure 2). But not only the trend of no exceedance looks promising, also the share of ecosystems with rather high exceedance (1000 eq ha^{-1} yr^{-1} and more) was reduced. In the years 1990 and 1995 about 60% of the ecosystem had such high exceedance, while the most recent modeled year showed only 1% in this category.

Setting the focus on eutrophying effects and Nitrogen abatement measures offers less positive results. Even if the share of highly polluted areas (more than 10 kg ha^{-1} yr^{-1}) was reduced beginning in the year 1990 with 90% and ending in the year 2009 with 15%, more than half of the area is still at risk to suffer from eutrophication. Nevertheless the trend of increasing share of protected ecosystem is visible. In the year 1990 only 1% of the area had no exceedance, but this changed a lot in the year 2007 with 22.5% and also in the year 2009 with 50% (see Figure 3).

As contribution to the continuous process of further developing the Critical Load concept and widen the ways of application, this method was extended to the NATURA 2000 areas. In this second part of this project various approaches of assigning Critical Load for these specially protected areas were tested and compared. The focus in this approach was laid on including the habitat types documented in the Special Areas of Conservation (SAC). Generally the Critical Load modelled for the German dataset also represent protection targets of the NATURA 2000 areas, therefore the aim of having no Critical Load exceedance on national level should remain as priority target.

Figure 2. Trends of Exceedance of the Critical Load for Acidification

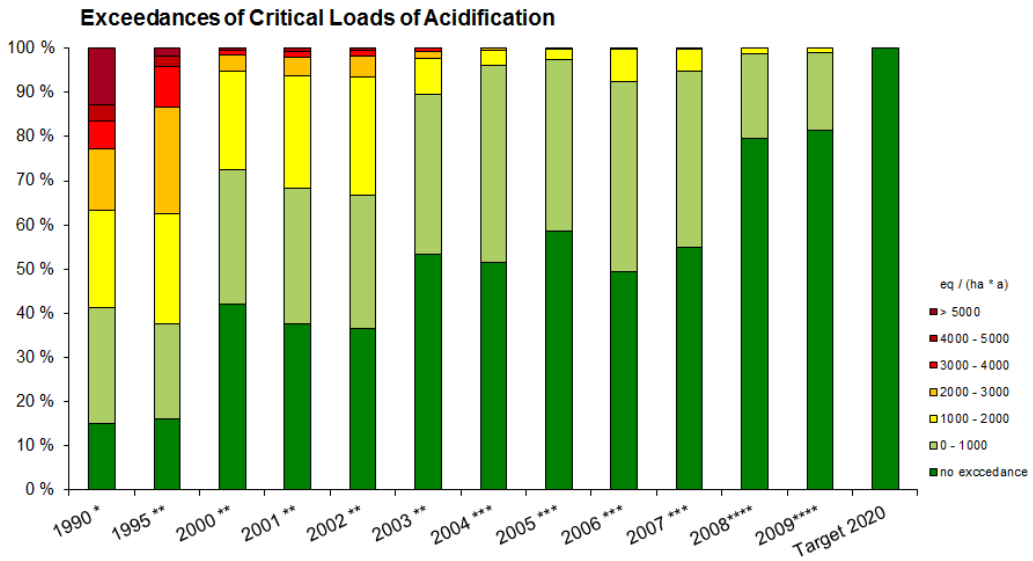

Source: Research projects of the Federal Environmental Agency (UBA): * FKZ 200 85 212 (2004), ** FKZ 204 63 252 (2008), *** FKZ 3707 64 200 (2011, MAPESI),****FKZ 3710 63 246 (2013, PINETI), Target 2020: to protect all ecosystems is a national CBD target for 2020 (BMU 2007)

Figure 3. Trends of the Exceedance of the Critical Load for Eutrophication

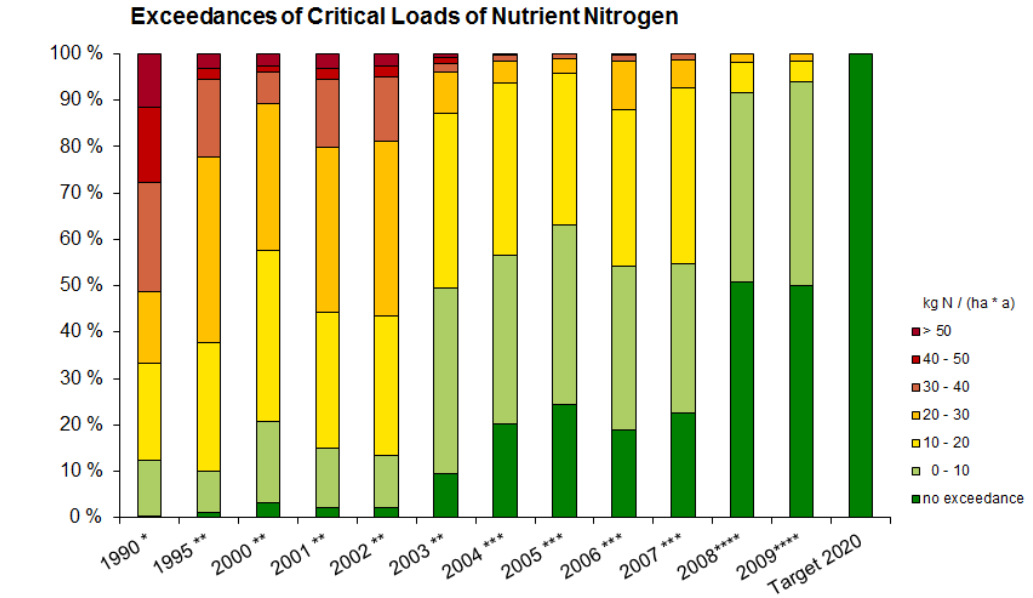

Source: Research projects of the Federal Environmental Agency (UBA) * FKZ 200 85 212 (2004), ** FKZ 204 63 252 (2008), *** FKZ 3707 64 200 (2011, MAPESI), **** FKZ 3710 63 246 (2013, PINETI), Target 2020: to protect all ecosystems is a national CBD target for 2020 (BMU 2007)

1 Introduction

Biodiversity in Europe is strongly affected by the deposition of nitrogen and sulfur on terrestrial ecosystems. Therefore, TNO, FUB and ÖKO-DATA assess the deposition of these atmospheric substances over Germany and calculate the exceedance of critical loads for sensitive ecosystems. Assessing is done by combining measurements and model calculations.

There are different forms of deposition: dry deposition, wet deposition and occult deposition. Measurements of dry deposition are very expensive and generally not available on a regular basis. Therefore, we have to rely on model calculations to estimate the dry deposition. For the wet deposition, however, there exist networks with more than 100 measuring stations in Germany. These measuring stations provide weekly, 2-weekly or 4-weekly measurements of concentrations of nitrogen, sulfur and base cations in rainwater. By combining these measurements with the modeled wet deposition fields, a high resolution map of the wet deposition over Germany is obtained. The occult deposition is estimated from the modeled moisture (or cloud) deposition and the concentrations of the different substances in the cloud or fog droplets (derived from the concentrations in rainwater from the wet deposition network). By adding the dry, wet and occult deposition, an overview of the total deposition over Germany is obtained, which is used to calculate Critical Load exceedances for different vegetation types (see Teilbericht 4).

In the previous MAPESI project (Builtjes et al., 2011), the wet deposition was based on the observed concentrations in rain water only and completely disconnected from the model calculations. The motivation for this approach was that modeled wet deposition and observed wet deposition differed substantially, i.e., the model underestimates the observed wet deposition. The obtained wet deposition field from the observations was considered to be more realistic than the rather low wet deposition field from the model. However, in the mass balance calculations of the model, the wet and dry deposition are in balance. This means that a low wet deposition is compensated by a higher dry deposition. Taking the wet deposition from the observations and the dry deposition from the model can therefore lead to an overestimation of the total deposition. As the model can still add spatial information to the wet deposition field, a new method to assess the wet deposition was developed within PINETI. In this new method both the modeled and the observed concentrations in precipitation are used. The new method has no feedback in the mass balance calculation yet, as a part of PINETI project concerns the improvement of the wet deposition modeling (see Teilbericht 2).

Another difference with the MAPESI project is the calculation of the occult deposition. In this study, more detailed hourly information on cloud liquid water content is available, which makes the existing method to assess the occult deposition less dependent on climatological constants, e.g., a fixed number of 1400 hours of clouds at the surface was assumed for areas over 250 m a.s.l., which is rather large for most of the areas.

These methodological changes lead to differences between the MAPESI and the PINETI project and will be investigated in more detail in another part of the PINETI project (see Teilbericht 3).

In the next chapters, we present the methods that were applied to obtain the total deposition in PINETI (Chapter 2) and discuss the results for 2008 and 2009 (Chapter 3). The differences between the final PINETI results and the sub-grid information that is used by ÖKO-DATA to calculate critical load exceedances are discussed in Chapter 4. The results from PINETI for the years 2008 and 2009 are compared with the MAPESI results for the year 2007 in Chapter 5. In Chapter 6 the results are compared with the EMEP results for 2008. Chapter 7 deals with uncertainties in the deposition results and this report is finished with a general discussion about the project results in Chapter 8.

2 Methods

In this chapter, an overview is given of the methods that are used to derive the total deposition of NH_x, NO_y, SO_x and the base cations over Germany for the years 2008 and 2009 on a 1 x 1 km² grid size resolution.

2.1 Emissions

The emissions for Germany for 2008 and 2009 rely on the emissions for Germany for 2005. These emissions are based on data from the UBA-database „Zentrales System Emissionen (ZSE)“ and lie on a regular grid with a resolution of 1/60° x 1/60° lon / lat (about 1.2 x 1.8 km^2). These emissions have been produced by the Institut für Zukunftsstudien und Technologiebewertung (IZT) and the Institut für Energiewirtschaft und Rationelle Energieanwendung (IER) from the University of Stuttgart within the PAREST project (Jörß et al., 2010). The focus of the PAREST project was on the present and future particulate matter loads in Germany. In contrast to the officially reported emissions inventories (based on an energy balance) the emissions within the PAREST project were determined based on the so called Inland-Prinzip, which means that they include the actual emissions in Germany. In this project, the PAREST emissions are scaled by a constant factor (for each substance) to the officially reported emission totals in 2012 by UNECE/CLRTAP (UBA, 2012), while the spatial distribution of PAREST is maintained.

The European emissions for 2008 and 2009 are based on the PAREST 2005 database that are on a regular grid with a resolution of 1/8° x 1/16° lon / lat (about 7 x 8 km^2). These emissions have been created by TNO within the PAREST project (Denier van der Gon et al., 2010). The European emissions for 2008 and 2009 are not scaled to the officially reported emission totals in 2012 by UNECE/CLRTAP (UBA, 2012), but in a conservative manner the original PAREST 2005 emissions were used to calculate the model boundary conditions for the years 2008 and 2009. Note that the German emissions in this PAREST database are scaled to the official UNECE/CLRTAP (UBA, 2012) emission totals, also for the boundary conditions.

The PAREST emission distributions for the year 2005 are shown in Figure 4. Note that in the previous project (MAPESI), for the years 2006 and 2007, the PAREST 2005 emissions were linearly interpolated between the reported 2005 emissions and a "current legislation emission scenario" (CLE) for the year 2010. In the current project, the PAREST 2005 emissions are scaled with factors derived from the reported country totals of the UNECE/CLRTAP emission inventory from 2012 for the years 2008 and 2009 (UBA, 2012). The spatial distributions for 2008 and 2009 are similar to the spatial distributions in Figure 4, only the scales will be different. The relative contribution of each SNAP category is assumed to be the same as in 2005. Table 4 gives an overview of the scaling factors (compared to PAREST 2005) that are used in this project. The trend in emissions between 2005 and 2010 according to the reported country totals of the UNECE/CLRTAP emission inventory 2012 (UBA, 2012) is shown in Figure 5.

Figure 4. Emission distribution of NO_x (a), NMVOC (b), SO_x (c), NH_3 (d), $PM_{2.5}$ (e), PM_{10} (f), CO (g) and CH_4 (h) at a 1/8th by 1/16th degrees grid size resolution for the year 2005. The years 2008 and 2009 have an equal distribution, but different scales.

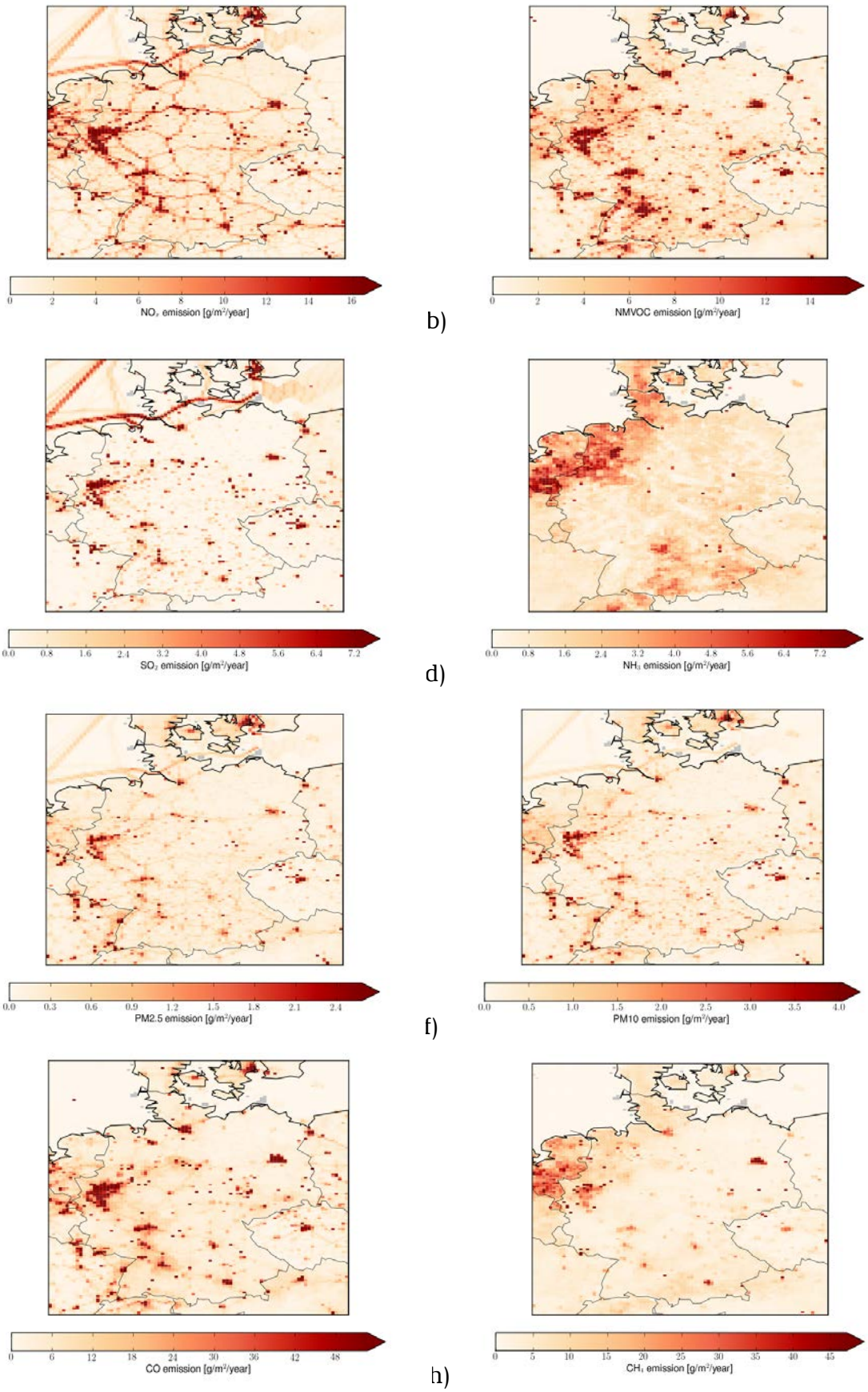

Table 4. Emission totals and scaling factors to obtain the reported country totals of the UNECE/CLRTAP emission inventory 2012 from original PAREST 2005 emissions assuming no changes in relative contribution of SNAP categories for the years 2005, 2008 and 2009. The low scaling factor for NMVOC is caused by the current exclusion of NMVOC-emissions from agriculture in the emission inventory.

Totals [Gg yr^{-1}]	NO_x	NMVOC	SO_x	NH_3	$PM_{2.5}$	PM_{10}	CO	CH_4
2005 PAREST	1544	1438	562	607	136	262	4043	2268
2005 UNECE/CLRTAP	1576	1143	517	573	121	207	3651	2725
2008 UNECE/CLRTAP	1415	1015	490	568	110	195	3387	2441
2009 UNECE/CLRTAP	1318	929	435	576	106	187	3002	2324
scaling factor between PAREST 2005 and UNECE/CLRTAP emissions								
2005	1.021	0.795	0.921	0.944	0.892	0.789	0.903	1.201
2008	0.916	0.706	0.873	0.936	0.809	0.742	0.838	1.076
2009	0.854	0.646	0.774	0.949	0.778	0.713	0.743	1.025

Figure 5. Trend in the emissions between 2005 and 2010 according to the reported country totals of the UNECE/CLRTAP emission inventory 2012.

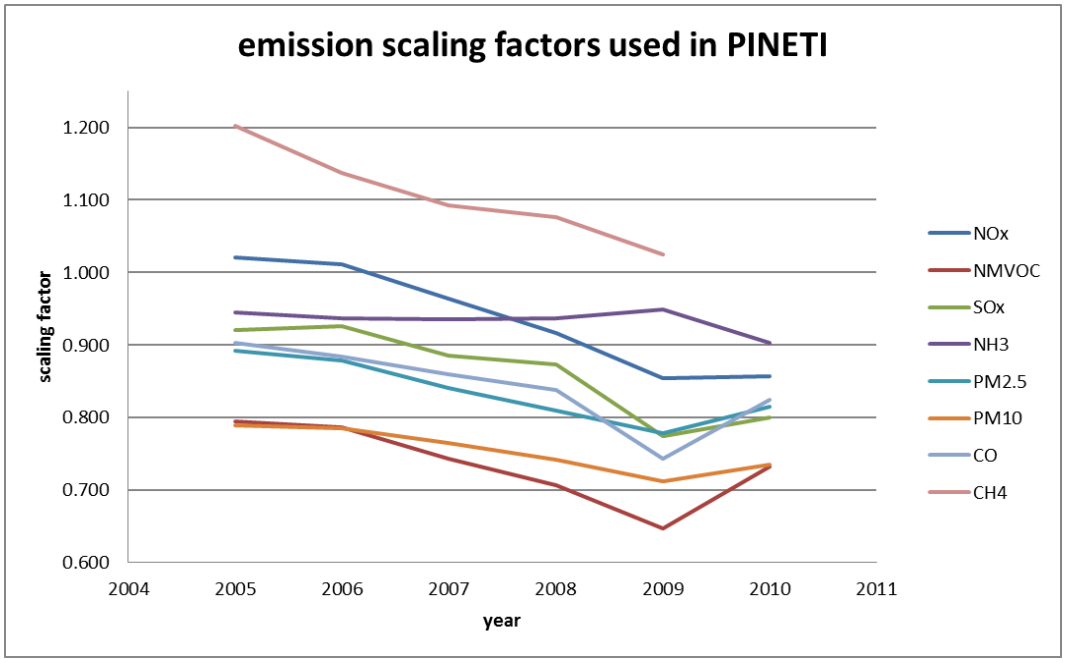

2.2 Land use

The LOTOS-EUROS model currently uses the land use dataset Corine Land Cover for the year 2000, CLC2000, for concentration and deposition calculations. This land use data set is a vector based data set, which is aggregated to a 1/60° x 1/60° latitude/longitude resolution, i.e., about 1.2 x 1.8 km^2. The available land use classes in CLC2000 are aggregated to 9 DEPAC land use classes. DEPAC is the DEPosition of Acidifying Components module that is developed and officially used by the National Institute for Public Health and the Environment (RIVM) in the Netherlands (Van Jaarsveld, 2004). LOTOS-EUROS also uses this module for the calculation of SO_x, NO_y, NH_x and base cation deposition, which are carried out on a 1/8° x 1/16° latitude/longitude resolution, i.e., about 7 x 7 km^2. Table 5 shows these 9 DEPAC land use classes and their corresponding roughness lengths. The fractions of each land use class within one grid cell of 7 x 7 km^2 in LOTOS-EUROS are shown in Figure 6.

The spatial distributions of the anthropogenic emissions (calculated by IER from Stuttgart University within the PAREST project) are also based on CLC2000 land use. For the biogenic isoprene emissions, more detailed information about tree species is required. Therefore, only for the biogenic isoprene emissions, we rely on a detailed "Tree Species Map for Europe" that was created by Joint Research Center in Ispra (Köble and Seufert, 2002). The tree species dataset is also on a 1/60° x 1/60° latitude/longitude resolution, i.e., about 1.2 x 1.8 km^2.

The critical load exceedance calculation is based on an updated version of the CLC2000 database, i.e., CLC2006, which has a higher resolution of 250 x 250 m^2.

Table 5. DEPAC categories and their corresponding roughness lengths.

DEPAC categories (abbreviation)	Roughness length (m)
Grassland (grs)	0.03
Arable land (ara)	0.25
Mixed forest (mix)	2.0
Coniferous forest (cnf)	2.0
Deciduous forest (dec)	2.0
Water (wat)	0.002
Urban area (urb)	3.0
Semi-natural vegetation (sem)	0.25
Other (oth)	0.1

Figure 6. Fractions of each CLC2000 land use class on a 1 x 1 km grid cell resolution (obtained from interpolation of 7 x 7 km^2 grid cell resolution). From upper left to lower right: grassland, arable land, mixed forest, coniferous forest, deciduous forest, water, urban area, semi-natural vegetation, other.

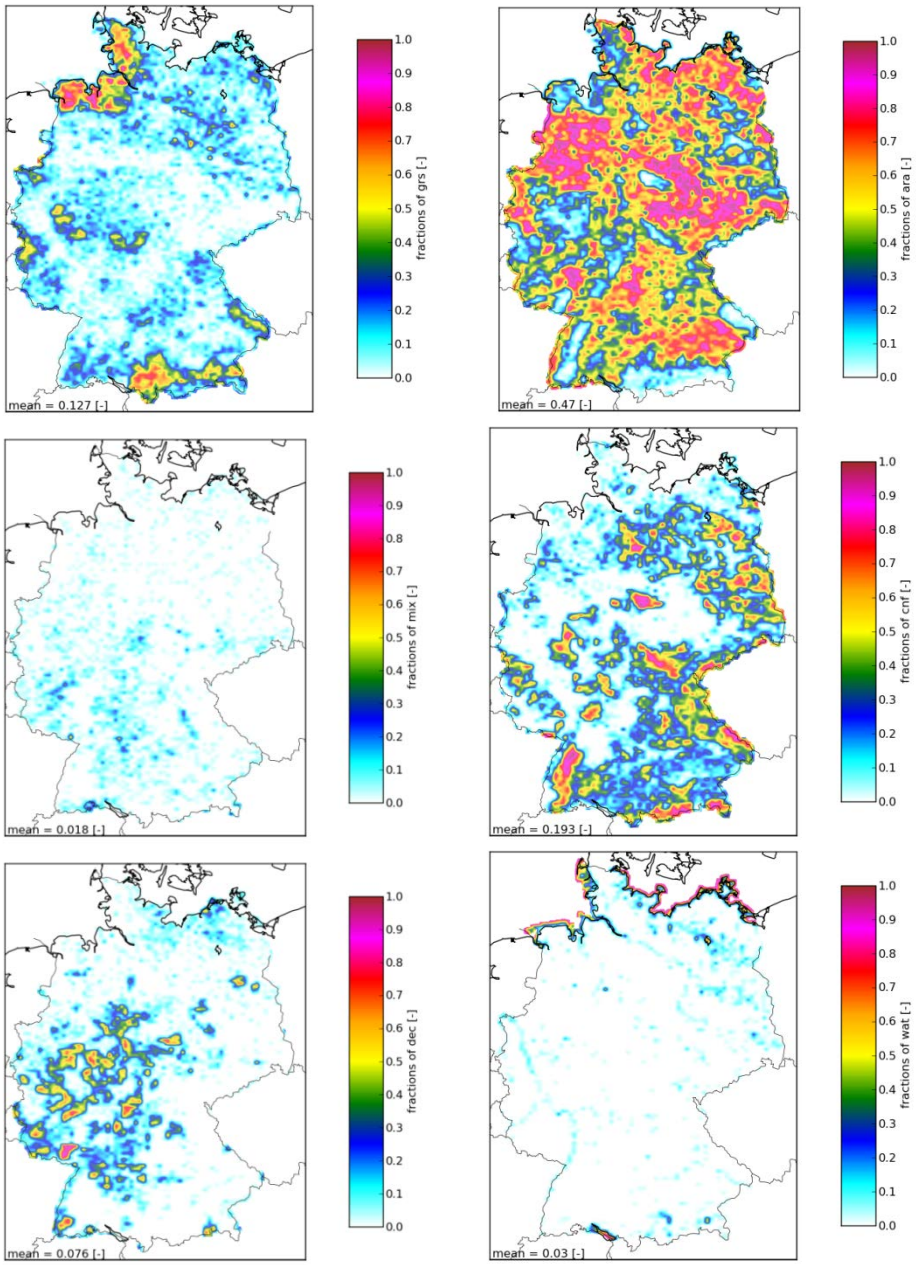

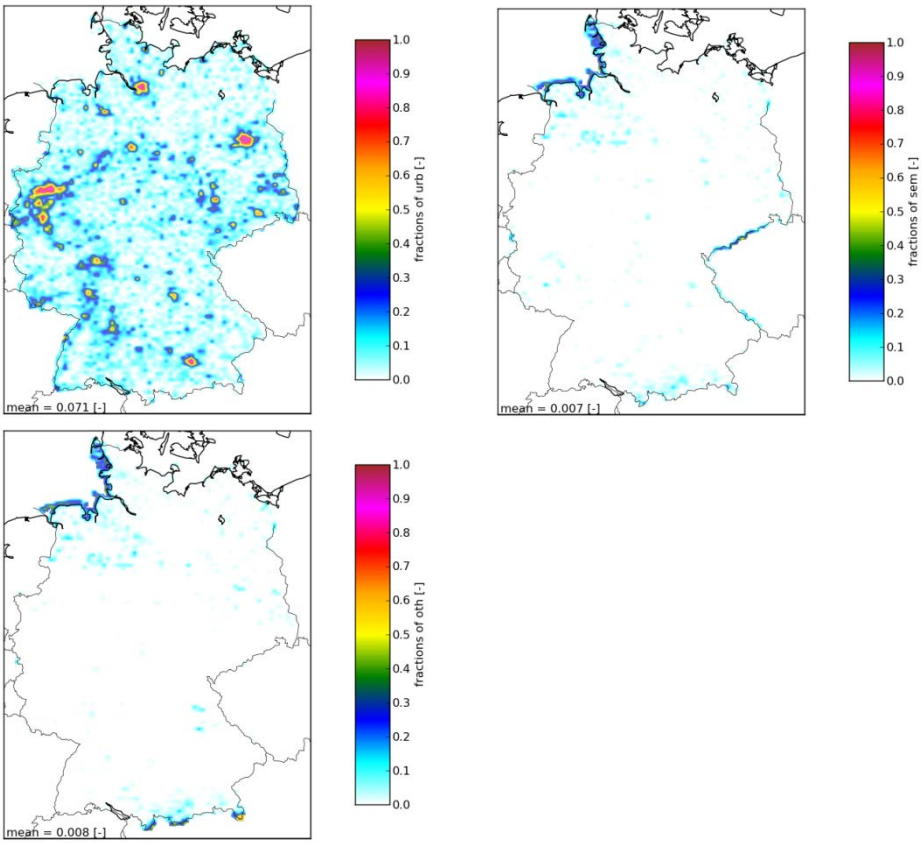

It is not ideal to use different land use datasets in the modeling process, but the biogenic emissions calculated with the detailed tree species map of JRC represent the real biogenic emissions better. Besides, it is quite common that models use different land use datasets as input for the calculation of different processes, e.g., the Unified EMEP model also uses different land use datasets for the calculation of biogenic emissions and deposition. The meteorological model from ECMWF uses again a different land use.

2.3 Meteorology

The LOTOS-EUROS model at TNO uses ECMWF meteorology which is provided by the Royal Dutch Meteorological Institute, i.e., KNMI (www.ecmwf.int). The meteorological input is provided on a 0.5° x 0.25° longitude/latitude resolution (~28 x 28 km^2) and is terrain following. This means that the meteorological data is calculated in a coordinate system relative to the earth's surface, so, accounting for the orography.

For the wet deposition calculation, the annual precipitation fields from DWD (http://www.dwd.de) are used on a 1 x 1 km^2 resolution. For the calculation of the occult deposition the liquid water content of DWD COSMO-EU are used. COSMO-EU runs at a 7 x7 km^2 resolution and uses 40 vertical levels with the lowest level 10 meter above ground. For the occult deposition, we will only use the data from this lowest level.

2.4 Dry Deposition

2.4.1 Introduction

Aim of the PINETI project is to determine the N-, S-, and base cation deposition for the years 2008 and 2009. The method to calculate the dry deposition in PINETI was roughly equal to the method that was used in the previous MAPESI project. However, some important methodological changes in the stability functions have been implemented. We start this chapter with a short overview of the equations that were used in the MAPESI project after which we will discuss the methodological changes in the stability functions. Differences between the calculated deposition values in different years (chapter 3) in principle have four different reasons:

5. Methodological changes in stability functions
6. Differences due to changes in the emissions in Germany and Europe
7. Changed chemical equilibriums due to the emissions changes mentioned in 1
8. Differences caused by different meteorological circumstances

The dry deposition is strongly dependent on land use and meteorology and can therefore show large spatial and temporal variations, e.g., annual, weekly, daily variations. Accurate deposition measurements are generally extremely expensive and labor intensive, and therefore sparse. To map the dry deposition over Germany based on measurements, a dense measurement network would be required.

To get an estimate of the spatial distribution of the dry deposition over Germany, we therefore rely on model calculations. The parameterizations that are used in the model are generally derived from measurement campaigns over specific vegetation types. Several models of varying complexity have been developed to describe the dry deposition. These models are all based on the same concept: resistance modeling using electrical circuit analogue (Monteith and Unsworth, 1990). In this modeling approach, the flux or current is modeled as the concentration difference or potential difference divided by the total resistance:

$$F = \frac{\Delta C}{R_{total}} \qquad \text{(Eq. 2.1)}$$

The total resistance, R_{total}, is the sum of the aerodynamic or atmospheric resistance, R_a, the quasi-laminar boundary layer resistance, R_b, and the surface resistance, R_c. The atmospheric resistance is dependent on atmospheric conditions, like wind speed and stability, and the roughness of the surface. The quasi-laminar boundary layer resistance is also dependent on the atmospheric conditions, but also on the characteristics of the substance that is transported through the atmosphere. The surface resistance represents the resistance against uptake by the surface, e.g. by the vegetation and soil, and is dependent on the characteristics of the substance and on the characteristics of the soil and vegetation (with meteorological variables as driving forces).

The necessary input data for the calculation of R_{total} are obtained from the ECMWF meteorology and the land use database.

2.4.2 Method for modeling of dry deposition

The dry deposition over Germany is calculated with the Chemical Transport Model (CTM) LOTOS-EUROS. CTMs calculate the 3-dimensional transport, chemical conversion and deposition of different atmospheric substances over an area typically the size of Europe or Germany. Concentration changes are calculated for each grid cell and for every hour.

The input data in a CTM consist of hourly meteorology, time and temperature dependent hourly emissions and land use data. The model contains parameterizations for transport, chemical conversion and dry and wet deposition for gaseous and particulate atmospheric substances. In each grid cell, the mass balance of the considered substance is calculated consistently based on the processes described above, where the total mass of the substance is maintained. So, the concentration of a substance in a grid cell is the result of many different processes, e.g., if one mole of NH_x is removed from a grid cell by dry deposition, the total mass in the grid cell is also reduced by one mole. As already mentioned in the introduction section, the dry deposition is calculated from the ambient concentration and several resistances:

$$F = \frac{C}{R_a+R_b+R_c} = v_d \cdot C \qquad \text{(Eq. 2.2)}$$

The reciprocal of the sum of the resistances is also called the deposition velocity, i.e., v_d. The dry deposition flux is a loss term for mass in a CTM grid cell. This means that besides emissions, chemical conversions and transport in and out of a grid cell, wet and dry deposition fluxes also affect the mass and consequently the concentration in a grid cell. In PINETI, the calculated dry deposition flux is directly applied in the mass balance calculation to keep the modeling system mass conservative.

For the calculation of the dry deposition, we have applied the following procedure:

1. In the mass balance calculations of the model, the dry deposition of SO_x (SO_2+SO_4^{2-}), NO_y (NO+NO_2+NO_3^-+HNO_3) and NH_x (NH_3+NH_4^+) is calculated by the LOTOS-EUROS model on a 7 x 7 km² grid cell resolution by accumulating the fractions of each land use class present in the grid cell multiplied by the land use specific v_d (at 25 m height) and the grid cell average concentration in the lowest model layer (at 25 m height) of LOTOS-EUROS. The land use specific v_d are calculated using land use specific u_*. The dry SO_x deposition is initially calculated by the model without a sea salt contribution, but the sea salt contribution is added to the dry SO_x deposition in a postprocessing procedure based on the sodium concentration.
2. The land use dependent dry depositions of SO_x, NO_y and NH_x are saved as separate outputs. These outputs may be used to create maps for the landuse specific deposition (needed for example for the critical load exceedance calculations).

3. Dry deposition of Na^+, Ca^{2+}, Mg^{2+}, K^+ are calculated in a post-processing procedure using the results of the wet deposition calculations, i.e. the concentrations in rain are converted in concentrations in air following Draaijer et al. (1996):

   $[C]_{air} = ([C]_{rain} * 1200)/(188 * e^{(0.227*MMD)})$

   where:

   $MMD = a *[C]_{rain} + b$

   with a = 0.574, 2.778, 1.520, 2.740 for Na^+, Mg^{2+}, Ca^{2+} and K^+ respectively

   b = 6.082, 5.694, 6.316, 4.096 for Na^+, Mg^{2+}, Ca^{2+} and K^+ respectively

4. The obtained air concentrations are multiplied by the land use specific v_d. Na^+, Ca^{2+}, Mg^{2+} are treated as coarse particles, i.e. particles between 2.5 and 10 μm, while K^+ is treated as fine particles, i.e. particles smaller than 2.5 μm. Examples of the v_d fields for coarse and fine particles over grassland are shown in Figure 7a and Figure 7b respectively. In PINETI, the dry deposition of Cl^- was not calculated, neither were the wet and occult deposition of Cl^-.

5. The dry depositions of non-sea salt components, i.e., Ca^{2+}-nss, Mg^{2+}-nss, K^+-nss, are calculated from the fields including the sea salt fraction minus the sea salt fraction of this component. The sea salt fraction of each component is calculated by multiplying the Na^+-field with a component specific factor, which represents the fraction of this component in fresh sea salt (CLRTAP (2004); see Table 6).

6. In addition to the land use specific dry deposition maps from step 3 and 4, a composite map on 7 x 7 km^2 is created based on the CLC2000 land use fractions in each grid cell with their corresponding deposition fluxes.

Table 6. Conversion table for sea salt fractions (CLRTAP (2004); Table 2.1)

	Ca^{2+}	Mg^{2+}	K^+	Na^+	Cl^-	SO_4^{2-}
eq X/eq Na^+	0.043	0.228	0.021	1.000	1.166	0.120
g X/g Na^+	0.037	0.120	0.036	1.000	1.797	0.250

Figure 7. Example of a deposition velocity field of coarse particles (between 2.5 and 10 µm; left) and fine particles (smaller than 2.5 um; right) at 2.5 meters height over Germany in 2007 for grassland.

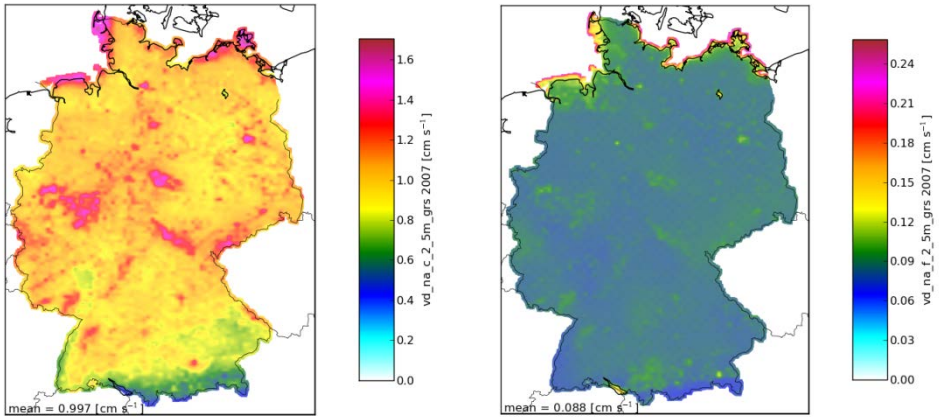

2.4.3 Changes in stability functions and displacement height

At the beginning of the PINETI project, some inconsistencies in the method to calculate the friction velocity u* from the wind speed at 10 meters (from the meteorology) were resolved. In the calculation of u*, the 10 meter wind speed is scaled up to 50 meters using the grid cell average roughness lengths from the meteorological input. At this height, the influence of the vegetation below is assumed to be negligible. In the MAPESI project this calculation occurred with the stability function for heat (which is equal to the stability function of mass), while the stability function for momentum should have been used for the calculation of the wind speed at 50 meter, i.e., heat and mass are transferred more efficiently than momentum. In PINETI, the stability function for momentum is used to obtain the wind speed at 50 meters. From the wind speed at 50 meters, the land use dependent u* are calculated with the stability functions for momentum using the roughness lengths of the land uses that are present in the deposition routine. For the calculation of the atmospheric resistance, R_a, which is used to calculate the dry deposition flux, the stability functions for heat (and thus mass) is used in combination with the land use specific u*.

Besides the changes in the stability functions, some inconsistencies in the treatment of the displacement height for land use classes forest were removed. In MAPESI the displacement height was erroneously set to the canopy height, while in micrometeorological literature, two-third of the canopy height is generally given as a more realistic estimate for the displacement height (e.g., in the Mapping Manual (CLRTAP, 2011) a 0.7 times the canopy height is proposed). In PINETI, the displacement heights are therefore set at two-third of the canopy height, i.e., 13 meters for deciduous, coniferous and mixed forest.

These changes have resulted in a decrease in the dry deposition especially over the larger forest areas, which can be seen in chapter 11 Appendix B.

2.4.4 Conversion of model results to high resolution 1 x 1 km^2

The 1 x 1 km^2 resolution dry deposition results presented in chapter 3.2 all result from the 7 x7 km^2 results of LOTOS-EUROS, either directly, i.e., NO_y, NH_x, SO_x, or indirectly (i.e for the base cations) in that the modeled v_d fields resulting from the 7 x7 km^2 DEPAC land use classes are used in combination with derived air concentrations from the concentrations in the precipitation. The deposition is calculated for each land use class separately and a 2-D

interpolation is carried out to obtain 1 x 1 km^2 results, which are provided as a separate dataset. The deposition fluxes presented in Figure 32 are obtained by multiplying the land use specific deposition fluxes with the land use fractions from CLC2000 (Figure 6).

For the critical load exceedance maps that are created by ÖKO-DATA, the land use specific deposition fields from LOTOS-EUROS interpolated to 1 x 1 km^2 are used in combination with the high resolution CLC2006 land use map. The dry deposition amounts calculated by the LOTOS-EUROS model for one 7 x 7 km^2 grid cell in the mass balance calculation approximately agree with the sum of the dry deposition to the 1 x 1 km^2 mosaic cells covering the same area. To illustrate that the differences in the land use databases used by TNO and ÖKO-DATA are small, a comparison of the interpolated 1 x 1 km^2 total deposition fields by TNO and the 'mosaic' field finally created by ÖKO-DATA to calculate the critical load exceedances over Germany is shown in chapter 4.

2.5 Wet deposition

2.5.1 Introduction

Wet deposition is the vertical chemical input of airborne compounds to a ground surface via precipitation. Airborne pollutants, which are attached to and dissolved in cloud droplets, rain drops, and snow, respectively, are either transported downwards to the ground surface by 'rain-out' ('in-cloud scavenging'), or they are taken up from the atmosphere by hydrometeors during the precipitation event ('wash-out', 'below-cloud scavenging').

The LOTOS-EUROS model tends to underestimate the observed wet deposition of SO_x, NO_y and NH_x by almost a factor of two. As many wet deposition measurements are available, the wet deposition maps in PINETI are obtained by applying a Kriging technique, which combines LOTOS-EUROS model calculations (Schaap et al., 2008) with wet deposition measurements (see paragraph 2.5.3). The wet deposition in LOTOS-EUROS is calculated using below-cloud scavenging coefficients only, leaving the in-cloud scavenging out of consideration, which likely explains part of the underestimation by the LOTOS-EUROS model. We have to mention here that the in-cloud scavenging was not included due to lacking meteorological input data. However, this shortcoming is likely partly compensated by the applied (higher) below-cloud scavenging coefficients.

The concentrations of the different components in precipitation in Germany are measured by an extensive countrywide measurement network made up of various national and regional monitoring programs.

2.5.2 Method for the calculation of wet deposition

For the calculation of the wet deposition of NH_x, NO_y and SO_x, we have applied the following method:

1. first the total annual wet deposition by the model is calculated using:

   air concentration x scavenging coefficients x precipitation amount (ECMWF) on an hourly basis

2. then, the average concentration in the precipitation is calculated from the total annual wet deposition and the total annual precipitation amount (units in mg l^{-1}).

   These model results are then combined with the wet deposition observations using the Kriging technique. However, before we can combine model results and observations, we need to pre-process the wet deposition observations.

3. Pre-processing and selection of wet deposition observations: Although many stations provide concentrations in precipitation on a weekly or 2-weekly basis, it's important to calculate the annual average concentration in precipitation from the total wet deposition and the total precipitation amount (at the measurement station). This is because the concentration in precipitation depends non-linearly on the precipitation amount, i.e., low precipitation amounts generally contain higher concentrations and occur more often (see Figure 8). Therefore, we first accumulate the wet deposition measurements calculated from the provided concentrations and precipitation amounts and then divide by the total precipitation amount at the measurement station (units in mg l^{-1}).

   A comparison of annual station precipitation to the annual DWD precipitation is not straight forward as almost all stations contain missing values (see upper panel in Figure 14) and the annual precipitation sum cannot be computed without gap filling. For a comparison of annual station precipitation with annual DWD precipitation, we refer to Gauger et al. (2010), who found that the difference between annual station precipitation and DWD precipitation was generally smaller than ±10% for most stations in 2005-2007. However, it is not clear if and how missing data were treated in that comparison.

4. then, we apply Kriging to combine the modeled and measured concentration in precipitation. For this purpose, we analyzed the spatial correlation between the time series of the difference between the modeled and observed concentrations in precipitation for pairs of stations (as a function of the distance between the stations), i.e., residual Kriging. The obtained correlation model will be used as input for the Kriging procedure in which the annual average modeled concentrations in precipitation are corrected towards the annual average observed concentrations in precipitation. A more extensive description of the Kriging procedure is given in chapter 2.5.4.

5. The Kriging procedure results in a field of the annual average concentration in precipitation on the 7x7 Km model grid. The concentrations are approximately equal to the observed values at the observation locations, and smoothed in between them.

6. To obtain the annual wet deposition we interpolate the annual average concentration in precipitation to 1 x 1 km^2 and we multiply this field with the 1 x 1 km^2 annual precipitation field from DWD (http://www.dwd.de).

Figure 8. Weekly precipitation sum versus concentration in precipitation for SO_4^{2-} (left), NO_3^- (middle) and NH_4^+ (right) at 12 UBA stations in 2008.

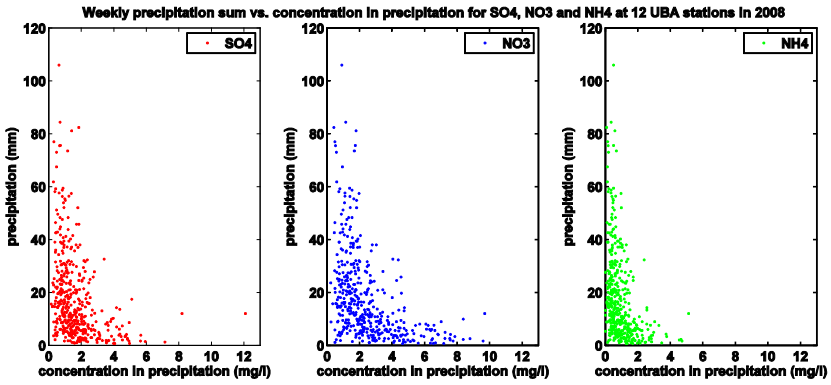

The annual average base cation concentrations in precipitation are calculated based on the observations only. To calculate the wet deposition a direct Kriging interpolation of the measured annual concentration in precipitation is applied. The resulting concentration field is multiplied by the annual precipitation field from DWD to obtain the corresponding wet deposition field.

The non-sea salt (-nss) part of SO_x and the base cations is calculated using the conversions in Table 6 (ICP Modeling and Mapping Manual, 2004).

2.5.3 Data processing of measurements of wet deposition

2.5.3.1 Introduction

In the following paragraphs, the dataset of wet deposition measurements used within PINETI for the Kriging procedure is described.

Concentrations of pollutants in rain water are measured using devices as shown in Figure 9. The instruments collect rain water during some time period, typically in a range from 1 week up to 1 month. Some of the devices (wet-only collectors) are equipped with a lid which opens only during precipitation events; thus minimizing the collection of deposition fluxes other than wet deposition such as dry sedimenting particles. In contrast, so called bulk-collectors are continuously exposed to the atmosphere. The collected bulk deposition also include an additional amount of dry deposited matter (particulates and gases) collected in dry periods (still the bulk deposition is not equal to the total deposition as particularly the collection of the dry deposition is incomplete).

Figure 9. Wet-only sampler (Firma Eigenbrodt, Germany) for measurements of wet deposition.

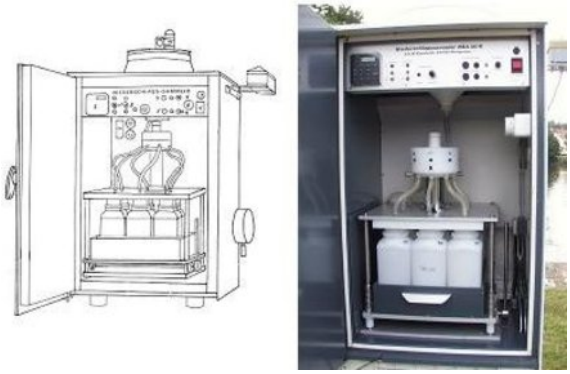

The data retrieved from the instruments is twofold:

1. the total precipitation amount p [mm water];
2. concentration c_{ion} [mg/l] of a particular ion.

Table 7 shows the observed ions that were used in this study.

From the observed amount of precipitation and the concentrations it is possible to compute the deposition flux:

$$F_{ion} = p \times c_{ion} \quad \left[\frac{mg}{m^2}\right] \qquad \text{(Eq. 2.3)}$$

Examples of the time series of weekly observed precipitation in 2007 (blue bars), sulphate concentrations (red line; multiplied by 10 to match scale), and computed deposition flux (green diamonds) are shown in Figure 10.

In this example, the instrument measured rain during most of the weeks; the only exceptions are a few dry weeks during spring and autumn. The amount of collected precipitation during a week shows large variations, ranging from a few millimeter to weeks with more than 100 millimeters of water collected. The observed concentrations show less variation; their value is usually determined by the location of the station, e.g. whether it is exposed to polluted air from urbanized areas or to relative clean air.

Figure 10. Example of time series of sulphate observations in Schmücke (one of the sites of the UBA network).

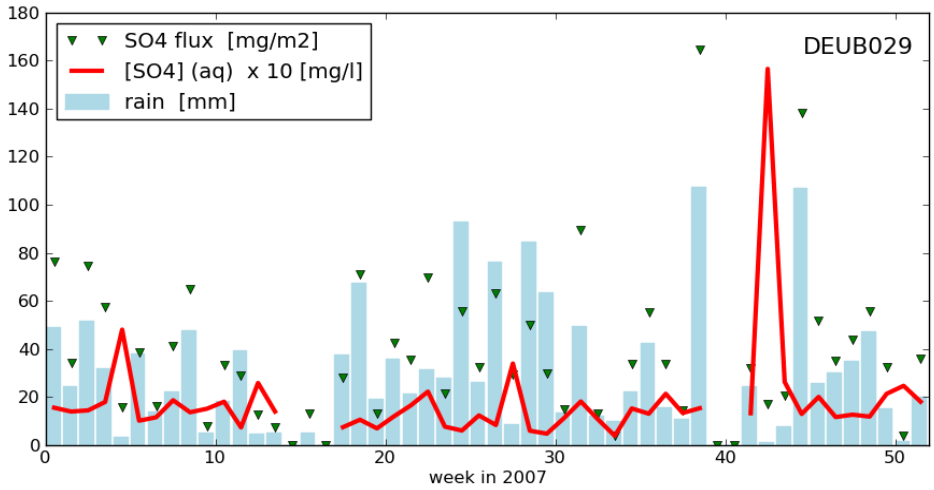

Due to the complexity of the measurement procedure, a rather large observation error has to be accepted. The relative measurement error has been estimated to be in the order of about 30% (Annex XVI, sec. 1.2.5; Builtjes et al. 2011). In the rest of the study, we will use this estimate to quantify the error variance, which is found to be in agreement with the observation data in section 2.5.4.3.

2.5.3.2 Description of data set

The concentrations of ions in precipitation that are used within PINETI have been provided by different monitoring networks operated by different institutions. This information is listed in Table 8, together with the available components, the type of sampler and the number of stations for the various monitoring networks for the relevant years 2007, 2008 and 2009. The corresponding metadata has been included in the UBA station data base (http://www.env-it.de/stationen/public/stationList.do). The service of the involved institutions (Table 8) is gratefully acknowledged.

The temporal resolution of the observations (weekly or 2-weekly) and the day of the week on which the measurements are performed vary between the different monitoring networks and stations. Hence, the data are not temporally synchronized. The measurements are delivered either as concentrations in precipitation in mg/l or as deposition fluxes in mg/m^2. In case deposition fluxes (mg/m^2) are delivered, the concentrations in precipitation are derived by dividing the wet deposition fluxes by the precipitation at the station (in mm).

Table 8 shows that the number of measured components varies for the different monitoring networks. Complete data sets (suitable for ion balance check) are marked in green. Besides, it was found that there is large variation in detection limits for the different components in the different monitoring networks (see Table 7). Depending on the monitoring network, the observations are either performed by means of bulk samplers or wet-only samplers. To correct the bulk deposition for the contribution of the dry deposition into the funnels, the bulk measurements are reduced by means of correction factors derived by Gauger et al. (2000;2008) (see section 2.5.3.3).

Table 7. Overview of observed ions and parameters used in this study.

ion	name	Range of detection limits due to different analytical procedure [mg/l]
SO_4^{2-}	sulphate	0.020-0.4
NO_3^-	nitrate	0.013-0.5
NH_4^+	ammonium	0.003-0.1
Na^+	sodium	0.006-0.1
K^+	potassium	0.002-0.1
Mg^{2+}	magnesium	0.001-0.1
Ca^{2+}	calcium	0.002-0.1
Cl^-	chloride	0.007-0.1

The quality of the station data is assured by several criteria, which are described in more detail in section 2.5.3.3 below. The resulting concentrations of SO_4^{2-}, NO_3^-, NH_4^+, Ca^{2+}, Mg^{2+}, Na^+, K^+ and H^+ in precipitation are used in the Kriging procedure. The number of stations per component, before and after quality checks for the years 2007, 2008 and 2009 is listed in the three bottom rows of Table 8.

Table 8. Available components, type of collector and the number of stations for the various measurement networks for the considered years. Complete data sets (suitable for ion balance check) are marked in green.

Region	Abbreviation	Institution	year	SO_4^{2-}	NO_3^-	NH_4^+	Mg^{2+}	Na^+	Ca^{2+}	K^+	Cl^-	H^+	Wet-only	Bulk	number of stations
Baden-Württemberg	BW	LUBW Landesanstalt für Umwelt, Messungen und Naturschutz Baden-Württemberg, Referat Luftqualität	2007	X	X	X							X		4
			2008	X	X	X							X		4
			2009	X	X	X							X		4
		FVA Forstliche Versuchs- und Forschungsanstalt Freiburg, Abteilung Boden und Umwelt	2007	X	X	X	X	X	X	X	X	X		X	26
			2008	X	X	X	X	X	X	X	X	X		X	25
			2009	X	X	X	X	X	X	X	X	X		X	26
Bayern	BY	LFU Bayerisches Landesamt für Umwelt, Medienübergreifende Umweltbeobachtung	2007												
			2008	X	X	X	X	X	X	X	X	X		X	28
			2009	X	X	X	X	X	X	X	X	X		X	29
		LFU Bayerisches Landesamt für Umwelt, Hydrologie des Grundwassers	2007	X	X	X	X	X	X	X	X	X		X	11
			2008	X	X	X	X	X	X	X	X	X		X	11
			2009	X	X	X	X	X	X	X	X	X		X	11
		LWF Bayerische Landesanstalt für Wald und Forstwirtschaft, Abteilung Boden und Klima	2007	X	X	X	X	X	X	X	X	X		X	6
			2008	X	X	X	X	X	X	X	X	X		X	6
			2009	X	X	X	X	X	X	X	X	X		X	6
Hessen	HE	NW-FVA Nordwestdeutsche Forstliche Versuchsanstalt – Abteilung Umweltkontrolle	2007	X	X	X	X	X	X	X	X	X		X	5
			2008	X	X	X	X	X	X	X	X	X		X	5
			2009	X	X	X	X	X	X	X	X	X		X	5
Mecklenburg-Vorpommern	MV	Landesamt für Umwelt, Naturschutz und Geologie	2007	X	X	X	X	X	X	X	X		X		2
			2008	X	X	X	X	X	X	X	X		X		2
			2009	X	X	X	X	X	X	X	X		X		1
Niedersachsen	NI	NLWKN Niedersächsischer Landesbetrieb für Wasserwirtschaft, Küsten- und Naturschutz	2007	X	X	X	X	X	X	X	X	X		X	54
			2008	X	X	X	X	X	X	X	X	X		X	53
			2009	X	X	X	X	X	X	X	X	X		X	53
		NW-FVA Nordwestdeutsche Forstliche Versuchsanstalt – Abteilung Umweltkontrolle	2007	X	X	X	X	X	X	X	X	X		X	1
			2008	X	X							X		X	15
			2009	X	X							X		X	16
Nordrhein-Westfalen	NW	LANUV Landesamt für Natur, Umwelt und Verbraucherschutz; Fachbereich Monitoring,	2007												
			2008												
			2009	X	X	X	X	X	X	X	X			X	3

Rheinland-Pfalz	RP	FAWF Forschungsanstalt für Waldökologie und Forstwirtschaft Rheinland-Pfalz	2007	X	X	X	X	X	X	X	X	X		X	4
			2008	X	X	X	X	X	X	X	X	X		X	4
			2009	X	X	X	X	X	X	X	X	X		X	4
Sachsen	SN	Sächsisches Landesamt für Umwelt, Landwirtschaft und Geologie, Referat Luftqualität	2007	X	X	X	X	X	X	X	X	X	X		10
			2008	X	X	X	X	X	X	X	X	X	X		10
			2009	X	X	X	X	X	X	X	X	X	X		10
Sachsen-Anhalt	ST	LAU Landesamt für Umweltschutz Sachsen-Anhalt	2007	X	X	X	X	X	X	X	X	X	X		2
			2008	X	X	X	X	X	X	X	X	X	X		2
			2009	X	X	X	X	X	X	X	X	X	X		2
Schleswig-Holstein	SH	Landesamt für Landwirtschaft, Umwelt und ländliche Räume des Landes Schleswig-Holstein, Technischer Umweltschutz	2007	X	X	X	X	X	X	X	X	X	X		10
			2008	X	X	X	X	X	X	X	X	X	X		12
			2009	X	X	X	X	X	X	X	X	X	X		11
Thüringen	TH	Thüringen Forst – Anstalt öffentlichen Rechts	2007	X	X	X	X	X	X	X	X	X		X	14
			2008	X	X	X	X	X	X	X	X	X		X	14
			2009	X	X	X	X	X	X	X	X	X		X	14
Bundesverwaltung	BUND	Thünen-Institut für Waldökosysteme	2007	X	X	X	X	X	X	X	X	X		X	70
			2008	X	X	X	X	X	X	X	X	X		X	64
			2009	X	X	X	X	X	X	X	X	X		X	59
		UBA Umweltbundesamt Abteilung Luft	2007	X	X	X	X	X	X	X	X	X	X		15
			2008	X	X	X	X	X	X	X	X	X	X		12
			2009	X	X	X	X	X	X	X	X	X	X		11
Deutscher Wetterdienst	DWD	Observatorium Hohenpeißenberg	2007	X	X	X	X	X	X	X	X	X	X		1
			2008	X	X	X	X	X	X	X	X	X	X		1
			2009	X	X	X	X	X	X	X	X	X	X		1
totals	all		2007	235	235	235	231	231	231	231	231	229	44	191	235
			2008	268	268	253	249	249	249	249	249	262	43	225	268
			2009	266	266	250	246	246	246	246	246	258	40	226	266
total complete sets (green)	all		2007	223	223	223	223	223	223	223	223	223	38	185	223
			2008	238	238	238	238	238	238	238	238	238	37	201	238
			2009	236	236	236	236	236	236	236	236	236	35	201	236
total after quality checks	all		2007	201	201	201	201	201	201	201	201	201	31	170	201
			2008	210	210	210	210	210	210	210	210	210	31	179	210
			2009	191	191	191	191	191	191	191	191	191	31	160	191

2.5.3.3 Quality Assurance, data selection and data transformation

The annual average concentration in the precipitation is computed as the total annual flux divided by the total annual precipitation. A minimum amount of 40% of the data in the time series available for a year needs to be valid. 40% percent is chosen such that not too many stations will fall out of the analysis, while the average of this 40% is representative to the real annual average. The assumption, that the annual average value for a station with more than 40% of valid data is representative for the annual average value for this station, is tested with different subsets of a dataset with 52 weekly measurements in Neuglobsow (see Figure 11). The figure shows the annual average concentration in precipitation for 1000 random subsets of the data for 5 different data availabilities, i.e., 100%, 80%, 60%, 40% and 20%. The standard deviation for these 1000 different subsets is represented by the error bars. The figure shows that the uncertainty in the annual mean concentration increases if data availability is smaller. For example, if a random subset of 20% of the data would be used to calculate the annual mean concentration for SO_4, the answer will be between 1.0 and 1.4 mg/l, with a most likely answer of 1.2 mg/l. If we increase data availability to 40%, the uncertainty reduces by a factor of 2, i.e., 1.2 ± 0.1 mg/l. The maximum error that we make for the annual mean concentration in the precipitation for a data availability of 40% is in the order of 10-20% depending on the component and station considered, e.g., the uncertainty in the K^+ concentrations is much more uncertain than that of SO_4^{2-}.

We initially intended to use the arbitrary 50% criterion, but with the 40% data availability we allow slightly larger errors in the mean, but by taking a lower threshold, we increase the number of stations especially in southern Germany (see Figure 14).

Figure 11. Uncertainty in the annual mean concentration in precipitation for different percentages of data availability for 9 ion components at UBA station Neuglobsow.

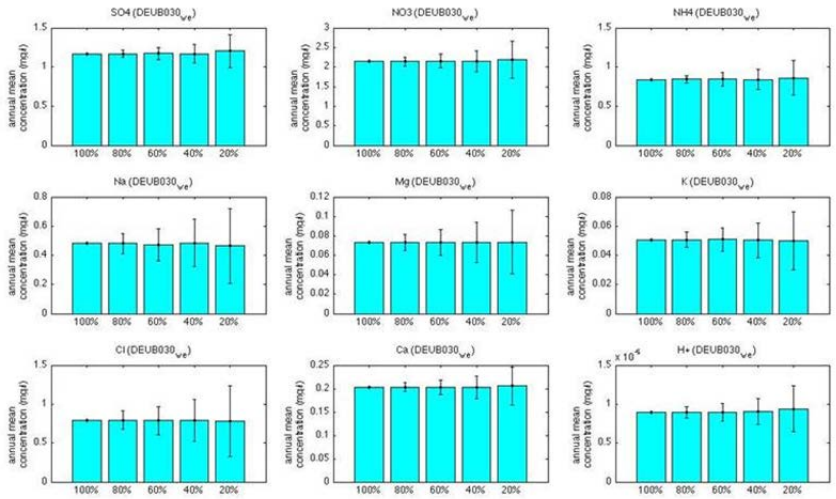

There are several reasons for lower data availability at a measuring station, i.e., no data reported, insufficient or no precipitation, large deviation in ion balance, outliers. These reasons will be discussed in more detail in the following sections.

No data reported

Status flags are reported per observed ion and for the amount of precipitation collected. If the status flag is set to 'no-data', then no observation is present for further unspecified reason.

The top-left panels of Figure 13 and Figure 14 show the fractions of no-data flags for nitrate observations found for the stations in the different networks for the time period 2007 to 2009. For the UBA network most stations have full data coverage for the selected time period, except for one site that observed for only 2 of the 3 years in 2007-2009 (Figure 13). For the other networks the amount of missing data is in the range of 10-80% (Figure 14).

Limited precipitation

No concentrations can be determined if the sampler did not catch any rain at all, i.e., 'no rain', or not enough rain to perform an analysis, i.e., 'tiny rain'. The UBA stations report this situation for about 10% of the time period (Figure 13, middle panels). For the other networks this percentage is more diffuse (Figure 14); since some stations collect precipitation and fluxes over rather long sampling periods (monthly or longer), it becomes unlikely that not a single rain event occurred during a sampling period; in addition, some stations might flag a case with no or hardly rain simply as 'no-data'.

Ion balance check

As a first quality check, each measurement at each measurement station is checked for the ion balance, i.e., the sum of the main ions and cations is calculated. The net ion-charge of the concentrations should be close to zero, thus no bias into positive or negative charges. If the net ion-charge exceeds ±20%, the measurement is rejected, like in the previous project MAPESI (Gauger et al., 2010).

The ion balance (IB) is described by the quality assurance handbook of the UBA monitoring network (2004), according to EMEP (EMEP, 1996) and WMO-GAW report 160 (2004), according to the following equation:

$$IB = ID * 100 / IS \qquad \text{(Eq. 2.4)}$$

with:

- ID = $eq^+ - eq^-$: difference between the sum of cations and the sum of anions
- IS = $eq^+ + eq^-$: sum of total ion concentration
- IB = deviation in %

Insertion of the relevant components leads to the formula:

$$IB[\%] = \frac{(NH_4^+ + Ca^{2+} + Mg^{2+} + K^+ + Na^+ + H^+) - (SO_4^{2-} + NO_3^- + Cl^-)}{(NH_4^+ + Ca^{2+} + Mg^{2+} + K^+ + Na^+ + H^+) + (SO_4^{2-} + NO_3^- + Cl^-)} \cdot 100 \qquad \text{(Eq. 2.5)}$$

The concentrations are given in [meq/l]. If the ion balance for a measurement exceeds ±20%, the specific data are replaced by a missing value status flag in the correspondent data series. To be able to calculate the ion balance following Eq. 2.5 all relevant components need to be available from the analysis of precipitation. In case one or more of the relevant components from Eq. 2.5 are missing, the specific measurement event or even the whole data set cannot be used for the purpose of this project, as a quality check is not possible.

For the time period 2007 to 2009 for the UBA network about 5-20% of the data is rejected due to ion-imbalances (Figure 13, top right). For the other networks, the variation between the stations is larger and about 5-60% of the data is rejected due to ion-imbalance (Figure 14, top right).

Bulk to Wet-only correction

The method that was applied to correct the bulk deposition fluxes for dry deposition into the funnels is based on earlier investigations in which measurements with wet-only samplers and bulk samplers were performed simultaneously (Gauger et al., 2000, 2008). The bulk measurements are reduced to wet-only inputs by means of the mean correction factors as listed in Table 9.

Table 9. Mean ratio between measured wet-only and bulk deposition fluxes (Gauger et al., 2008)

	K^+	Ca^{2+}	Mg^{2+}	Na^+	SO_4^{2-}-S	Cl^-	NO_3^--N	NH_4^+-N	pH	precip	H^+
simultaneous measurements n =	66	65	67	67	87	54	86	79	35	54	37
average ratio wet-only/bulk	0.62	0.63	0.76	0.81	0.82	0.85	0.9	0.95	0.97	1.03	1.34
Maximum	1.44	1.77	1.36	1.47	1.07	1.42	2.01	1.79	1.06	3.00	3.17
Minimum	0.09	0.21	0.18	0.22	0.26	0.32	0.3	0.29	0.83	0.84	0.48
Standard deviation	0.24	0.24	0.25	0.2	0.17	0.19	0.22	0.25	0.06	0.29	0.62

Check on detection limit

Each monitoring network reported a detection limit for each component. The resultant range of detection limits for each component is presented in Table 7.

Whenever the status flag indicates that concentrations are too low to be quantified the concentrations are set to values equal one half of the detection limit.

Synchronization of error flags

If one of the ion concentrations could not be determined and is reported with an error flag, then the total observation might be all corrupted, for example because of external pollution of the collection reservoir. Therefore, if for one of the ions the error flag is set, then the concentrations for the other ions are rejected, as well.

Log-transform

As shown in the example of Figure 10, concentrations of ions in rain water are often very low, but never exactly equal to zero. On the other hand, also extreme high values are rare. The distribution is therefore skewed, as illustrated by the histogram in the left panel of Figure 12.

In statistical analysis it is preferred to work with normal distributions. Therefore, a log-transformation is applied to all concentrations:

$$z = \log(c) \qquad \text{(Eq. 2.6)}$$

The histogram of log-concentrations has now a normal distribution, as shown by the histogram in the right panel of Figure 12.

Figure 12. Histograms of observed sulfate concentrations (left) and of the natural logarithm of the concentrations (right), as computed over all data from the UBA network for the years 2007-2009.

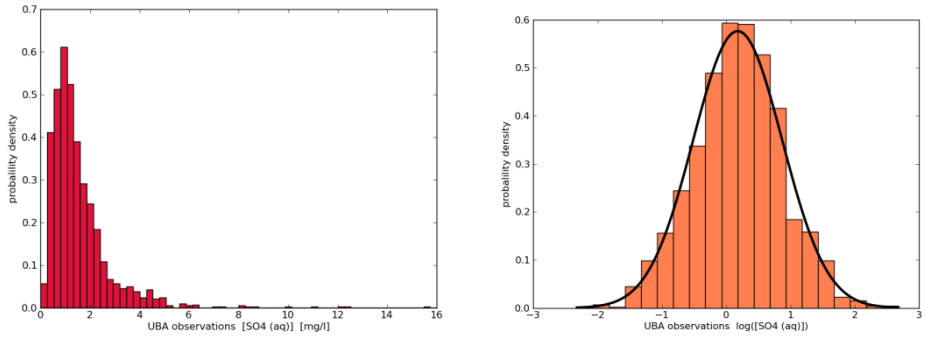

The log-normal distribution is often used in geophysical applications, for example because operations on log-values can never lead to negative real-values after inverse transformation. Formulas for conversion from and to a logarithmic state are available for the relevant statistical properties (here mean and variance). If the value of a log-concentration z is expressed in terms of normal distribution, then:

$$z \sim N(\mu, \sigma^2) \qquad \text{(Eq. 2.7)}$$

If the (arithmetic) mean and variance of a concentration c are known, the (arithmetic) mean and variance of the log-concentration are equal to:

$$\mu = \log\big(E(c)\big) - \frac{1}{2}\log\left(1 + \frac{Var(c)}{E(c)^2}\right) \quad \text{(Eq. 2.8)}$$

$$\sigma^2 = \log\left(1 + \frac{Var(c)}{E(c)^2}\right) \quad \text{(Eq. 2.9)}$$

In reverse, if the parameters of the log-normal distribution are known, then:

$$E(c) = e^{\mu + \frac{\sigma^2}{2}} \quad \text{(Eq. 2.10)}$$

$$Var(c) = \left(e^{\sigma^2} - 1\right)\left(e^{\mu + \frac{\sigma^2}{2}}\right)^2 \quad \text{(Eq. 2.11)}$$

Removal of outliers

An outlier in a time series of observations could strongly influence the results, and these should be removed from the dataset. Therefore, the outliers are removed from each time series over 2007-2009 that is available for a single station.

The algorithm is an implementation of the Grubbs test (Grubbs, 1969), which is an iterative procedure that removes entries from a series if they are regarded as an outlier; the procedure stops if no outliers are found anymore, or too many entries from the series are removed. Here the procedure is applied to the time series of log-concentrations. The algorithm is the following:

1. Compute the mean value of the series.
2. Select the value with the largest distance to the mean for removal; this is potentially an outlier.
3. Compute over the remaining samples the mean and the standard deviation.
4. Compute the distance between the selected sample and the new mean.
    a) If the distance is more than 3 times the standard deviation, then it is defined as an outlier, and is removed permanently from the time series.
    b) If the distance is smaller, then the selected sample is not regarded as an outlier; the screening procedure could stop.
5. If the new time series has 10 or less values, it is too short to compute reliable statistics for outlier detection, and therefore rejected completely.
6. The procedure starts again with step 1 to search for other outliers.

About 5% of the data of the UBA network is removed by the outlier screening (Figure 13, lower left); for the Länder data, this is in the range of 5-20% (Figure 14, lower left).

Combination of near-by stations

For the network of Länder stations it might occur that two or more stations are located close to each other. If the observations from these stations differ significantly from each other, the Kriging procedure might produce unrealistic gradients in the vicinity of these stations, since the current procedure uses a single variogram model for the entire domain (global homogeneity). The assumed observation error is with this assumption an average value that might be smaller than the locally found difference between nearby sites suggests. To avoid this problem, the time series from stations that are within about 1.3 km (0.01 degrees latitude/longitude) from each other are replaced by a single average. The original time series are thereto first homogenized into daily resolution, with for each day of an original period the same concentration and an equal contribution to the accumulated precipitation.

Computation of yearly averages

The Kriging procedure will be applied to yearly average values. A time series of observations should cover at least 40% of the year before a yearly average is computed; otherwise, it is rejected from the procedure.

For the stations in the UBA network about 60-70% of the possible data is present and not rejected by any of the screening procedures; yearly average values could therefore be computed for all of them. For the Länder stations the amount of valid data shows more variance, with fractions in a range of 10-90%.Note that even for an availability of 90% the actual number of data values might be limited, since some of the regional stations observe monthly values only.

Figure 15 shows the stations with sufficient data density for SO_4^{2-} after quality assurance for the years 2008 and 2009. Figure 15 illustrates that the amount of stations with sufficient data density is higher in 2008 than in 2009.

Figure 13. Fractions of nitrate concentrations in the data from the UBA network that were rejected for a particular reason, and the remaining data that is considered to be valid for usage in the Kriging procedure.

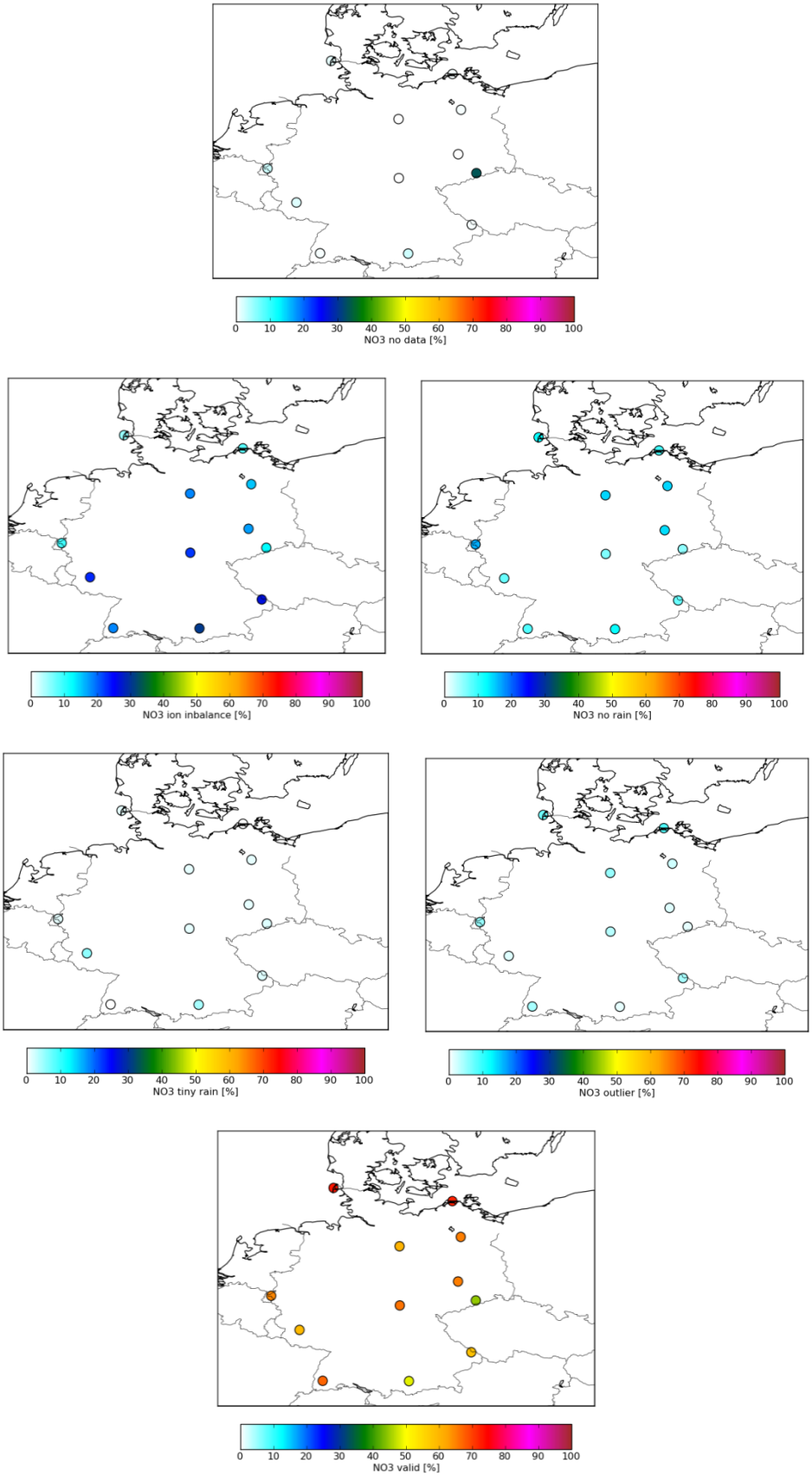

Figure 14. As the previous figure, but now for the Länder data.

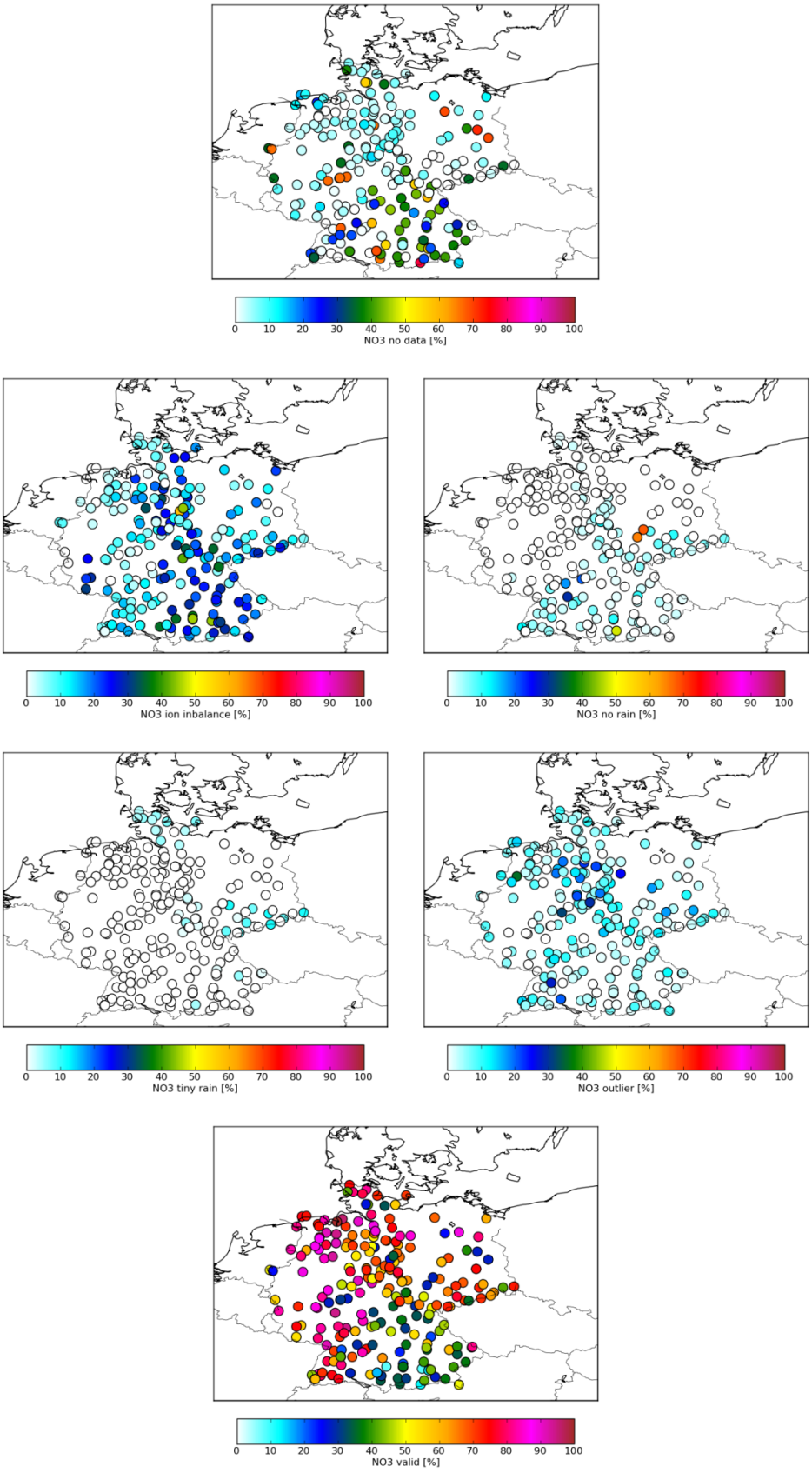

Figure 15. stations with sufficient data density for SO_4^{2-} after quality assurance for the years 2008 (a) and 2009 (b)

(a) (b)

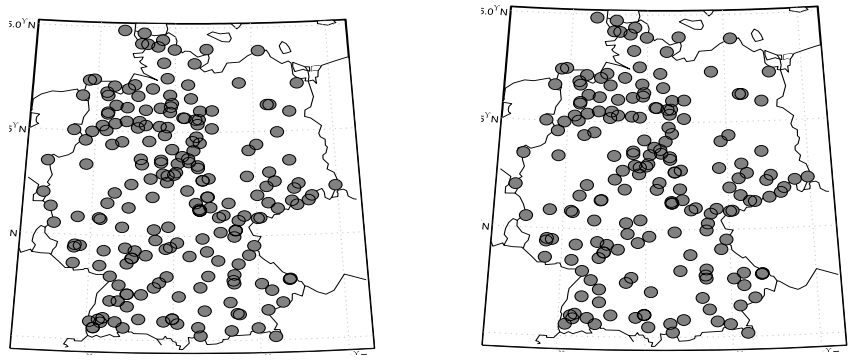

2.5.4 Kriging of wet deposition observations

2.5.4.1 Introduction

Wet deposition is an important removal process for pollutants from the atmosphere. A rain shower is able to clean up parts of the atmosphere in a short time period.

Wet deposition fields could be obtained by using observations and/or model simulations. Observations are performed by collecting rain water and analyzing its ion composition. These data provide a valid estimate of the wet deposition at the observation site. To cover a large area, an expensive network of observation sites is needed. Model simulations are in that respect cheaper, since they could provide simulations at virtually all locations. However, simulation of concentrations in rain water with a model is rather difficult. A simulation of wet-deposition relies strongly on simulation of the atmospheric concentrations as well as the amount, location, and time span of rain events. Simulated wet deposition fluxes could therefore differ substantially from the observations. This is illustrated in Figure 16 where it shows that LOTOS-EUROS generally underestimates the average of and the variability in the observed wet deposition fluxes.

Combination of observations and simulations provide a valuable area-wide estimate of the wet deposition field as the model information is used to interpolate between the measurements. A common technique to combine observations and simulations is the use of a Kriging method. The technique was developed during the nineteen fifties/sixties for applications in geo-sciences, and has found its way to many other disciplines, too (Cressi, 1993). The remainder of this chapter describes how the Kriging technique has been used to combine observations of concentrations in rain water at sites in Germany with simulations of the LOTOS-EUROS model.

Figure 16. Statistical comparison of LOTOS-EUROS modeled (Mod) and observed (OBS) wet deposition fluxes across all wet deposition sites used in PINETI (>100 stations)

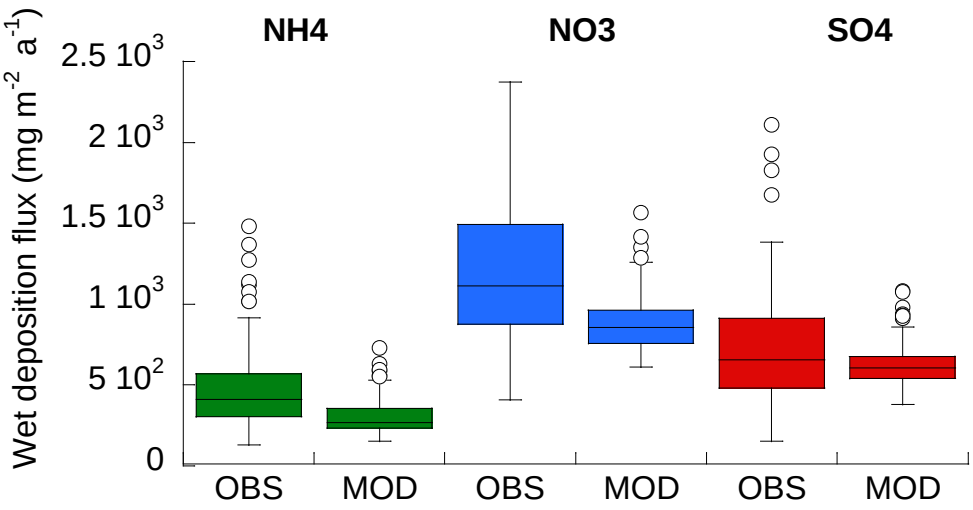

2.5.4.2 The Kriging method

To apply a Kriging technique, the following elements should be present:

- A set of spatially distributed observations.
- A specification of the (assumed) spatial covariance present in a field of the observed entity. This includes a specification of the uncertainty present in the observations too.
- A target grid, e.g. a domain and resolution on which an estimate of the observed entity should be presented.

What is defined as 'observations' could differ per application. The observations could be real observed quantities, in which case the Kriging method acts as an interpolator between observation sites. Alternatively, the observations could also denote a difference between a real observation and its simulation by a model; in that case, the Kriging procedure acts as an interpolation between observations and model.

The different components of the Kriging procedure used in this study are discussed in the following sections.

2.5.4.3 Yearly averages or averages over the year?

The end result of the method should be a set of maps with the best possible estimate of the average aqueous concentrations of various tracers. Two options have been considered for this:

1. Application of the Kriging method directly on yearly average observations. Since only one Kriging operation has to be performed per year, the result can be obtained fast. It might be hampered however by the fact that yearly average observations are influenced by extreme rain events, and time series might have gaps without any data. In addition, a substantial amount of yearly averages should be available with high spatial coverage. For the Länder networks this is available, but the UBA network is not dens enough.

2. Application of the Kriging method on a higher frequency (monthly, weekly, or even daily), and computation of the yearly average afterwards.

   This option is computationally more expensive. It will be necessary to harmonize the time series of observations onto a joint temporal resolution. The only suitable temporal resolution is probably daily, since this is the only common frequency between stations reporting on weekly, two-weekly, monthly, or even 2-monhly base with different start and end dates for each period.

To limit the computation demand, the first option was chosen for the current project, thus application of the Kriging method only once per year based on yearly averages. However, as we shall see in the following sections, the temporal information present in the observation time series will still be used to some extend in the determination of the variogram model used in the Kriging procedure.

2.5.4.4 Spatial variability models

Definition

To infer values at unobserved locations from the values at the measurement sites, a model for the spatial correlation is needed. In the Kriging procedure the spatial correlation is expressed in terms of the semi-variance between two data at locations x_1 and x_2 of the field of interest $Z(x)$:

$$\gamma(x_1, y_2) = \frac{1}{2} Var[Z(x_1) - Z(x_2)] \quad \text{(Eq. 2.12)}$$

The function $\gamma(x_1,x_2)$ is sometimes referred to as the 'semi'-variogram, where the 'semi' refers to the ½ factor. The name 'variogram' is in that case reserved for:

$$2\,\gamma(x_1, y_2) = Var[Z(x_1) - Z(x_2)] \quad \text{(Eq. 2.13)}$$

However, this difference is a constant source of confusion. Bachmaier and Backes (2011) stated that the name 'semi'-variogram should not be used, since the half factor is a natural element of the definition and should not be amplified. Here we will follow this convention too, and use the name 'variogram' for the function defined above.

The variogram is related to the covariance function:

$$c(x_1, x_2) = E[(Z(x_1) - E[Z(x_1)])(Z(x_2) - E[Z(x_2)])] \quad \text{(Eq. 2.14)}$$

by:

$$\gamma(x_1, x_2) = 1/2(\,Var[Z(x_1)] + Var[Z(x_2)] - 2\,P(x_1, x_2) + (E[Z(x_1)] - E[Z(x_2)])^2) \quad \text{(Eq. 2.15)}$$

If the statistical properties of the field *Z(x)* are independent of *x*, e.g.

$$E[Z(x_1)] = E[Z(x_2)] = \mu \qquad Var[Z(x_1)] = Var[Z(x_2)] = \sigma^2 \qquad \text{(Eq. 2.16)}$$

the field is called stationary, and the covariance and variogram reduce to:

$$c(x_1, x_2) = c_s(x_1 - x_2) = c_s(r)$$
$$\gamma(x_1, x_2) = \gamma_s(x_1 - x_2) = \gamma_s(r) = c(0) - c_s(r) \qquad \text{(Eq. 2.17)}$$

where r is the distance between the locations x_1 and x_2. For large distances the covariances between two locations will vanish to zero, and the variogram will reduce to the over-all variance:

$$\lim_{r\to\infty} \gamma_s(r) = c_s(0) = \sigma^2 \qquad \text{(Eq. 2.18)}$$

Spatial variability model based on variogram of yearly averages

The first step in deriving a spatial variability model for the concentrations in rainwater is to estimate the variogram from the available observations, as a function of the distance between the observation sites. In this study, the yearly average log-concentrations will be used as described in section 2.5.3.3. To have enough samples available to compute statistics, the spatial variability model will be based on the samples from all 3 available years, i.e., 2007, 2008 and 2009, together. In the combined data sets from the UBA and Länder networks for these years, many pairs of observations can be found at any distance. The average variance is calculated for each distance increment (lag size) of 25 km if at least 50 pairs (x_i , x_j) are available:

$$\gamma_s(r) \approx {}^1\!/_2 \frac{1}{|Q(r)|} \sum_{(i,j)\in Q(r)} \left(Z_i - Z_j\right)^2 \qquad \text{(Eq. 2.19)}$$

An example of a computed empirical variogram is shown in Figure 17. The variogram increases with distance, since the observations become less correlated. The sample variance is a reasonable estimate for the sill (i.e. the theoretical maximum of the variogram). In the figure it is seen that the computed variances exceed this number in this case after distances of more than 400 km. This can be explained from the fact that the assumption of a stationary field is probably not valid. If a gradient in the field is present, the mean is not represented well everywhere by a single constant value. At large distance from each other, samples could therefore become anti-correlated with respect to the joint mean, and the variance could exceed the overall value. At short distances however, the variogram is still valid since it reflects the

variability on local scale which is not influenced by the large scale gradient. From zero to nearly-zero distance the variogram shows a jump, which partly reflects the intrinsic uncertainty in the observations as well as the stochastic nature of the atmosphere.

Figure 17. Empirical variogram for yearly average log-concentration differences of nitrate (circles). All station pairs of the network are grouped into 25 Km distance intervals and includes the studied three years. The orange line denotes the overall variance over all samples in the network. The fitted variogram model is added in red, as well as a description of its shape

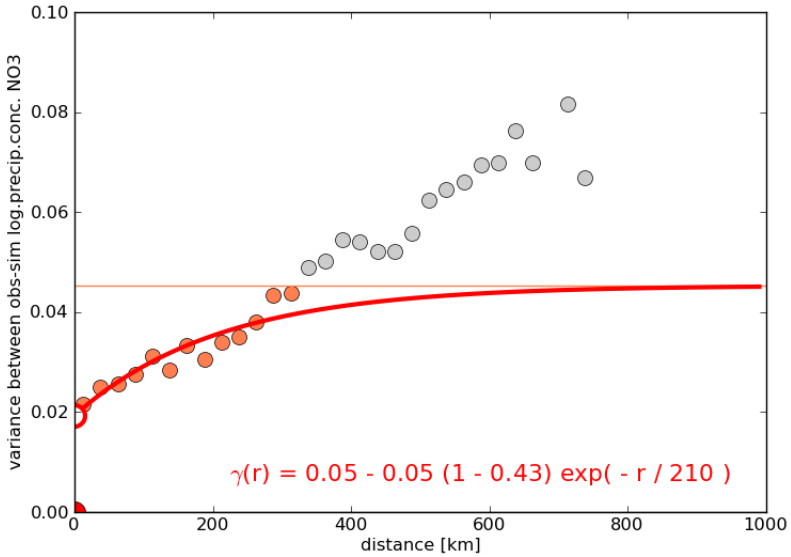

The next step in the procedure is to fit a variogram function to the data. An exponential curve was found to be a proper estimate of the observed decay in the covariances . The following function is therefore used to describe the variogram:

$$\gamma_s(r) = \begin{cases} 0 & ,r = 0 \\ s - (s-\eta)\exp\left(-\frac{r}{L}\right) & ,r > 0 \end{cases} \qquad \text{(Eq. 2.20)}$$

In here, r is the distance between the observation sites, and L is the length scale of the spatial decay. As the data are distributed over an area much larger than the variogram range (<600 km) the overall sample variance should provide a reasonable (heuristic) estimate of the variogram sill. The nugget value η is the limit value of the variogram for distances approaching towards zero. The discontinuity at zero distance (the presence of a nugget value) is related to the instrumental error. If two observations are made next to each other with similar equipment, the time series won't be exactly the same since both suffer from random instrumental errors. The correlation at near-zero distance will therefore not be equal to 1.0 but somewhat less, and therefore the covariance is not continuous but will show a drop at zero. For the Kriging procedure the relevant parameter is actually the ratio between nugget and sill (η/s),

which represents the relative instrumental error. The variogram model is therefore rewritten into:

$$\gamma_s(r) = \begin{cases} 0 & ,r = 0 \\ s - s(1 - \eta/s)\exp(-\frac{r}{L}) & ,r > 0 \end{cases} \quad \text{(Eq. 2.21)}$$

To fit the model to the computed covariances, first the sill value is set to overall sample variance. Then, nugget and length scale are determined using a least-squares fit.

The computed variograms are provided in Appendix A: spatial variability models, together with other spatial variability models. In each of the tables, the variogram obtained from the yearly averaged concentrations are shown in the upper-left corner. A description of the variogram with the obtained values for s, η/s, and L, is added as text to the figures.

For most of the components, the sampled variances show a clear decay towards a nugget value at zero distance. Exceptions are those found for Na^+ and Ca^{2+}, which suffer from a large overall gradient in the domain (Na^+) or other irregular patterns (Ca^{2+}). The variogram length scale parameters L found are about 250 km. The nugget/sill ratios are in a range of 18% for SO_4^{2-} to 74% for K^+, with outliers for Na^+ and Ca^{2+} due to the problematic fitting.

As the results for Na^+ and Ca^{2+} show, the variogram model could be rather sensitive for the data selection. The yearly averages used here might be influenced by exceptional values, although the outlier filtering should have removed most of them. In addition, the computation of a yearly average might suffer from the data gaps and different temporal resolutions present in time series. A more robust result could be obtained if the original time series are maintained as much as possible, which would substantially increase the amount of data. A procedure to do this is given in the next section.

Spatial variability model based on covariances in time series

By analyzing the original time series of observations, the amount of data available to determine spatial variability increases significantly. A time series is considered as a set of independent samples. If the number of samples is large enough, the covariance between two sets (two time series) observed at different locations is a measure for the spatial variability.

As shown above, the variogram used in the Kriging procedure could be expressed as a covariance too:

$$\gamma_s(r) = c_s(0) - c_s(r) \quad \text{(Eq. 2.22)}$$

In this section we will use the covariance representation instead of the variogram, since the first is more common used when analyzing time series.

The first step in the procedure is to make a collection of all possible pairs of stations. For each pair, the time series of observations should be harmonized onto the same time axis. For the

UBA network, where all sites observe with a weekly frequency, this requirement is automatically fulfilled. For the Länder data however, which is presented on a wide variety of temporal resolutions, this requirement is implemented by first creating time series of daily values by assigning the observations valid for a time interval (weekly, or monthly, etc) to each of the individual days. The two time series in a pair should have a significant number of data values available at the same times to be able to compute their covariance.

For the weekly UBA data a minimum of 50 common values is required, and for the to-daily-distributed Länder data, the threshold was set to 300 common values; in both cases, that means that the stations should have observed at the same times during 1/3 of the 3 year period 2007-2009.

Then, for each pair, the covariance between the time series of the log-concentrations is computed and plotted versus the distance between the sites. Figure 18 shows examples of this for the nitrate observations from the two networks. The plots show that, as expected, the covariance decreases with distance, although especially for the data from the Länder networks the result is rather noisy. Experiments showed that the computation of covariances is rather sensitive to the data screening; especially the removal of outliers helped to limit the scatter. The figures also include covariances computed over time series with less elements than the required minimum, which are not found to be very different; the length of the time series therefore seems to be sufficient for computation of the covariances. The wide spread in temporal resolutions and observation methods present in the Länder data hampers the reduction of noise in the results; a more intensive study on harmonization of this data and implementation of screening methods dedicated to computation of the spatial covariances would be useful.

Figure 18. Spatial covariances between aqueous log-concentrations of nitrate observed at sites in the UBA network as (left) or the Länder networks (right), as a function of their distance. The grey dots are covariances found without any restrictions on the data availability; the total number of pairs and the number of pairs with minimum joint coverage are displayed at the top. The red line is the exponential correlation function with sill value fitted through the data, the parameters of the fit are shown in red.

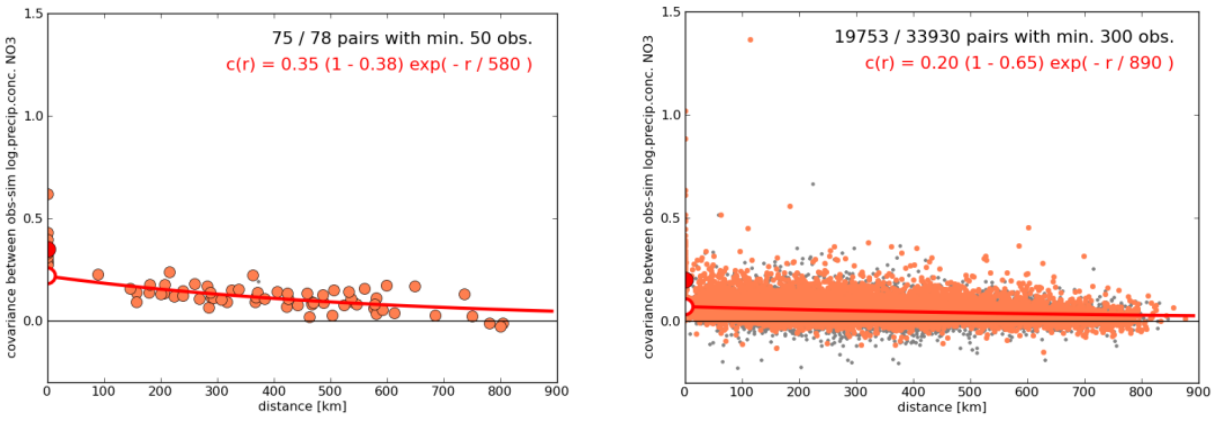

The next step in the procedure is the fitting of a covariance function to the data. Similar as for the variogram method, an exponential curve was found to be a proper estimate of the observed decay in the covariances. The following function is therefore used to describe the covariance:

$$c_s(r) = \begin{cases} s & ,r = 0 \\ s(1 - \eta/s)\exp\left(-\frac{r}{L}\right) & ,r > 0 \end{cases} \qquad \text{(Eq. 2.23)}$$

The interpretation of the sill value s, the nugget η, and the len
variogram. To fit the model to the computed covariances, first the sill value is set to the mean of the variances obtained for the individual sites; an alternative would have been to simply take the variance over all available samples. Then, nugget and length scale are determined using a least-squares fit.

Figures of all sampled covariances and fitted covariance models are in Appendix A: spatial variability models; the middle and lower panel of the left column show the results based on UBA and all data respectively. As seen already for the nitrate observations, the covariances found in the Länder data are much more scattered than those found for the UBA data. The covariance length scales present in the UBA data is in the range of 400-600 km; for the Länder data much longer scales are sometimes found. The nugget/sill ratio representing the relative observation error are for the UBA stations in a range of 33-43% for the inorganic components, which is in agreement with the 30% error variance fraction found in section 2.5.3; for the base cations, the ratio is in a range of 15% for Na^+ to 55% for K^+. For the covariances including the Länder data, the results are more scattered.

Discussion

As the results in Appendix A: spatial variability models show, the description of the spatial variability (length scales, nugget/sill ratios) could differ significantly based on the chosen method. As will be shown in section 2.5.4.7, the best results for the residual Kriging method are obtained with the variability model based on covariance between harmonized times series using all data; especially the rather low nugget/sill ratio improves the results here. Since this product is regarded as the final one, we choose to use the variability models based on harmonized times series from all stations for the Kriging.

This choice is subject of discussion, and might change in future when more data become available. For a consistent procedure, the spatial variability should have been calculated over yearly averaged concentrations, since it will be used to analyze yearly averages too. However, only 3 years of observation data were available for this study, which is too short to compute covariances based on yearly averages. Therefore, the spatial variability models will be based on the best available common temporal resolutions, which is weekly for the UBA data and daily-equivalent for the Länder data.

A dedicated study on the construction of suitable covariance models is left for future research. If yearly averaged concentrations will be used, the study should focus on how to improve their computation taking into account data gaps and outliers. If higher temporal resolutions are used, the harmonization procedure should get more attention, including how representative monthly averages are for weekly or daily values. Another option is to use a localized approach for the variability model, with different parameterizations for each point in the domain based on locally available observations only, instead of estimating numbers valid for the whole domain.

2.5.4.5 Kriging procedure

Kriging is a statistical technique that can be used to obtain an estimate of a field of values given isolated observations (Cressi, 1993). It could therefore be seen as an interpolation method that fills the gaps between observations. The result is a field that is exactly equal to the observations at the observation locations, and is a weighted average of the observations in between them. The Kriging or analyzed field is accompanied with an accuracy estimate in terms of an error variance. Observation errors have no impact on the analyzed field, but only on the computed error variance.

The two most popular Kriging methods are *simple* and *ordinary* Kriging. The difference between these two is mainly in the assumption on the mean value of the field: for simple Kriging a zero value is assumed, and for ordinary Kriging it is set to the average of the observations. In this study we will use the ordinary method, since no other knowledge on the mean value is available and therefore the average of the observations is a suitable first guess.

Kriging equations

The target of the Kriging procedure is to obtain an estimate of the variable *Z(x)* on spatial locations *x*. In this application, *Z*(x) is a 2D field of ion log-concentrations in rain water. The value of *Z* at a particular location is expressed in terms of a probability density of a normal distribution, and is therefore described completely by a mean and a variance:

$$\mu(x) = \mathrm{E}[Z(x)]$$
$$\sigma^2(x) = \mathrm{E}[(Z(x) - \mu(x))^2] \qquad \text{(Eq. 2.24)}$$

To let (μ,σ^2) represent the best possible description of the field, the variance should be as small as possible.

For the ordinary Kriging method, the following assumptions and requirements are needed:

The mean or expected value of the distribution of *Z(x)* is an unknown constant:

$$\mathrm{E}[Z(x)] = \mu(x) = \mu_0 \qquad \text{(Eq. 2.25)}$$

The spatial covariance between two locations is known:

$$\mathrm{Cov}[Z(x_1), Z(x_2)] = c(x_1, x_2) \qquad \text{(Eq. 2.26)}$$

In this study we will use the spatial homogeneous covariance functions defined in section 2.5.4.3, thus:

$$\mathrm{Cov}[Z(x_1), Z(x_2)] = c_s(|x_1 - x_2|) \qquad \text{(Eq. 2.27)}$$

The Kriging estimator is now defined as a field $Z_K(x)$ that at every possible location x is formed from a weighted combination of the available observations $z_1,..,z_n$:

$$Z_K(x) = \sum_{i=1}^{n} \lambda_i(x)\, z_i \qquad \text{(Eq. 2.28)}$$

The interpolation weights $\lambda_i(x)$ are chosen such that the expected value of the estimator matches with the assumed expectation of the (true) field, and that the expected difference between the estimator and the (true) field is as small as possible in terms of its variance:

$$\mathrm{E}[Z_K(x)] = \mu_0$$
$$\mathrm{Var}[Z_K(x) - Z(x)] = S_K^2(x) = \text{ minimal} \qquad \text{(Eq. 2.29)}$$

Under these requirements, the interpolation weights (and in addition the expected mean value μ) should be solved from the following system:

$$\begin{pmatrix} c(x_1,x_1) & \cdots & c(x_1,x_n) & 1 \\ \vdots & \ddots & \vdots & \vdots \\ c(x_n,x_1) & \ldots & c(x_n,x_n) & 1 \\ 1 & \ldots & 1 & 0 \end{pmatrix} \begin{pmatrix} \lambda_1(x) \\ \vdots \\ \lambda_n(x) \\ \mu_0 \end{pmatrix} = \begin{pmatrix} c(x_n,x) \\ \vdots \\ c(x_n,x) \\ 1 \end{pmatrix} \qquad \text{(Eq. 2.30)}$$

or in matrix-vector notation:

$$\boldsymbol{A}\,\boldsymbol{\lambda}(x) = \boldsymbol{b}(x) \qquad \text{(Eq. 2.31)}$$

The last equation in the system ensures that the sum of the interpolation weights is equal to one (unbiased condition). For the variance of the error in the Kriging estimate the following expression is available:

$$S_K^2(x) = \boldsymbol{b}(x)^T \boldsymbol{\lambda}(x) \qquad \text{(Eq. 2.32)}$$

Note that in this system the A matrix only depends on the observation locations; the right-hand side b depends on the location x. The system needs to be solved many times, e.g. for all locations x in the domain of interest. For computation efficiency it is therefore preferable to use an algorithm that can solve the system for multiple right-hand sides.

The Kriging procedure is illustrated in Figure 19 for a 1-dimensional example. The input to the procedure is a set of 3 observations (colored squares in upper panel), for which also observation errors are prescribed (error bars).

The observation error is used as a sill value, which together with an assumed spatial correlation length describes at each location the covariance with the observation location; the values are shown in the lower panel. For each location, the matrix system is solved with a different right-hand side, providing the weight factors for the contributions of each observation. Their values are plotted in the middle panel. The highest weight is assigned to the nearby observation, but due to the assumed observation errors all observations contribute everywhere. Far away from the observations the Kriging estimator will converge to a common mean value. The error in the Kriging estimator is displayed in the upper panel in terms of a 1-standard deviation band around the estimator; the smallest values are found near the observations.

Figure 19. Example of ordinary Kriging in a single dimension. The top panel shows three observations including an observation error distributed along the axis. The (prescribed) spatial covariance with each of the three observation locations is shown in the bottom panel. The middle panel shows the interpolation weights for each position. The resulting Kriging estimate is plotted in the top panel as a solid line in the top panel, with the 1-standard deviation Kriging error as dashed lines.

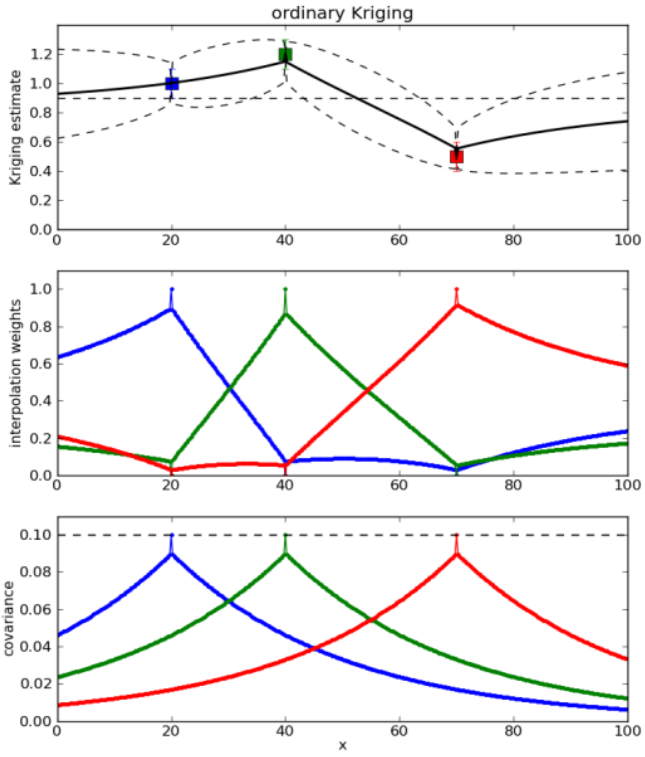

2.5.4.6 Observational Kriging

In a first application, the Kriging procedure has been applied to the observed concentrations. The use of Kriging in this way is often referred to as *observational* Kriging.

Figure 20 illustrates the data flow for the current application. All concentrations available from the observation data (including error definition) are transformed into log-concentrations following the formula in section 2.5.3.3.

To this dataset the Kriging procedure is applied, including an estimation of a spatial variability model following the procedure described in section 2.5.4.4 . The result is formed by 2D fields representing the analyzed (or Kriging) estimate and the associated error field. Finally, the inverse-log-transform from section 2.5.3.3 is applied to obtain an analyzed mean and uncertainty for real concentrations.

Figure 20. Data flow during Kriging of observations.

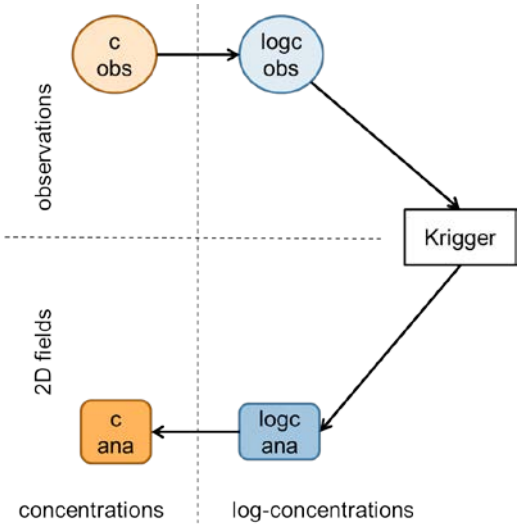

An example of the input, intermediate fields, and final results is shown in Figure 21. Here, the Kriging procedure is applied to yearly average nitrate concentration from the UBA network for 2008. The figures show the mean values (left column) as well as the associated error standard deviation (right column).

The top panel shows the values for the observed concentrations. Note that the constant background field of 1 for the mean values is an artifact of the combined implementation of observational and residual Kriging, which will be explained in the next section; the only relevant data in this panel are the concentrations at the observation sites.

The second panel shows the observed values after log-transformation. This will be used as input for the Kriging procedure. The spatial correlation model is based on the 3-year time series of observation available for the shown network.

After application of the Kriging procedure, an estimate of the log-concentrations is available at the full domain. The field approximates the observed values in the vicinity of the stations, showing elevated values in two regions. To the edge of the domain, where no stations are nearby, the Kriging estimate converges to a constant value. The associated standard deviation field (an estimate of the quality) is high near the edges, and drops to lower values near the site locations since the availability of observations decreases the uncertainty here. The decreased uncertainty is the same for all stations due to the assumption of a constant error fraction of 30% (absolute values in a range from 0.05 to 0.13 in this example), which becomes an additive error with constant variance after the log-transformation.

The final row shows the mean and error of the concentrations, which has similar features as the log-transformed results.

Figure 21. Example of the Kriging input, intermediate fields, and final result for application of observational Kriging to yearly-average nitrate concentrations from the UBA network for 2008. Left: Kriging field (mean values); right: quality estimate (std.dev.). Rows from top to bottom: observed concentrations, log-transform, Kriging estimates, and analyzed concentrations after inverse log-transform.

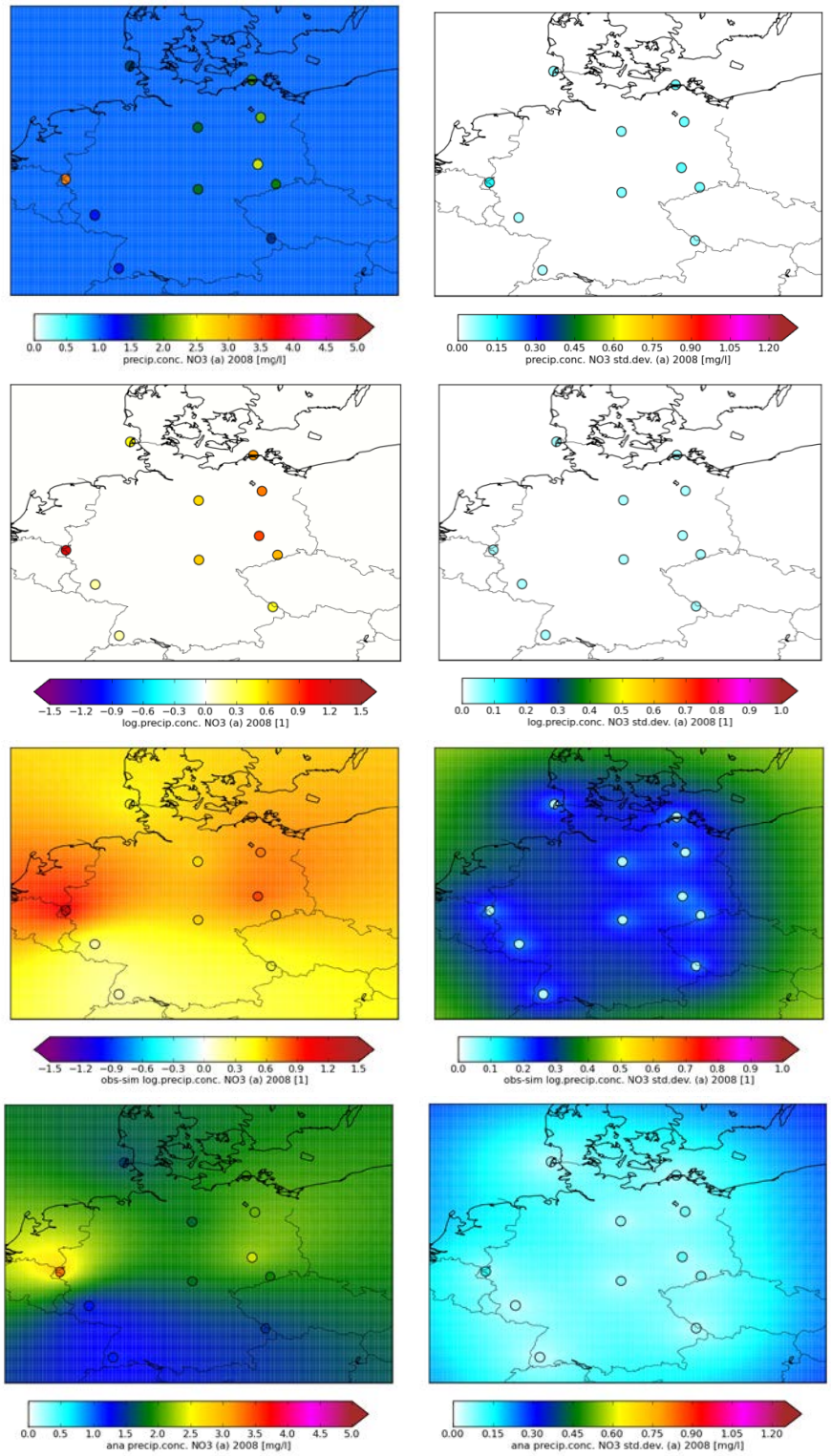

2.5.4.7 Residual Kriging of model simulations

The LOTOS-EUROS model in general underestimates concentration in precipitation in comparison to observations (Figure 19). Thus, in a second application, the Kriging procedure was applied to the difference between observations and model simulations from the LOTOS-EUROS model. This application is often referred to as residual Kriging. In another study by Denby et al. (2008) residual Kriging was also applied to this model to combine simulations of PM with observations.

The data flow for the residual Kriging in this study is shown in Figure 22. A second input is provided by a simulation model. The model produces 2D fields of concentrations, for which we assume a zero error when transforming to log-concentrations. The log-concentration fields from the model are sampled at the station locations and provide simulated log-concentrations.

The idea behind residual Kriging is now to obtain a 2D correction field distributing the difference between observed and simulated log-concentrations in space. This correction field is then added to the simulated log-concentration field. After inverse log-transformation to concentrations, the result is a model field that is corrected for the bias with the observations by multiplication with a field with correction factors. The difference between simulated and observed log-concentrations (the residue) is computed, and used as input for the Kriging procedure.

Similar as for the observational Kriging, the spatial covariance functions are based on time series of residues. The results are shown in Appendix A: spatial variability models in the right column of the tables. The covariance functions obtained with residual Kriging can differ significantly from the covariance functions obtained for the observational Kriging. In general, the length scales are shorter and the nugget/sill ratios are smaller. This is an indication that the large scale patterns are indeed captured by the model, and the residues that are left have a smaller amplitude and are spatially less correlated. The sill values are larger, however. This is a result of the log-transformation of simulations with a wide range of values, which leads to a wide range of differences between simulated and observed log-concentrations too. For the observational Kriging, the ‘simulated’ log-concentration is not present and therefore implicitly equal to zero; the range of ‘differences’ is therefore smaller.

Figure 22. Illustration of the data flow in the residual Kriging procedure.

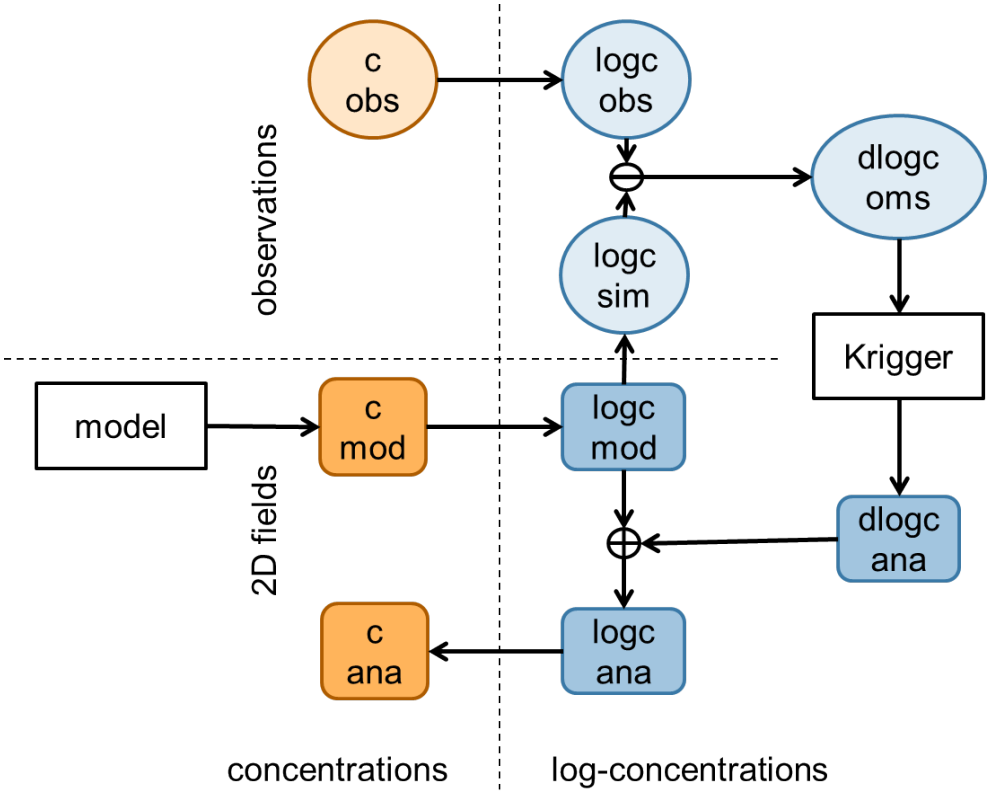

Comparing the spatial variability parameters based on yearly averages (variograms) and harmonized time series (spatial covariances), the latter has smallest nugget/sill ratios. Especially for nitrate the difference is significant, with a value of 61% for the variograms based on yearly averages and only 6% for the spatial covariances based on the time-series, respectively. The difference between observed and analyzed values will therefore be much smaller using the second approach, as illustrated by scatter plots of analyzed versus observed values in Figure 24. For this, the spatial variability model used throughout this study has been based on the harmonized time series.

After application of the Kriging procedure, a 2D field with residue corrections is obtained. These are added to the (log-transformed) model fields that were also used to compute the difference-values. The result is then inversely log-transformed to obtain a 2D field of concentration values again.

The procedure used for residual Kriging is actually a generalization of the procedure for observational Kriging. If the model field is set to a constant value of 1, then the log-transformation becomes zero and effectively an observational Kriging procedure is applied. The unity background field in the upper left panel of Figure 21 is the result of this.

The net result of the log-transformations is that the concentration field is adjusted with a correction factor field. The Kriging procedure provides a field of correction values that is added to the modeled field in log-space:

$$\mu_{ana} = \mu_{mod} + \delta\mu_K \quad \text{(Eq. 2.33)}$$

After reverse log-transform, the analyzed concentration mean becomes (using the zero assumption for the model error):

$$\mathrm{E}[c_{ana}] = \exp(\mu_{mod} + \delta\mu_K + \sigma_K^2/2) = E[c_{mod}] \times \exp(\delta\mu_K + \sigma_K^2/2) \quad \text{(Eq. 2.34)}$$

Due to the exponential function, the correction factors are always positive which ensures that concentrations cannot become negative.

Examples of the input, intermediate fields, and final results of the residual Kriging procedure are shown in Figure 23. Similar as for the example of observational Kriging, the procedure is applied to the 2008 yearly average nitrate concentrations, using observations from the UBA network and simulations from the LOTOS-EUROS model. The figures show the mean values (left column) as well as the associated error standard deviation (right column).

The top panel shows the values for the observed concentrations in the station locations, and the simulated concentrations in the background. The model clearly underestimates the observations in this case. A gradient over the domain is visible for the simulations, with lower values in west and south and higher values to the east, which is not reflected by the observations.

The second row shows the same values after log-transformation. The difference between observations and simulations seen here (the residues) form the input for the Kriging procedure.

The correction fields computed by the Kriging algorithm are shown on the third row. The field approximates the residue values in the vicinity of the stations, with a strong increment around a site near the border with The Netherlands due to the relatively large difference between the observed and the simulated concentration here. The associated error field is high near the edges, and drops to lower values near the site locations; since no error was assigned to the model simulations, the error computation is based on the assumed observation errors only, and therefore the same as for the observational Kriging.

The final row shows the mean and error of the concentrations, obtained after adding the correction field to the original modeled log-concentrations and application of the inverse log-transform. The result shows much more spatial structures than before the correction, with for example strongly increased concentrations near the border with the Netherlands.

Figure 23. Example of the Kriging input, intermediate, and output fields for application of residual Kriging to yearly-average nitrate concentrations from the UBA network and the LOTOS-EUROS model for 2008. Left: mean values; right: error. Rows from top to bottom: concentrations, log-transform, correction field from Kriging, and analyzed concentrations after adding correction to log-concentration field from the model and inverse log-transform.

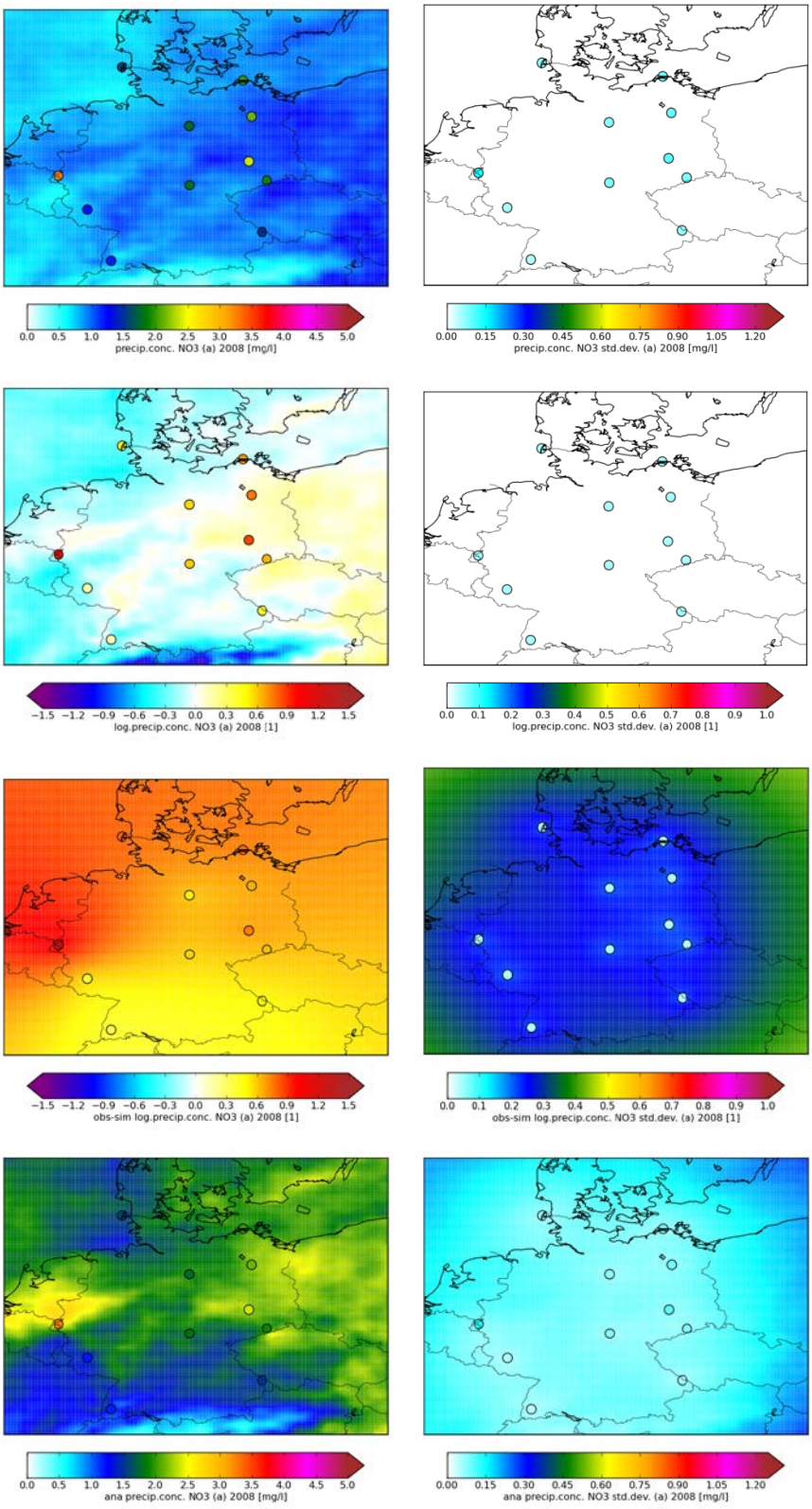

Figure 24. Difference between observed and analyzed nitrate concentrations for each of the available stations, obtained with residual Kriging using the variogram model (left) and using the covariance between harmonized time series (right). The scatter in the later version is much smaller due to the smaller nugget/sill ratios.

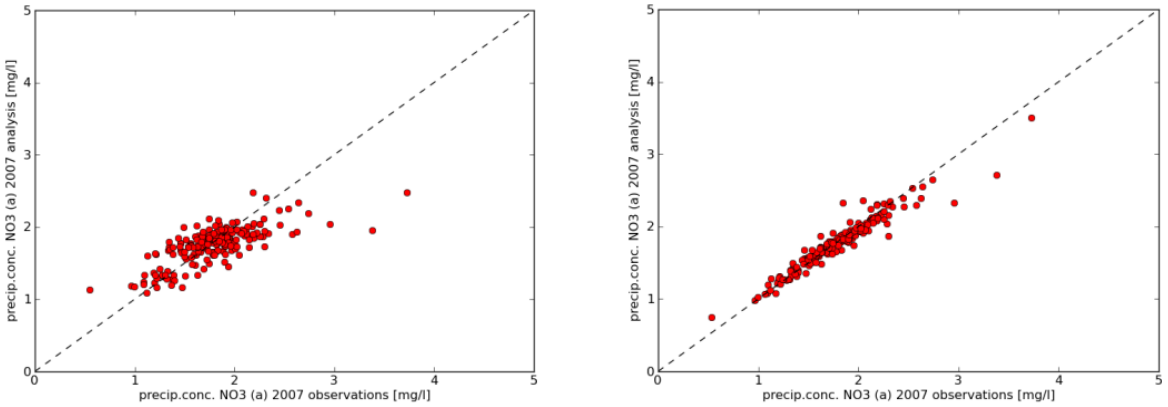

2.5.5 Analysis and validation sites

For proper validation of data-assimilations like Kriging it is essential to divide the available observations in two groups. The first group consists of the observations that will be used in the analysis as input for the Kriging. Hence, the difference between analysis and observation will (almost by definition) be smaller than between the simulated and observed values. To assess the quality of the spatial interpolation a second group of stations should be withheld from the kriging procedure and should be used for validation of the interpolated field. If the comparison to the observations for the analysis and validation stations are similar, the procedure is proven to be robust, and not too sensitive to the choice of observation data.

Table 10. shows the different options for division of the available data over analysis and validation sets that were tested in this study. The first option is to use the UBA data for the analysis, and the Länder data for the validation. The second set uses all available Länder and UBA data for the analysis, without any data left for validation. The third option uses 80% of all available data for the analysis and 20% for validation.

Table 10. Overview of tested options for division in analysis and validation stations.

option	analysis stations	validation stations
1	UBA	Länder
2	UBA + Länder	
3	80 % mixed	20 % mixed

The distribution of the analysis and the validation stations is shown in Figure 25.

Figure 25. Distribution of analysis stations (left) and validation stations (right) for 3 different options (upper plots = option 1, middle plots = option 2 and lower plots = options 3 according to Table 10).

option 1:

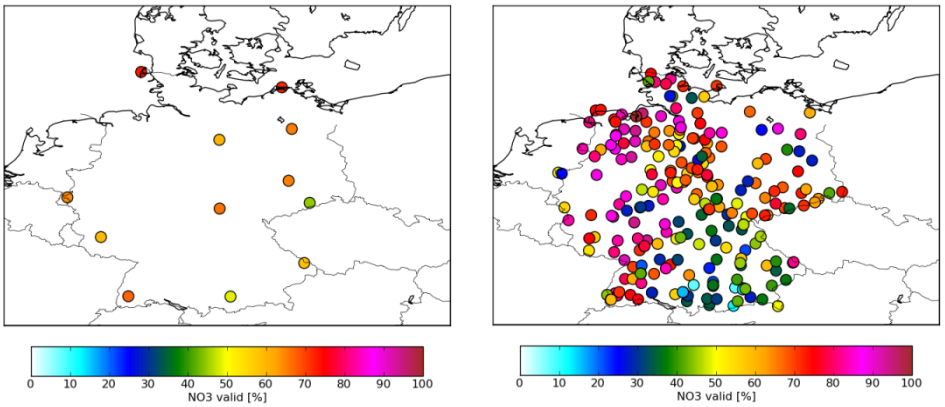

option 2:

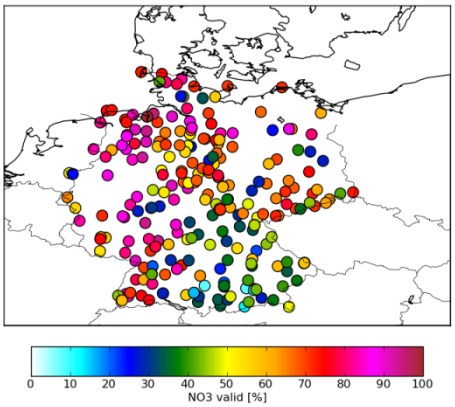

option 3:

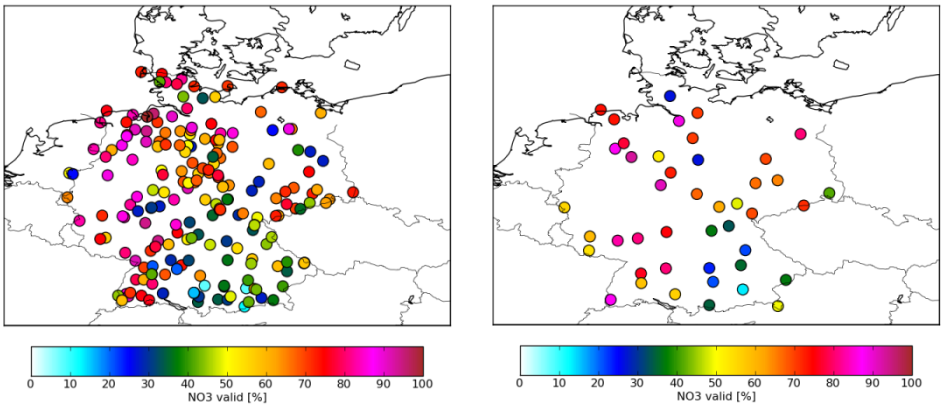

Figure 26. Validation results for 3 different options (upper plots = option 1, middle plots = option 2 and lower plots = options 3 according to Table 10) for 2007.

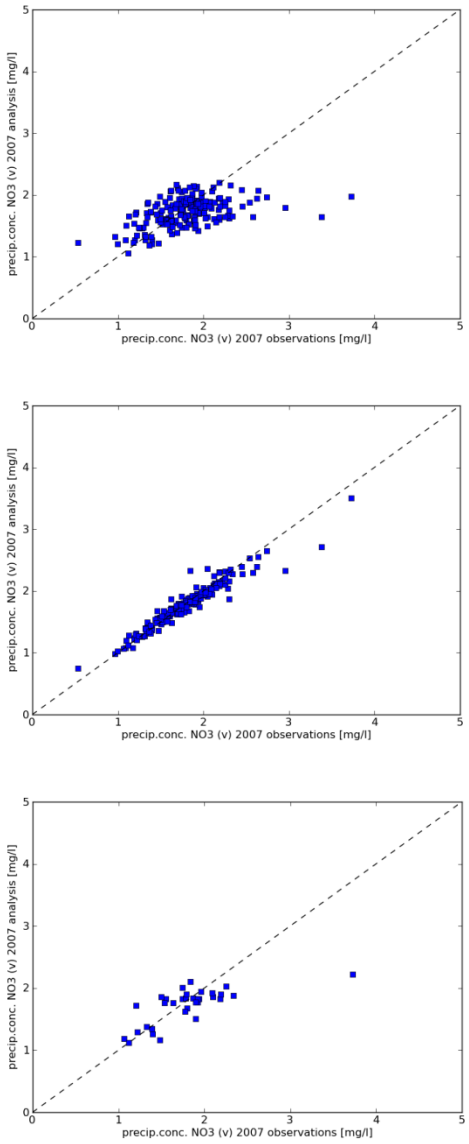

Figure 26 shows that the best results are obtained with option 2. With this option, the highest amount of spatial detail can be introduced in the result since both the data from the dense Länder networks and the UBA data are used in the analysis. This option is therefore used to create the final wet deposition results of this study.

The first option had the disadvantage that the UBA network has only a limited number of stations, which are on large distance from each other. The high spatial resolution present in the Länder data cannot be resolved by using only this small amount of stations. The third option had the disadvantage that some of the spatial information is not used.

2.5.6 Computation of wet deposition fluxes

High resolution maps of wet deposition fluxes have been computed by combining observations and model simulations. Figure 27 shows the data flow of the procedure.

Figure 27. Dataflow for computation of maps of wet deposition fluxes using model simulations from LOTOS-EUROS (which use meteorological data from ECMWF), observations of ion-concentrations from the UBA or Länder networks, and high resolution rain fields from DWD (Figure 31).

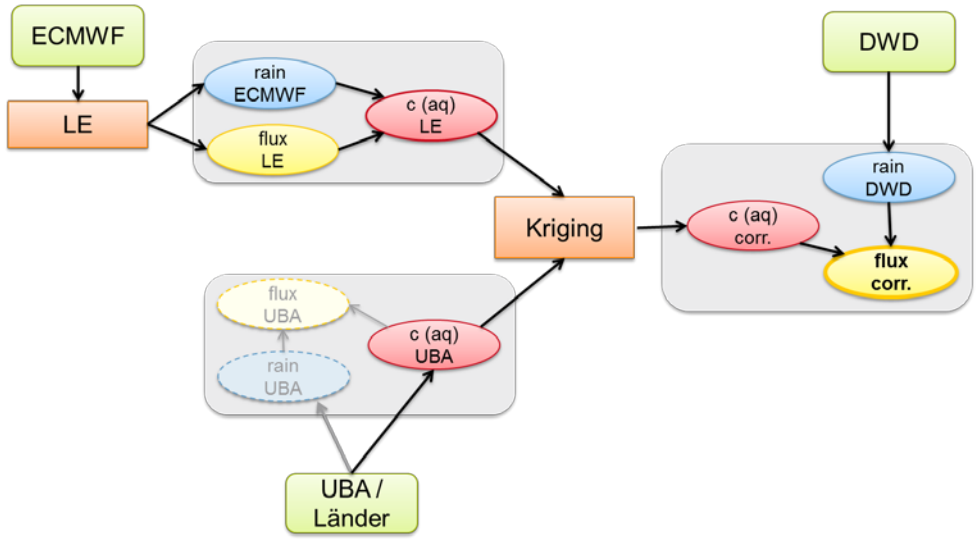

2.6 Occult deposition

2.6.1 Introduction

Nutrient or pollutant input in ecosystems by deposition of fog or cloud droplets is called occult deposition. The computation of the occult deposition flux is performed following the approach by Bleeker et al. (2000) and is performed in a post-processing procedure, i.e., the occult deposition is not (yet) included in the LOTOS-EUROS model.

The occult deposition computed within PINETI refers to input by orographic fog, which is the result of condensation processes in moist air lifted by mountains (= orographic cloud) or by intrusion of mountaintops into a low level cloud deck (Bleeker et al., 2000). Bleeker et al. (2000) use the following formulation to calculate the occult deposition flux:

$$F_{occult} = C_{cloud} \cdot LWC_{Klima} \cdot v_d \cdot (\text{duration of cloud occurrences})_{Klima} \qquad \text{(Eq. 2.35)}$$

with: $C_{cloud} = a \cdot z^b \cdot C_{rain}$ = concentration in cloud droplets

LWC_{Klima} = climatological Liquid Water Content (= 0.15 g/m^3)

v_d = cloud deposition velocity (≈ Ra(at 4m)$^{-1}$)

$(\text{duration of cloud occurrences})_{Klima}$ = 1400 hours

For the calculation of C_{cloud}, Bleeker et al. (2000) derived height-dependent relations between the concentration in cloud droplets and the concentration in rain water based on former investigations at different sites in mountainous areas at different altitudes. The sites were all located higher than 350m a.s.l. and therefore the approach by Bleeker et al. (2000) was only applied for areas above 350m a.s.l.. In MAPESI, the Bleeker approach was applied down to an altitude of 250m a.s.l.. In this study, we try to stay consistent with MAPESI and therefore also apply the Bleeker approach down to 250m a.s.l.. The coefficients a and b are taken from Bleeker et al., 2000 (Table 11), z is the altitude in meters obtained from a detailed orography map from DGM50 „Digitales Geländemodell Gitterweite 50 m" provided by the Bundesamt für Kartographie und Geodäsie (http://www.bkg.bund.de; Figure 28), and C_{rain} is the concentration of a specific component in precipitation obtained from the wet deposition calculation.

Table 11. Best-fit-Parameter a and b according to Bleeker et al., 2000.

Component	a	b
SO_4^{2-}	341	-0.64
NO_3^-	912	-0.77
NH_4^+	25.60	-0.24
H^+	15.30	-0.24
Na^+	9.10E+05	-1.9
Mg^{2+}	6.00E+07	-2.5
Ca^{2+}	1.30E+05	-1.6
K^+	2.20E+03	-0.99
Cl^-	3.00E+06	-2.09

Figure 28. Detailed orography map from DGM50 „Digitales Geländemodell Gitterweite 50 m" provided by the Bundesamt für Kartographie und Geodäsie (http://www.bkg.bund.de).

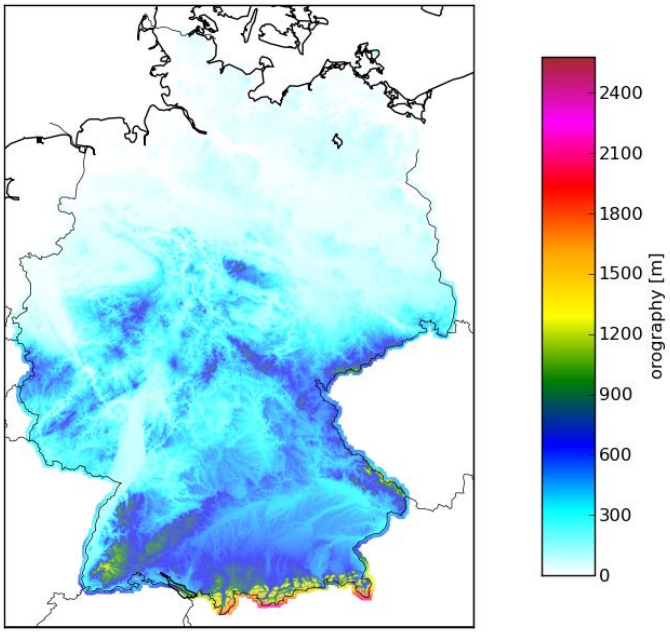

The climatological values used in Bleeker et al. (2000) were derived for the mountainous area Schwarzwald and do not have to be valid in other mountainous areas. In fact, in this study, LWC is available on a high time resolution gridded over the whole of Germany from COSMO-EU at a 7 x 7 km^2 grid size resolution. Figure 29 shows the duration of LWC occurrence over Germany in 2008 and 2009. The figure shows that the climatological average duration of cloud occurrences used in Bleeker et al. (2000) can only be found in a few mountainous areas. On average, the duration of cloud occurrences is much lower and in the order of 200 hours. This is significantly lower than the climatological value used by Bleeker et al. (2000).

Figure 29. Overview of LWC occurrence over Germany as calculated by COSMO-EU over Germany in 2008 and 2009.

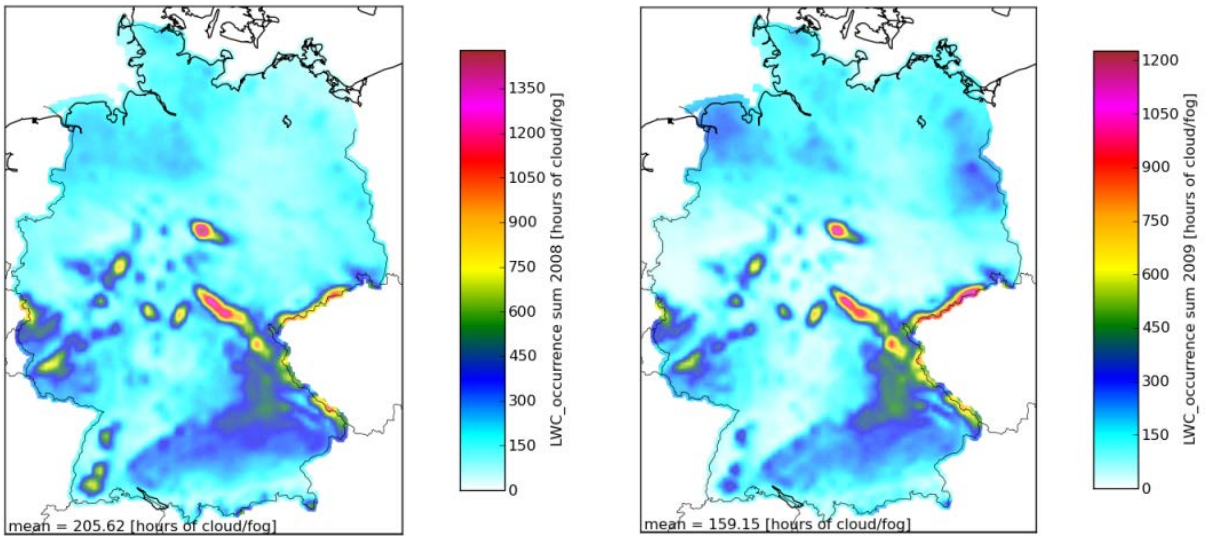

Therefore, a slightly modified formulation from Bleeker et al. (2000) is used in this study applying the annually accumulated LWC of the COSMO-EU model on a 7x7 km^2 grid resolution (analogue to the formulation used by Gauger et al., 2008):

$$F_{occult} = C_{cloud} \cdot \sum_{t=1}^{n} LWC(t) \cdot \overline{v_d(lu)} \qquad \text{(Eq. 2.36)}$$

with: $C_{cloud} = a \cdot z^b \cdot C_{rain}$ (Eq. 2.37)

$\sum_{t=1}^{n} LWC(t)$ = accumulated LWC [kg water/m^3 air]

$\overline{v_d(lu)}$ = annual average (land use dependent) deposition velocity for coarse particles

Figure 30 shows the accumulated LWC of the year 2008 derived from COSMO-EU model output.

Figure 30. Accumulated LWC of the COSMO-EU model for the year 2008

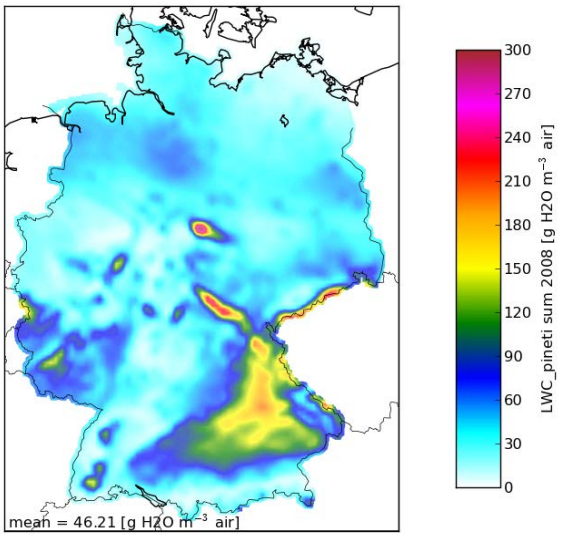

2.6.2 Method for modeling of occult deposition

For the calculation of the occult deposition, we have applied the following method:

1. First, the accumulated LWC over the whole year is calculated. The LWC is obtained from DWD COSMO-EU Model on a 7 x 7 km grid cell resolution. The LWC of the lowest model layer is used.
2. Then, the annual average deposition velocity for cloud droplets is calculated, i.e., the cloud droplets are assumed to deposit from the atmosphere in the same way as coarse particles. Note that due to this multiplication with the deposition velocity, the occult deposition is land use dependent.

3. The concentrations of the different substances in cloud droplets are calculated using Eq. 2.37 (with coefficients a and b from Table 11), from the high-resolution orography map and the concentrations in precipitation, which are obtained by the wet deposition calculation as described in the section 2.5.
4. Finally, the occult deposition is calculated for all areas above 250 m in a post-processing procedure using Equation 2.36 and 2.37.

2.7 Total deposition

The total deposition is calculated as the sum of dry, wet and occult deposition. The total deposition is the sum of land use dependent and land use independent data, which makes the total deposition land use dependent in the end.

3 Results

3.1 Meteorology

Figure 31 shows the precipitation amounts for the years 2007 (upper plot), 2008 (middle plot) and 2009 (lower plot) over Germany as obtained on a 1 x 1 km^2 grid size resolution from DWD (www.dwd.de). The figures on the right show the absolute difference between 2008/2009 and 2007. It can be seen that the regional differences between the individual years can be large, but in general, 2007 appeared to be a relatively wet year.

Figure 31. Precipitation 2007 – 2009

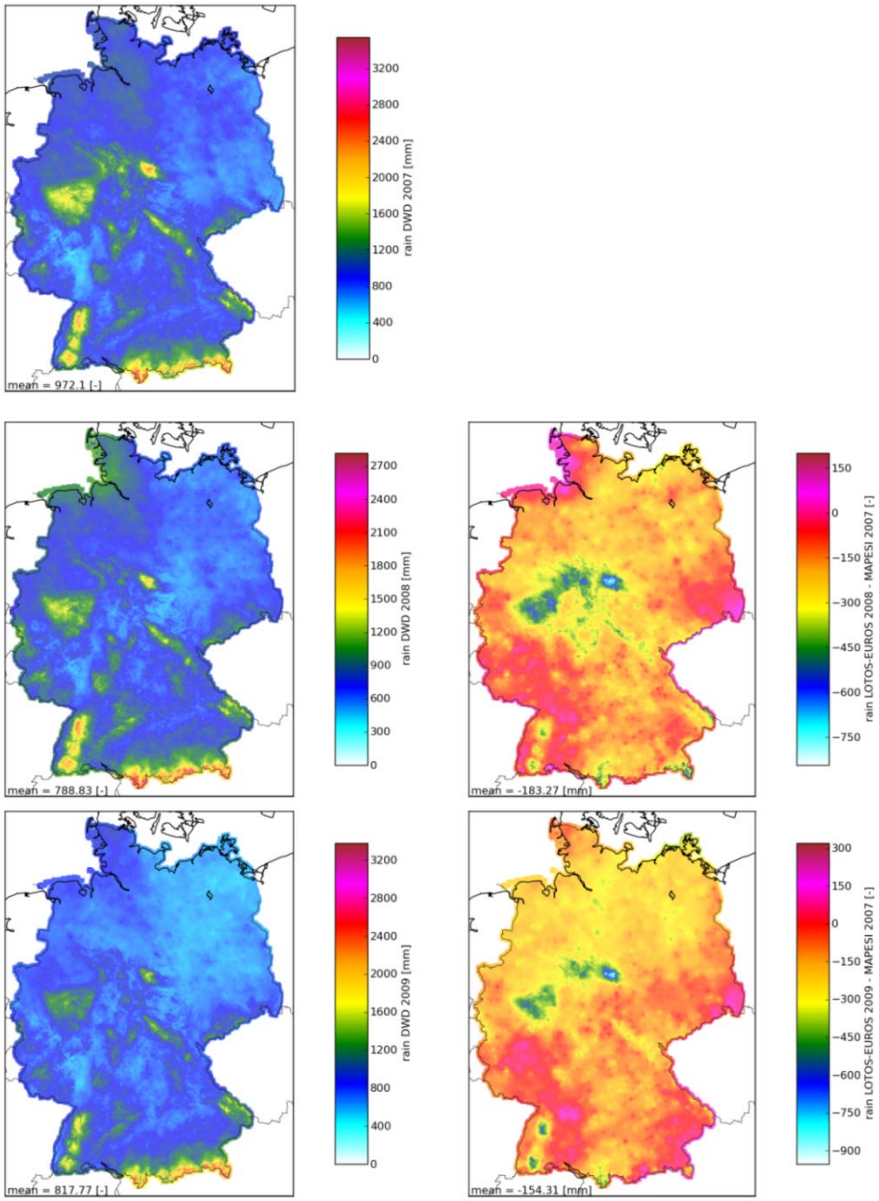

3.2 Dry deposition

Figure 32 shows the interpolated 1 x 1 km^2 dry deposition fields per component over Germany in 2008 as obtained from the described procedure in section 2.4. Note that this is the best estimate for the grid cell resolution of the model (7 x 7 km^2) interpolated to a 1 x 1 km^2 grid cell resolution. The country average dry depositions of the different components in Germany in 2008 and 2009 are given in Table 12.

Note that the tabulated values for Mg-nss refer to the averages of the distribution in which large areas have no or negative Mg-nss estimates, meaning that the impact of Mg-nss is negligible and that the Mg-nss is largely determined by the measurement uncertainty in both ions.

Mosaic plots, which show the land use specific deposition on a 1 x 1 km^2 grid cell resolution coupled to the actual land use in the 1 x 1 grid cell, might give more detailed sub-grid information. These plots will only be presented for the total deposition and will be compared with the 'best estimate' plots in Chapter 4.

Table 12. Overview of the LOTOS-EUROS modeling results of dry deposition flux.

DRY DEPOSITION		2008	2009
SO_x-S-nss	eq ha^{-1} yr^{-1}	189.8	179.1
SO_x-S	eq ha^{-1} yr^{-1}	212.9	196.2
NH_x-N	eq ha^{-1} yr^{-1}	487.0	479.5
NO_y-N	eq ha^{-1} yr^{-1}	202.4	201.4
N	eq ha^{-1} yr^{-1}	689.8	681.4
Na^+	eq ha^{-1} yr^{-1}	191.9	142.2
Ca^{2+}	eq ha^{-1} yr^{-1}	79.9	67.6
Mg^{2+}	eq ha^{-1} yr^{-1}	56.4	42.9
K^+	eq ha^{-1} yr^{-1}	17.6	17.1
Ca^{2+}-nss	eq ha^{-1} yr^{-1}	72.2	62.0
Mg^{2+}-nss **	eq ha^{-1} yr^{-1}	9.6	9.3
K^+-nss	eq ha^{-1} yr^{-1}	14.4	14.8
BC-nss	eq ha^{-1} yr^{-1}	96.1	86.2

** mean value for Mg^{2+}-nss is based on non-zero values in the distribution only. Based on tabulated data 12.2 and 7.6 eq ha^{-1} yr^{-1} are estimated for 2008 and 2009, respectively

Figure 32. Dry deposition of NH_x, NO_y, SO_x, Na^+, Ca^{2+}, Ca^{2+}-nss, Mg^{2+}, Mg^{2+}-nss, K^+ and K^+-nss in Germany in 2008.

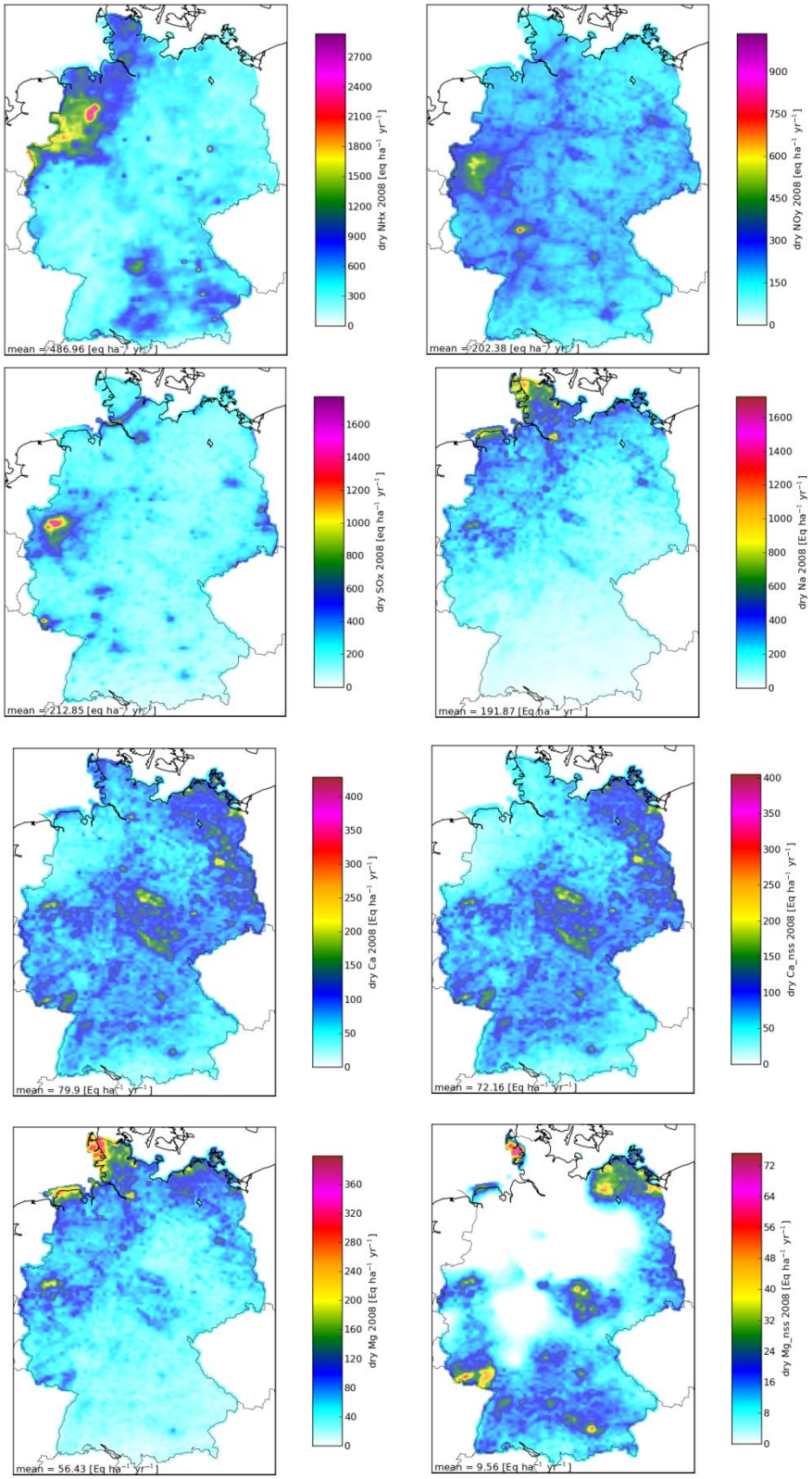

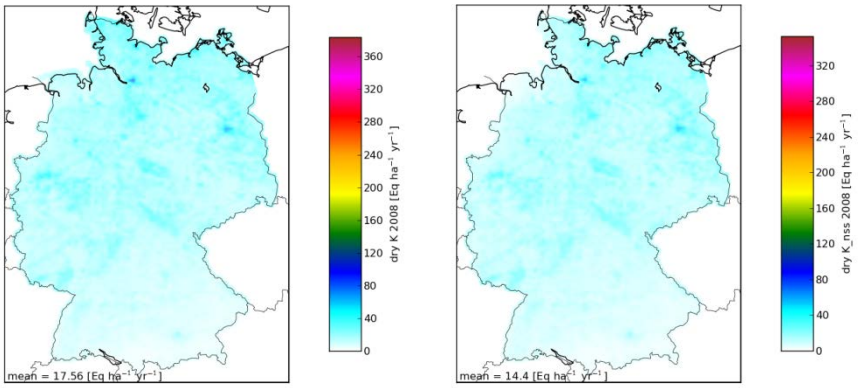

Table 13 shows the averaged effective deposition velocities as calculated from the model results. The effective deposition velocity is the annual average flux divided by the annual averaged concentration at 2.5 meters height. Effective deposition velocities are not given for base cation because no fluxes and concentrations are calculated by the model for these components.

Table 13. Deposition velocities 2009

Effective deposition velocities at 2.5 m height (cm/s)								
Landuse/Tracer	SO_4^{2-}	SO_2	NO_3^-	NO_2	NO	NH_4^+	NH_3	HNO_3
grs	0.11	0.67	0.11	0.21	0.11	0.11	1.27	1.21
ara	0.12	0.70	0.12	0.16	0.12	0.12	1.59	1.65
cnf	0.61	0.87	0.59	0.26	0.12	0.59	1.84	2.17
dec	0.61	0.73	0.59	0.12	0.12	0.59	1.72	2.17
mix	0.61	0.73	0.59	0.12	0.12	0.59	1.90	2.17
wat	0.10	0.53	0.10	0.05	0.11	0.10	1.07	0.83
urb	0.62	0.34	0.60	0.08	0.19	0.59	0.80	2.27
sem	0.12	0.65	0.12	0.11	0.12	0.12	1.60	1.65
oth	0.12	0.28	0.12	0.07	0.11	0.12	1.13	1.45

3.3 Wet deposition

Figure 33 shows the 1 x 1 km^2 wet deposition fields per component over Germany in 2008 as obtained from the described procedure in section 2.5. In contradiction to the dry deposition, the wet deposition is independent on land use and the obtained wet deposition amounts have shown to be in good agreement with the observations (middle plot in Figure 26). The country average wet depositions of the different components in Germany in 2008 and 2009 are given in Table 14.

Table 14. Overview of the LOTOS-EUROS modeling results of wet deposition

WET DEPOSITION		2008	2009
SO_x-S-nss	eq ha^{-1} yr^{-1}	173.0	169.8
SO_x-S	eq ha^{-1} yr^{-1}	197.7	188.2
NH_x-N	eq ha^{-1} yr^{-1}	312.7	318.8
NO_y-N	eq ha^{-1} yr^{-1}	244.5	246.5
N	eq ha^{-1} yr^{-1}	557.3	565.3
Na^+	eq ha^{-1} yr^{-1}	206.3	153.3
Ca^{2+}	eq ha^{-1} yr^{-1}	81.2	75.3
Mg^{2+}	eq ha^{-1} yr^{-1}	52.8	41.7
K^+	eq ha^{-1} yr^{-1}	21.2	22.4
Ca^{2+}-nss	eq ha^{-1} yr^{-1}	72.5	68.8
Mg^{2+}-nss **	eq ha^{-1} yr^{-1}	8.8	9.3
K^+-nss	eq ha^{-1} yr^{-1}	16.8	19.1
BC-nss	eq ha^{-1} yr^{-1}	98.1	97.2

** mean value for Mg^{2+}-nss is based on non-zero values in the distribution only. Based on tabulated data 5.4 and 6.4 eq ha^{-1} yr^{-1} are estimated for 2008 and 2009, respectively

Figure 33. Wet deposition of NH_x, NO_y, SO_x, Na^+, Ca^{2+}, Ca^{2+}-nss, Mg^{2+}, Mg^{2+}-nss, K^+ and K^+-nss in Germany in 2008.

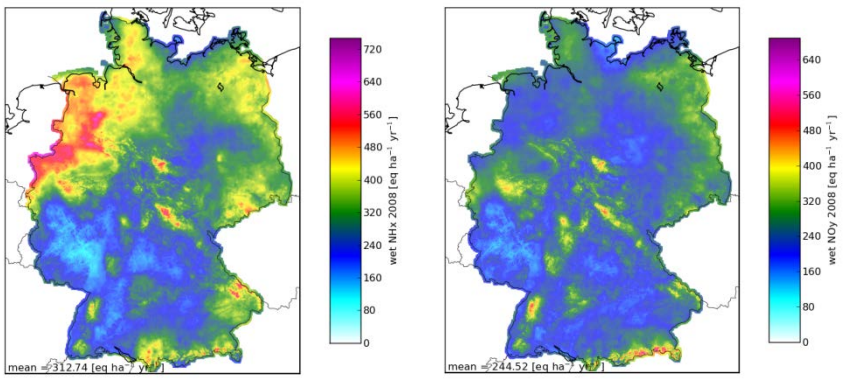

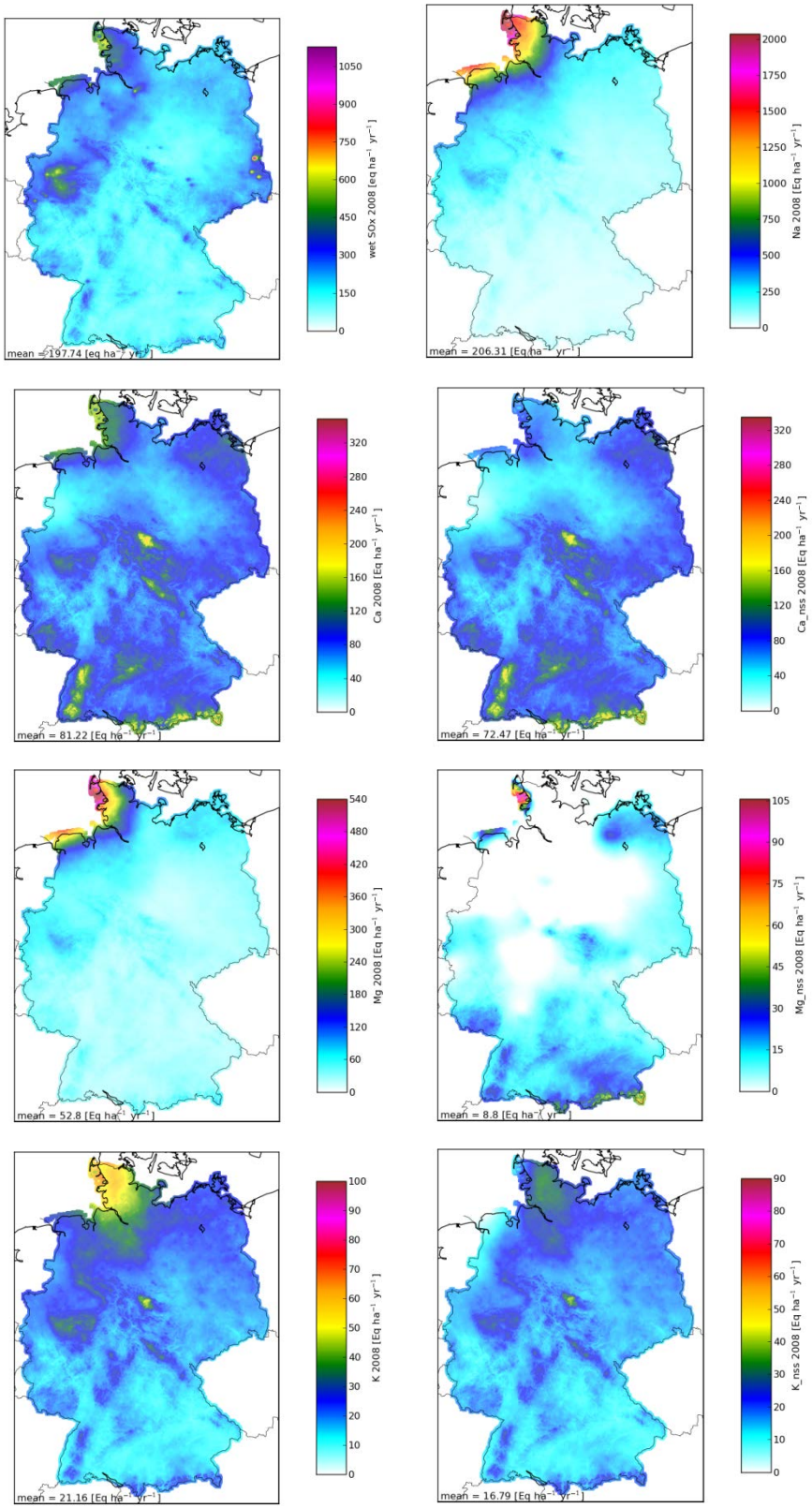

3.4 Occult Deposition

Figure 34 shows the 1 x 1 km^2 occult deposition fields per component over Germany in 2008 as obtained from the described procedure in section 2.6. Note that this is the best estimate for the

grid cell resolution of the model (7 x 7 km^2) interpolated to a 1 x 1 km^2 grid cell resolution. The country average occult depositions of the different components in Germany in 2008 and 2009 are given in Table 15.

Table 15. Overview of the LOTOS-EUROS modeling results of occult deposition

OCCULT DEPOSITION		2008 PINETI	2009 PINETI
SO_x-S-nss	eq ha^{-1} yr^{-1}	2.00	0.94
SO_x-S	eq ha^{-1} yr^{-1}	2.20	1.02
NH_x-N	eq ha^{-1} yr^{-1}	3.84	2.02
NO_y-N	eq ha^{-1} yr^{-1}	3.94	1.95
N	eq ha^{-1} yr^{-1}	7.78	3.97
Na^+	eq ha^{-1} yr^{-1}	1.97	0.80
Ca^{2+}	eq ha^{-1} yr^{-1}	1.41	0.63
Mg^{2+}	eq ha^{-1} yr^{-1}	1.21	0.49
K^+	eq ha^{-1} yr^{-1}	0.07	0.04
Ca^{2+}-nss	eq ha^{-1} yr^{-1}	1.34	0.60
Mg^{2+}-nss **	eq ha^{-1} yr^{-1}	0.38	0.17
K^+-nss	eq ha^{-1} yr^{-1}	0.06	0.03
BC-nss	eq ha^{-1} yr^{-1}	1.78	0.80

** mean value for Mg2+-nss is based on non-zero values only

Figure 34. Occult deposition of NH_x, NO_y, SO_x, Na^+, Ca^{2+}, Ca^{2+}-nss, Mg^{2+}, Mg^{2+}-nss, K^+ and K^+-nss in Germany in 2008.

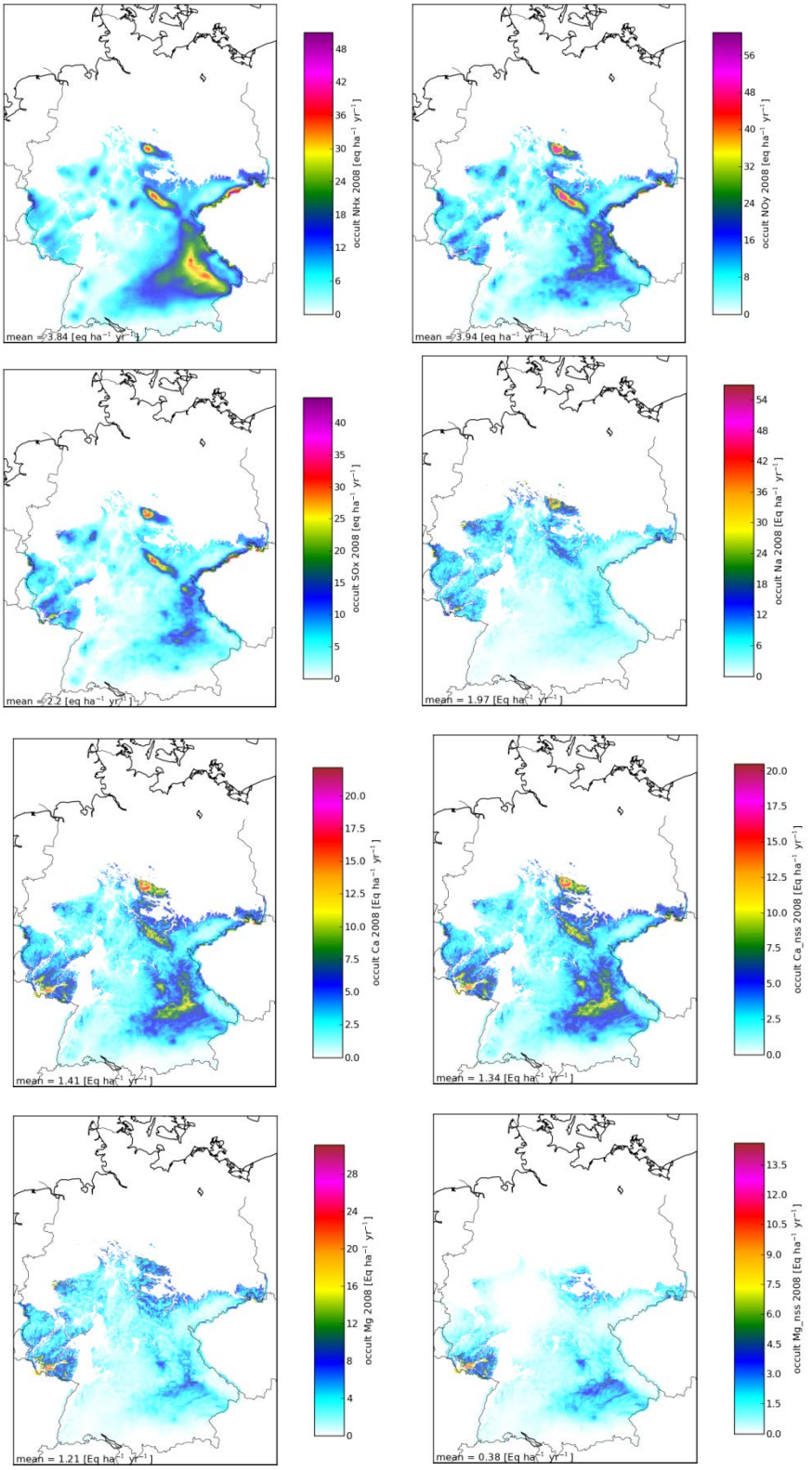

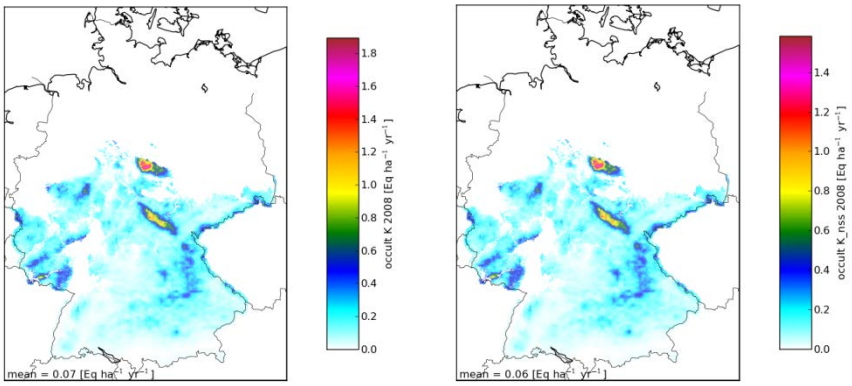

3.5 Total deposition

Figure 35 shows the 1 x 1 km^2 total deposition fields per component over Germany in 2008 as obtained from the described procedure in section 2.7. The results for the year 2009 are presented in Appendix D: Total deposition over Germany in 2009. Note that this is the best estimate for the grid cell resolution of the model (7 x 7 km^2) interpolated to a 1 x 1 km^2 grid cell resolution. Mosaic plots, which show the land use specific deposition on a 1 x 1 km^2 grid cell resolution coupled to the actual land use in the 1 x 1 grid cell, give more detailed sub-grid information and will be used for Critical Load Exceedance calculations. In Chapter 4, the total deposition fields presented in Figure 35, will be compared with the 'mosaic' plots of the total deposition.

The country average total depositions of the different components in Germany in 2008 and 2009 are given in Table 16.

Table 16. Overview of the PINETI results of total deposition flux.

TOTAL DEPOSITION		2008 PINETI	2009 PINETI
SO_x-S-nss	eq ha^{-1} yr^{-1}	364.9	349.9
SO_x-S	eq ha^{-1} yr^{-1}	412.8	385.4
NH_x-N	eq ha^{-1} yr^{-1}	803.5	800.4
	kg ha^{-1} yr^{-1}	11.25	11.21
NO_y-N	eq ha^{-1} yr^{-1}	450.8	449.9
	kg ha^{-1} yr^{-1}	6.31	6.30
N	eq ha^{-1} yr^{-1}	1254.9	1250.7
	kg ha^{-1} yr^{-1}	17.57	17.51
Na^+	eq ha^{-1} yr^{-1}	399.6	296.3
Ca^{2+}	eq ha^{-1} yr^{-1}	162.3	143.6
Mg^{2+}	eq ha^{-1} yr^{-1}	110.3	85.0

TOTAL DEPOSITION		2008 PINETI	2009 PINETI
K^+	eq ha^{-1} yr^{-1}	38.7	39.5
Ca^{2+}-nss	eq ha^{-1} yr^{-1}	145.8	131.5
Mg^{2+}-nss	eq ha^{-1} yr^{-1}	18.7	18.7
K^+-nss	eq ha^{-1} yr^{-1}	31.2	34.0
BC-nss	eq ha^{-1} yr^{-1}	195.7	184.2

Figure 35. Total deposition of NH_x, NO_y, SO_x, Na^+, Ca^{2+}, Ca^{2+}-nss, Mg^{2+}, Mg^{2+}-nss, K^+, K^+-nss and total N in Germany in 2008.

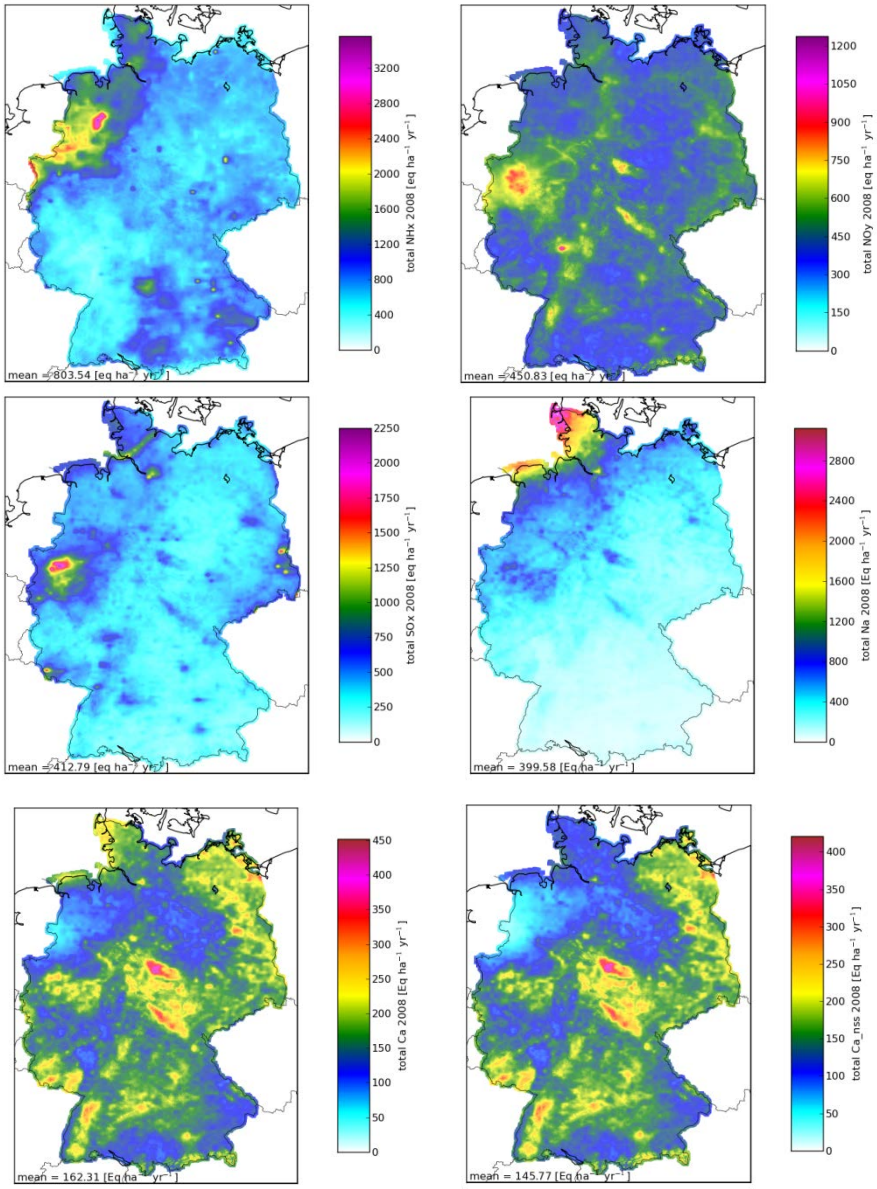

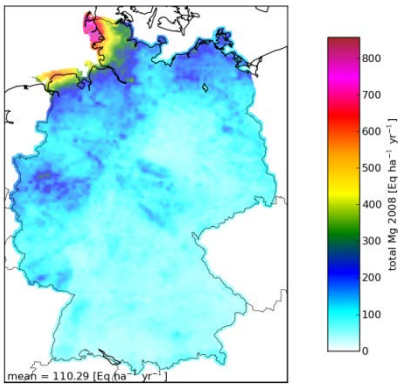
mean = 110.29 [Eq ha⁻¹ yr⁻¹]

800
700
600
500
400
300
200
100
0
total Mg 2008 [Eq ha⁻¹ yr⁻¹]

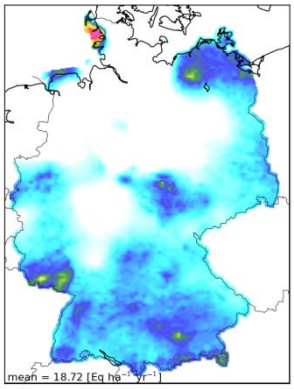
mean = 18.72 [Eq ha⁻¹ yr⁻¹]

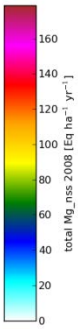
160
140
120
100
80
60
40
20
0
total Mg_nss 2008 [Eq ha⁻¹ yr⁻¹]

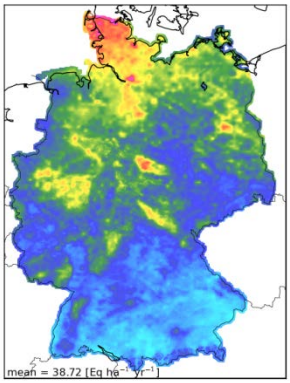
mean = 38.72 [Eq ha⁻¹ yr⁻¹]

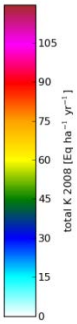
105
90
75
60
45
30
15
0
total K 2008 [Eq ha⁻¹ yr⁻¹]

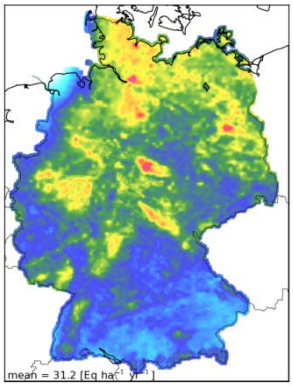
mean = 31.2 [Eq ha⁻¹ yr⁻¹]

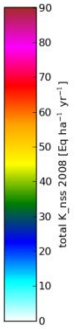
90
80
70
60
50
40
30
20
10
0
total K_nss 2008 [Eq ha⁻¹ yr⁻¹]

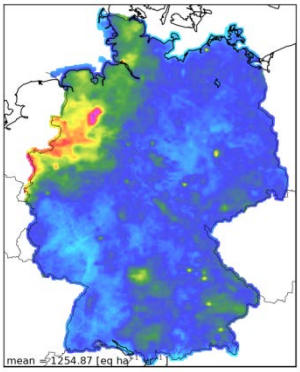
mean = 1254.87 [eq ha⁻¹ yr⁻¹]

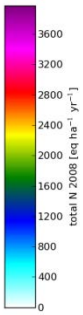
3600
3200
2800
2400
2000
1600
1200
800
400
0
total N 2008 [eq ha⁻¹ yr⁻¹]

4 TNO 1 x 1 km^2 map versus ÖKO-DATA 1 x 1 km^2 map

In the following figures, the TNO 1 x 1 km^2 'best estimate' maps (from Figure 35) are compared with ÖKO-DATA 1 x 1 km^2 'mosaic' maps for the total SO_x (Figure 36) and total N deposition (Figure 38). The ÖKO-DATA 1 x 1 km^2 'mosaic' maps are composed from the land use specific TNO 1 x 1 km^2 maps in combination with the land use in the CLC2006 database as described in 2.4.4. In the upper plots, the TNO 1 x 1 km^2 'best estimate' maps are shown, in the lower plots, the ÖKO-DATA 1 x 1 km^2 'mosaic' maps are shown. As the land use maps that TNO and ÖKO-DATA use, i.e., CLC2000 and CLC2006 respectively, are very similar, the 'mosaic' maps only give extra sub-grid information, no different deposition totals. As a check, the absolute and relative difference maps between the TNO 1 x 1 km^2 'best estimate' and the ÖKO-DATA 1 x 1 km^2 'mosaic' maps are shown in Figure 37 and Figure 39. The differences between both maps are nicely distributed around zero, supporting the statement that the deposition totals over Germany are the same, while the spread in the differences gives us information about the sub-grid variability in the deposition.

Figure 36 and Figure 38 clearly show that the patterns are very similar in both approaches. The 'mosaic' plots just add some extra detail on the local scale, as expected. This can also be seen in the deposition distribution plots on the right-hand side of both figures, in which more extreme values are found in the ÖKO-DATA 'mosaic' plots due to the higher level of detail.

The absolute and relative difference plots (Figure 37 and Figure 39) show that there are no spatial patterns in the absolute or relative differences between the two maps. The distribution plots on the right-hand side of the plots show that the differences are nicely distributed around zero. For total SO_x, only 1.3% of the grid cells in the ÖKO-DATA 'mosaic' differ more than 20% from the TNO 'best estimate'; for total N deposition this is even only 0.5%.

Figure 36. Best estimate of the total SO_x deposition over Germany in 2008 (upper plot) and ‚mosaic' of the total SO_x deposition using land use specific depositions for each 1 x 1 km^2 grid cell (lower plot).

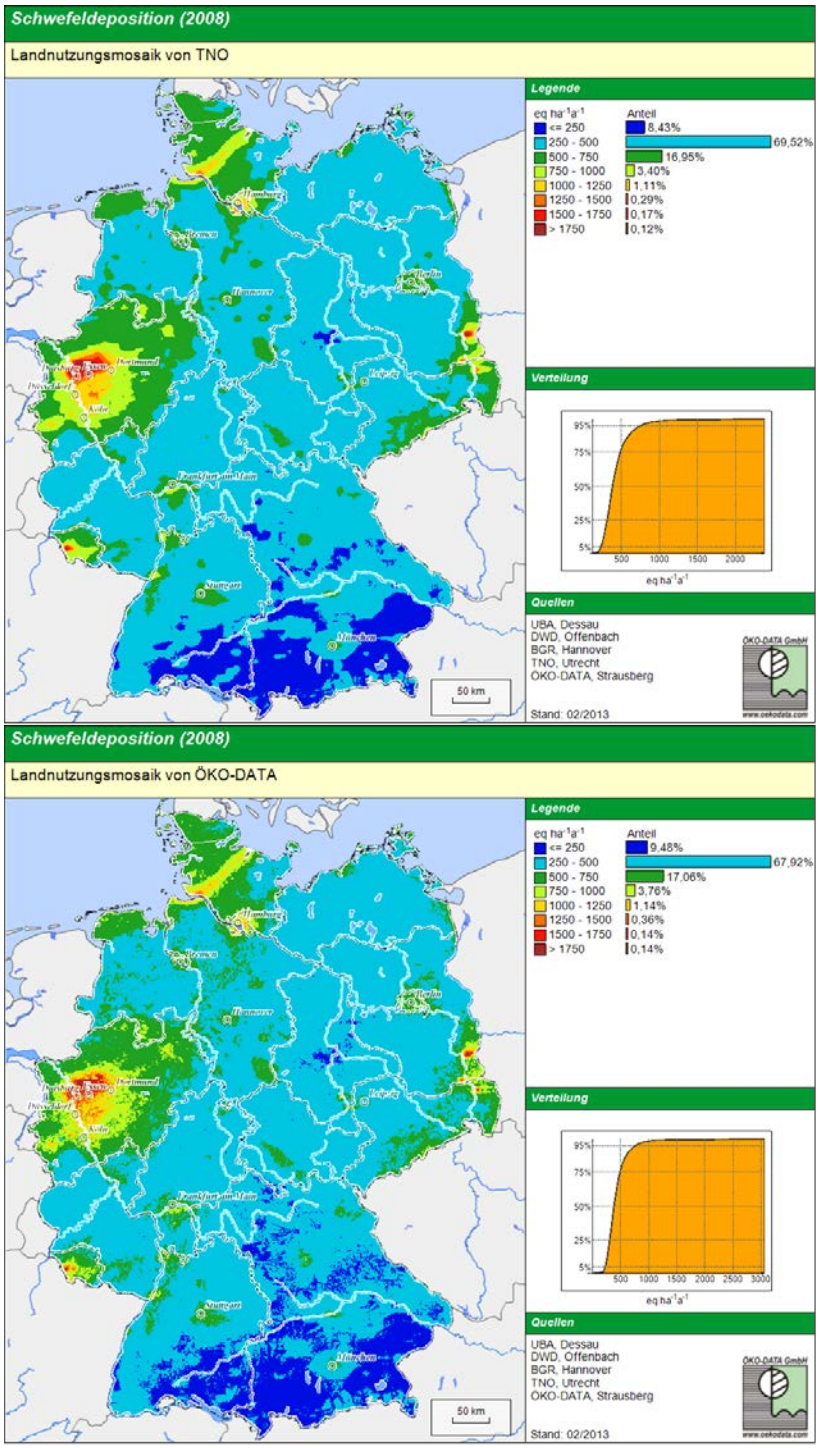

Figure 37. Absolute (upper plot) and relative (lower plot) difference between the best estimate of the total SO_x deposition over Germany in 2008 and the ‚mosaic' of the total SO_x deposition using land use specific depositions for each 1 x 1 km^2 grid cell.

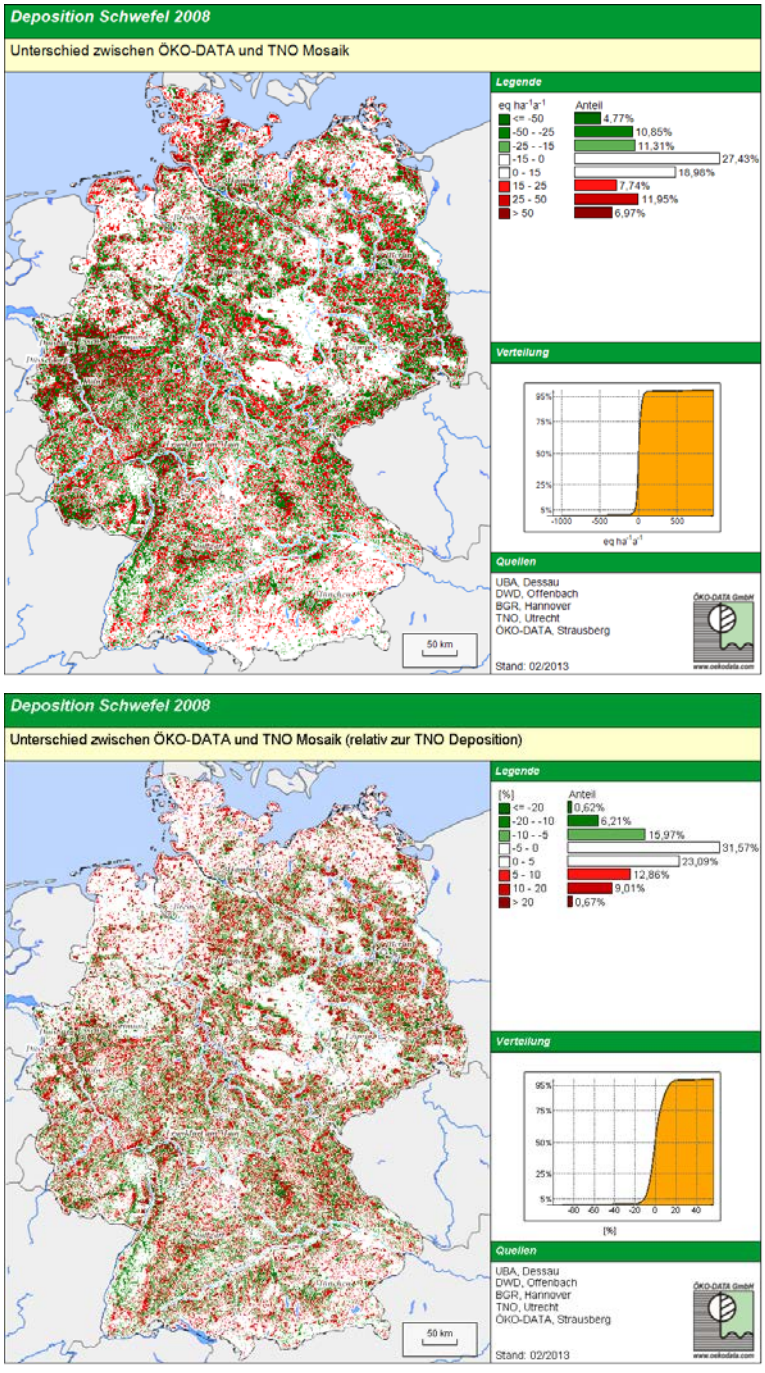

Figure 38. Best estimate of the total N deposition over Germany in 2008 (upper plot) and ‚mosaic' of the total N deposition using land use specific depositions for each 1 x 1 km^2 grid cell (lower plot).

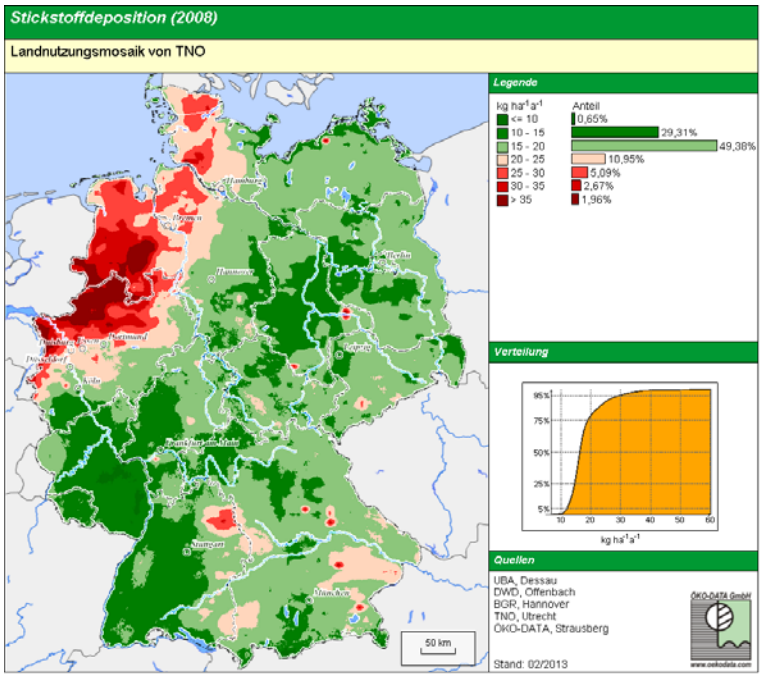

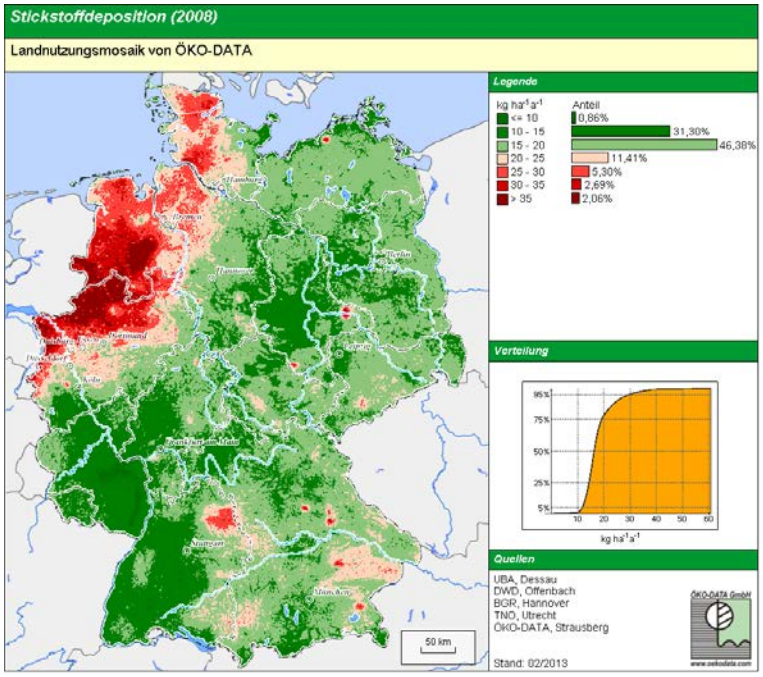

Figure 39. Absolute (upper plot) and relative (lower plot) difference between the best estimate of the total N deposition over Germany in 2008 and the ‚mosaic' of the total N deposition using land use specific depositions for each 1 x 1 km^2 grid cell.

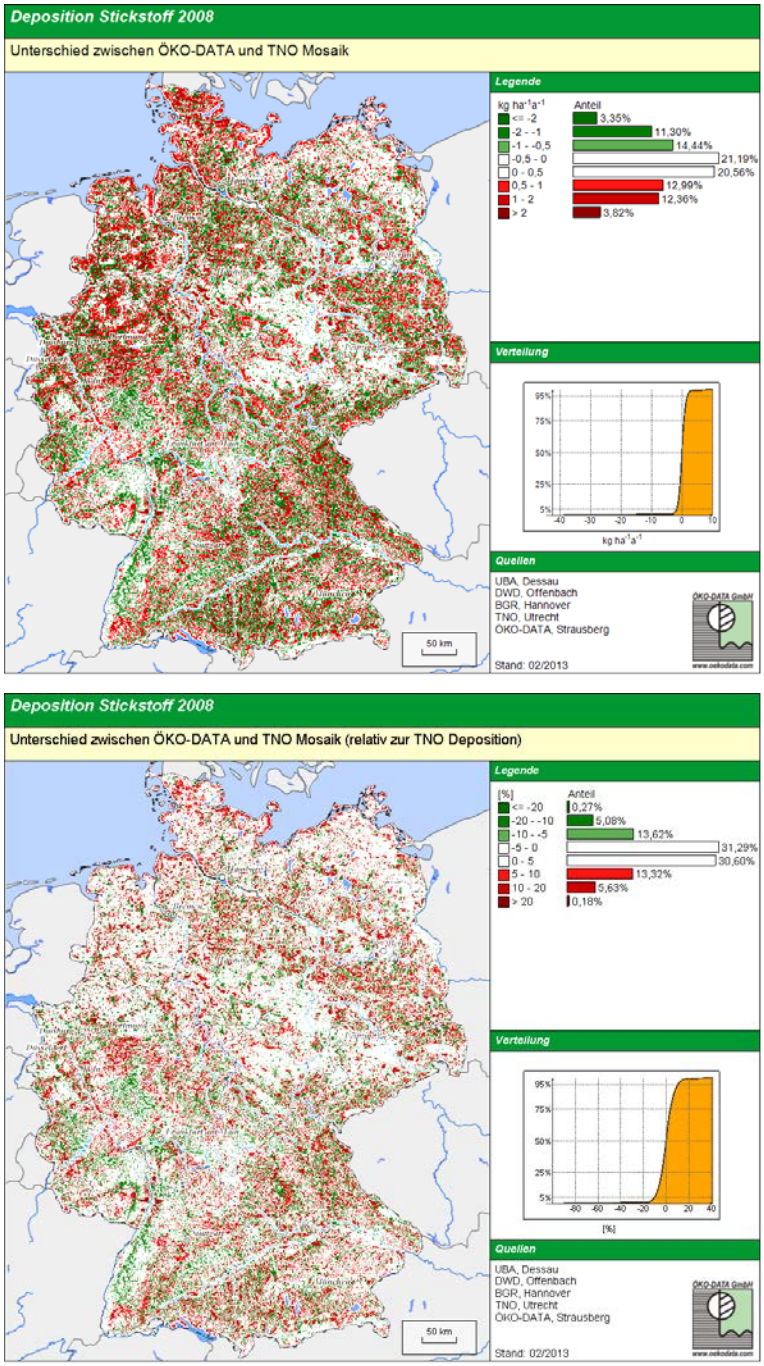

5 Comparison with MAPESI results

In the following sections, a comparison between the total deposition fluxes calculated in PINETI for the year 2008 and in MAPESI for the year 2007 is made. Per component, the MAPESI results for 2007 are presented in the upper left figure. The PINETI results for 2008 are shown in the upper right figure. The relative and absolute difference between the PINETI 2008 and MAPESI 2007 results are shown in the lower left and right figure, respectively. Note that a direct comparison is not possible as the meteorological conditions (see section 3.1, differences in precipitation) and the emissions are not the same for the different years. Despite these shortcomings, it is useful to compare the PINETI 2008 results with the MAPESI 2007 results to get an impression of the spatial variations of the differences, which might partly be caused by methodological differences. In this chapter, only the total deposition of the different components is considered. For an overview of the differences per removal process, i.e., dry, wet and occult deposition, between MAPESI 2007 and PINETI 2008, see Appendix B: Comparison of dry, wet and occult deposition fluxes in MAPESI 2007 and PINETI 2008. Results are discussed in chapter 8.

Note that in Teilbericht 3 a comparison between PINETI and MAPESI for 2007 is made, which provides more insight in methodological induced differences. In short, largest changes are induced by the (change in methodologies for) wet deposition and occult deposition. The first may explain up to 50% of the change between the studies. Other impacts are due the dry depositon modelling and different meteorology.

Table 17. Overview of German average annual deposition results of MAEPSI 2007 and PINETI 2008.

TOTAL DEPOSITION		MAPESI 2007	PINETI 2008
SO_x-S	eq ha^{-1} yr^{-1}	470	413
NH_x-N	eq ha^{-1} yr^{-1}	978	804
NO_y-N	eq ha^{-1} yr^{-1}	549	451
Na^+	eq ha^{-1} yr^{-1}	508	400
Ca^{2+}	eq ha^{-1} yr^{-1}	217	162
Mg^{2+}	eq ha^{-1} yr^{-1}	107	110
K^+	eq ha^{-1} yr^{-1}	124	39
Ca^{2+}-nss	eq ha^{-1} yr^{-1}	197	146
Mg^{2+}-nss **	eq ha^{-1} yr^{-1}	15	19
K^+-nss	eq ha^{-1} yr^{-1}	108	31

5.1 SO_x

Figure 40. Total deposition of SO_x in MAPESI 2007 (upper left), PINETI 2008 (upper right), relative difference between PINETI 2008 and MAPESI 2007 (lower left) and absolute difference between PINETI 2008 and MAPESI 2007 (lower right).

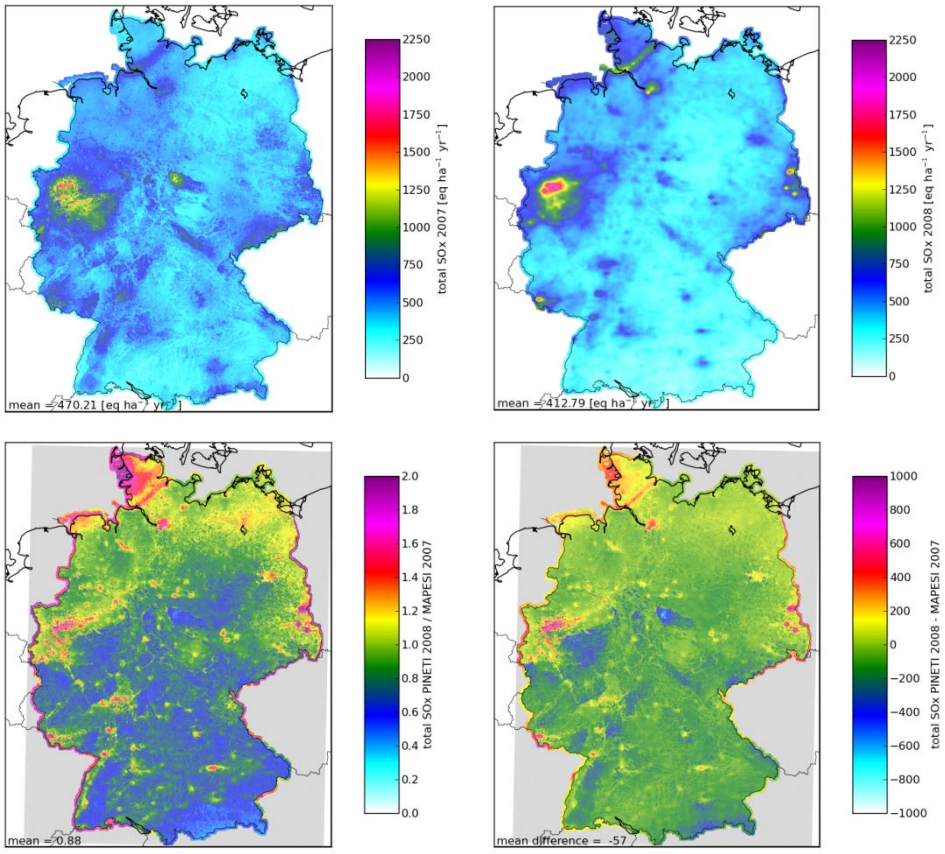

5.2 NH_x

Figure 41. Total deposition of NH_x in MAPESI 2007 (upper left), PINETI 2008 (upper right), relative difference between PINETI 2008 and MAPESI 2007 (lower left) and absolute difference between PINETI 2008 and MAPESI 2007 (lower right).

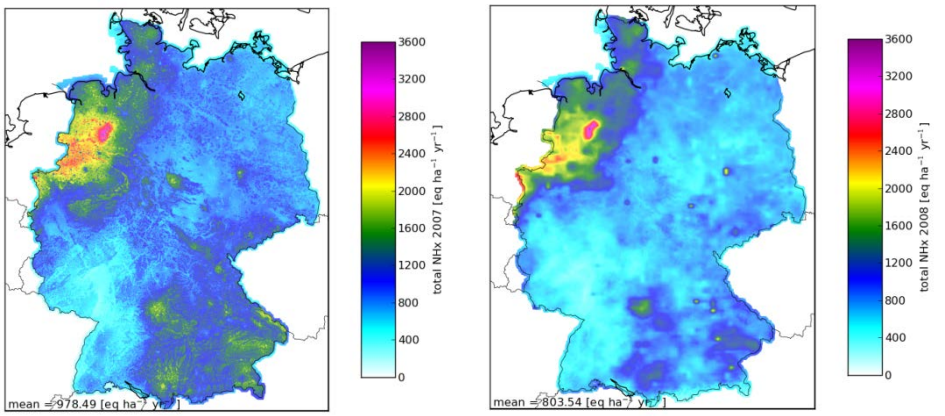

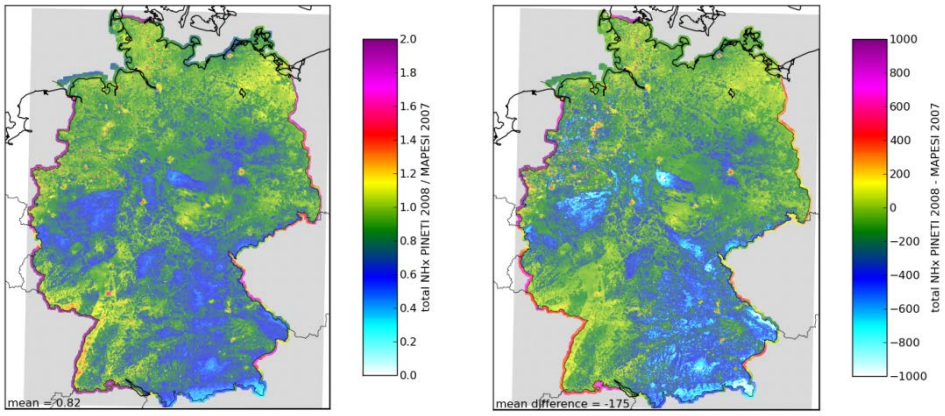

5.3 NO_y

Figure 42. Total deposition of NO_y in MAPESI 2007 (upper left), PINETI 2008 (upper right), relative difference between PINETI 2008 and MAPESI 2007 (lower left) and absolute difference between PINETI 2008 and MAPESI 2007 (lower right).

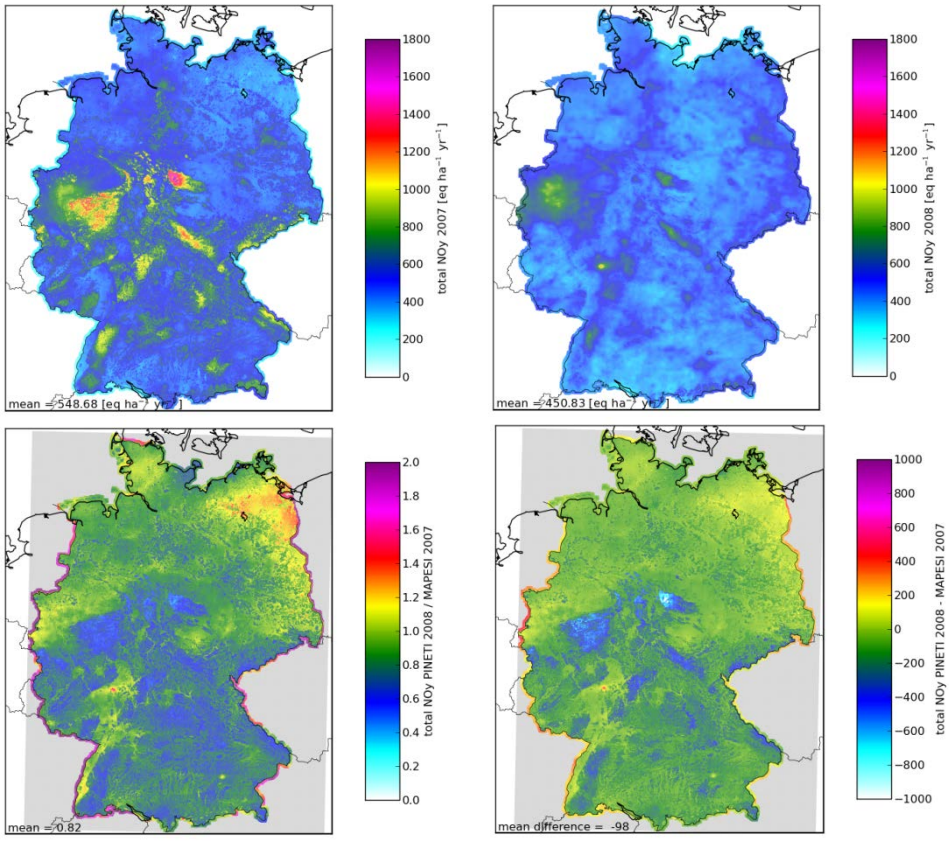

5.4 Na^+

Figure 43. Total deposition of Na^+ in MAPESI 2007 (upper left), PINETI 2008 (upper right), relative difference between PINETI 2008 and MAPESI 2007 (lower left) and absolute difference between PINETI 2008 and MAPESI 2007 (lower right).

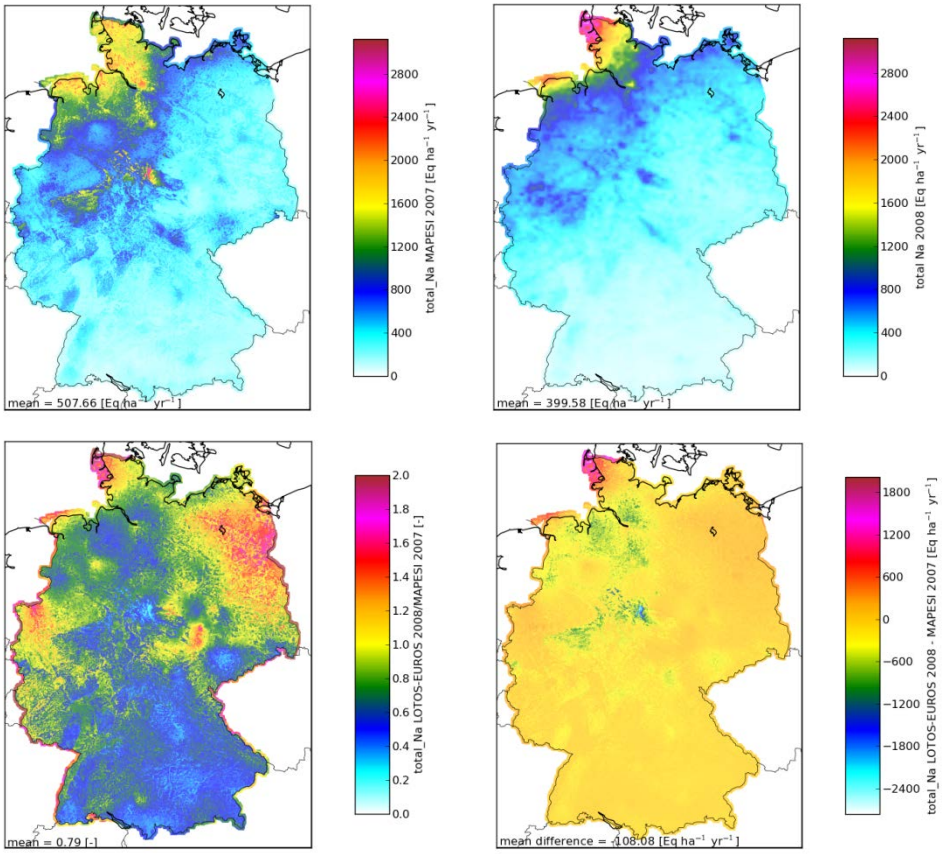

5.5 Ca^{2+}

Figure 44. Total deposition of Ca^{2+} in MAPESI 2007 (upper left), PINETI 2008 (upper right), relative difference between PINETI 2008 and MAPESI 2007 (lower left) and absolute difference between PINETI 2008 and MAPESI 2007 (lower right).

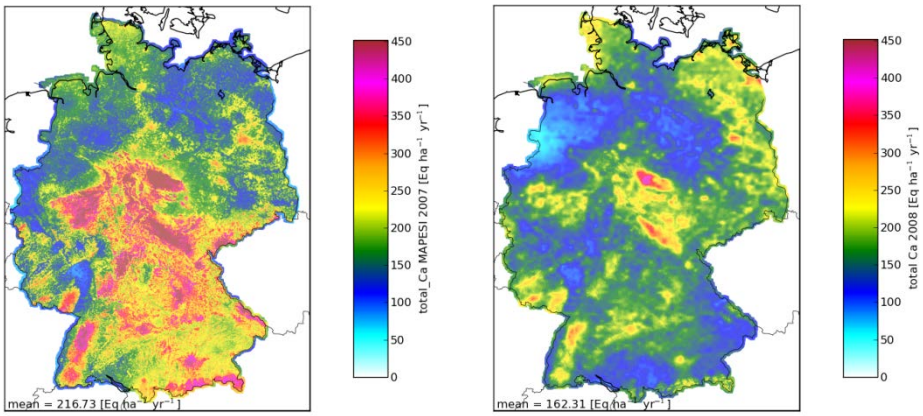

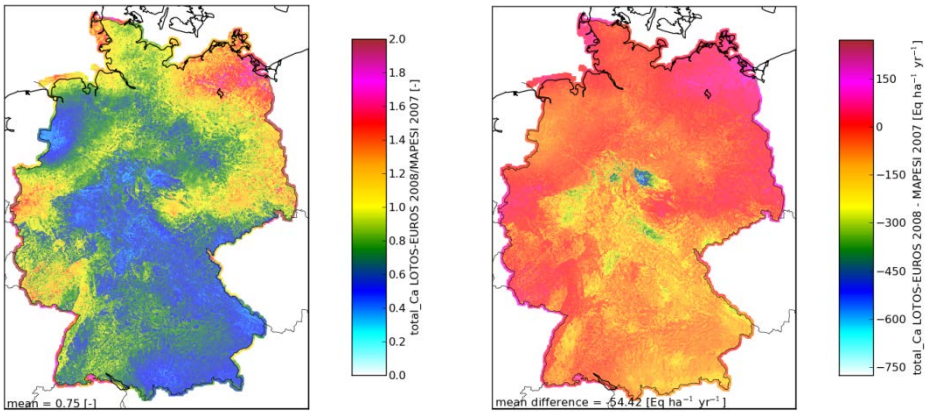

5.6 Mg^{2+}

Figure 45. Total deposition of Mg^{2+} in MAPESI 2007 (upper left), PINETI 2008 (upper right), relative difference between PINETI 2008 and MAPESI 2007 (lower left) and absolute difference between PINETI 2008 and MAPESI 2007 (lower right).

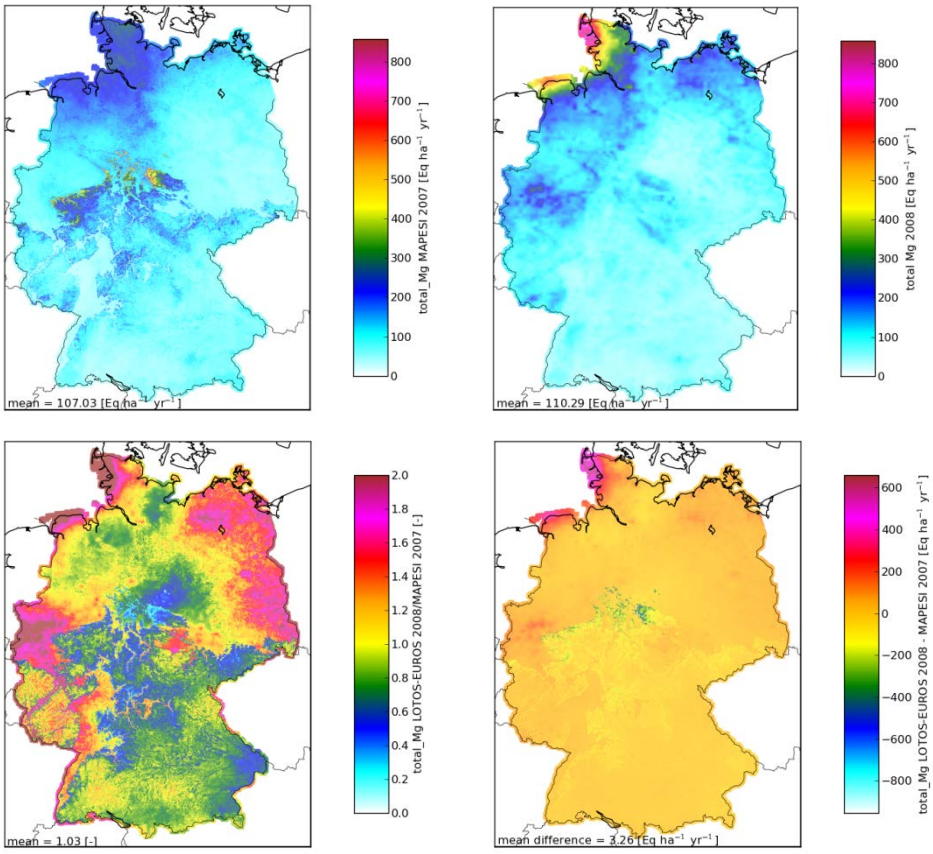

5.7 K^+

Figure 46. Total deposition of K^+ in MAPESI 2007 (upper left), PINETI 2008 (upper right), relative difference between PINETI 2008 and MAPESI 2007 (lower left) and absolute difference between PINETI 2008 and MAPESI 2007 (lower right).

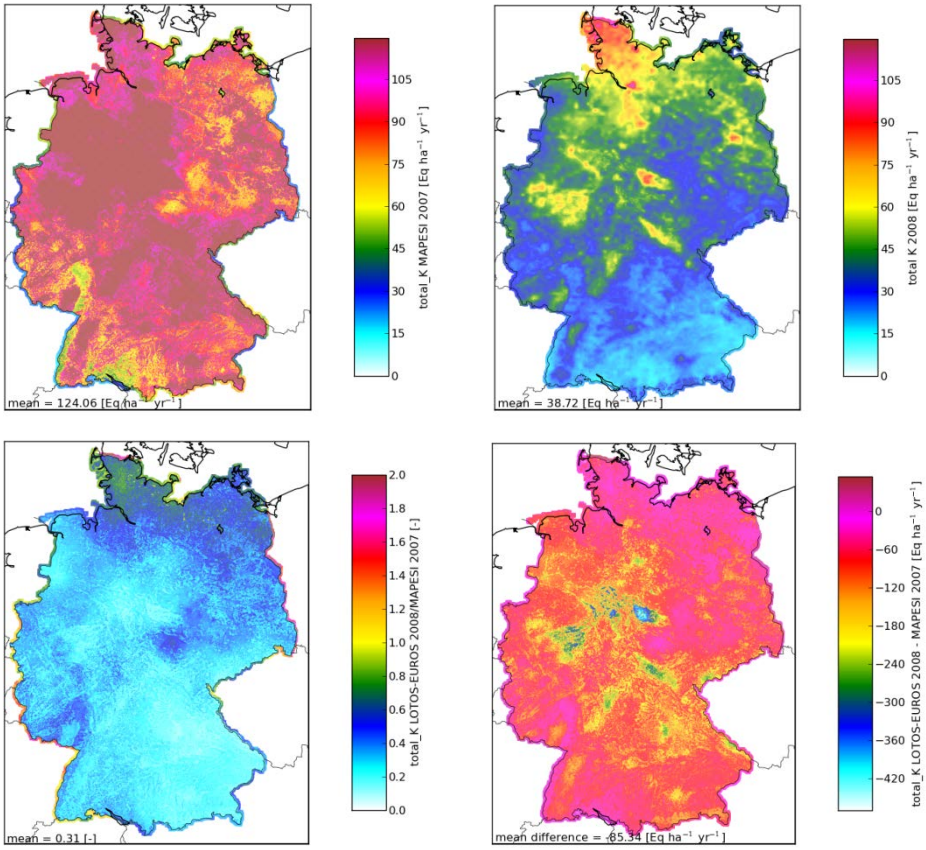

5.8 Ca^{2+}-nss

Figure 47. Total deposition of Ca^{2+}-nss in MAPESI 2007 (upper left), PINETI 2008 (upper right), relative difference between PINETI 2008 and MAPESI 2007 (lower left) and absolute difference between PINETI 2008 and MAPESI 2007 (lower right).

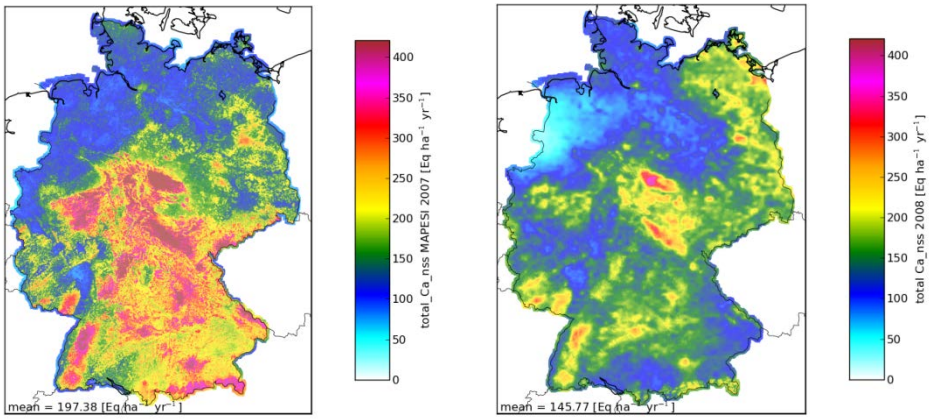

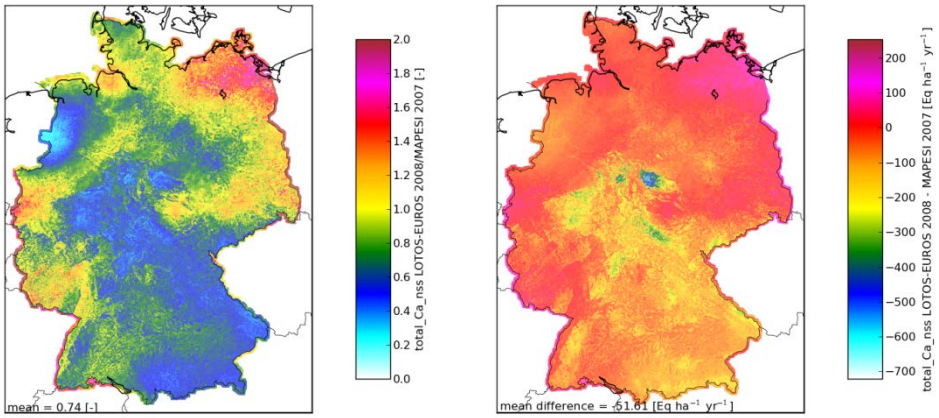

5.9 Mg^{2+}-nss

Figure 48. Total deposition of Mg^{2+}-nss in MAPESI 2007 (upper left), PINETI 2008 (upper right), relative difference between PINETI 2008 and MAPESI 2007 (lower left) and absolute difference between PINETI 2008 and MAPESI 2007 (lower right).

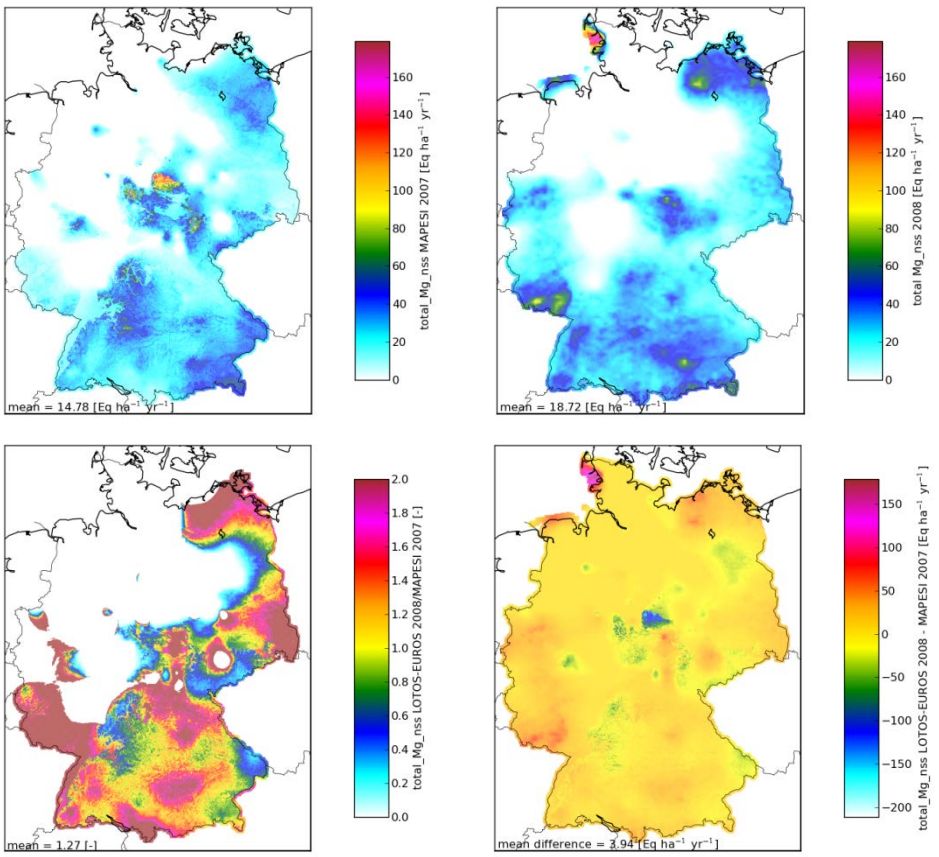

5.10 K^+-nss

Figure 49. Total deposition of K^+-nss in MAPESI 2007 (upper left), PINETI 2008 (upper right), relative difference between PINETI 2008 and MAPESI 2007 (lower left) and absolute difference between PINETI 2008 and MAPESI 2007 (lower right).

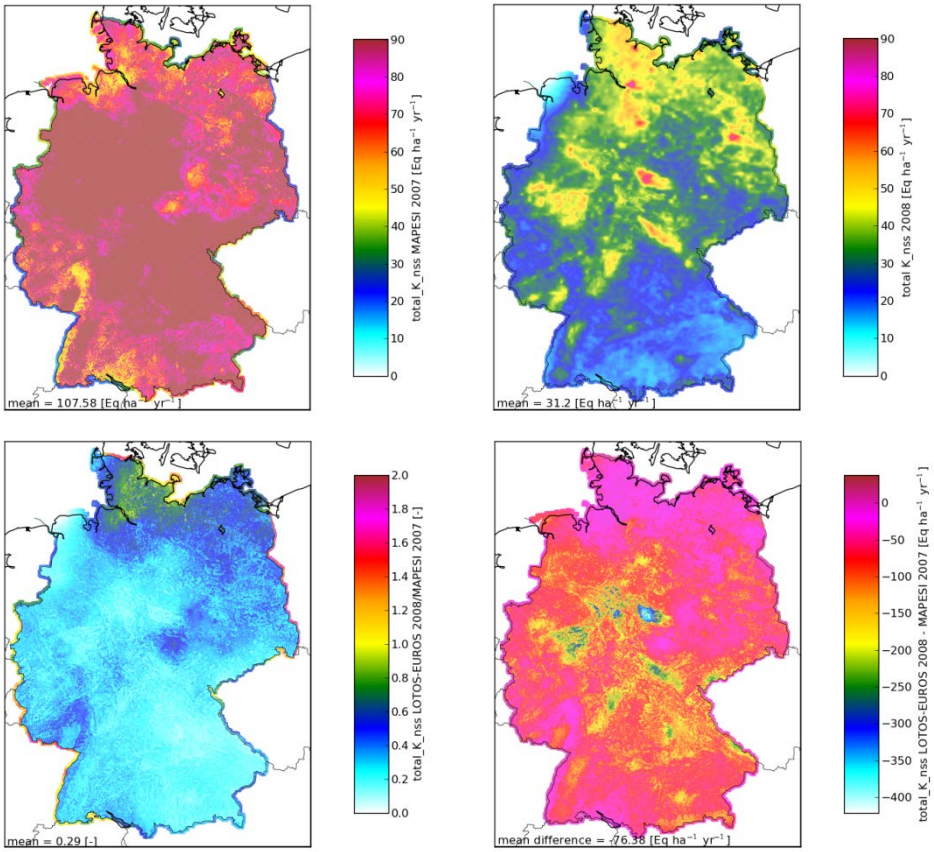

6 Comparison with EMEP deposition

In this chapter, the results from PINETI are compared with the EMEP results for the years 2008 (Unified EMEP model version rv3.6; www.emep.int). Note that the EMEP model operated at a resolution of 50 Km. Table 18 shows the country average dry, wet and total deposition of SO_x, NH_x and NO_y over Germany in 2005, 2008 and 2009 from EMEP MAPESI and PINETI. Note that the total deposition in this case only consists of the dry and the wet deposition and that the occult deposition is not considered here as this process is not explicitly modeled by EMEP. This explains the small differences between PINETI results presented in Table 16 and Table 18.

For comparison, model results from EMEP and LOTOS-EUROS (L-E) for the year 2005 are also included. These results were obtained from MAPESI-Bericht Anhang IV (Builtjes et al., 2011). The LOTOS-EUROS model results from the MAPESI study for the year 2005 will be called L-E hereafter. Note that the wet deposition results of the LOTOS-EUROS model were not officially used in MAPESI, i.e., the official wet deposition in MAPESI was derived from observations only. The final results from MAPESI for the year 2005 are therefore also presented in Table 18 and originate from the figures in MAPESI-Bericht Anhang XI (Builtjes et al., 2011). Note that the dry deposition in MAPESI is slightly different from the original modeled dry deposition by LOTOS-EUROS (L-E), which is likely due to the conversion to the 1 x 1 km^2 grid.

The table shows that the dry deposition of all components is generally larger in the PINETI/MAPESI results than in the EMEP results. In contrast, the wet deposition of all components is smaller in the PINETI/MAPESI results than in EMEP results. Note that the PINETI wet deposition results are based on a combination of measurements and LOTOS-EUROS model results, while MAPESI results are based on measurements only, and the L-E and EMEP results are based on model results only. It is therefore likely that the EMEP results slightly overestimate the wet deposition. As a consequence of this overestimated removal of mass by wet deposition in the EMEP model, less mass is available for dry deposition. This could explain the lower values for the dry deposition in the EMEP results. We have to remark here that the LOTOS-EUROS model underestimates the wet deposition of all components. This is reflected by the lower modeled wet deposition results from L-E in 2005 as compared to the wet deposition results in MAPESI in 2005, in which only observations were used or the wet deposition results in PINETI in 2008 and 2009, in which the model results were adjusted with the observed wet deposition. There is, however, no feedback mechanism in the model yet to account for this correction by the measurements, and therefore, the corrections are not included in the mass balance calculations. As a consequence, the dry deposition results of LOTOS-EUROS in MAPESI and PINETI might be on the high side.

If we look at the total deposition, we see that the L-E results for 2005 were lower than the ones for EMEP in 2005, but for 2008 and 2009 this is the other way around, i.e., the PINETI results are higher than the EMEP total deposition for 2008 and 2009. This is mainly due to the correction of the wet deposition in the PINETI results, but also due to a rather large reduction in the dry deposition of NO_y and SO_x in the EMEP results. The overall differences between EMEP and PINETI results are in the order of about 15% and are well within the estimated model uncertainty for annual average deposition fluxes of about 30%.

Table 18. Overview of annual average deposition results of PINETI and EMEP for SO_x, NH_x and NO_y in 2008 and 2009. Annual averages in 2005 are the EMEP and LOTOS-EUROS (L-E) results from MAPESI-Bericht Anhang IV (Builtjes et al., 2011). MAPESI results for 2005 originate from MAPESI-Bericht Anhang XI (Builtjes et al., 2011).

model eq ha^{-1} yr^{-1}	2005 EMEP	2005 L-E	2005 MAPESI	2008 EMEP	2008 PINETI	2009 EMEP	2009 PINETI
dry SO_x-S	201	214	213	152	213	134	196
wet SO_x-S	283	120	231	205	198	209	188
total SO_x-S (dry + wet)	484	334	444	357	411	344	384
dry NH_x-N	313	511	511	276	487	289	480
wet NH_x-N	434	136	371	422	313	449	319
total NH_x-N (dry + wet)	747	647	882	698	800	739	799
dry NO_y-N	208	260	265	116	202	102	201
wet NO_y-N	290	177	267	248	245	256	247
total NO_y-N (dry + wet)	498	437	532	364	447	359	448

In the following figures the spatial distributions of the EMEP results are compared with the spatial distributions in PINETI for the year 2008. Table 19 can be used to convert the units in the EMEP results to the units that are used in the PINETI results vice versa.

Table 19. Conversion factors to convert from mg (N/S) m^{-2} to eq ha^{-1} yr^{-1}

conversion factors	eq = mg / atomic weight * valence
mg S m^{-2}	eq ha^{-1} yr^{-1}
1.00	0.63
mg N m^{-2}	eq ha^{-1} yr^{-1}
1.00	0.71

6.1 Comparison between dry deposition EMEP 2008 and PINETI 2008

dry SO_x-nss EMEP 2008	dry SO_x-nss PINETI 2008
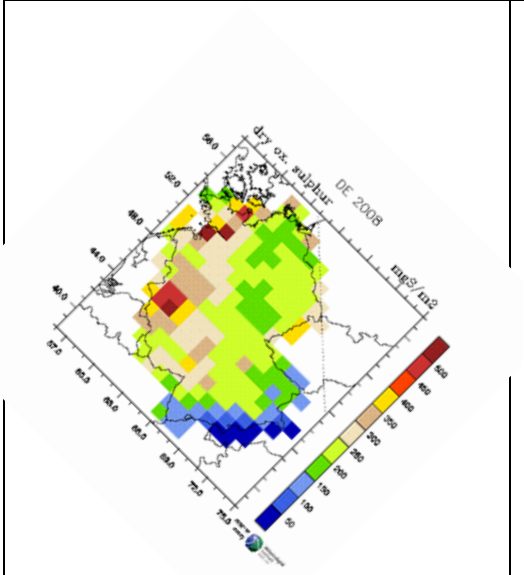	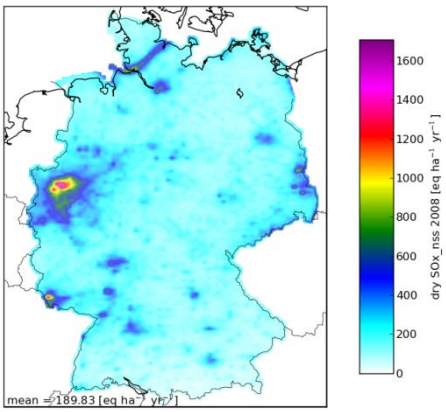
dry NH_x EMEP 2008	dry NH_x PINETI 2008
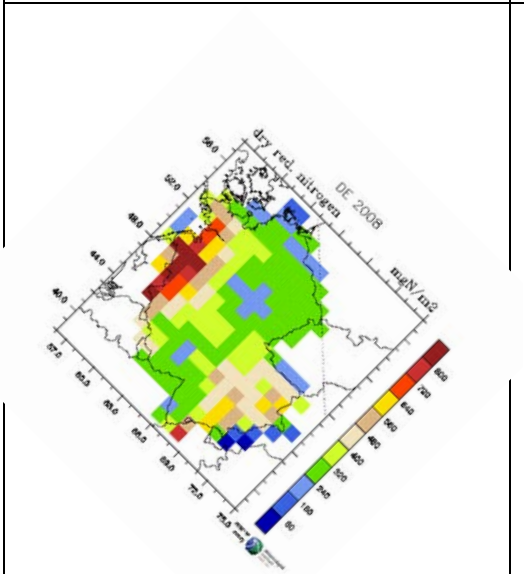	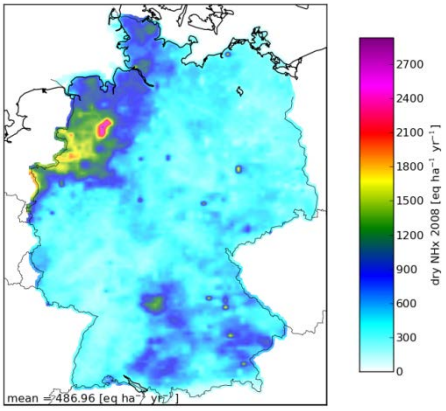

dry NO_y EMEP 2008	dry NO_y PINETI 2008
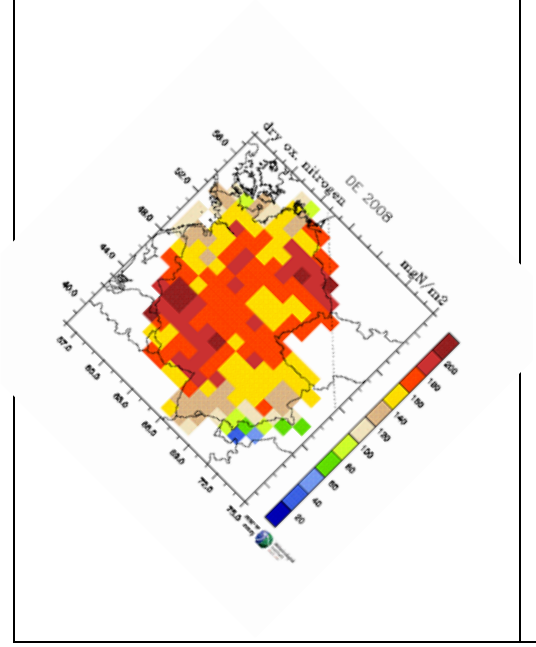	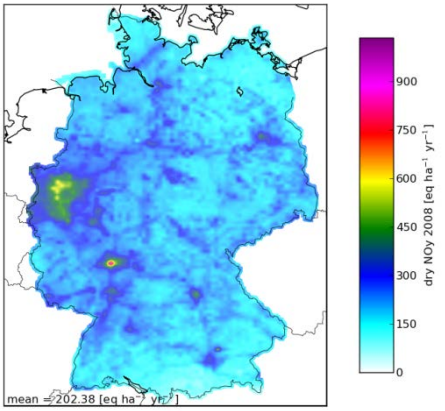

6.2 Comparison between wet deposition EMEP 2008 and PINETI 2008

wet SO_x-nss EMEP 2008	wet SO_x-nss PINETI 2008
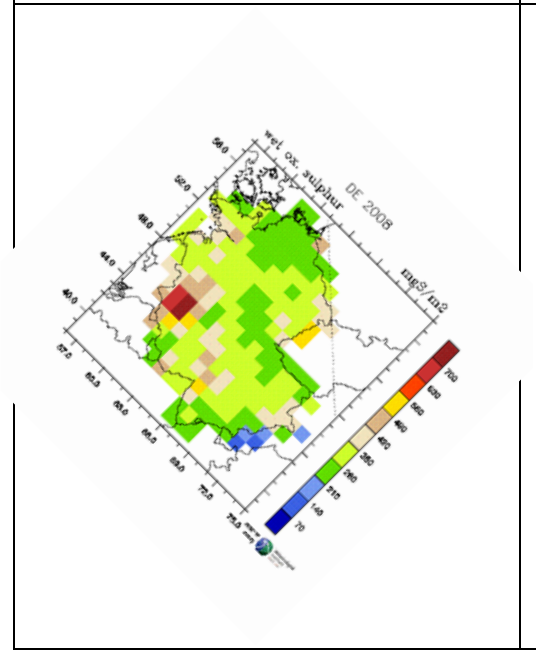	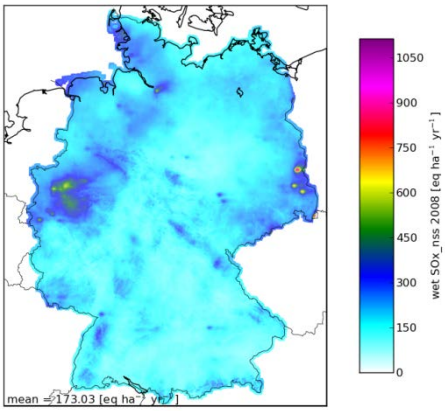

wet NH_x EMEP 2008	wet NH_x PINETI 2008
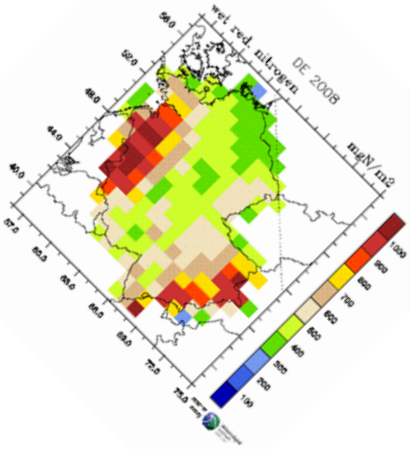	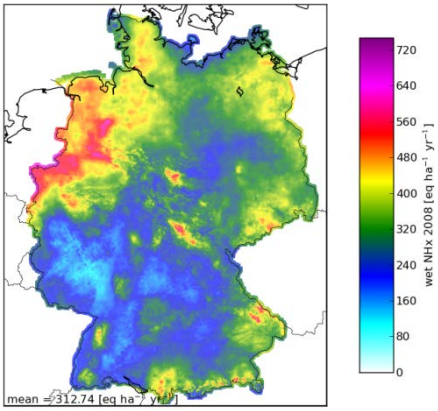
wet NO_y EMEP 2008	wet NO_y PINETI 2008
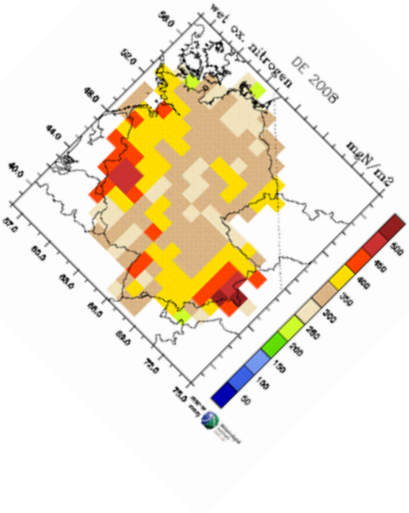	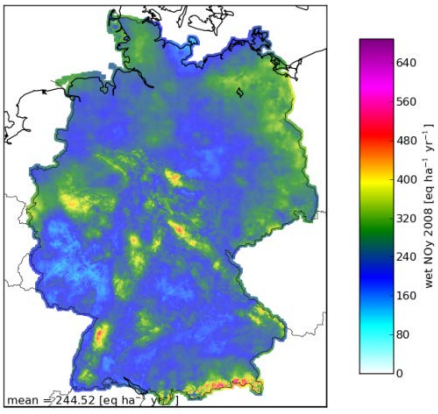

precipitation EMEP 2008	precipitation PINETI 2008
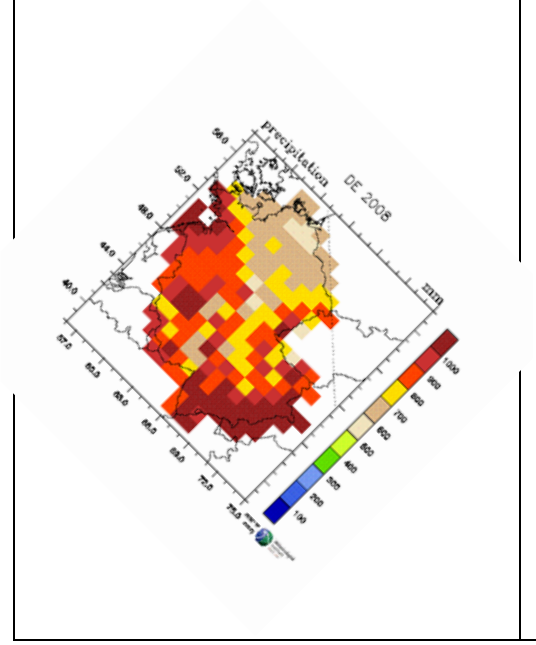	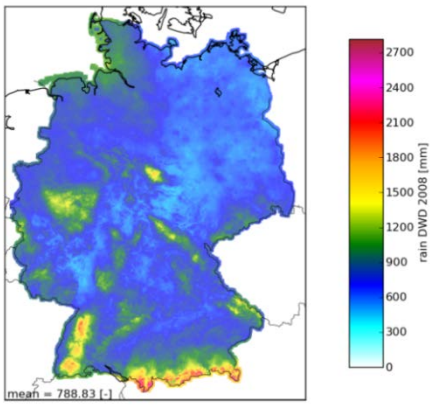

6.3 Comparison between total deposition EMEP 2008 and PINETI 2008

total SO_x-nss EMEP 2008	total SO_x-nss PINETI 2008
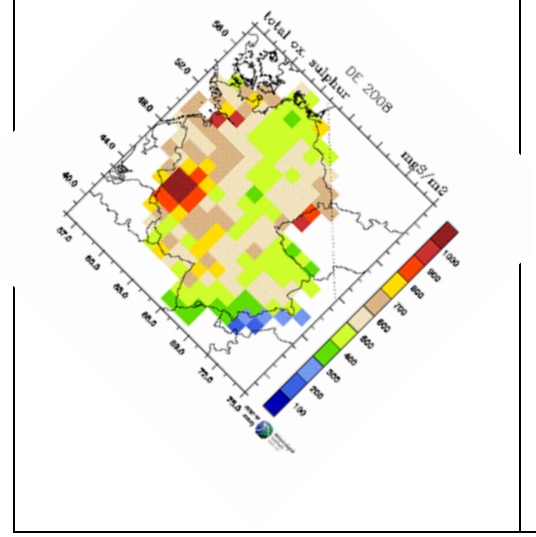	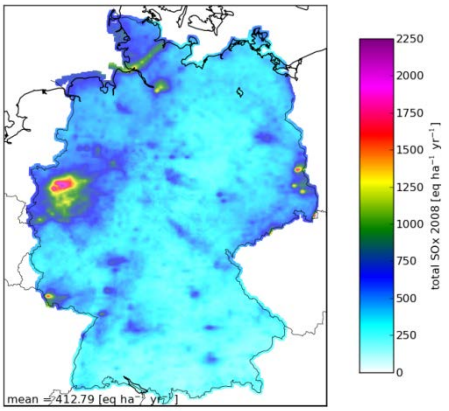

total NH_x EMEP 2008	total NH_x PINETI 2008
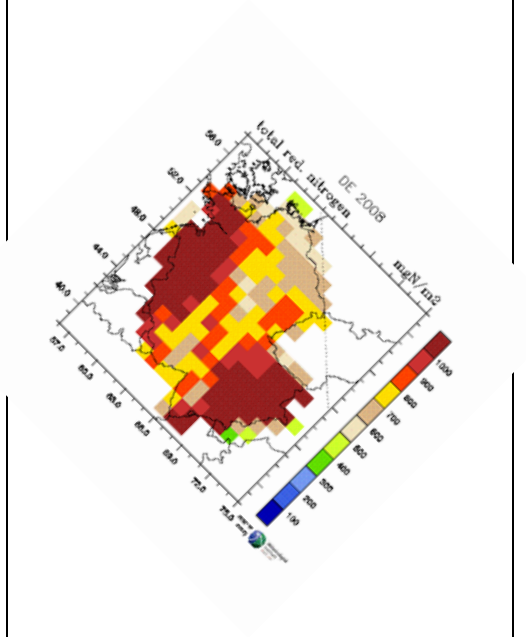	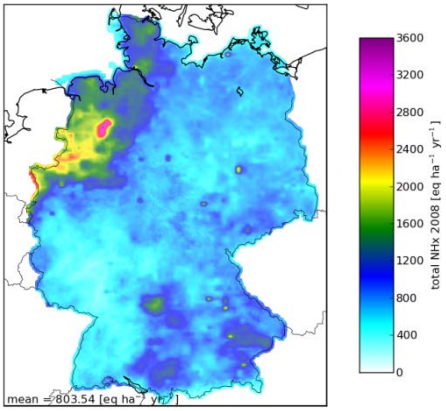
total NO_y EMEP 2008	total NO_y PINETI 2008
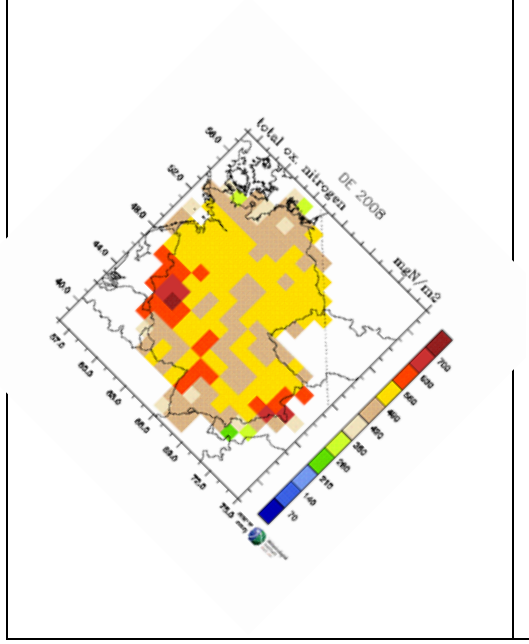	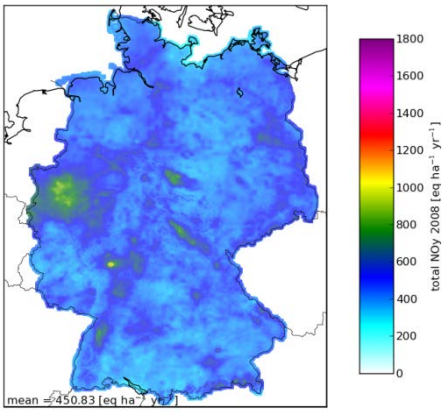

7 Uncertainty analysis within PINETI

7.1 Introduction

General aspects

The purpose of this chapter is to address the item “uncertainty” with the focus on the uncertainty of the most relevant aspect of the PINETI-project, which is the uncertainty of the total yearly averaged N-deposition. The chapter should be seen as a discussion paper, and it is recommended that it will be discussed further with national and international experts.

The discussion will first address the N-deposition over Germany, with a grid-resolution of about 7 x 7 km^2, which is 0.0625 x 0.125 long/lat, later on, the uncertainty on the scale of 1 x 1 km^2 will be addressed. The aim is to derive quantitative information over Germany of the uncertainty (expressed as one-sigma) for the determined total yearly averaged N-deposition.

The focus here is on the total N-deposition. It is well known that the uncertainty in the deposition of reduced N will be larger than that of oxidized N, due to the fact that the uncertainty in NH_3-emissions is most likely larger than in NO_x-emissions, and that NH_3 is a more local phenomena due to a shorter lifetime in the atmosphere and local emission sources. A detailed analysis of the differences between uncertainties of NH_3 and NO_x is however beyond the limits of the analysis made here.

Uncertainty and observations

The uncertainty results that will be produced will be presented on 7 x 7 km^2. The reason is that the basic information of the calculated total N-deposition is based on information on this 7 x7 km^2 grid-scale. The downscaling to 1 x 1 km^2, which is the requested grid-resolution by UBA due to the effects of N-Deposition, is prepared as a post-processing, and creates its own extra uncertainty. This extra uncertainty will also be discussed, but only after the discussion for the coarser grid. It should also be mentioned that the determined deposition on 7 x 7 km^2 as well as on 1 x 1 km^2 should be viewed as background-deposition load. It is often thought that a higher grid resolution will automatically lead to better results and is assumed to improve the model performance, as details, e.g. in orography or emissions, are better resolved. However, this is only the case if indeed emissions and especially also meteorology are accurately known on the higher resolution. Also, mostly the orography on a higher resolution is in fact not taken into account explicitly , as the meteorology is based on a coarser resolution.

A distinction should be made between variability and uncertainty, although the two are connected. The total N-deposition will be different from year to year, mainly because of meteorological variability and because of emission changes. Emission changes will be visible mostly as –often rather gradual- trends, whereas meteorological variability will show up in year to year changes, and more in wet than in dry deposition. An indication of the meteorological variability can be found in Andersson et al, 2007. Over a 44 year period the fractional bias (defined as averaged bias over the 44 year period based on the value for a specific year minus the value averaged over all years divided by the average over all years) for an area containing Germany is about +/- 10 % for total dry N-deposition and about +/- 15 % for total wet deposition.

A change from one year to another can of course be substantially larger. It is also clear that a change from one year to another for a specific grid of 7 x 7 km^2 will again be larger than the values of 10 and 15 % given above for a large area as Germany. Changes of total N-deposition for a grid of 7 x 7 km^2 from one year to another due to only meteorological variability of up to 50 % might well be possible. So, both variability and uncertainty increase at higher resolution.

It should be noted that the total uncertainty can be due to 1) complexity and chaotic behavior as well as 2) lack of knowledge and information. It should be clear that the uncertainty mentioned under item 1), which can be partly considered as inherent variability, can in principle not be reduced.

The uncertainty, which also could be called bandwidth, could be defined as the difference between the given total yearly averaged N-deposition for a grid of 7 x 7 km^2, in comparison to the "real" value. In chemistry transport model evaluation studies this "real" value is the observed concentration. Ideally, this observed concentration should be representative for the 7 x 7 km^2 grid, or should be the averaged of a number of observations within such a grid. Numerous studies have been carried out to study this comparison between calculated and observed concentrations, often using a number of chemistry transport models, including the LOTOS-EUROS model which is the model used in the PINETI-project. See for example Vautard (2007, 2009), van Loon (2007). A vital aspect in these studies is the fact that in a "correct" comparison, the observed concentration should be representative for the considered model grid. In fact, rather complex chemistry transport models like the LOTOS-EUROS model cannot just simply be validated against observations. These models have to be judged on the quality of the science, through documentation, reviews, and assessments (Raes, 2012). These above-mentioned model intercomparison studies, show that modeled and observed concentrations of several species like O_3, NO_x are in general within 20-30 %. A similar conclusion is drawn in the UBA-PAREST project (Stern, 2010).

Concerning total N-deposition the main challenge is the lack of direct observations of total N-deposition. Total N-deposition is divided in dry deposition, wet deposition and occult/cloud/fog deposition. Of these 3 types of deposition the dry deposition is only measured in special campaigns and only at a very few locations. The purpose of these dry deposition measurements is to study the dry deposition process and to derive process descriptions. Consequently, these observations cannot be used to perform a model evaluation study over Germany. The same holds for the occult deposition. There is no regular monitoring of the occult deposition, and observations are only carried out at specific locations and in specific campaigns. Additionally, the observations of dry and occult deposition do not really measure dry and occult deposition. Theoretical considerations and local modeling are needed to derive dry and occult deposition from these observations. For a more detailed analysis of occult deposition, see Task 1 of the Extension report (Teilbericht 3).

Concerning wet deposition, the uncertainty analysis is different from that for the dry deposition. Wet deposition is measured routinely over Germany at a large number of sites. The drawback for a detailed comparison with modeled wet deposition is that the wet deposition samples are generally only collected weekly (and sometimes even 2-weekly), and that the modeled wet deposition is provided on an hourly basis, which makes a process oriented comparison not directly possible. In addition, modeling wet deposition is directly related to the rain information given by the meteorological input data. Errors in rain intensity and location,

which occur frequent, also due to the not always spatial representativeness of rain/wet deposition observations, are difficult to estimate.

In the following we sketch tentative assessments of the uncertainty of the N-deposition, separated in dry and wet N-deposition (see chapter 7.4 for the occult deposition). Given the paucity of dedicated studies the estimates are based on both available literature and expert judgments. The uncertainty of the modelled N-deposition in Germany has been discussed already in Builtjes et al, 2011. Below, the discussion will be continued by summarizing the current state of knowledge, proposing estimations of the different uncertainties, and sketch possible ways to derive a more quantitative estimate in the future.

7.2 The uncertainty of yearly averaged dry deposition data over Germany and over grids of 7 x 7 km^2

7.2.1 Methodology

As stated, there is no regular monitoring network that measures dry deposition over Germany/Europe. There is, however, the Airbase, including EMEP, monitoring network that measures concentrations throughout Germany and Europe, mainly measuring $NO/NO_2/HNO_3$ and sometimes NH_3 as well as aerosol-components containing N, e.g. NH_4^+ and NO_3^-. The dry deposition in the LOTOS-EUROS model is determined by the resistance approach, following the approach by Zhang (2001). This means that the uncertainty of the calculated dry deposition will be based on the uncertainty of the modeled concentration, and the uncertainty in the Zhang-approach.

7.2.2 Input data

The uncertainty with respect to the comparison between modeled and calculated annual mean concentrations on 7 x 7 km^2 is estimated to be about 20-30 % on average, see the discussion above. This 20-30 % is valid for areas without strong orography and large spatial emission changes, and only when the observations are representative for larger areas, e.g., background/rural observations.

The uncertainty of the dry deposition calculated by the model is obviously larger than the uncertainty in the concentrations, as the dry deposition flux calculation contains more parameters, i.e., all the resistance parameters. All these parameters are based on values valid for and averaged over the 7 x 7 km^2 grid. This means that these values are no point, local values, but are averaged values over this 7 x 7 km^2 grid.

The atmospheric resistance is rather well known, but especially parameters like the stomatal resistance contain large uncertainties. A separate analysis per parameter is beyond the scope of the analysis given here, and it is also unlikely that such a detailed analysis would lead to a difference in the overall uncertainty. As stated, the largest uncertainty in the determination of dry deposition might well be with the stomatal resistance. No approach is known by which this uncertainty can be diminished, this inherent uncertainty has to be accepted.

7.2.3 Estimation of the uncertainty

Taking everything into account the uncertainty per 7 x 7 km^2 grid for the dry deposition will be about 40 %; in regions characterized by strong heterogeneity in, e.g., orography or

emissions the uncertainty may be increased further. This increased uncertainty is due to the fact that in general the detailed information of the heterogeneity is lacking. Only in case this information would be available with a high precision, an improvement in the uncertainty might be possible.

The overall uncertainty in the dry deposition of N over the whole of Germany will be less than the 40 % for a grid of 7 x 7 km^2, because this dry deposition over Germany is the result of the mass balance over Germany as a whole. The best estimate for the uncertainty in the yearly averaged total dry deposition of N-deposition over Germany would be about 30 %. This value has also been mentioned and discussed before within the MAPESI-project (Builtjes et al, 2011).

7.3 The uncertainty of yearly averaged wet deposition data over Germany and over grids of 7 x 7 km^2

7.3.1 Methodology

In the PINETI-project, the wet N-deposition on 7 x 7 km^2 is determined by combining the modeled wet deposition with the observed wet deposition using a kriging method. This is done on the basis of annual averaged model results as well as annual averaged observations. Finally, the fields are combined with annual averaged precipitation fields on a 1 x 1 km^2 grid to obtain the wet deposition field.

The reason for combining the model results with observations and not using the model results directly is that the current operational model version of LOTOS-EUROS uses a simple scavenging approach for the wet deposition to cover both in-cloud and below-cloud processes, and neglects the influence of changing pH-values, and in general resulting in lower modelled wet deposition than observed. The drawback of not being able to use the modeled wet deposition directly is that by combining the modeled with the observed wet deposition, there is no feedback of the resulting wet deposition on the modeled concentrations. This leads to inconsistencies, and a slightly too high dry deposition, and to the fact that the impact of emission scenarios cannot be calculated directly.

7.3.2 Input data

The modeled concentration data are not explicitly used to calculate the wet deposition, because wet deposition is determined by a combination of model results and observations. A separate uncertainty of the observed wet deposition, based on the spatial representativeness and the measurement uncertainty as such, seems not to be available in the current literature, but is unlikely to be less than 30 %.

7.3.3 Estimation of the uncertainty

The uncertainty in the determined wet deposition will be smaller than for the dry deposition, because the combined modeled and observed wet deposition obtained with the kriging method are close to each other. It can be estimated that the uncertainty in the yearly averaged wet deposition by applying this method for grids of 7 x 7 km^2 will be about 20 %, and in case of strong heterogeneity about 30 %. For the total wet deposition over Germany the uncertainty is estimated to be about 15 %, see Andersson, 2007

In case the determination of the wet deposition, as for the dry deposition, is based on the chemical transport model alone, the total wet deposition uncertainty will still be about 15 %. No approach is known by which this uncertainty can be diminished, this inherent uncertainty has to be accepted.

It should be mentioned that the wet and dry deposition, and so their uncertainties are related. The reason is that the concentration will be influenced by the magnitude of the dry deposition:in the example of a large dry deposition the remaining concentration available for wet deposition is lower, leading to a lower wet deposition and obviously, also vice versa.

7.4 The uncertainty of yearly averaged occult deposition data over Germany

For a more detailed analysis, the reader is referred to Task 1 of the extension report (Teilbericht 3). Here, for completeness, only a number of remarks is made.

The occult deposition, in literature also called cloud or fog deposition, is a phenomenon that occurs when clouds/ fog get in contact with the vegetation over a certain area, often in mountainous regions and in situations with low wind speed. The phenomenon is thought to be important/relevant especially in areas in Germany like the Black Forest and the Bayrian Forest with large orography. In the PINETI-project, the occult deposition was determined following the empirical method by Bleeker, 2000. Due to the very local (sub grid) character of the phenomena and the many empirical factors and choices in the method by Bleeker, the uncertainty of the modelled occult deposition is estimated to be about a factor of 2 for a grid of 7 x7 km^2. It might even be questioned whether the occult deposition can be modeled in a way that high quality results can be achieved at all (Klemm et al, 2007). Consequently, the yearly averaged occult deposition will add to the uncertainty in the total N-deposition in areas with clear orography. Because the occult deposition is only relevant in certain areas of Germany - the Bleeker method considers occult deposition only to occur at levels above 250 m a.s.l. - an uncertainty over the whole of Germany is consequently not relevant, and is location dependent.

7.5 The uncertainty of yearly averaged total N-deposition data over Germany

Based on the analysis given above, the uncertainty of the total yearly averaged N-deposition over Germany will be close to 30 %, and is mainly determined by the uncertainty in the dry deposition.

The average grid-scale uncertainty of the total N-deposition per 7 x 7 km^2 is about 30 to 50 %. In very inhomogeneous grids (e.g., strong orography or close to sources) the uncertainty can be well above this estimate. Similar values are given for the UK, Dore, 2012, Denmark, Geels et al, 2012 and the Netherlands (Velders et al, 2012, Erbrink, 2012)

7.6 Increasing resolution and uncertainty, from 7 x 7 km^2 to 1 x 1 km^2

7.6.1 Estimation of the uncertainty

As stated, the determination of the 1 x 1 km^2 deposition is performed in a post-processing procedure, and is not calculated directly within the model. Differences in land use and cover within a grid of 7 x 7 km^2 are taken into account, but the concentration and the meteorology is still the 7 x 7 km^2 averaged values. In case the computer-power and –storage was large enough,

a “real “calculation on 1 x 1 km^2 with the full model could be performed, in principle leading to better results.

However, to be realistic this would mean that all input parameters: meteorology, emissions, land use, should be available, and be reliable, on this 1 x 1 km^2 scale. This is in fact only to some extent the case for the land use and the emissions. But even for the land use and the emissions the real land use and the emissions with all its gradients is not represented in data bases. The same holds for meteorological data. Also here, as mentioned above, one has to live with inherent uncertainties that are not possible to decrease further. This all means that the uncertainty on a grid of 1 x 1 km^2 will in generally be larger than for the averaged values on the 7 x 7 km^2 scale. However quantifying this increase requires further elaborations (cf. next chapter). As a first tentative estimate we expect in a generic sense that the confidence interval may enlarge by a factor of about 1.5. It should be noted that the best estimate is still the average value resulting from the model.

Possibilities to determine sub grid scale processes further within a 1 x 1 km2 grid would be to use local point and line sources (Gaussian type) or even more refined local models like CFD-Computational Fluid Dynamics models or LES-models. Comparing such a detailed approach with averaged values for a 1 x 1 km2 and 7 x 7 km2 grid, respectively could provide a much more reliable estimate of the uncertainties involved. It should be noted that such a study would be very time consuming.

The recent study by Dore, 2012 using different grid sizes of 50 x 50 km^2, 5 x 5 km^2 and 1 x 1 km^2 over the UK shows the clear benefits of using a grid size of 1 x 1 km^2, provided the emission data and the meteorology-especially the rain fall- is available and reliable on the small grid scale. A similar study concerning NH_3 has been performed by Geels et al. (2012) in combining a chemistry transport model with a smallest grid size ca. 6 x 6 km^2 with a local model down to 400 x 400 m^2. Again, the study shows improved results at the small scale providing that especially the NH_3-emission data are available on that scale. A nested model run going from the 7 x 7 km^2 of the LOTOS-EUROS model down to 1 x 1 km^2, and adding a local Gaussian type model for the even smaller features, would show the impact of such a calculation, relative to the post-processing used in the current PINETI-project.

Additional insight could be provided by further sensitivity studies, e.g., by varying emissions and meteorological input parameters in a systematic way and studying the effects on the overall result.

7.6.2 Some additional remarks

Uncertainties will show up and play a large role in especially local studies. Here, attempts should be made to use consistent models and input data going from the larger to the local scale.

Uncertainties will also show up across country borders. Differences in total N-deposition will show up due to the fact that –slightly- different models and methods, and input data are used from one country to another. However, on the mentioned grid scale of 7 x 7 km^2, these differences should in general not exceeded values of 50 %.

7.6.3 Uncertainty communication

The way that uncertainty is communicated has a substantial impact on the way people perceive uncertainty. A good example is the method how in climate change the inherent uncertainty is expressed by the IPCC, by giving a bandwidth for the expected temperature increases. Also the way in which uncertainty is visualized will affect the way how uncertainty is perceived.

7.6.4 Summary

The uncertainty of the determined total N-deposition is most likely dominated by the uncertainty in the dry deposition. It should be stressed that the provided total N-deposition in this project is the best estimate according to present knowledge.

For local applications sub-grid scale phenomena like abrupt changes in land use, orography and emissions will increase the uncertainty.

It is recommended that the aspect of uncertainty should be elaborated further in future research projects and discussed within a wider international community.

7.6.5 References

Andersson, C, J.Langner, R.Bergstrom, 2007. „Interannual variation and trends in air pollution over Europe due to climate variability durinh 1958-2001 simulated with a regional CTM coupled to the ERA40 reanalysis". Tellus, 59B, 77-98.

Bleeker, et al, 2000. Deposition of acidifying components and base cations in Germany in the period 1987-1995. RIVM report 722108027, Bilthoven, the Netherlands. 124 pp.

Builtjes, P., et al, 2011: Modelling of Air Pollutants and Ecosystem Impact (MAPESI), In German, FKZ 3707 64 200.

Dore et al, 2012, The influence of model grid resolution on the estimation of national scale nitrogen deposition and exceedance of critical loads. Biogeosciences 9, 1597-1609.

Dore, T. et al, 2012: Evaluation and Inter-comparison of Acid Deposition Models for the UK. Proceedings, 32 th ITM on Air pollution modeling and its application, Utrecht, the Netherlands. 505-510.

Erbrink, J.J, 2012. How to proceed with calculations of N-deposition (in Dutch), Magazine Air, 8, nr 6, 29-30.

Geels, C, et al, 2012, Improved modeling of atmospheric ammonia over Denmark using the coupled modeling system Damos. Biogeosciences , 9, 2625-2647.

Klemm, O, et al, 2007, Fog deposition fluxes of water and ions to a mountainous site in Central Europe, Tellus, 59,705-714.

Loon, van M., R. Vautard, M. Schaap, R. Bergström, B. Bessagnet, J. Brandt, P.J.H. Builtjes, J. H. Christensen, K. Cuvelier, A. Graf, J.E. Jonson, M. Krol, J. Langner, P. Roberts, L. Rouil, R. Stern, L.

Raes, Frank, 2012 . Air and Climate, Conversations about molecules and planets, with humans in between. JRC-Report, ISBN 978-92-79-25195-5

Stern, R., 2010. Analysis of the uncertainties/bandwidth in the PAREST-project in the chain Emission-Transport-Concentration (in German) UBA-Report FKZ 206 43 200/01

Tarrasón, P. Thunis, E. Vignati, L. White, P. Wind (2007), Evaluation of long-term ozone simulations from seven regional air quality models and their ensemble average, Atmospheric Environment, 41 (10), 2083-2097.

Vautard, R., Builtjes, P. J.H., Thunis, P., Cuvelier, K., Bedogni, M., Bessagnet, B., Honoré, C., Moussiopoulos, N., Pirovano G., Schaap, M., Stern, R., Tarrason, L., Van Loon, M. (2007), Evaluation and intercomparison of Ozone and PM10 simulations by several chemistry-transport models over 4 european cities within the City-Delta project, Atmospheric Environment*, 41, 173-188*.

Vautard, R., Schaap, M., Bergström, R., Bessagnet, B., Brandt, J., Builtjes, P.J.H., Christensen, J.H., Cuvelier, C., Foltescu, V., Graff, A., Kerschbaumer, A., Krol, M., Roberts, P., Rouïl, L., Stern, R., Tarrason, L., Thunis, P., Vignati, E., Wind, P. (2009) Skill and uncertainty of a regional air quality model ensemble. Atmospheric Environment, DOI: 10.1016/j.atmosenv.2008.09.083.

Velders, G, et al, 2012. Large scale concentration and deposition maps over the Netherlands (in dutch). RIVM-Report 680362002/2012.

Zhang, M et al, 2001. A comparison of models to estimate in-canopy photosynthetical active radiation and their influence on canopy stomatal resistance, Atm. Env 35, 4463-4470.

8 Discussion, conclusions and outlook

The PINETI project aimed at assessing the risk associated with the deposition of nitrogen and sulfur compounds in Germany. This report summarizes the estimation of the deposition loads. The risk assessment and further technical developments and validations are summarized in reports 2-4.

Numerous studies show that high resolution deposition data allow for reliable risk assessments (e.g., Geels et al., 2012). However such high resolution modeling may increase the single plot uncertainty and is strongly dependent on the availability of high resolution input data (e.g., meteorology and emissions; cf. Chapter 7). Finally, the estimation of the pollutant deposition load is not only dependent on the spatial resolution chosen but also on the particular modeling techniques.

In this concluding chapter we will thus briefly discuss the results of the PINETI project in comparison to the results of the European consensus model EMEP (operating on a much larger model domain with a coarser resolution) and the results of the previous MAPESI project. We will conclude with a concise outlook regarding further technical improvements and open research questions.

8.1 Comparison with EMEP

In chapter 6, we have seen that the magnitude of the total deposition fluxes in PINETI compare well with the results of the EMEP model (within 25% difference). The same holds for the overall pattern of the spatial distribution. Due to the smaller grid size (PINETI: 1 x 1 km^2; EMEP: 50 x 50 km^2; since 2013: approximately 25 x 25 km^2) the PINETI results provide a more detailed picture for Germany. This also leads to 'hot spots' being clearly visible in the distributions and being much more pronounced than in the EMEP data. For example, power plants are clearly visible in the SO_x deposition fields close to the north-eastern border of Germany.

In PINETI the wet deposition flux is determined empirically and replaces the LOTOS-EUROS wet deposition results. Differences between EMEP and PINETI results can be explained by differences in the ratio of dry and wet deposition in LOTOS-EUROS and EMEP models. These are induced by the combined differences in model parameterizations for chemistry, dry and wet deposition, etc. The lower wet deposition by LOTOS-EUROS and thus higher dry deposition explains why PINETI sum of modelled dry and empirical wet deposition yields somewhat higher total deposition fluxes than the EMEP model.

8.2 Comparison with MAPESI

Differences between the deposition loads for the year 2007 (MAPESI) and 2008/2009 (PINETI) are partly due to changes in emissions and a variable meteorology, e.g., the average precipitation decreased from 2007 to 2008 by 183 mm, which reduces the amount of wet deposition accordingly. Besides, it was agreed within the framework of the PINETI project to address two methodological improvements:

1. Evaluation of the use of model data to further improve the geostatistical interpolation between the measurement sites for the wet deposition estimate and
2. Evaluation of the current scheme for calculating cloud deposition fluxes and update the required input data.

Both evaluations resulted in improved calculation schemes. The use of these improved calculation schemes provide another reason for differences between the calculated deposition loads of the two projects.

8.2.1 Wet deposition

The use of residual Kriging (i.e., combination with model results) instead of observational Kriging resulted in a modified spatial distribution of the deposition loads (cf. chapter 5, Appendix C). In addition the average wet deposition load of reduced nitrogen calculated within PINETI is about 20% smaller than the one calculated within MAPESI, while the difference for oxidized nitrogen and sulfur is below 5% (see Teilbericht 3). Available (cross-) validations suggest that the improved method provides a physically more realistic estimate.

One consequence of the use of model data for the interpolation of the wet deposition field is the occurrence of wet deposition hotspots around large point sources. The total area affected by such a hot spot deposition is very small (likely only a few kilometers around the source), since the number of large point sources and the spatial extend of the effect is limited. As the measurement sites used for the geostatistical interpolation are not located in the close vicinity of these point sources, this hotspot pattern was fully absent in the maps obtained from the MAPESI method. An increased wet deposition around point sources is plausible and known from local measurements; however a comprehensive validation of magnitude and spatial extend of the modeled effect has not been done to date (see Teilbericht 3).

The method for calculating the national wet deposition field of base cations was only slightly adapted in comparison to the MAPESI project and the results of both projects are in reasonable agreement with each other and the results of a recently published study comprising a number of measurement sites in Germany (Dämmgen et al., 2013).

8.2.2 Occult deposition

The overall contribution of the cloud deposition flux to the national average deposition load is rather small (<5%). Locally it may however be much more important or even dominant. Obviously incorporating such a highly local phenomena into a national model is extremely challenging.

The general method to calculate the cloud deposition was not changed. We used the method as described by Bleeker et al. (2000) but using the more accurate hourly liquid water content (LWC) data from COSMO-EU. In this way, we avoided the use of climatological values for the LWC and cloud duration, which made the method more general to apply. As a result the cloud deposition load decreased quite strongly, particularly in mountainous regions such as the Rothaargebirge and the Harz. Literature results and measurements from the Bavarian Forest (Integrated Monitoring station Forellenbach) support the updated calculation scheme (see Teilbericht 3). Still, there are indications that the cloud deposition flux at very local, highly exposed sites (such as summits) is underestimated. Possible further improvements of the calculation scheme were gathered and assessed in a literature study (see Teilbericht 3).

8.2.3 Further changes

In the PINETI project, some inconsistencies in the method to calculate u* from the wind speed at 10 meters (from the meteorology) were resolved. In the calculation of u*, the 10 meter wind

speed is scaled up to 50 meters using the grid cell average roughness lengths from the meteorological input.

At this height, the influence of the vegetation below is assumed to be negligible. In the MAPESI project this calculation occurred with the stability function for heat (which is equal to the stability function of mass), while the stability function for momentum should have been used for the calculation of the wind speed at 50 meter, i.e., heat and mass are transferred more efficiently than momentum. In PINETI, the stability function for momentum is used to obtain the wind speed at 50 meters. From the wind speed at 50 meters, the land use dependent u* are calculated with the stability functions for momentum using the roughness lengths of the land uses that are present in the deposition routine. For the calculation of the atmospheric resistance, R_a, which is used to calculate the dry deposition flux, the stability functions for heat (and thus mass) is used in combination with the land use specific u*.

Besides the changes in the stability functions, some inconsistencies in the treatment of the displacement height for land use classes forest were removed. In MAPESI the displacement height was erroneously set to the canopy height, while in micrometeorological literature, two-third of the canopy height is generally given as a more realistic estimate for the displacement height. In PINETI, the displacement heights are therefore set at two-third of the canopy height, i.e., 13 meters for deciduous, coniferous and mixed forest.

These changes have resulted in a decrease in the dry deposition especially over the larger forest areas, which can be seen in Figure 32.

Within the MAPESI project the dry deposition results of LOTUS-EUROS were downscaled from the original 7 x 7 km² to the 1 x 1 km² grid by the use of a (observational) Kriging scheme. This allows taking into account the local-to-regional correlation. The application of the Kriging scheme involves however the important drawback of data smoothing meaning that single extreme values (minima or maxima) will diminish (see Figures 18, 20 and 22 from Appendix XVI of the MAPESI report, Builtjes et al., 2011). In the PINETI project the downscaling is done by using the 7 x 7 km² LOTOS-EUROS value in each 7 x 7-grid-center and interpolating linearly between these values by using a 2-dimensional interpolation scheme. As a result the hotspots of the dry (as well as the total) deposition are more pronounced in the maps of the PINETI project compared to the MAPESI project. For the area of the Frankfurt airport this means for the example of the LUC mixed forests that the deposition at the emission center is about 6 kg N ha^{-1} yr^{-1} higher compared to the MAPESI results. This local hotspot effect decreases strongly with distance: after about 5 km the surrounding background value is obtained.

8.3 Outlook and conclusion

Concerning model development, future research should focus on closing the mass balance. One of the current weaknesses in the modeling is the underestimation of the wet deposition process, which likely leads to a slight overestimation of the dry deposition. Although the modeled wet deposition is corrected with wet deposition observations, the modeled dry deposition is not due to a lack of dry deposition observations. This means that reducing the underestimation of the modeled wet deposition is a key priority to avoid an overestimation of the dry deposition and consequently an overestimation of the total deposition. Besides, new insight in the surface-atmosphere exchange of ammonia in the Netherlands indicate that dry deposition of ammonia is overestimated in especially the agricultural areas (Wichink Kruit et al., 2007, 2010). A new bi-directional surface-atmosphere exchange parameterization was developed (Van Zanten et el. 2010). This new parameterization leads to a shift of ammonia

deposition from agricultural areas to (semi-) natural areas. It is recommended to include this new bi-directional surface-atmosphere exchange parameterization in future model calculations.

9 References

Andersson, C, J. Langner, R. Bergstrom, 2007. „Interannual variation and trends in air pollution over Europe due to climate variability during 1958-2001 simulated with a regional CTM coupled to the ERA40 reanalysis". Tellus 59B, 77-98.

Bachmaier, M., Backes, M., 2011. Variogram or Semi-variogram? Variance or Semi-variance? Allan Variance or Introducing a New Term? Mathematical Geosciences 43, 735-740. doi:10.1007/s11004-011-9348-3

Bleeker, A., Draaijers, G.P.J., Klap, J.M., van Jaarsveld, J.A., 2000. Deposition of acidifying components and base cations in Germany in the period 1987-1995. RIVM report 722108027, Bilthoven, the Netherlands. 124 pp.

Builtjes, P.J.H., Hendriks, E., Koenen, M., Schaap, M., Banzhaf, S., Kerschbaumer, A., Gauger, T., Nagel, H.-D., Scheuschner, T., Schlutow, A., 2011. Erfassung, Prognose und Bewertung von Stoffeintraegen und ihren Wirkungen in Deutschland (in German). MAPESI-Project: Modeling of Air Pollutants and Ecosystem Impact. UBA Bericht zu BMU/UBA FE-Nr. 3707 64 200; Texte 38/2011; ISSN 1862-4804; Umweltbundesamt, Dessau-Roßlau, 2011.

CLRTAP, 2004. Manual on Methodologies and Criteria for Modelling and Mapping Critical Loads and Levels and Air Pollution Effects, Risks and Trends. (www.icpmapping.org)

CLRTAP, 2011. Mapping Manual. Chapter 3. Update June 2011. (www.icpmapping.org)

Cressi, 1993. Statistics for spatial data, Rev. ed edn, Wiley, New York.

Dämmgen, U., Matschullat, J., Zimmermann, F., Strogies, M., Grünhage, L., Scheler, B., Conrad, J., 2013. Emission reduction effects on bulk and wet-only deposition in Germany – evidence from long-term observations. Part 3: Sulphur and nitrogen compounds. Gefahrstoffe-Reinhaltung der Luft 73, 7/8 – July/August.

Denby, B., Schaap, M., Segers, A., Builtjes, P., Horálek, J., 2008. Comparison of two data assimilation methods for assessing PM10 exceedances on the European scale. Atmospheric Environment 42, 7122-7134.

Denier van der Gon, H.A.C., Visschedijk, A., van der Brugh, H., Dröge, R., 2010. A high resolution European emission data base for the year 2005. A contribution to UBA-Projekt PAREST: Particle Reduction Strategies, TNO report TNO-034-UT-2010–01895_RPT-ML, Utrecht, 2010.

Dore et al, 2012. The influence of model grid resolution on the estimation of national scale nitrogen deposition and exceedance of critical loads. Biogeosciences 9, 1597-1609.

Dore, T. 2012, Proceedings, 32th ITM on Air pollution modeling and its application, Utrecht, the Netherlands.

Draaijers, G. P. J., Van Leeuwen, E.P., de Jong, P.G.H., Erisman, J.W., 1996. Deposition of base-cations in Europe and its role in acid neutralization and forest nutrition. RIVM Report 722108017, Bilthoven, the Netherlands. 79 pp.

Erbrink, J.J, 2012. How to proceed with calculations of N-deposition (in Dutch). Magazine Air 8, nr 6, 29-30.

Geels, C., Andersen, H.V., Ambelas Skjøth, C., Christensen, J.H., Ellermann, T., Løfstrøm P., Gyldenkaerne, S., Brandt, J., Hansen, K.M., Frohn, L.M., Hertel, O., 2012. Improved modeling of atmospheric ammonia over Denmark using the coupled modeling system Damos. Biogeosciences 9, 2625-2647.

Grubbs, F., 1969. Procedures for Detecting Outlying Observations in Samples. Technometrics 11, 1-21.

Jörß, W., Kugler, U., Theloke, J., 2010. " Emissionen im PAREST Referenzszenario 2005-2020", Parest-Bericht Mai 2010.

Katata, G., H. Nagai, T. Wrzesinsky, O. Klemm, W. Eugster, and R. Burkard, 2008. Development of a land surface model including cloud water deposition on vegetation, J. Appl. Meteorol. Climatol., 47, 2129–2146, doi:10.1175/2008JAMC1758.1.

Katata, G., Kajino, M., Hiraki, T., Aikawa, M., Kobayashi, T., Nagai, H., 2011. A method for simple and accurate estimation of fog deposition in a mountain forest using a meteorological model. Journal of Geophysical Research , Vol. 116, No. D20, doi:10.1029/2010JD015552.

Klemm, O, et al, 2007. Fog deposition fluxes of water and ions to a mountainous site in Central Europe. Tellus 59, 705-714.

Köble, R and Seufert, G, 2002. Novel maps for tree species in Europe. Proc. of the 8th European Symposium on the Physico-Chemical Behaviour of the pollution. JRC-Ispra.

Kuenen, J., Denier van der Gon, H., Visschedijk, A., van der Brugh, H., van Gijlswijk, R., 2011. MACC European emission inventory for the years 2003-2007. TNO-060-UT-2011-00588, Utrecht, the Netherlands. 49 pp.

Loon, van M., R. Vautard, M. Schaap, R. Bergström, B. Bessagnet, J. Brandt, P.J.H. Builtjes, J. H. Christensen, K. Cuvelier, A. Graf, J.E. Jonson, M. Krol, J. Langner, P. Roberts, L. Rouil, R. Stern, L. Tarrasón, P. Thunis, E. Vignati, L. White, P. Wind, 2007. Evaluation of long-term ozone simulations from seven regional air quality models and their ensemble average. Atmospheric Environment 41, 2083-2097.

Monteith, J.L., Unsworth, M.H., 1990. Principles of environmental physics 2nd edn. Edward Arnold, London, 291 pp.

Raes, Frank, 2012 Air and Climate, Conversations about molecules and planets, with humans in between. JRC-Report, ISBN 978-92-79-25195-5.

Schaap, M., Sauter, F., Timmermans, R., Roemer, M., Velders, G., Beck, J., Builtjes, P., 2008. The LOTOS-EUROS model: description, validation and latest developments. International Journal of Environmental Pollution 32, 270–290.

Stern, R., 2010. Analysis of the uncertainties/bandwidth in the PAREST-project in the chain Emission-Transport-Concentration (in German). UBA-Report FKZ 206 43 200/01

Tarrasón, P. Thunis, E. Vignati, L. White, P. Wind (2007), Evaluation of long-term ozone simulations from seven regional air quality models and their ensemble average, Atmospheric Environment, 41 (10), 2083-2097.

UBA, 2012.
http://www.umweltbundesamt.de/sites/default/files/medien/419/dokumente/2012_02_09_em_entwicklung_in_d_trendtabelle_luft_v1.1.0.xls

Van Jaarsveld, J.A., 2004. The Operational Priority Substances model. Description and validation of OPS-Pro 4.1. Report 500045001. RIVM, Bilthoven.

Van Zanten, M.C., Sauter, F.J., Wichink Kruit, R.J., Van Jaarsveld, J.A., Van Pul, W.A.J., 2010. Description of the DEPAC module. Dry deposition modeling with DEPAC_GCN2010. RIVM Report 680180001/2010, Bilthoven, the Netherlands. 76 pp.

Vautard, R., Builtjes, P. H. J., Thunis, P., Cuvelier, K., Bedogni, M., Bessagnet, B., Honoré, C., Moussiopoulos, N., Pirovano G., Schaap, M., Stern, R., Tarrason, L., Van Loon, M., 2007. Evaluation and intercomparison of Ozone and PM10 simulations by several chemistry-transport models over 4 european cities within the City-Delta project. Atmospheric Environment 41, 173-188.

Vautard, R., Schaap, M., Bergström, R., Bessagnet, B., Brandt, J., Builtjes, P.J.H., Christensen, J.H., Cuvelier, C., Foltescu, V., Graff, A., Kerschbaumer, A., Krol, M., Roberts, P., Rouïl, L., Stern, R., Tarrason, L., Thunis, P., Vignati, E., Wind, P., 2009. Skill and uncertainty of a regional air quality model ensemble. Atmospheric Environment, DOI: 10.1016/j.atmosenv.2008.09.083.

Velders, G, et al, 2012. Large scale concentration and deposition maps over the Netherlands (in dutch). RIVM-Report 680362002/2012.

Wichink Kruit R.J., Van Pul W.A.J., Otjes R.P., Hofschreuder P., Jacobs A.F.G., Holtslag A.A.M., 2007. Ammonia fluxes and derived canopy compensation points over non-fertilized agricultural grassland in the Netherlands using the new gradient ammonia-high accuracy-monitor (GRAHAM). Atmospheric Environment 41, 1275-1287.

Wichink Kruit R.J., Van Pul W.A.J., Sauter F.J., Van den Broek M., Nemitz E., Sutton M.A., Krol M.C., Holtslag A.A.M., 2010. Modeling the surface-atmosphere exchange of ammonia. Atmospheric Environment 44, 945-957.

WMO-GAW report 160, 2004. Manual for the GAW precipitation chemistry programme. Guidelines, Data Quality Objectives and Standard Operating Procedures. WMO TD No. 1251.

Zhang, M et al, 2001. A comparison of models to estimate in-canopy photosynthetical active radiation and their influence on canopy stomatal resistance, Atmospheric Environment 35, 4463-4470.

10 Appendix A: spatial variability models

The following sections show for each of the components of interest the various spatial variability models considered:

1. The variogram based on yearly average concentrations from all stations. Each circle represents a mean value over pairs of observations with a certain distance range from each other.
2. The spatial covariance based on weekly concentrations from the UBA stations. Each circle is the sample covariance between two time series of observations.
3. The spatial covariance based on data of all stations, harmonized into a daily temporal resolution. Each orange dot represents a covariance between two harmonized time series, gray dots were rejected because time series were considered too short. The variability models obtained in this way are used for the final computations.

The parameters of the fitted variability model (sill, nugget fraction of sill, and length scale) are shown in red.

For the secondary inorganic components (SO_4^{2-}, NO_3^-, and NH_4^+), results are available for both observational and residual Kriging; for the metals (Na^+, K^+, Mg^{2+}, and Ca^{2+}), no model simulations are available and therefore only observational Kriging is present.

10.1 SO_4^{2-}

	observation Kriging	residual Kriging
variogram (yearly av.)	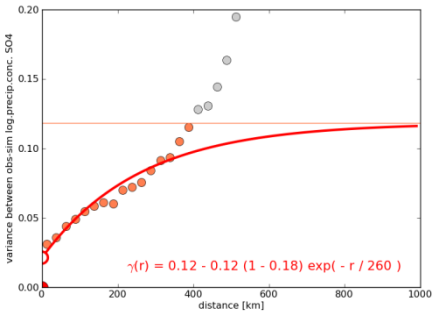	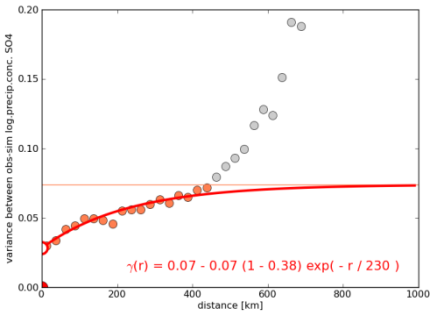
spatial covariance (UBA, weekly)	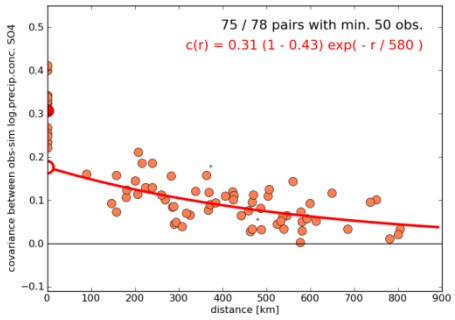	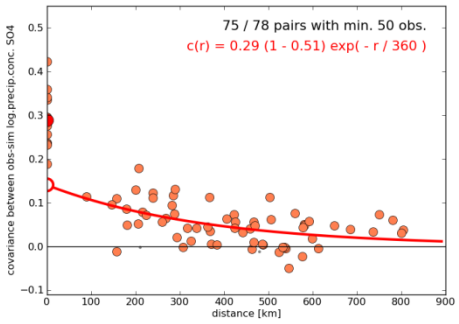
spatial covariance (all data, "daily")	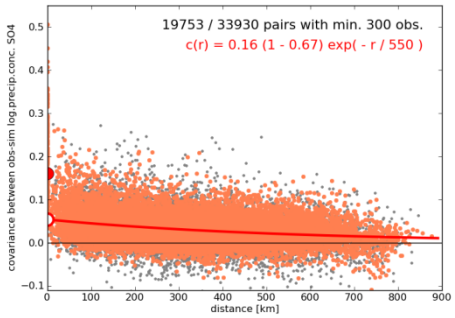	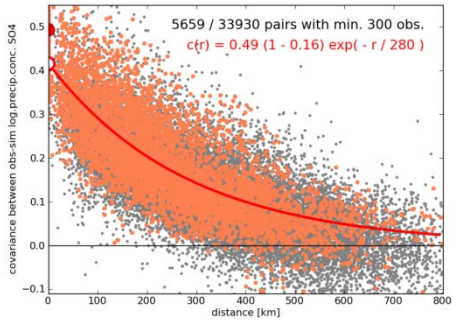

10.2 NO_3^-

	observation Kriging	residual Kriging
variogram (yearly av.)	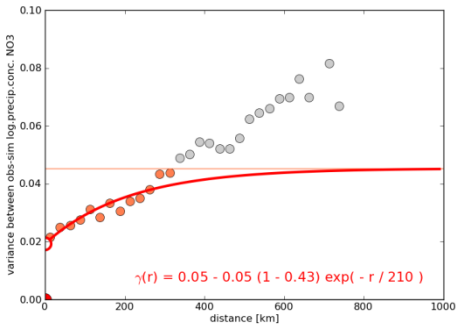	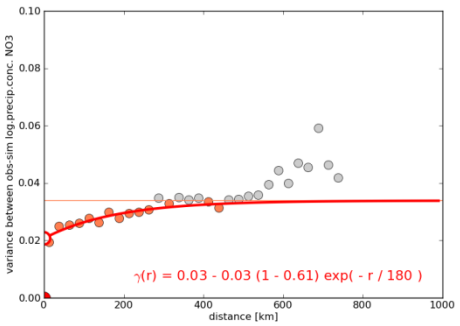
spatial covariance (UBA, weekly)	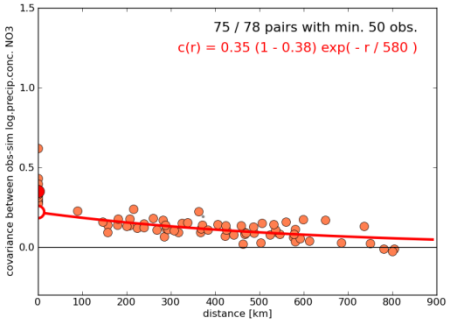	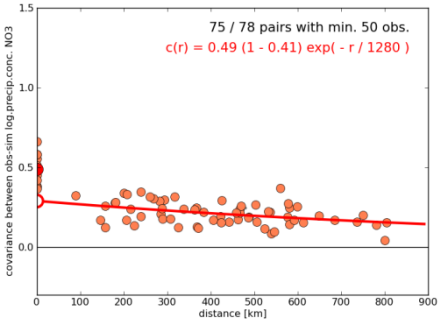
spatial covariance (all data, "daily")	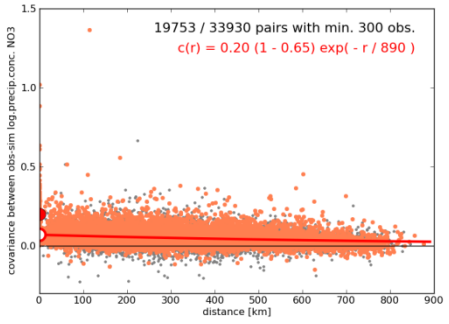	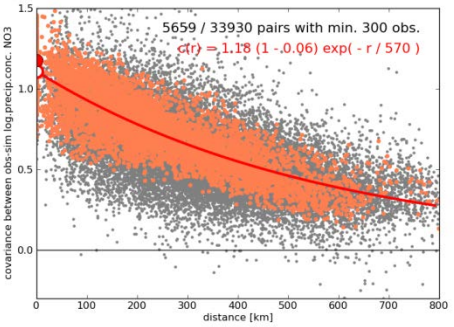

10.3 NH_4^+

	observation Kriging	residual Kriging
variogram (yearly av.)	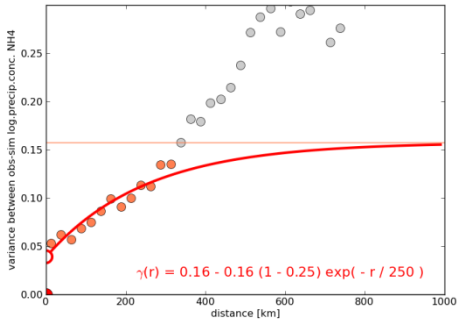	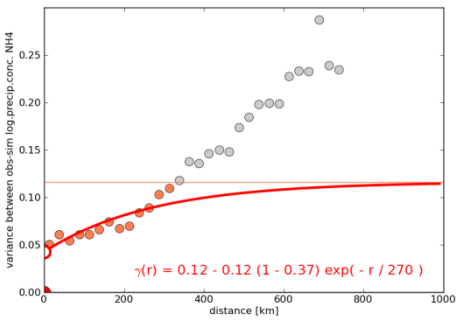
spatial covariance (UBA, weekly)	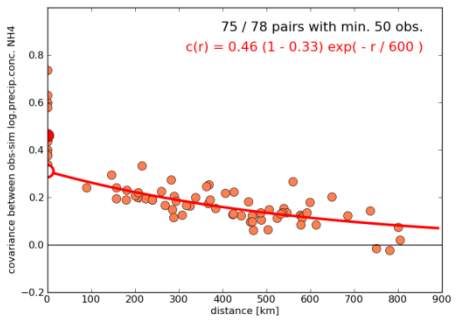	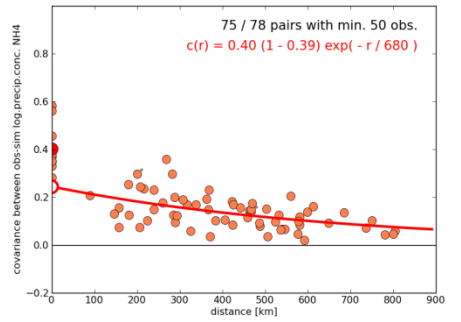
spatial covariance (all data, "daily")	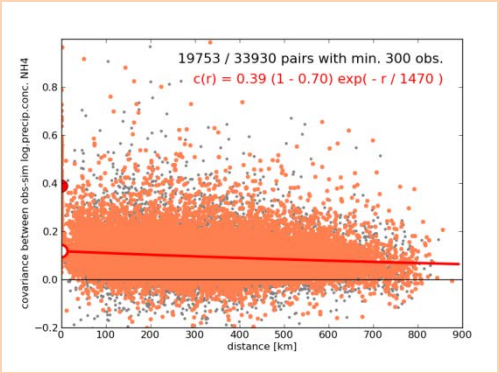	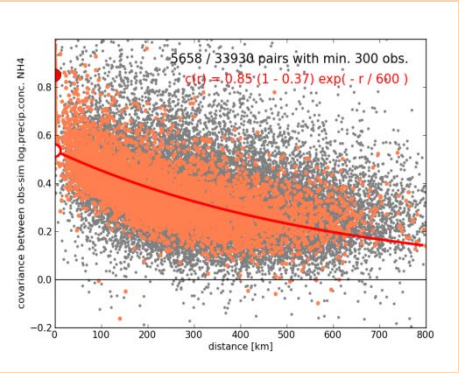

10.4 Na^+

	observation Kriging
variogram (yearly av.)	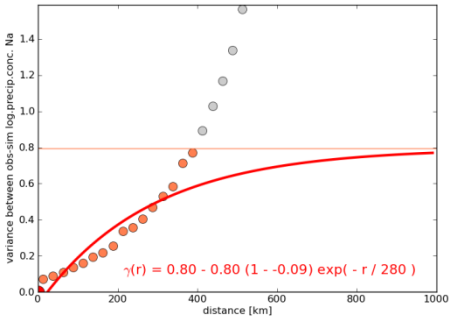
spatial covariance (UBA, weekly)	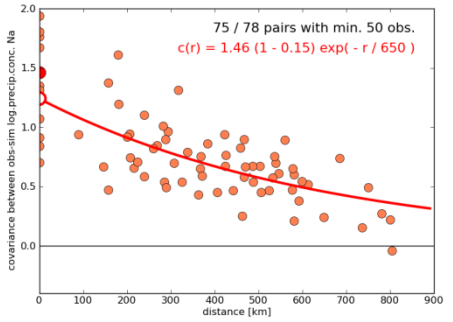
spatial covariance (all data, "daily")	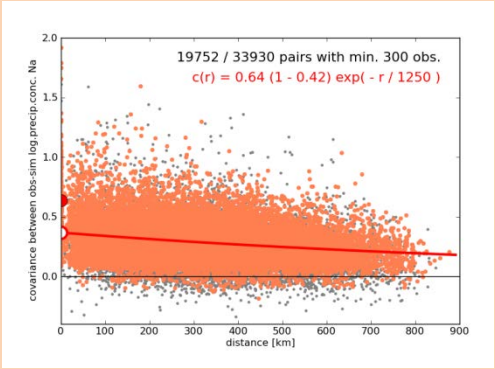

10.5 K^+

	observation Kriging
variogram (yearly av.)	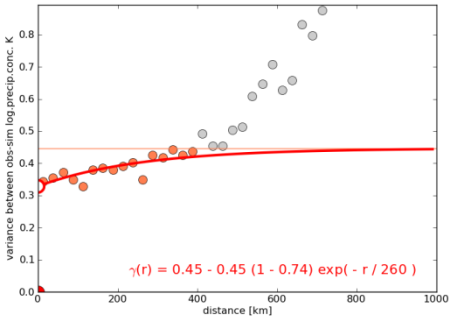
spatial covariance (UBA, weekly)	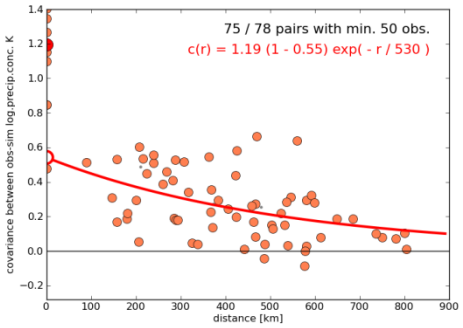
spatial covariance (all data, "daily")	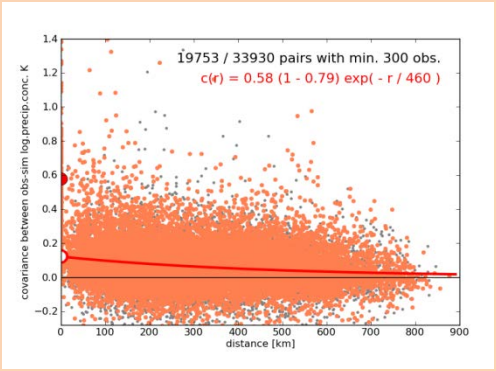

10.6 Mg^{2+}

	observation Kriging
variogram (yearly av.)	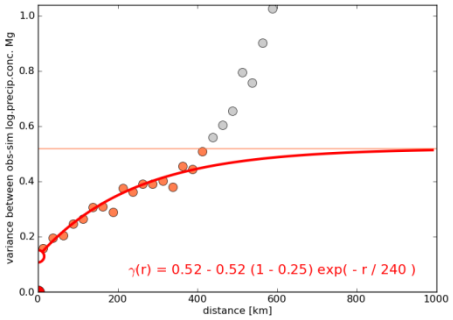
spatial covariance (UBA, weekly)	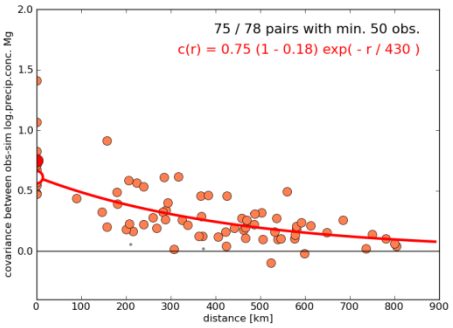
spatial covariance (all data, "daily")	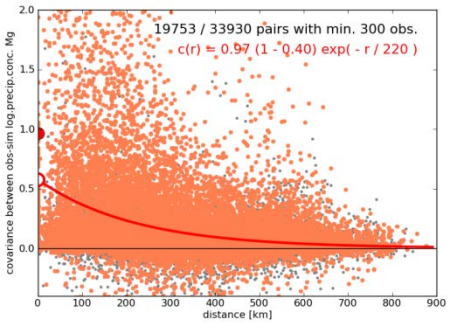

10.7 Ca^{2+}

	observation Kriging
variogram (yearly av.)	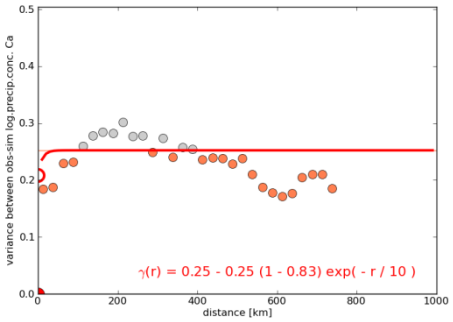
spatial covariance (UBA, weekly)	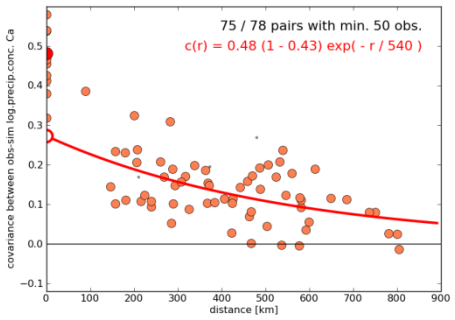
spatial covariance (all data, "daily")	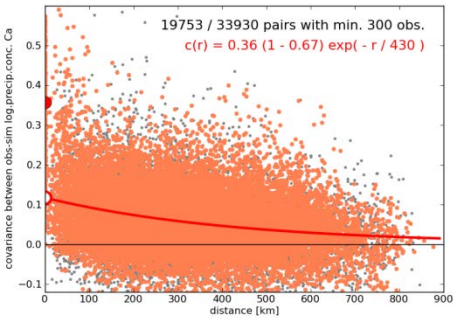

11 Appendix B: Comparison of dry, wet and occult deposition fluxes in MAPESI 2007 and PINETI 2008

11.1 SO_x

Dry deposition:

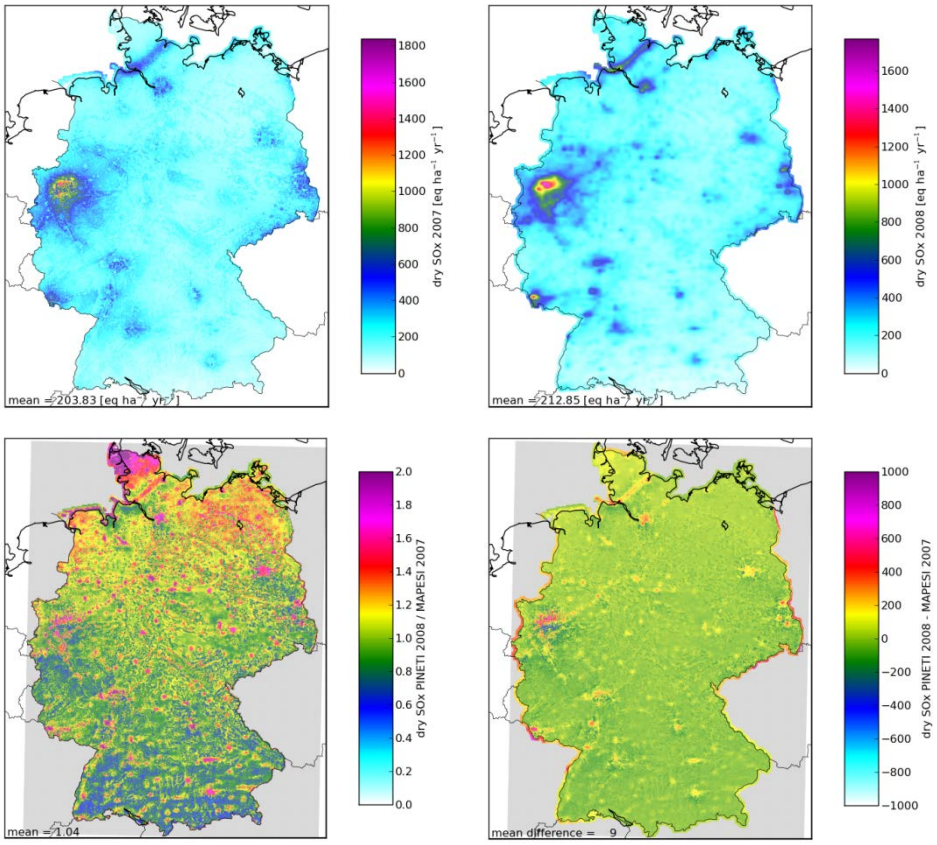

Wet deposition:

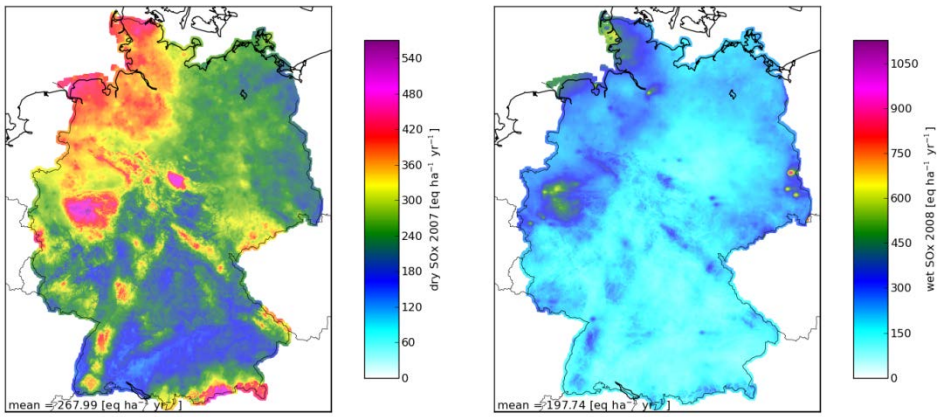

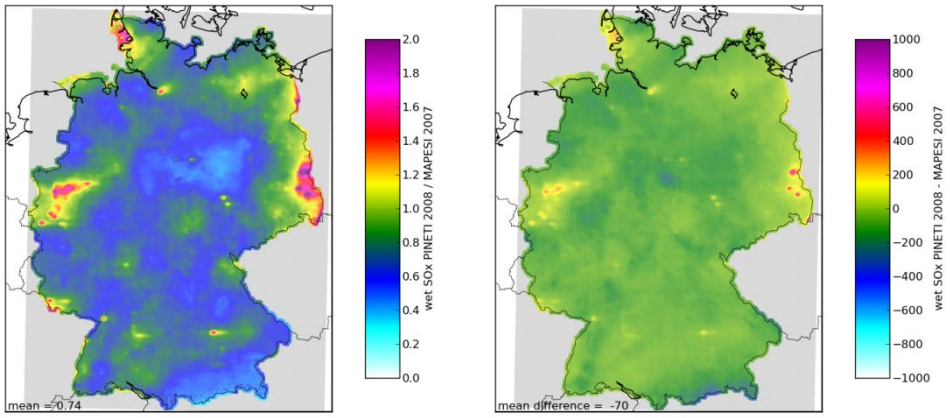

Occult deposition:

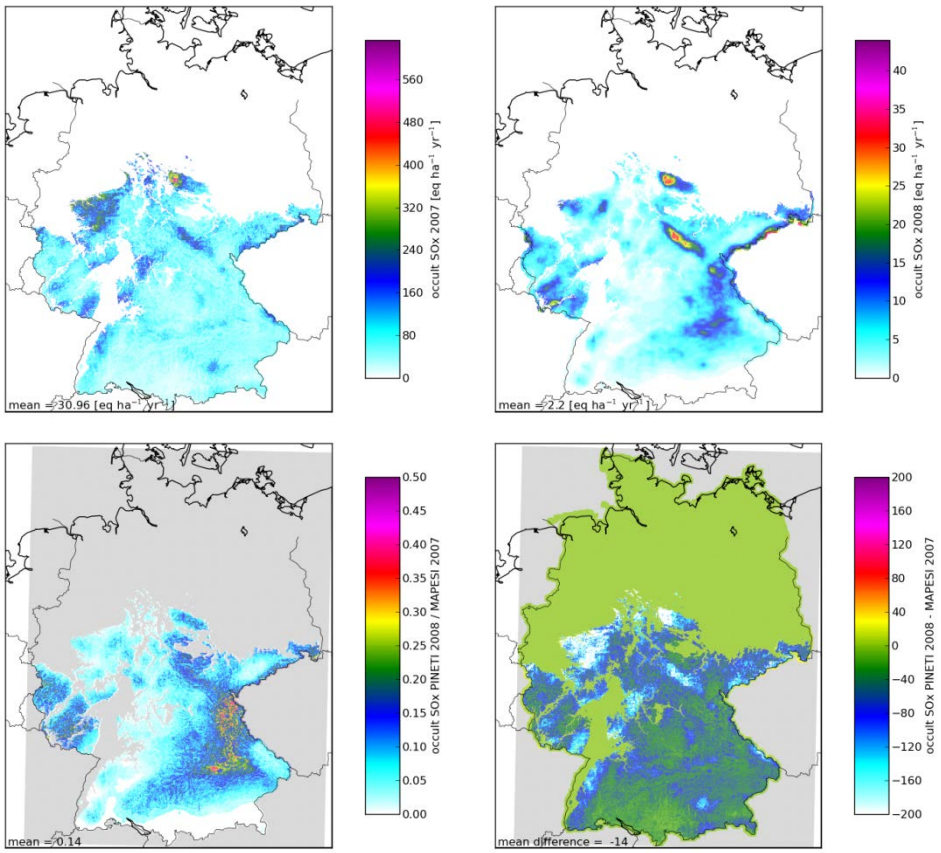

11.2 NH_x

Dry deposition:

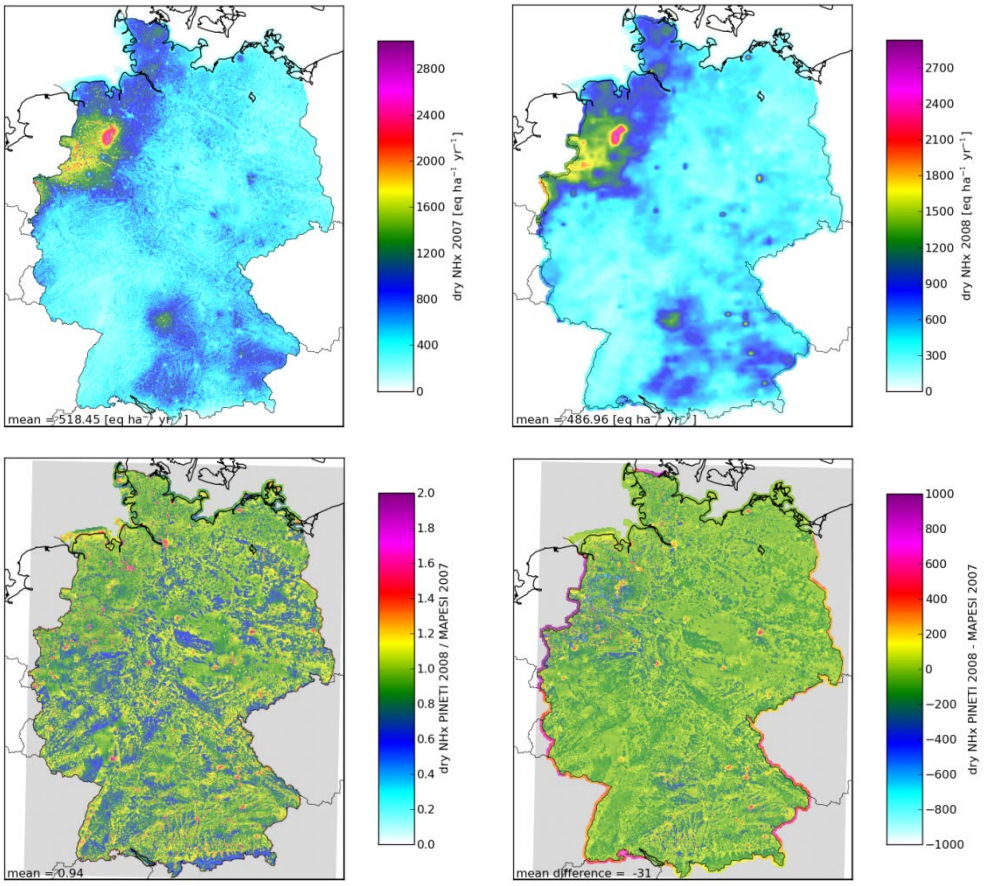

Wet deposition:

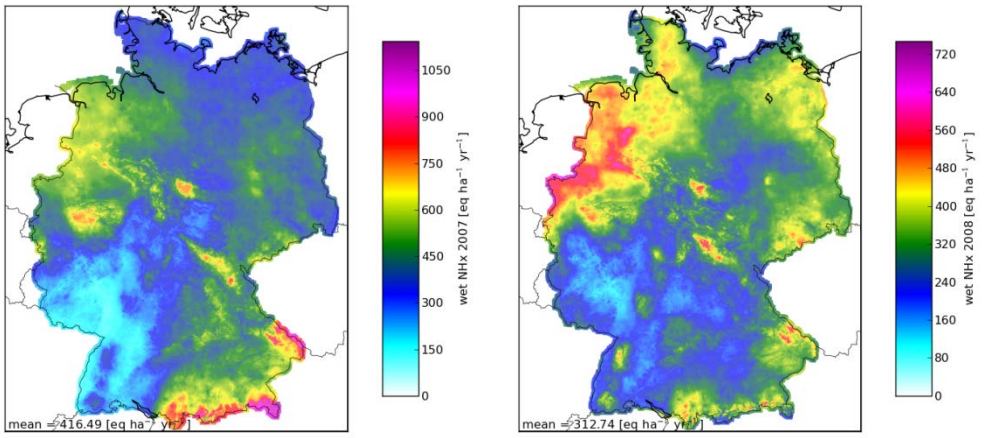

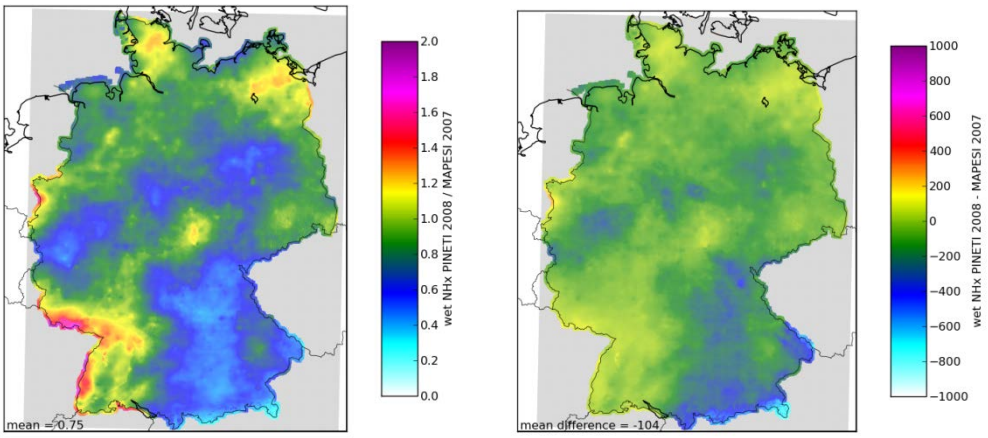

Occult deposition:

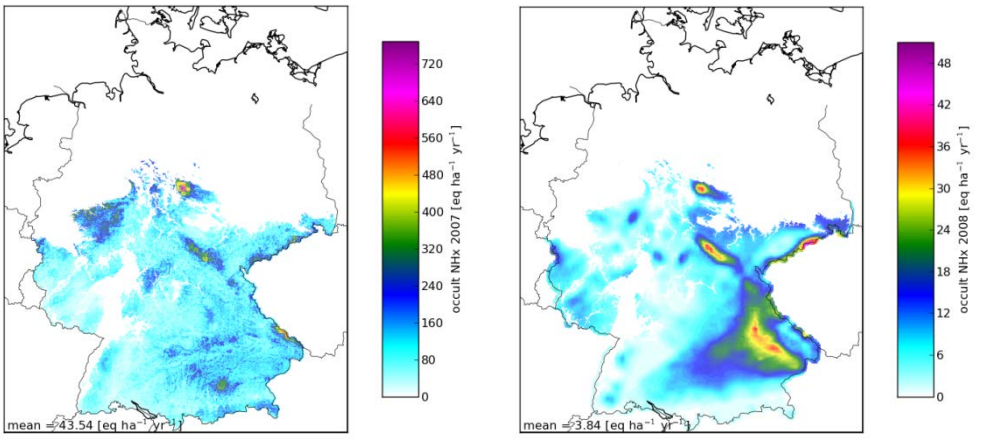

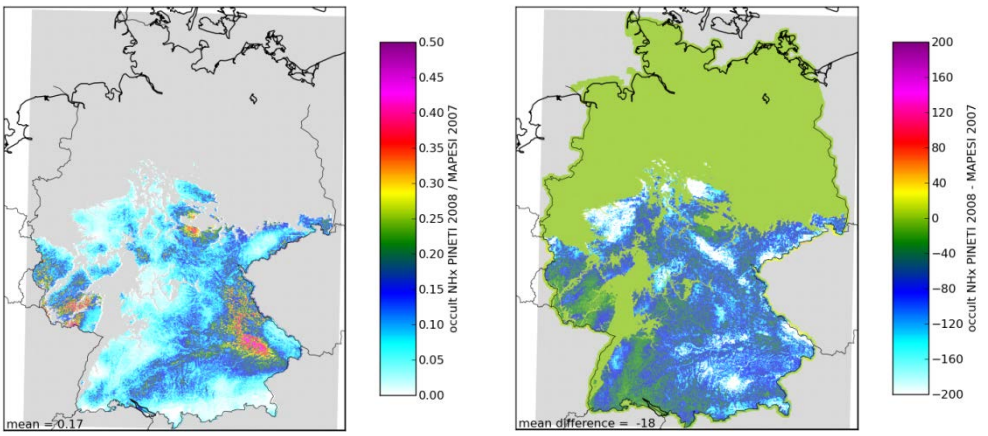

11.3 NO_y

Dry deposition:

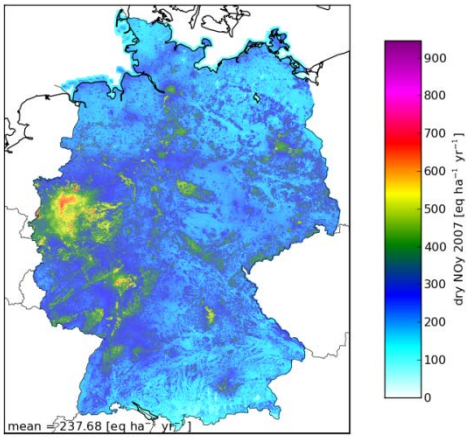

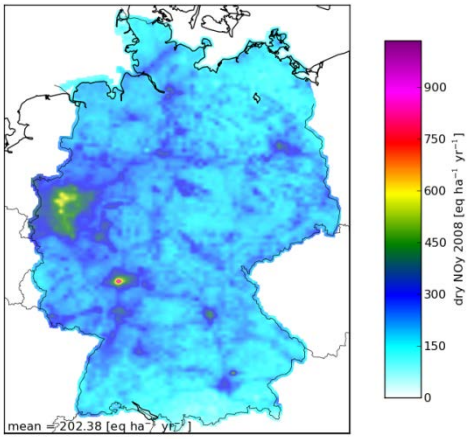

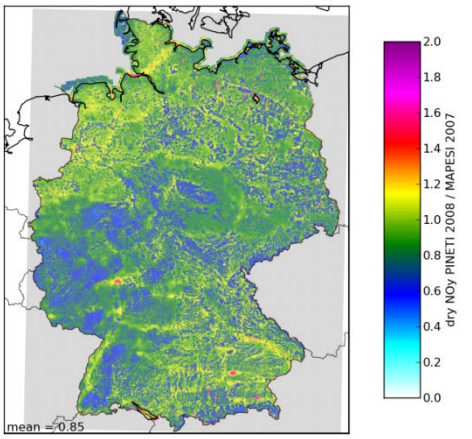

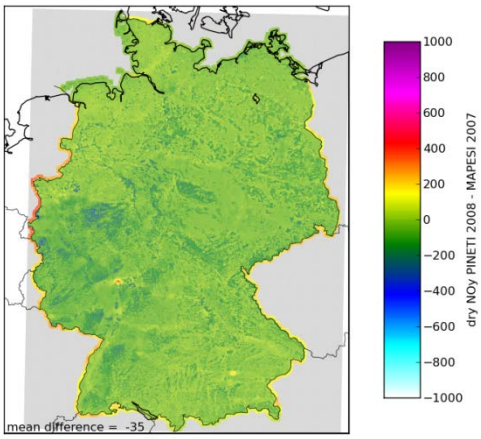

Wet deposition:

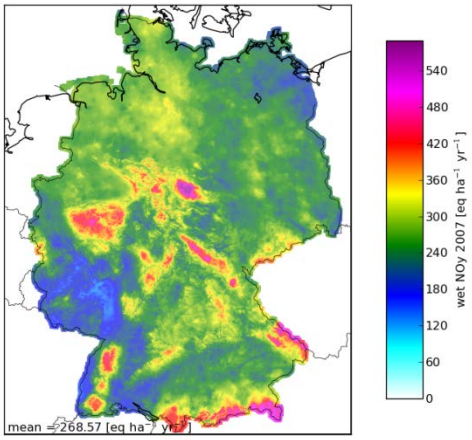

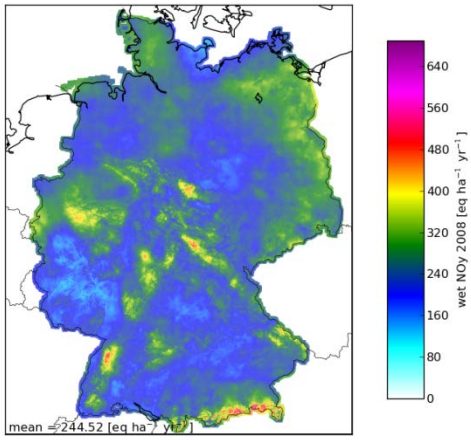

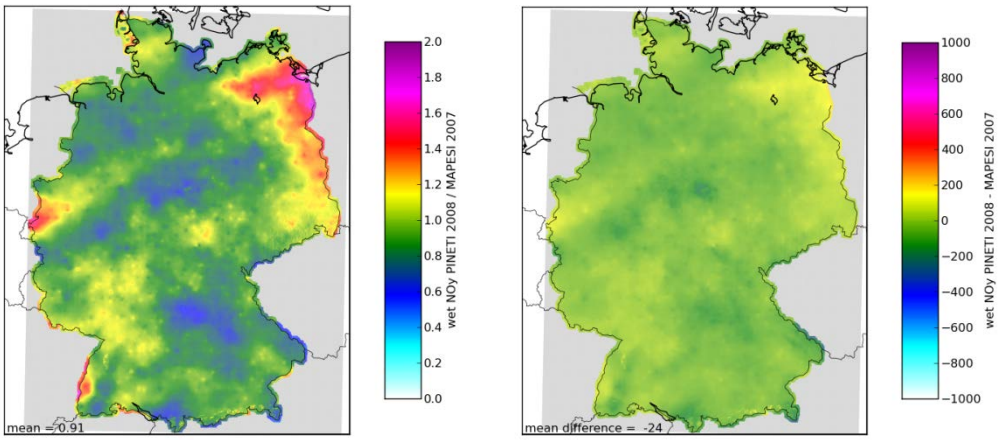

Occult deposition:

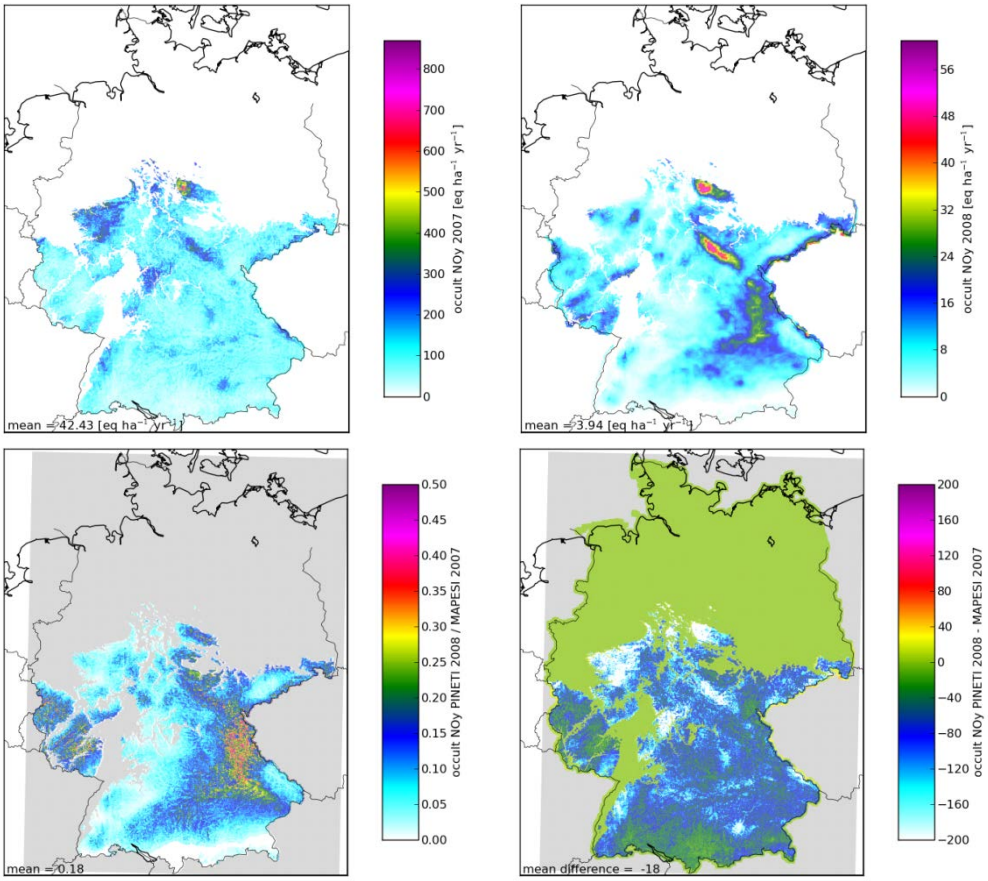

11.4 Na^+

Dry deposition:

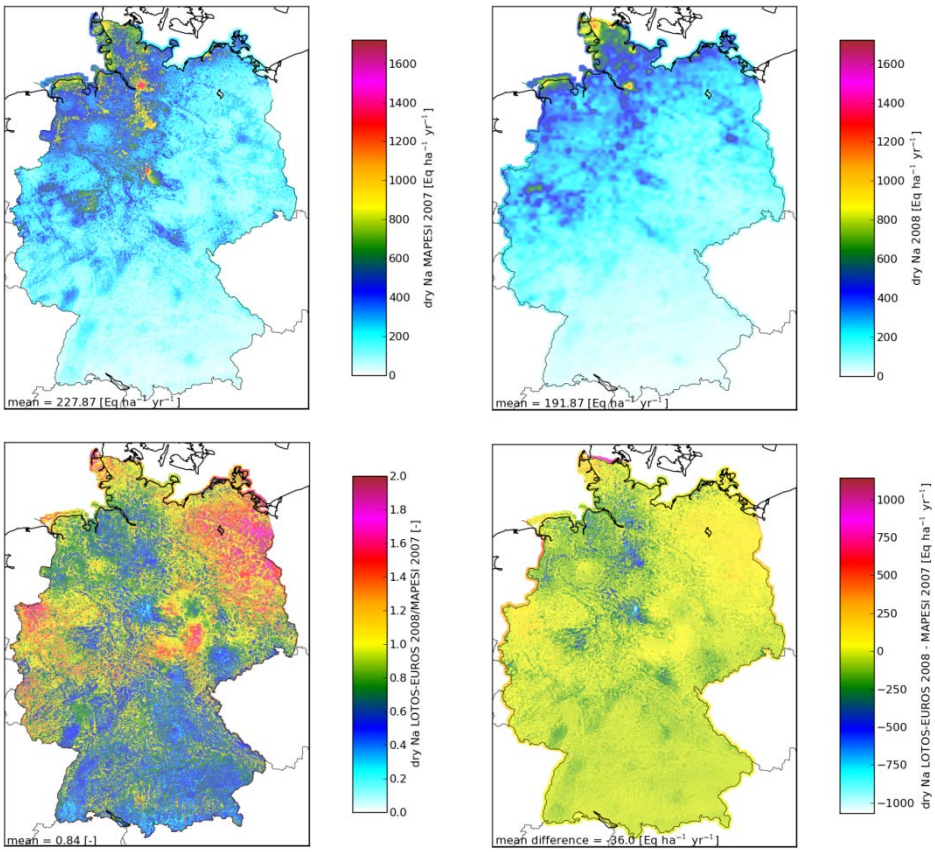

Wet deposition:

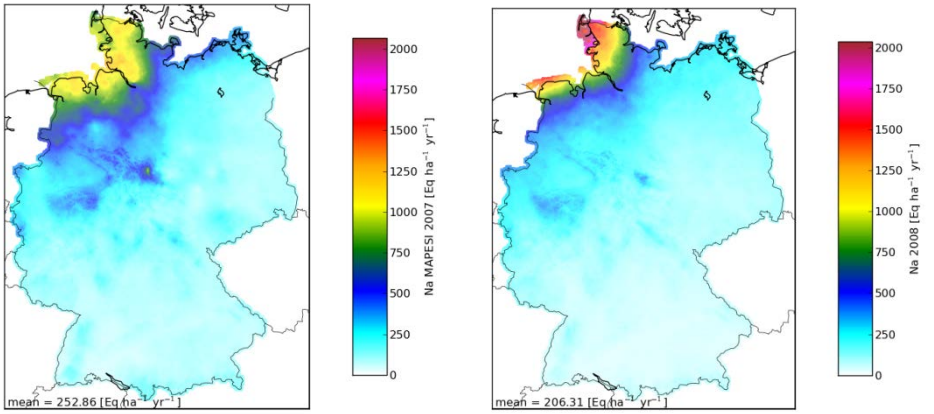

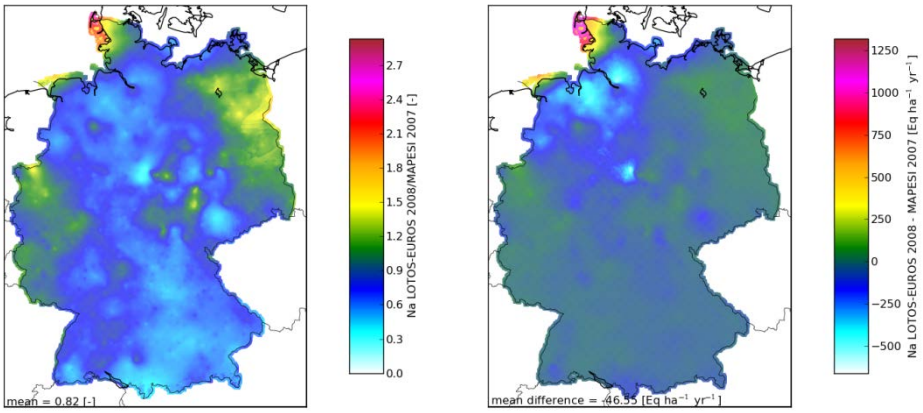

Occult deposition:

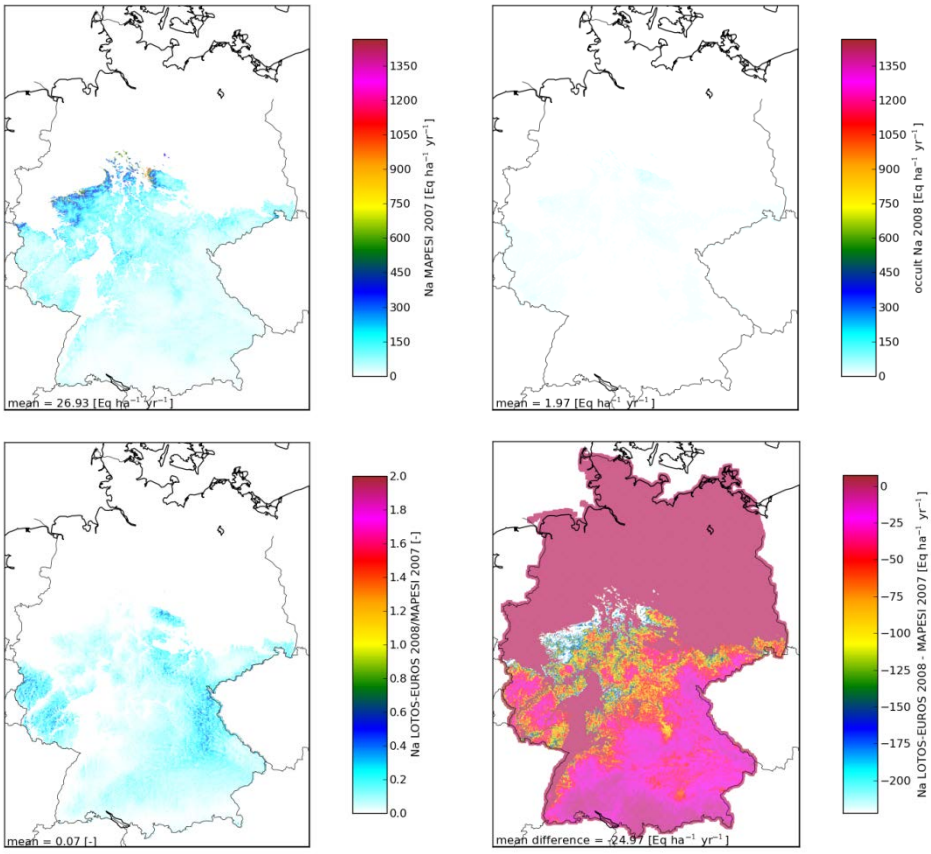

11.5 Ca^{2+}

Dry deposition:

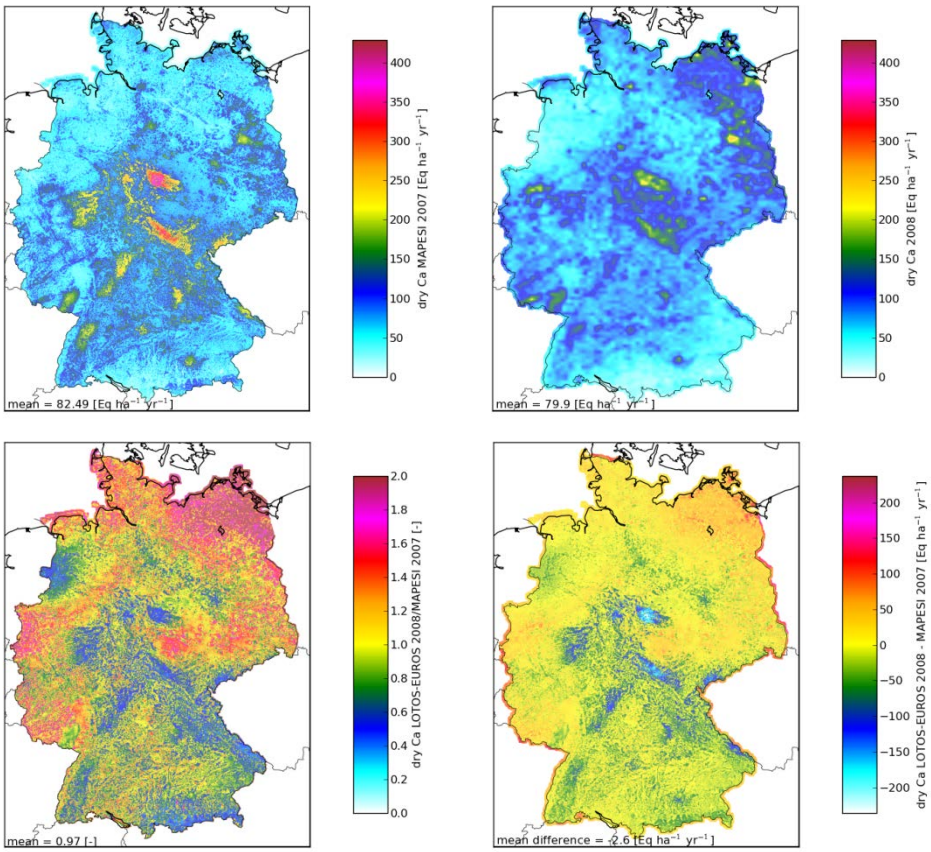

Wet deposition:

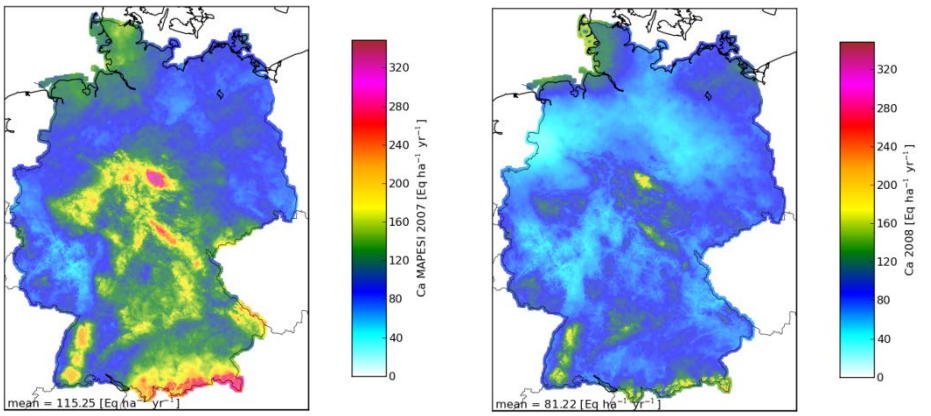

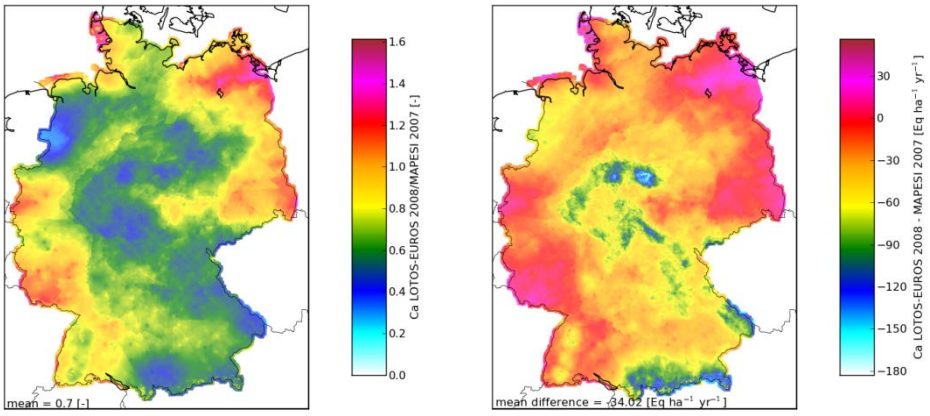

Occult deposition:

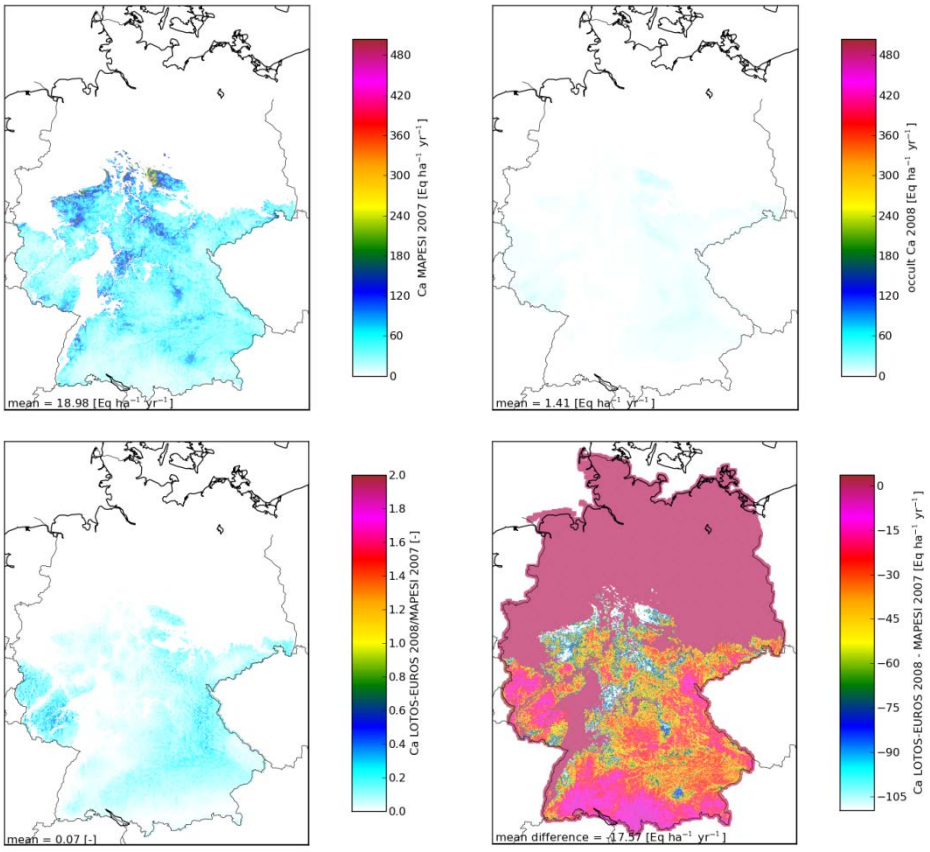

11.6 Mg^{2+}

Dry deposition:

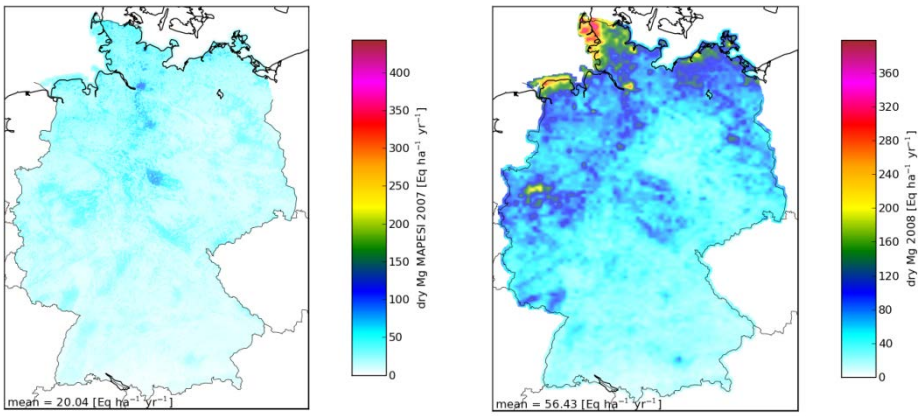

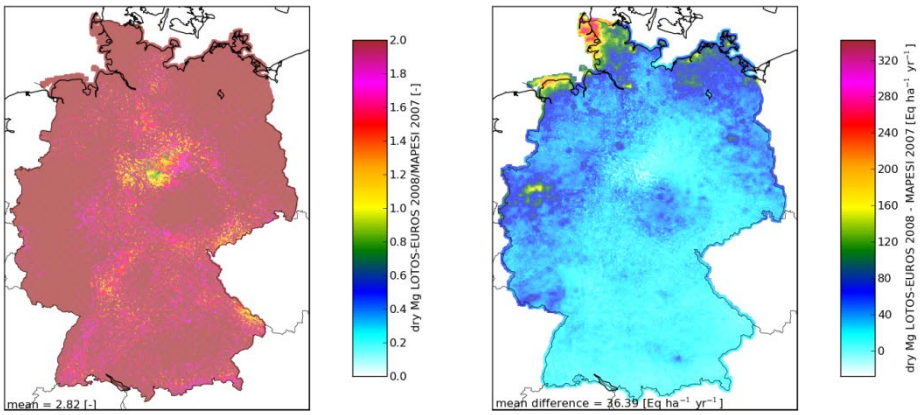

Wet deposition:

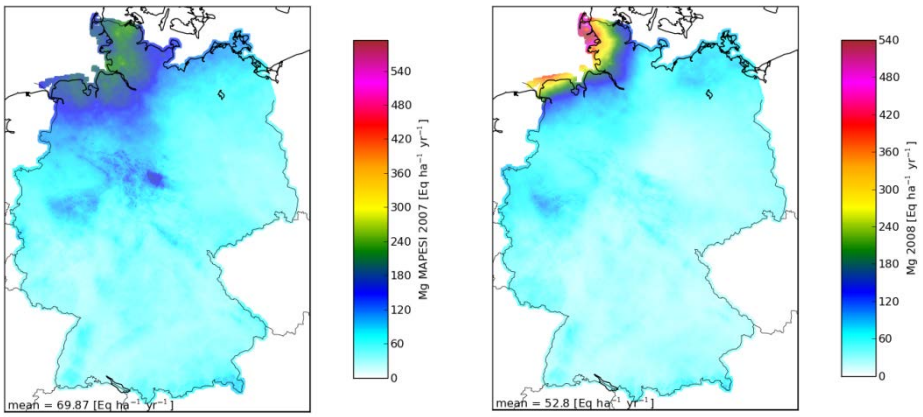

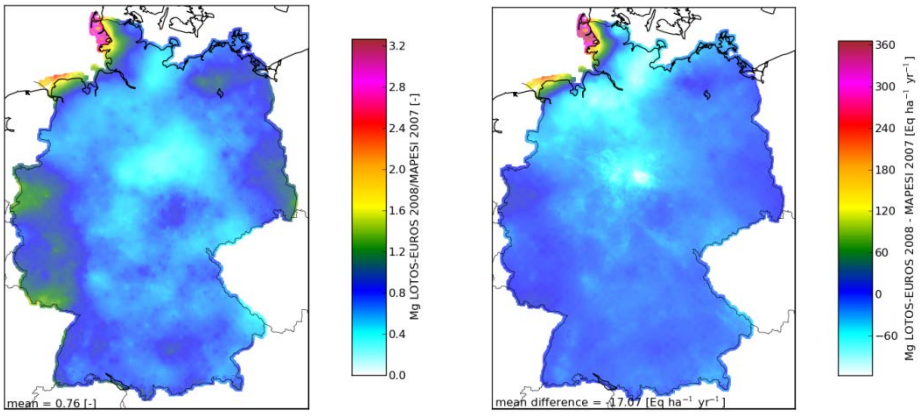

Occult deposition:

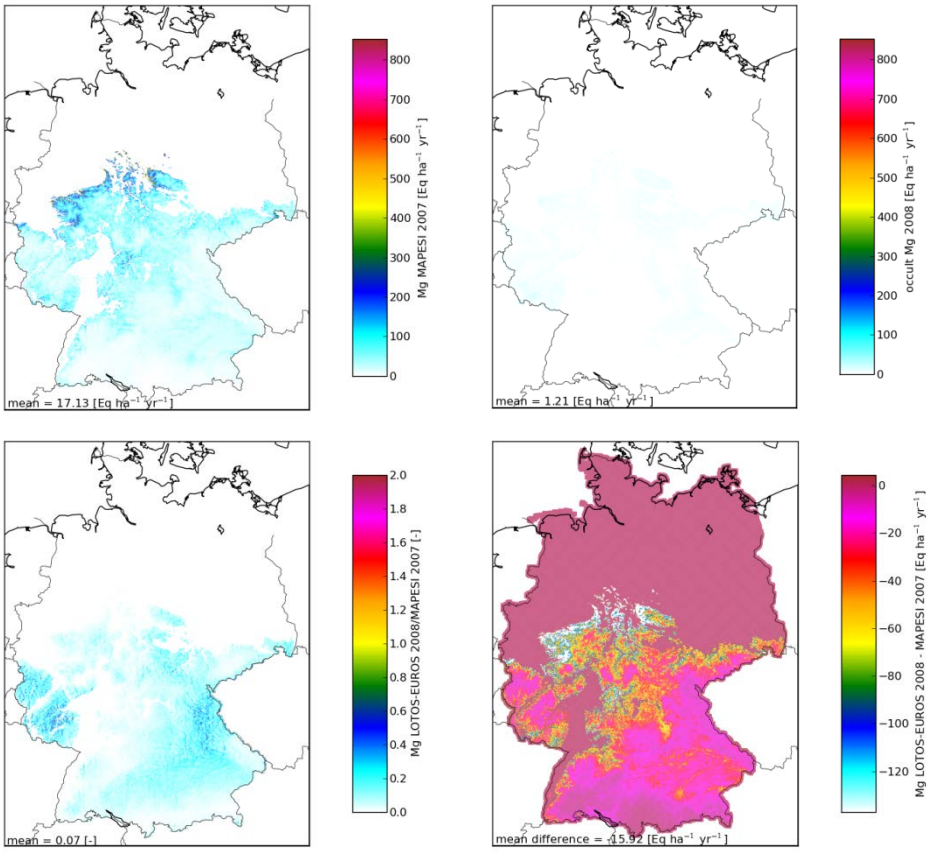

11.7 K^+

Dry deposition:

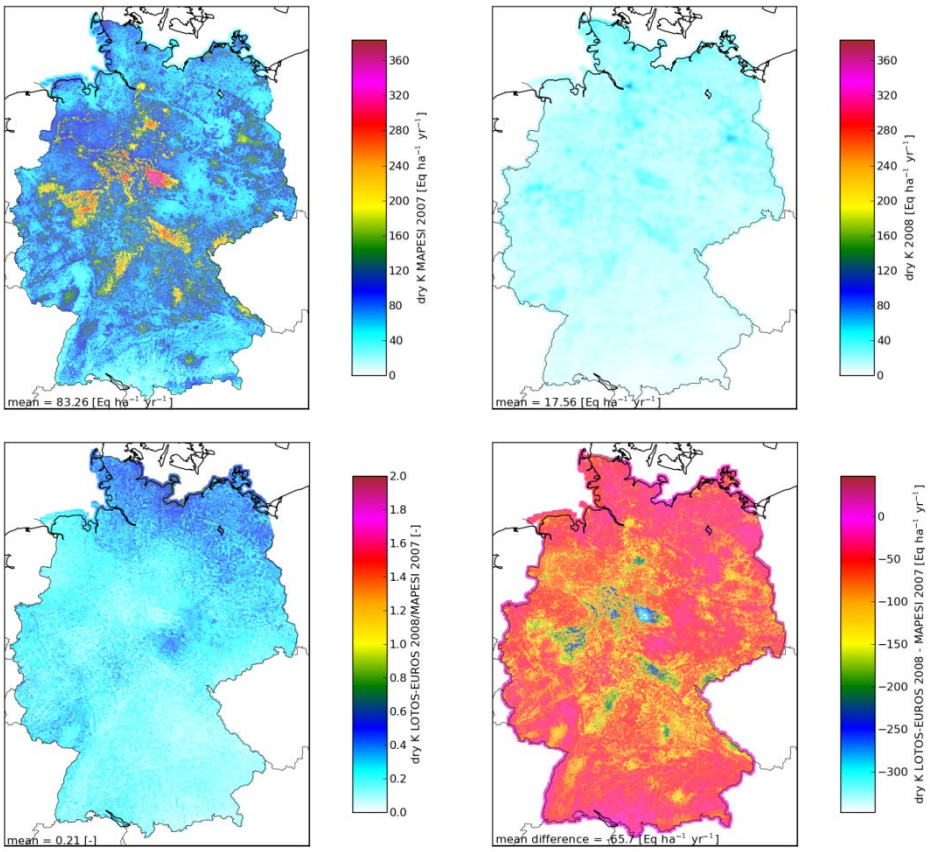

Wet deposition:

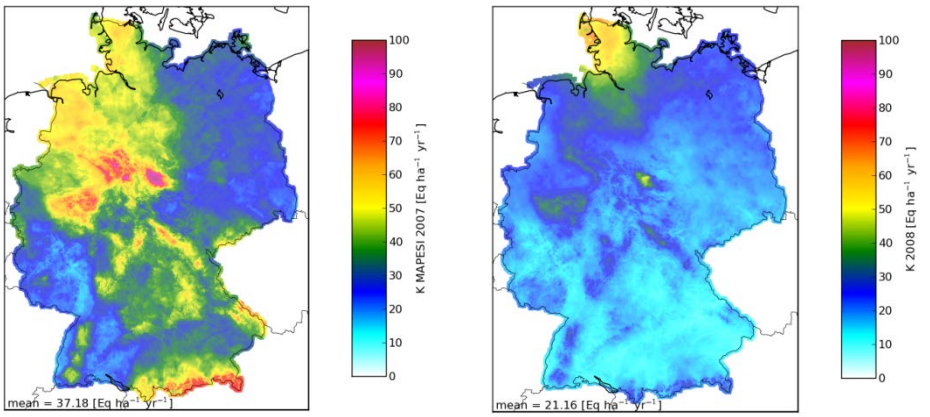

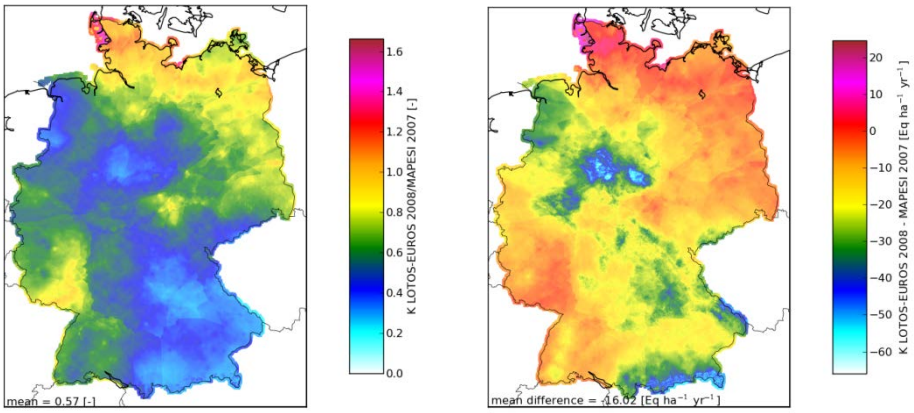

Occult deposition:

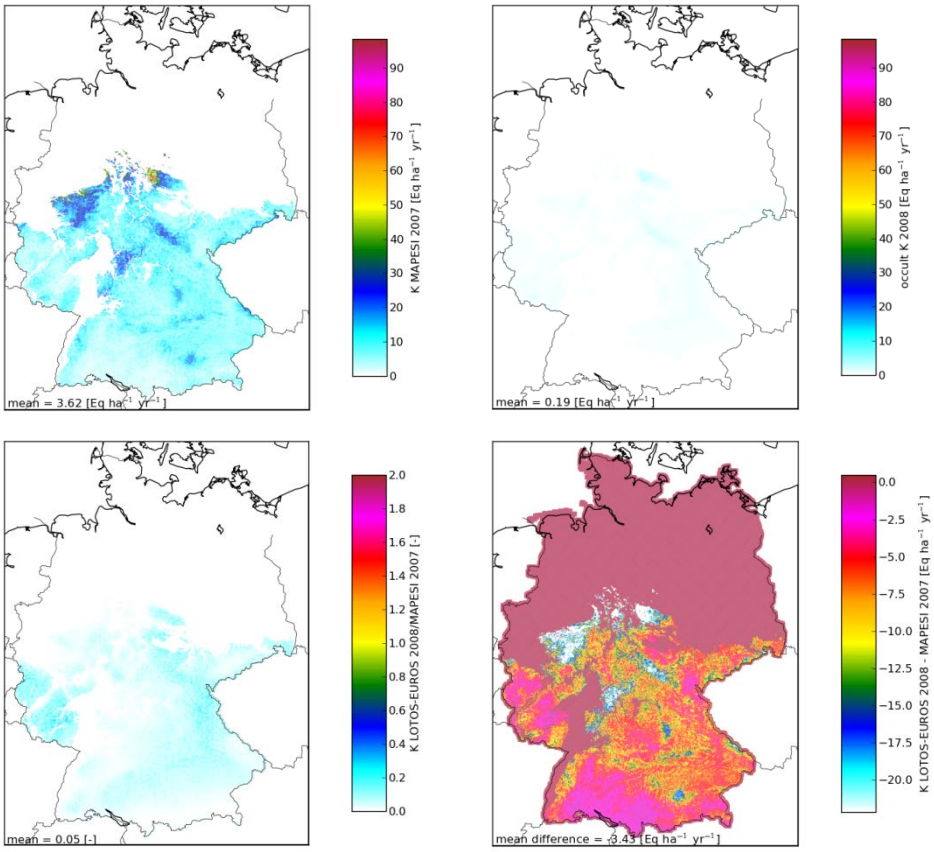

11.8 Ca^{2+}-nss

Dry deposition:

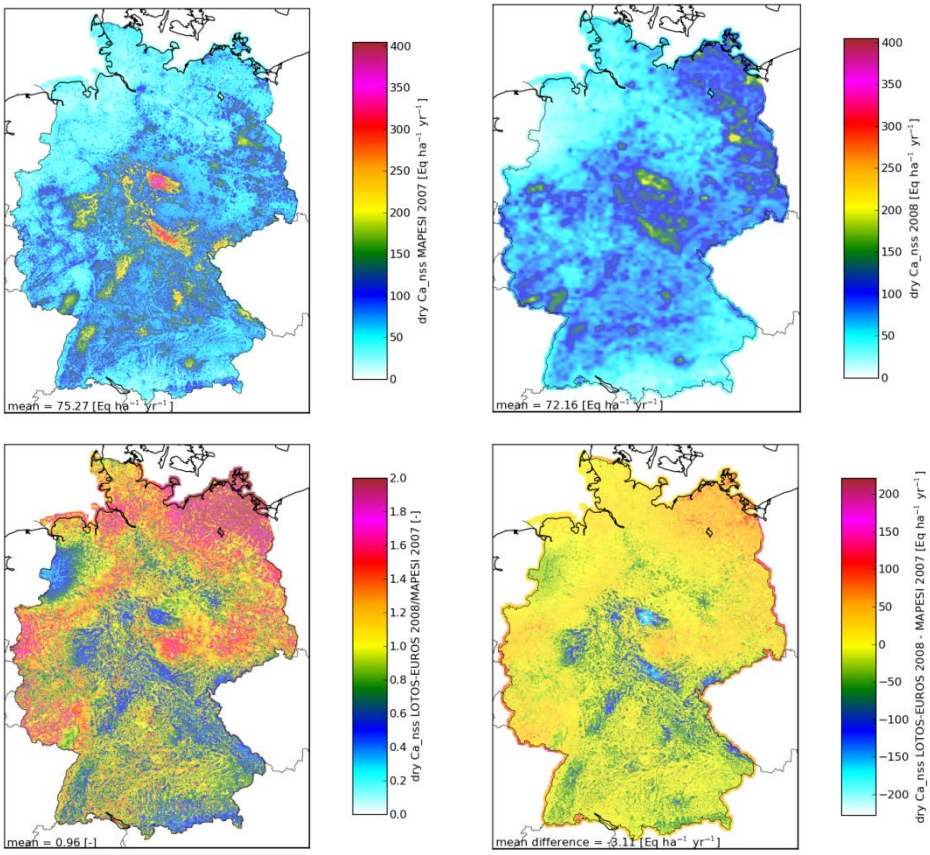

Wet deposition:

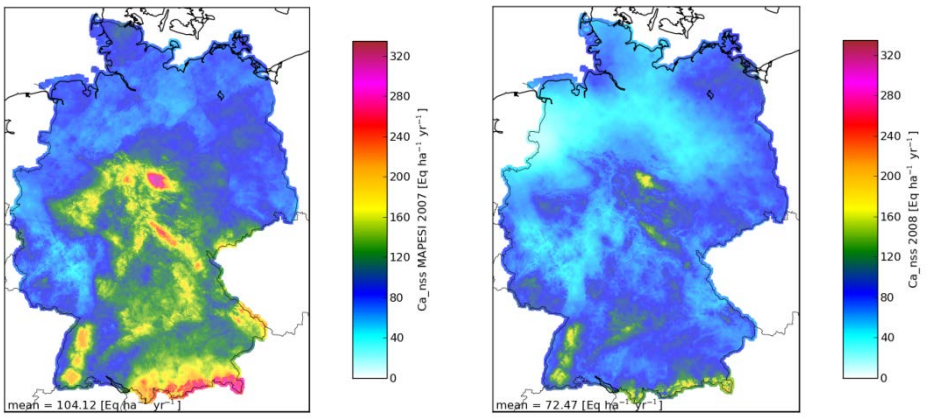

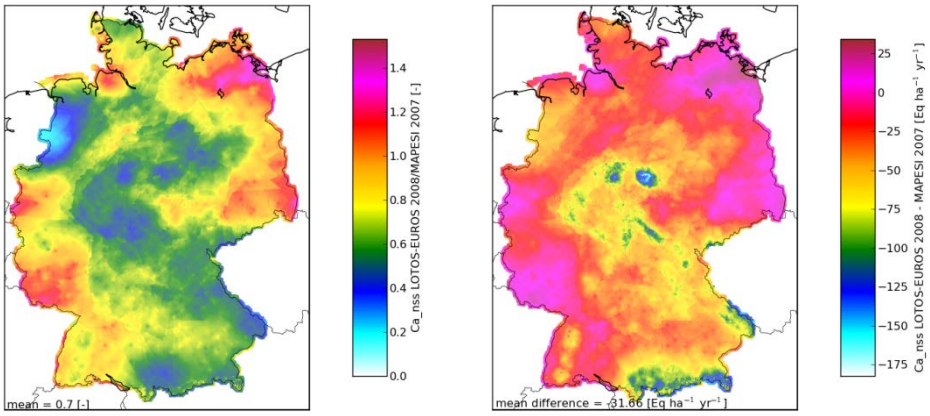

Occult deposition:

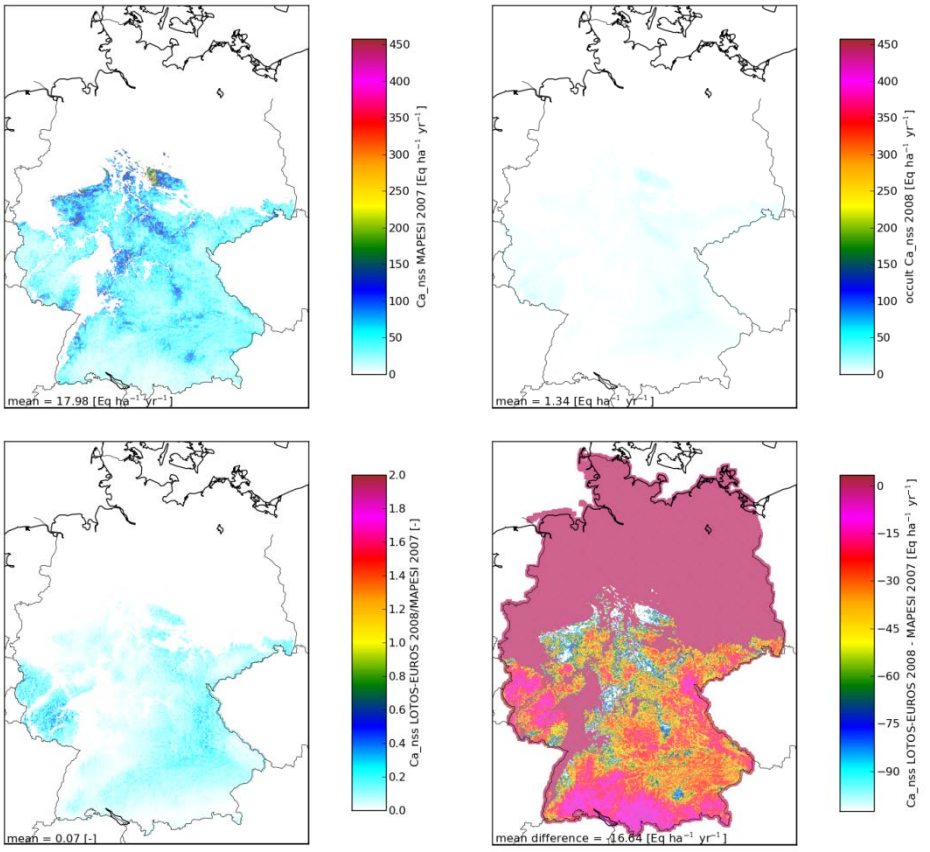

11.9 Mg^{2+}-nss

Dry deposition:

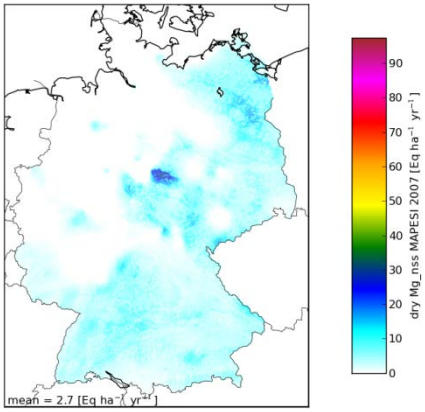

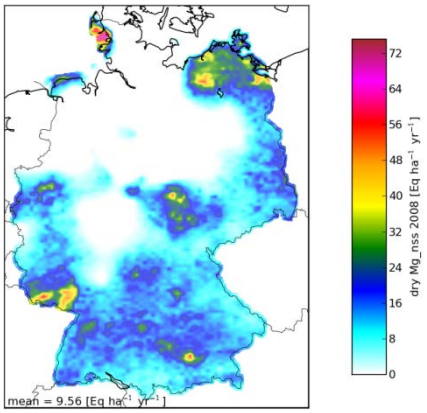

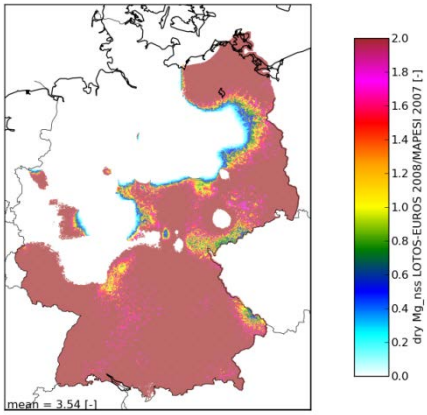

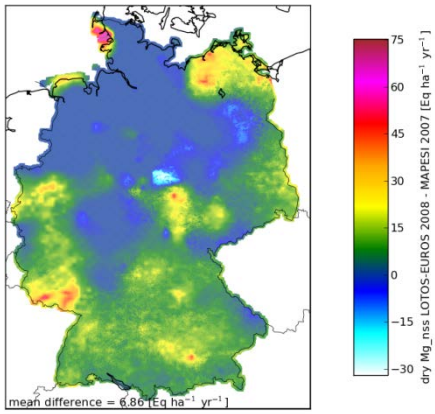

Wet deposition:

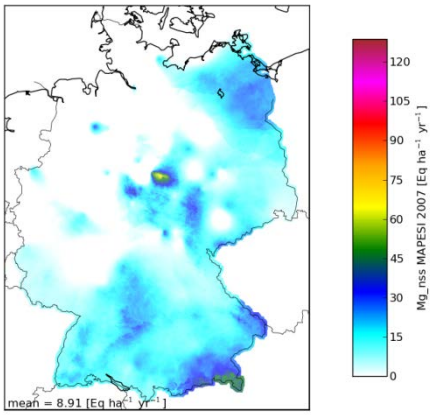

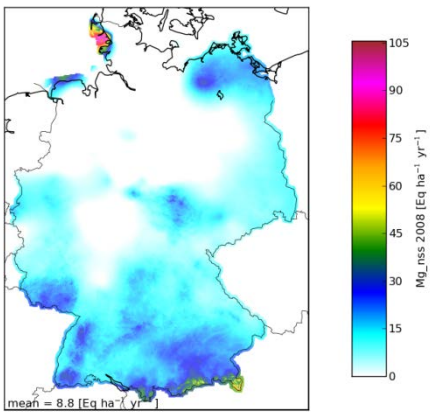

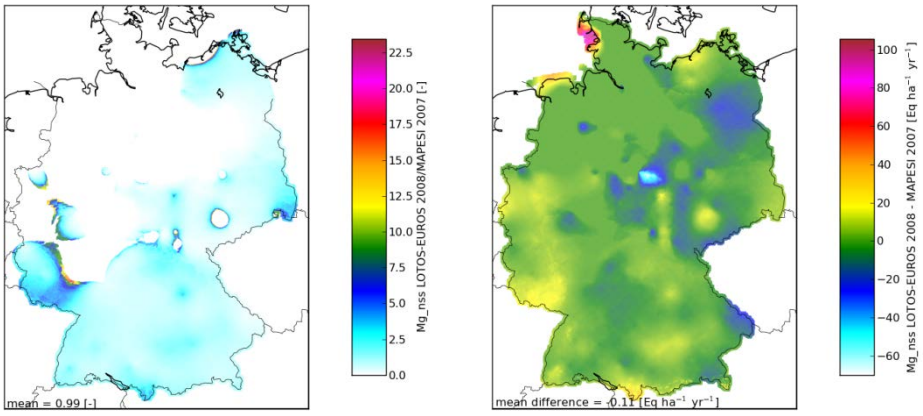

Occult deposition:

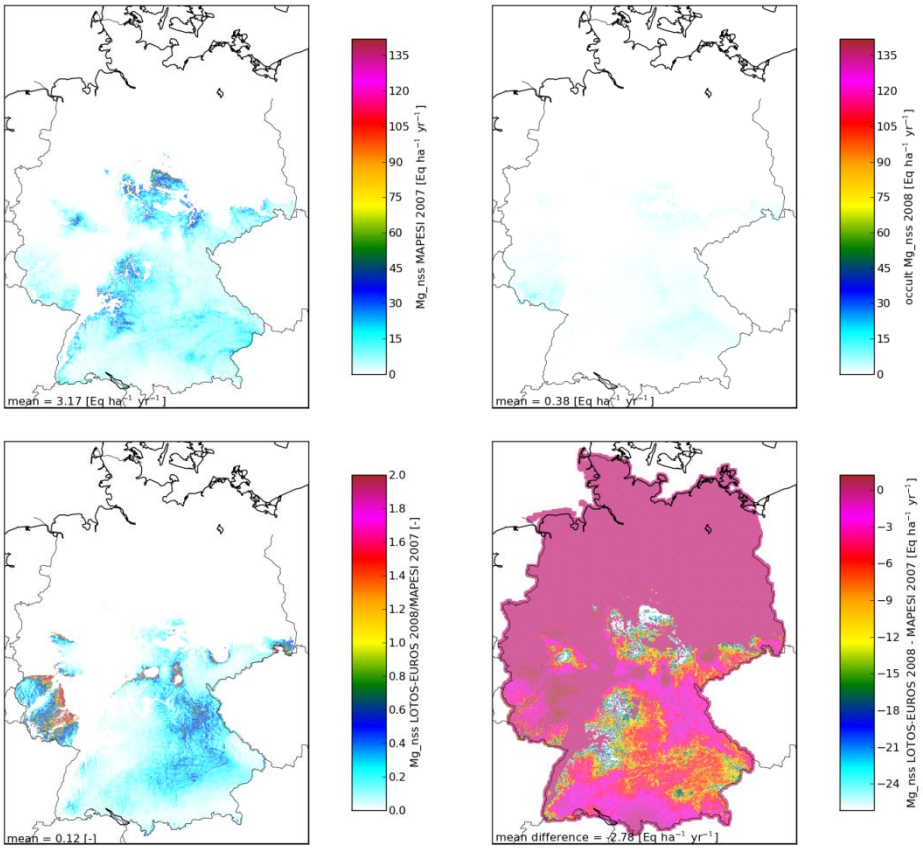

11.10 K^+-nss

Dry deposition:

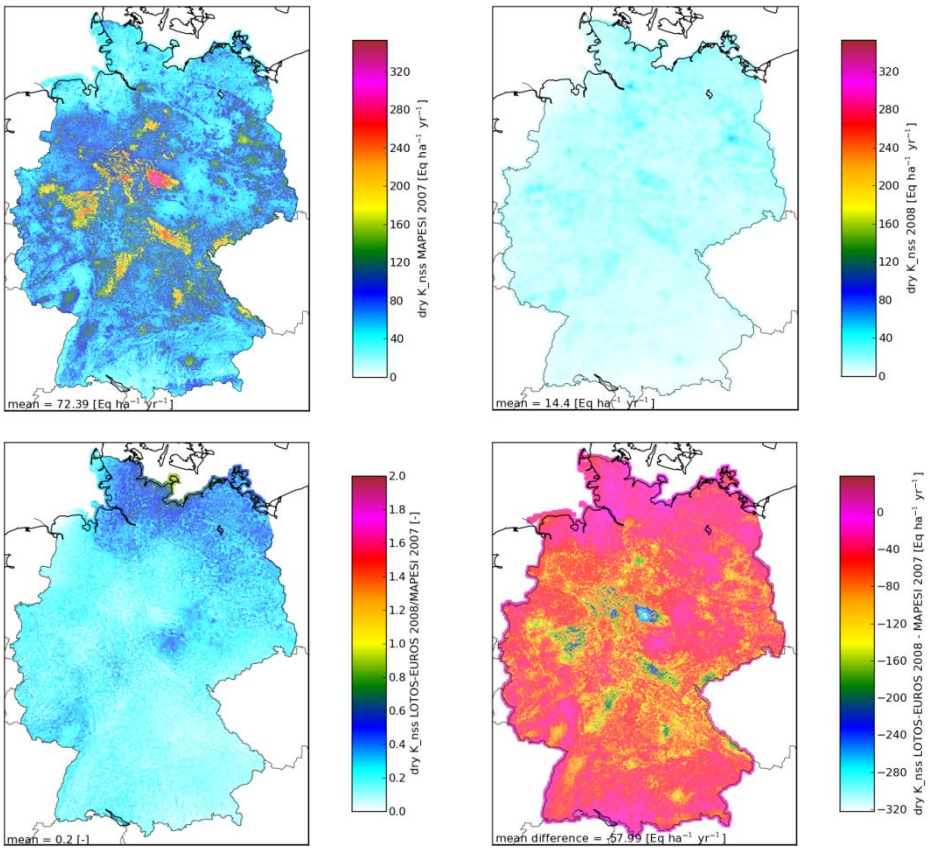

Wet deposition:

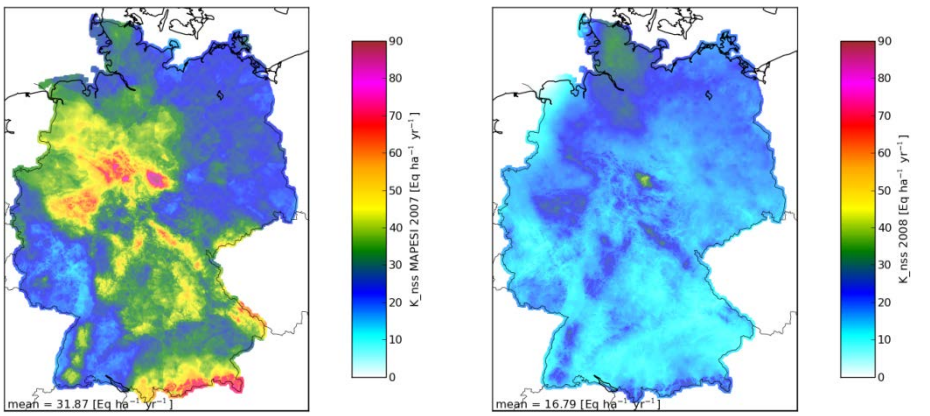

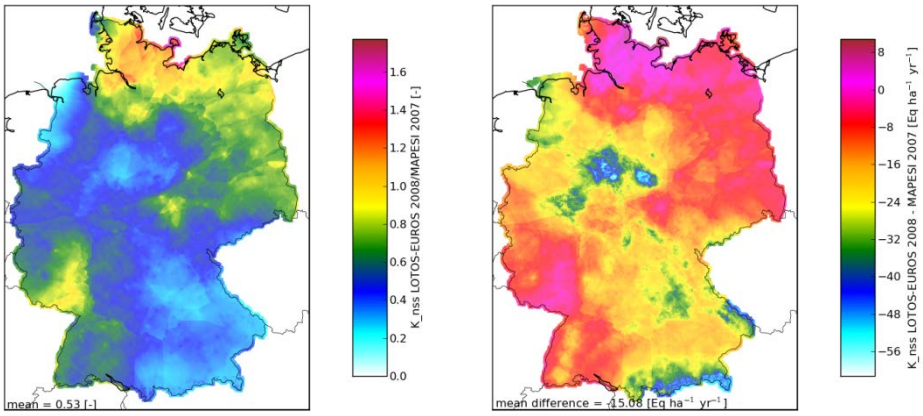

Occult deposition:

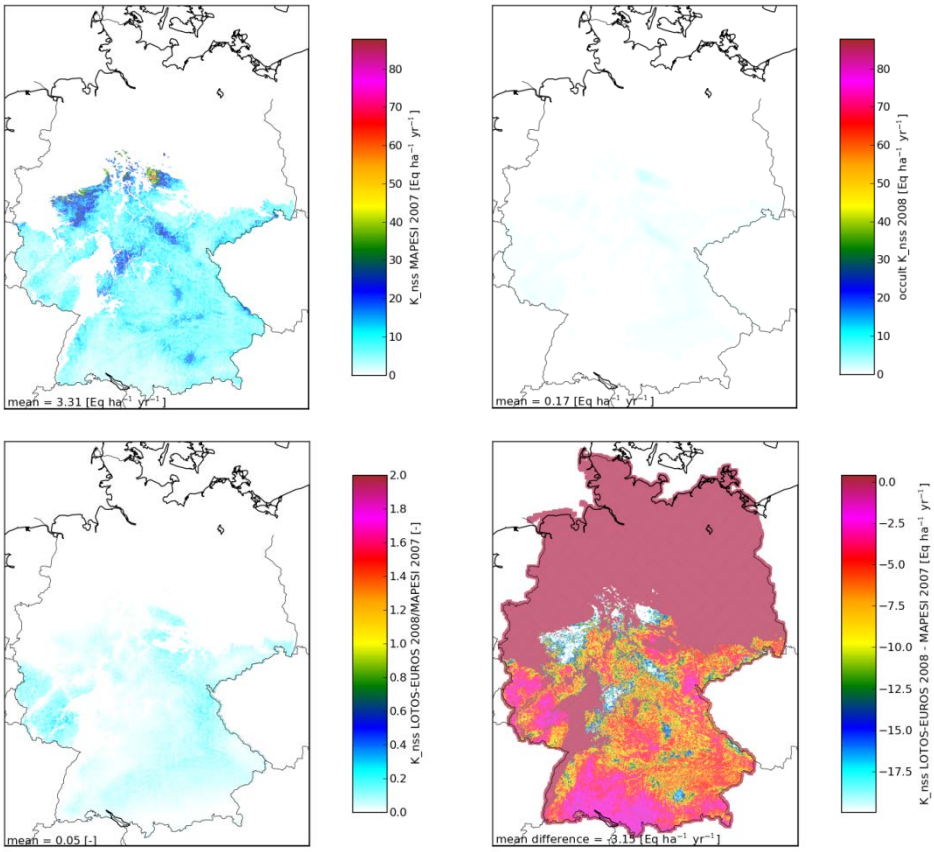

12 Appendix C: Overview of the average total deposition amounts over Germany from MAPESI and PINETI for the years 2004 till 2009

The total deposition as calculated in the MAPESI project (Builtjes et al., 2011) and in this PINETI project are summarized in Table 20.

Table 20. Summary of total deposition in MAPESI (Builtjes et al., 2011) and PINETI (this study).

TOTAL DEPOSITION		2004 MAPESI	2005 MAPESI	2006 MAPESI	2007 MAPESI	2008 PINETI	2009 PINETI
SO_x-S-nss	eq ha^{-1} yr^{-1}	512	499	552	479	365	350
NH_x-N	eq ha^{-1} yr^{-1}	972	934	1021	1006	804	800
NO_y-N	eq ha^{-1} yr^{-1}	601	572	538	563	451	450
N	eq ha^{-1} yr^{-1}	1573	1506	1559	1569	1255	1251
Na^+	eq ha^{-1} yr^{-1}	319	370	402	504	400	296
Ca^{2+}	eq ha^{-1} yr^{-1}	202	214	233	222	162	144
Mg^{2+}	eq ha^{-1} yr^{-1}	91	80	88	107	110	85
K^+	eq ha^{-1} yr^{-1}	81	85	152	128	39	40
Ca^{2+}-nss	eq ha^{-1} yr^{-1}	189	191	219	202	146	131
Mg^{2+}-nss	eq ha^{-1} yr^{-1}	21	12	17	15	19	19
K^+-nss	eq ha^{-1} yr^{-1}	72	74	139	110	31	34
BC-nss	eq ha^{-1} yr^{-1}	282	277	375	327	196	184

13 Appendix D: Total deposition over Germany in 2009

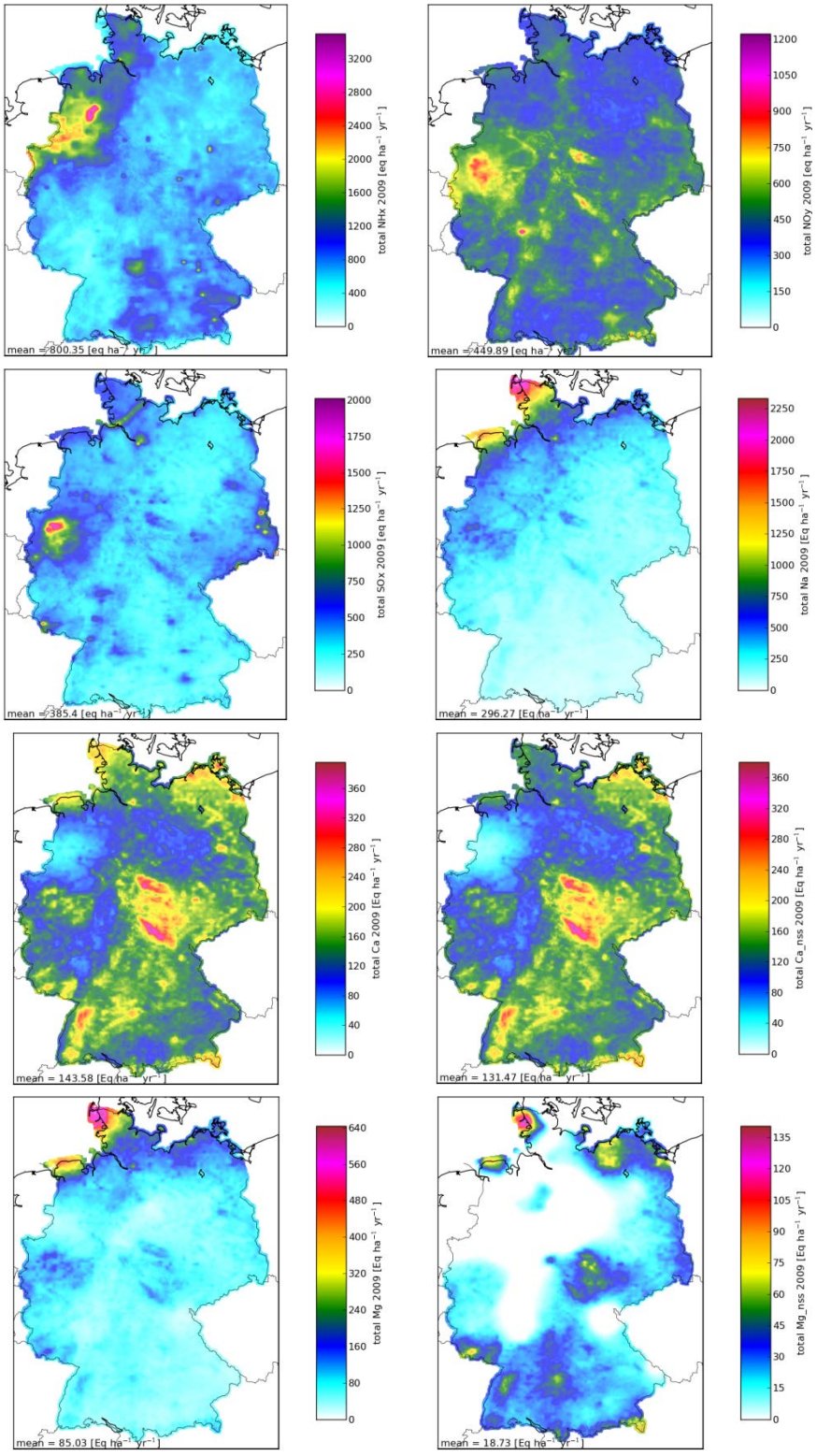

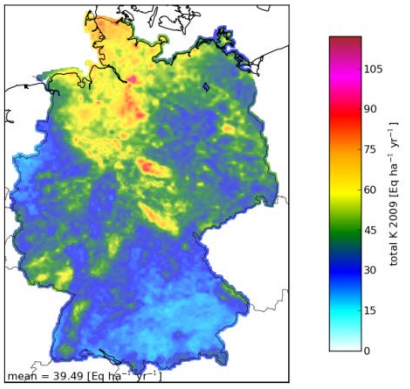
mean = 39.49 [Eq ha⁻¹ yr⁻¹]

105
90
75
60
45
30
15
0
total K 2009 [Eq ha⁻¹ yr⁻¹]

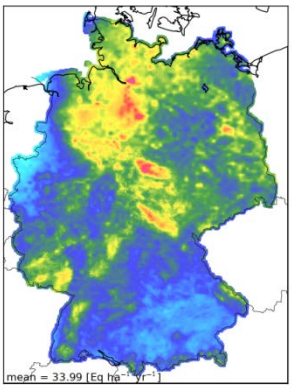
mean = 33.99 [Eq ha⁻¹ yr⁻¹]

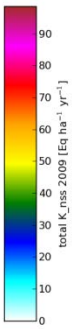
90
80
70
60
50
40
30
20
10
0
total K_nss 2009 [Eq ha⁻¹ yr⁻¹]

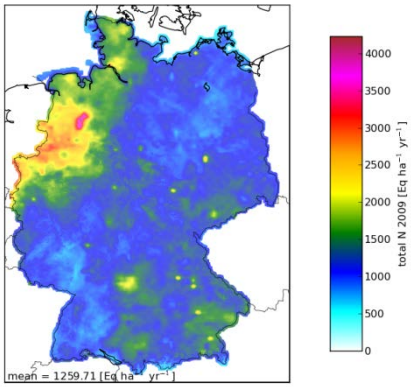
mean = 1259.71 [Eq ha⁻¹ yr⁻¹]

4000
3500
3000
2500
2000
1500
1000
500
0
total N 2009 [Eq ha⁻¹ yr⁻¹]